The 6th international conference

Fundamental Problems of Superconductivity

September 28 – October 4, 2025
Moscow

The 6th international conference **«Fundamental problems of superconductivity-2025»** will be held in an on-site format in the Hotel Izmailovo «Beta» **from September 28 to October 4, 2025**.

PREFACE

The conference **«Fundamental Problems of High Temperature Superconductivity-2025»** (FPS'25), is the 6th conference in row, organized by the P.N. Lebedev Physical Institute.

The years preceding FPS'25 were extremely impressive and fruitful for this field due to the discovery 10 years ago of hydrogen sulfide superconductivity with a record critical T_c value 203 K, with impressive achievements in the interfacial superconductivity, including $LaAlO_3$ / $SrTiO_3$ interface and FeSe monolayers on the $SrTiO_3$, and with the emergence of very interesting physics of the topologically non-trivial materials, including the topological superconductivity. In the fall of 2016, the HTS-community commemorated the 100th birthday of Vitaly Ginzburg, a Nobel laureate, great scientist and a great enthusiast of the High temperature superconductivity. Subsequent conferences after FPS'15 have been postponed due to the pandemic and other unforeseen events that prevented the meeting of participants from different regions and countries.

The discovery of the high-temperature superconductivity in the whole class of binary and ternary polyhydrides (whose T_c reaches now 260 K) is important not only due to their record high T_c value. More importantly, it has breathed new life into the conventional electron-phonon pairing, already revitalizing with the discovery of MgB_2. This finding and subsequent experiments give reason for hoping that superconductivity can even occur at room temperature and at ambient pressure. Also, this discovery opens up routes and encourages researchers for designing new superconducting materials capable for practical applications.

Despite the almost 40-year history of HTSC in cuprates, their extremely complex physics continues to pose a challenge to researchers. Magnetism, which has traditionally been viewed as the antagonist of superconductivity, has recently introduced new physics in superconductors with magnetic ordering of atoms. Another new twist in research promises combinations of topological properties and superconductivity, either in a single material or in layered structures.

On the practical application side, new iron-based supersonductors and (Cu,C)-1234 HTSC materials obtain a good chance to become successors of REBCO, Nb_3Sn

and NbTi wires, due to their superior performance and a simpler manufacturing technology.

The FPS Conference considers complexity and promise of the novel materials, and causes the scientific community to more freely share the ideas and results in the field of superconductivity. It became a tradition to publish selected FPS'15 papers collection in the Journal Superconductivity and Novel Magnetism (Springer). This FPS'25 conference is no exception to this tradition. We will be delighted to have received contributions from the leading researchers in the field.

The main topics of the FPS'25 conference are as follows:

- **(M)** Fundamentals of high temperature superconductivity (mechanisms, pairing symmetry, etc);
- **(RTS)** Superconductivity at high pressures. Routes to «room» temperature superconductivity at atmospheric pressure;
- **(SQ)** Properties of superconductors and quantum/topological materials;
- **(SM)** Superconductivity and magnetism;
- **(A)** Applied superconductivity.

We welcome all participants of FPS'25, wish them creative success and look forward to new discoveries!

Michael Sadovskii *(Institute of Electrophysics, RAS, Ekaterinburg, Russia)*
Vladimir Pudalov *(P.N. Lebedev Physical Institute, RAS, Moscow, Russia)*
Co-Chairs, Program Committee

ORGANIZERS

ФИАН
1934 2024

Physical Sciences Division RAS

POCATOM

Program Committee

Co-chair

Vladimir M. Pudalov
P.N. Lebedev Physical Institute RAS
Russia

Co-chair

Michael V. Sadovskii
Institute of Electrophysics RAS
Russia

Scientific Secretary

Tatiana E. Kuzmicheva
P.N. Lebedev Physical Institute RAS
Russia

Iman N. Askerzade
Ankara University &
Institute of Physics AAS
Turkey / Azerbaijan

Igor S. Burmistrov
Landau Institute of Theor.
Physics RAS
Russia

Alexander I. Buzdin
University of Bordeaux
France

Evgueni V. Chulkov
Donostia International
Physics Center
Spain

Ali Gencer
Ankara University
Turkey

Vadim A. Grinenko
Tsung-Dao Lee Institute
China

Maxim M. Korshunov
Kirensky Institute of Physics
RAS
Russia

Alexander S. Mel'nikov
Moscow Institute for Physics
and Technology & Institute
for Physics of
Microstructures RAS | Russia

Igor A. Nekrasov
Institute of Electrophysics
RAS
Russia

Sergey G. Ovchinnikov
Kirensky Institute of
Physics RAS
Russia

Alexander L. Rakhmanov
Institute of Theor. and
Applied Electrodynamics,
RAS | Russia

Dmitrii V. Semenok
Center for High Pressure
Science and Technology
Advanced Research | China

Viktor V. Struzhkin
Shanghai Advanced Research in Physical Sciences | China

Valery V. Valkov
Kirensky Institute of Physics RAS
Russia

Vitaly S. Vysotsky
Russian Scientific R&D Cable Institute
Russia

Evgeny P. Krasnoperov
NRC "Kurchatov Institute"
Russia

Grigory N. Gol'tsman
Moscow State Pedagogical University
Russia

Organizing Committee

Chairman

Andrey V. Sadakov

Vice Chairman

Alena Yu. Levakhova

Organizing Secretary

Leonid A. Morgun

Andrey E. Borisov

Georgy V. Rybal'chenko

Ginzburg Centre.
LPI RAS

GINZBURG CENTER

(M) FUNDAMENTALS OF HIGH TEMPERATURE SUPERCONDUCTIVITY (MECHANISMS, PAIRING SYMMETRY, ETC)

Plenary

Invited

Oral

Posters

(RTS) SUPERCONDUCTIVITY AT HIGH PRESSURES. ROUTES TO «ROOM» TEMPERATURE SUPERCONDUCTIVITY AT ATMOSPHERIC PRESSURE

Plenary

Invited

Oral

(SQ) PROPERTIES OF SUPERCONDUCTORS AND QUANTUM/TOPOLOGICAL MATERIALS

Plenary

Invited

Oral

Posters

(SM) SUPERCONDUCTIVITY AND MAGNETISM

Invited

Oral

Posters

(A) APPLIED SUPERCONDUCTIVITY

Plenary

Invited

Oral

Posters

(M) FUNDAMENTALS OF HIGH TEMPERATURE SUPERCONDUCTIVITY (MECHANISMS, PAIRING SYMMETRY, ETC)

Plenary

A universal low-temperature fluctuation of unconventional superconductors revealed

Anthony Hegg, Ruoshi Jiang, Jie Wang, Jinning Hou,
Tao Zeng, Yucel Yildirim, Wei Ku

Tsung-Dao Lee Institute & School of Physics and Astronomy, Shanghai Jiao Tong University, Shanghai 200240, China,
Department of Materials Science and Metallurgy, University of Cambridge, Cambridge CB3 0FS, United Kingdom,
Department of Energy Systems Engineering, Bilgi University, Istanbul 34060, Turkey,
Key Laboratory of Artificial Structures and Quantum Control (Ministry of Education), Shanghai 200240, China,
Shanghai Branch, Hefei National Laboratory, Shanghai 201315, China

Unconventional superconductivity remains an unsolved mystery since its inception several decades ago. The low-temperature superfluid density in these materials is the key property that illuminates the correct quantum theory while eliminating others. Based on data from almost 20 families of bulk $3D$ superconductors, we identify a universal T^3 reduction of the superfluid density that rules out all previously proposed theories of superflow. We then develop a Galilean consistent theory for bosonic superfluidity that generically reproduces this T^3 depletion. This result leaves charged superfluidity of emergent bosons as the only known explanation for superconductivity in these materials.

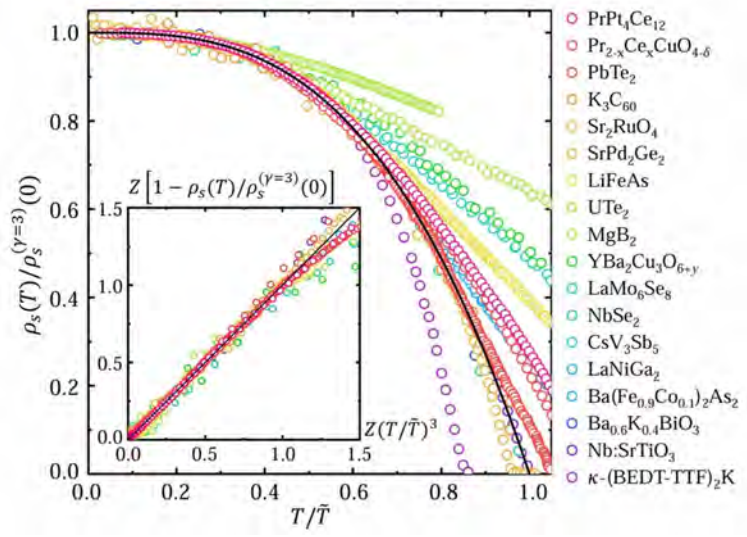

Low-temperature thermal fluctuations offer an essential window in characterizing the true nature of a quantum state of matter, a quintessential example being Fermi liquid theory. In the long-standing pursuit toward a fundamental understanding of unconventional superconductivity, the most essential low-temperature thermal fluctuation of superfluidity has unfortunately been greatly overlooked. Here, we examine the leading thermal fluctuation of the superfluid density across numerous families ranging from relatively conventional to highly unconventional superconductors (MgB_2, bismuthates, doped buckyballs, heavy fermions, UTe_2, doped $SrTiO_3$, Chevrel clusters, intermetallics, κ-organics, transition metal dichalcogenides, ruthenates, iron-pnictides, cuprates, and kagome metals). Amazingly, in all of them an unprecedented universal T^3 depletion materializes in the low-temperature superfluid density, even in the believed-to-be-conventional MgB_2. This reveals a new quantum superfluid state of matter and requires a necessary change of paradigm in describing modern superconductors. We demonstrate that such unorthodox yet generic behavior can be described by a Galilean invariant theory of bosonic superfluidity hosting a long-lived `true condensate'.

Unconventional superconductivity in low density electron systems and conventional superconductivity in metallic hydrogen and hydrogen metallic alloys

M.Yu. Kagan

P.L. Kapitza Institute for Physical Problems, Moscow, Russia

We consider different mechanisms of anomalous superconductivity in the variety of low density electron systems ranging from Kohn-Luttinger mechanism of SC in purely repulsive systems (described by Fermi gas, Hubbard and shubin-Vonsovsky models) and Frohlich mechanism of the acoustic plasmon exchange in RPA approximation for the two-band metals till spin-exchange mechanism for the high T_c cuprates in the framework of the t-J model.

We apply the obtained results for quantum gases, superfluid He-3 and He-3-He-4 mixtures, high-T_c, heavy fermion and iron based superconductors, monolayer and bilayer graphene etc.

We discuss BCS-BEC crossover between extended Cooper pairs and compact (local) pairs in quantum gases and superconductors.

We analize formation of the order parameter droplets in the 2D Hubbard model with strong on-site attraction in the presence of strong disorder.

We also advocate local pair formation and superconductivity in bismuth oxides BaKBiO within the scenario of space-separated Fermi-Bose mixture.

In the end of the talk we return back to the famous Eliashberg mechanism of superconductivity and calculate the critical temperatures (revealing also their non-trivial pressue dependence) in metallic hydrogen and different hydrogen metallic alloys.

We present an estimate for the lifetime and discuss interesting properties of different metastable phases of metallic hydrogen including highly anisotropic fillamentous phase with proton chains embedded in 3D electron Fermi liquid.

We reveal important analogies between the vibrational spectrum of this phase and vortex crystals in rotating superfluid helium.

Developing Ashcroft ideas, we propose a scenario with the formation of two Bose condensates in fillamentous and planar phases of metallic hydrogen with Cooper pairs in electron subsystem and bi-proton pairs on one or neighboring chains or planes in ionic subsystem.

References

1. *M.Yu. Kagan, M.M. Korovushkin, V.A. Mitskan*, Physics Uspekhi, **58**, 733-761 (2015).
2. *M.Yu. Kagan, M.M. Korovushkin, V.A. Mitskan, K.I. Kugel, A.L. Rakhmanov, A.V. Rozhkov, A.O. Sboychakov*, JETP Letters, **121**, 749 (2025).
3. *V.M. Silkin, D.V. Efremov, M.Yu. Kagan*, Physica Scripta, **100**, 045943 (2025). Open access.
4. *M.Yu. Kagan, E.A. Mazur*, ZHETP, **159**, 696 (2021).

5. *A.P. Menushenkov, A.V. Kuznetsov, K.V. Klementiev, M.Yu. Kagan*. Journ. Supercond. Nov. Magn., **29**, 701-705 (2016).
6. *M.Yu. Kagan, E.A. Mazur, R.Sh. Ikhsanov, I.A. Kovalev, A.V. Krasavin*, JETP, **166**, N 1 (7), 89-97 (2024).
7. *M.Yu. Kagan*, Modern Trends in Superconductivity and Superfluidity. Lecture Notes in Physics, vol. 874. (Springer, Dodrecht, 2013). – 550 pages.
8. *M.Yu. Kagan, K.I. Kugel, A.L. Rakhmanov, A.O. Sboychakov*, Electronic Phase Separation in Magnetic and Superconducting Materials. Recent advances, Springer Series in Solid-State Sciences, vol. 201, (Springer International Publishing, 2024). – 379 pages.

Impurity effect on an unconventional superconducting state in iron-based materials

M.M. Korshunov, Yu.N. Togushova, V.A. Shestakov

Kirensky Institute of Physics, Federal Research Center KSC SB RAS, 660036 Krasnoyarsk, Russia,
Siberian Federal University, 660041 Krasnoyarsk, Russia

Disorder can result in interesting and unexpected effects in unconventional superconductors having other than the usual uniform *s*-wave gap symmetry. Random-phase approximation spin fluctuation approach applied to the iron-based superconductors gives the sign-changing $s_{\pm}$ state as the main instability. The state got experimental support from neutron scattering and Andreev reflection measurements. Here we focus on the role of the nonmagnetic disorder that leads to the change in the gap structure from the $s_{\pm}$ to the sign-preserving s_{++} state within the multiband Eliashberg theory for a two-band model of Fe-based systems.

Disorder – impurities and defects violating an ideal order – is always present in solids. It can result in interesting and unexpected effects in unconventional superconductors having other than the usual uniform *s*-wave gap symmetry. Discovery of superconductivity in iron pnictides in 2008 boosted an interest in multiband systems [1]. The ideas appeared some time ago in application for MgB_2 [2] got a new life for iron-based superconductors [3]. Different presently discussed mechanisms of Cooper pairs formation result in the distinct superconducting gap symmetry and structure. In particular, the random-phase approximation spin fluctuation approach in the clean limit gives the extended *s*-wave gap that changes sign between hole and electron Fermi surface sheets – the so-called $s_{\pm}$ state – as the main instability for the wide range of doping concentrations [4]. The state got experimental support from neutron scattering [1], quasiparticle interference imaging [5], and Andreev reflection measurements [6]. A remarkable property giving prominence to iron based superconductors amongst a huge family of unconventional superconductors is their robustness to the suppression of superconductivity via nonmagnetic impurities. This property is associated with the possibility of changing structure of a superconducting order parameter upon the addition of nonmagnetic impurities [7]. The change of the order parameter structure is seen as the transition from the $s_{\pm}$ state to the state with s_{++} sign-preserving gap function [8]. The possibility of the experimental observation of this transition may be provided by the considering the London's penetration depth for a superconductor with nonmagnetic disorder [9] and there are at least two independent groups claiming the experimental observation of it [10, 11]. The transition is significantly affected by the strength of an impurity potential: for a weak scattering potential in the Born limit, the transition is characterized by the abrupt change of the gap function while for stronger potentials it is smooth with one of the gaps going through zero. In the unitary limit of strong scattering impurity potential, the multiband analogue of the Anderson's theorem is

held, and the transition is absent. To study thermodynamical properties of the disorder-induced transition between $s_{\pm}$ and s_{++} superconducting gaps, we calculate the difference $\Delta\Omega$ between the grand thermodynamic potentials in the normal and the superconducting states. The nonmagnetic disorder is considered within the multiband Eliashberg theory for a two-band model of Fe-based systems. Based on the $\Delta\Omega$ calculations, phase diagram is plotted representing the energetically favourable $s_{\pm}$ and s_{++} states and the transition between them. At finite temperature, a first order phase transition line in the vicinity of the Born limit is limited by a critical end point. Above that point, the sharp $s_{\pm}$ to s_{++} transition transforms to a crossover between $s_{\pm}$ and s_{++} states [12].

The study was supported by the Russian Science Foundation grant N 25-22-20043, https://rscf.ru/project/25-22-20043/, grant of the Krasnoyarsk Regional Science Foundation.

References

1. *Hirschfeld P.J., Korshunov M.M., Mazin I.I.* Rep. Prog. Phys. **74**, 124508 (2011).
2. *Golubov A.A., Mazin I.I.* Physica C **243**, 153 (1995).
3. *Mazin I.I., Singh D.J., Johannes M.D., Du M.H.* Phys. Rev. Lett. **101**, 057003 (2008).
4. *Korshunov M.M.* Phys.-Usp. **57**, 813 (2014).
5. *Hirschfeld P.J.* C. R. Phys. **17**, 197 (2016).
6. *Korshunov M.M., Kuzmichev S.A., Kuzmicheva T.E.* Materials **15**, 6120 (2022).
7. *Korshunov M.M., Togushova Y.N., Dolgov O.V.* Phys.-Usp. **59**, 1211 (2016).
8. *Efremov D.V., Korshunov M.M., Dolgov O.V., Golubov A.A., Hirschfeld P.J.* Phys. Rev. B **84**, 180512 (2011).
9. *Shestakov V.A., Korshunov M.M., Togushova Y.N., Dolgov O.V.* Supercond. Sci. Technol. **34**, 075008 (2021).
10. *Schilling M.B. et al.* Phys. Rev. B **93**, 174515 (2016).
11. *Ghigo G., Torsello D., Ummarino G.A., Gozzelino L., Tanatar M.A., Prozorov R., Canfield P.C.* Phys. Rev. Lett. **121**, 107001 (2018).
12. *Shestakov V.A., Korshunov M.M.* Supercond. Sci. Technol. **38**, 055002 (2025).

Upper limit for superconducting transition temperature in electron – phonon superconductors: very strong coupling

M.V. Sadovskii

Institute for Electrophysics, Russian Academy of Sciences,
Ural Branch, Amundsen str. 106, Ekaterinburg 620016, Russia

We present a brief review of some recent works introducing an upper limit for superconducting transition temperature with the emphasis on the very strong coupling limit of Eliashberg – McMillan theory.

We present a critical analysis of some recent attempts to introduce an upper limit for superconducting transition temperature [1–8]. This can be done for different models, starting from the simplest possible jellium model for metallic hydrogen [2], leading to rather pessimistic results, through purely dimensional analysis [3], and up to the results for the very strong coupling limit of Eliashberg – McMillan theory for electron – phonon superconductors, leading to the possibility of room – temperature superconductivity [4–8].

References

1. *I. Esterlis, S.A. Kivelson, D.J. Scalapino*, Quantum Materials **3**, 59 (2018).
2. *D. van der Marel, C. Berthod*, Newton **1**, 100002 (2025).
3. *K. Trachenko, D. Montserrat, M. Hutcheon, C.J. Pickard*, ArXiv: 2406.08129.
4. *P.B. Allen, R.C. Dynes*, Phys. Rev. **12**, 905 (1975).
5. *M.V. Sadovskii*, Physics – Uspekhi **65**, 724 (2022).
6. *E.G. Maksimov*, Physics – Uspekhi **51**, 567 (2008).
7. *D.V. Semenok, B.L. Altshuler, E.A. Yuzbashyan*, ArXiv: 2407.12922.
8. *M.V. Sadovskii*, JETP Letters **120**, 205 (2024).

Invited

Numerical evidence of pair density wave superconductivity in strongly correlated systems

Yi-Fan Jiang

School of Physical Science and Technology, ShanghaiTech University

Pair-density-wave (PDW) is a long-sought exotic state with oscillating superconducting order without external magnetic field. So far it has been rare in establishing a 2D microscopic model with PDW long-range order in its ground state. In this talk, we will discuss our recent works about the emergence of PDW in two strongly correlated models. By performing a state-of-the-art density-matrix renormalization group (DMRG) simulation, we show that PDW ordering established in the ground state of a minimal model of spinless fermions on the honeycomb lattice with density interaction. Remarkably this PDW state persists on the wider cylinder with 2D-like Fermi surfaces (FS), which provided probably the first controlled numerical evidence of PDW in systems with 2D-like FS. The evidence of PDW is also observed in our recent DMRG study of the Hubbard model on wide diagonal square lattice. We will discuss the exotic states, such as infinite-length stripes, holon Wigner crystal, and incommensurate PDW, found in the spinful model on the new sort of diagonal lattice geometry.

References

1. *Y.F. Jiang, H. Yao*, PRL **133** (17), 176501 (2024). Editors' Suggestion.
2. *S.K. Jian, Y.F. Jiang, H. Yao*, PRL **114** (23), 237001 (2015). Editors' Suggestion.
3. *Z. Xu, G.X. Liu, Y.F. Jiang*, arXiv: 2409.18833.

Electronic structure, orbital-selective renormalizations, and magnetic correlations in nickelate superconductors

I.V. Leonov

M.N. Mikheev Institute of Metal Physics, Russian Academy of Sciences, 620108 Yekaterinburg, Russia

The discovery of superconductivity in bulk Ruddlesden-Popper phases of $La_{n+1}Ni_nO_{3n+1}$ (LNO) with $n = 2$ (bilayer, $Ni^{2.5+}$) and $n = 3$ (trilayer, $Ni^{2.67+}$) with T_c comparable to that in cuprates, ~80 K (for $n = 2$) and 20-40 K ($n = 3$), opens up a new route to design high-T_c materials. Here, we discuss the effects of electron corrections, chemical doping and pressure on the electronic structure and magnetic properties of these systems. Using *ab initio* band structure and DFT+dynamical mean-field theory methods we show the proximity of the Ni 3*d* states in LNO to orbital-dependent localization, complicated by strong spin and charge correlations. We propose that spin and charge stripe fluctuations play an important role to tune superconductivity in LNO.

The discovery of unconventional superconductivity in hole-doped infinite-layer nickelate thin films $RNiO_2$ (R = Sr, Ca, REE) with a nominal low-valence Ni^+ state below $T_c \sim 15$ K has stimulated intensive experimental and theoretical efforts to understand the unusual properties of this novel class of superconducting materials [1, 2]. More recently, it has been demonstrated that under pressure bulk single- and polycrystalline Ruddlesden-Popper phases of $La_{n+1}Ni_nO_{3n+1}$ (LNO) with n=2 (bilayer, $Ni^{2.5+}$) and n=3 (trilayer, $Ni^{2.67+}$) exhibit superconductivity (SC) with a high transition temperature, comparable to that in cuprates, ~80 K (for n=2) and 20-40 K (n=3), opening up a new route to high-T_c SC [3, 4]. Here, we discuss the effects of electron corrections, chemical doping and pressure on the normal state electronic structure, orbital-dependent quasiparticle renormalzations, Fermi surface, and magnetic properties of the bilayer and trilayer RP LNO [5-7]. Using *ab initio* band structure and DFT+dynamical mean-field theory (DFT+DMFT) methods we show significant orbital-dependent quasiparticle renormalizations of the Ni x^2-y^2 and $3z^2-r^2$ orbital states, in agreement with experimental estimates. Our results for the $\boldsymbol{k}$-dependent spectral functions and Fermi surfaces reveal significant incoherence of the Ni $3z^2-r^2$ states, implying the proximity of the Ni 3*d* states to orbital-dependent localization. Our analysis of the static magnetic susceptibility evaluated within DFT+DMFT suggests the possible formation of the spin and charge (or bond) density wave stripe states in LNO, implying strong spin and charge correlations. We propose that spin and charge stripe fluctuations play an important role to tune superconductivity in LNO under pressure. Superconductivity in LNO seems to be associated with the suppression of spin and charge density wave stripe ordering under pressure, which leads to a sharp increase of spin fluctuations.

References

1. *D. Li et al.*, Nature (London) **572**, 624 (2019).
2. *M. Osada et al.*, Adv. Mater. **33**, 2104083 (2021).
3. *H. Sun et al.*, Nature **621**, 493 (2023).
4. *Y. Zhang et al.*, Nat. Phys. **20**, 1269 (2024).
5. *D.A. Shilenko, I.V. Leonov*, Phys. Rev. B **108**, 125105 (2023).
6. *I.V. Leonov*, Phys. Rev. B **109**, 235123 (2024).
7. *I.V. Leonov*, arXiv: 2410.15298.

Nonlocal superconducting pairing at interfaces of hybrid structures: new directions for engineering of the type of Cooper pairs

A.S. Mel'nikov, A.A. Kopasov, D. Annenkov

Moscow Institute of Physics and Technology, Dolgoprudnyi, Moscow Region 141701, Russia,
Institute for Physics of Microstructures, Russian Academy of Sciences, 603950 Nizhny Novgorod, GSP-105, Russia,
National University of Science and Technology «MISIS», Moscow 119049, Russia

Proximity phenomena and induced superconducting correlations in heterostructures are shown to be strongly affected by the nonlocal nature of the electronic attraction. The latter can trigger the formation of Cooper pairs consisting of electrons localized in neighboring layers even in the absence of direct quasiparticle transfer between the layers. We investigate the manifestations of such nonlocal pairing and resulting unconventional induced superconductivity in several exemplary layered systems in the presence of the energy band offset. The band offset is shown to induce the odd-frequency superconducting correlations, affect the phase diagram and the magnetic response of the system. The model of interlayer pairing and results of calculations are discussed in the context of possible explanation of recent experimental data on the interplay between ferroelectricity and superconductivity in van der Waals bilayers.

The mechanism of the interlayer superconducting pairing across the interface has been first addresses in 60s in the pioneering work by M.H. Cohen and D.H. Douglass [1]. Later the scenario of interlayer pairing has been discussed by A.I. Larkin and K.B. Efetov [2] to explain the extremely high upper critical fields in TaS_2 (pyridine) which were shown to exceed the paramagnetic limit. An important property of such interlayer pairing is that due to the nonlocality of the Cooper pair wave function (or more rigorously, the anomalous Green function) the Pauli principle doesn't impose severe restrictions on the spins of electrons in the pair which usually hamper the formation of triplet superconducting correlations. These theoretical considerations of the interlayer pairing have been further developed in the context of extensive studies of superconductivity in cuprates which also can be well described by the model of identical superconducting layers.

All the above theoretical works were devoted to the study of natural layered compounds and, thus, assumed the coinciding electronic structure of the individual layers. We revisit the problem of nonlocal interlayer pairing focusing on its effect on the properties of different types of superconducting hybrid structures. The difference between the electronic spectra in neighboring layers can produce the effect similar to the effect of the momentum dependent exchange field on Cooper pairing. The resulting superconducting state can reveal all the features typical for the systems with odd-frequency superconducting correlations such as unusual phase diagram, inhomogeneous superconducting order parameter and paramagnetic contribution to the supercurrent. The interest to these issues is also stimulated by recent progress in the study of superconductivity in van der Waals heterostructures which reveal the

interplay between ferroelectric and superconducting orderings [3]. Besides combining different materials in a hybrid structure, even for identical layers in a stack the band structure is highly sensitive to a relative layer twist and can be also controlled by an external electric field. Such modifications of the electronic spectrum provide the way for electrostatic control of the superconducting state. The ferroelectric domain walls in such structures can cause the formation of localized domain wall superconductivity with the critical temperature exceeding the one inside the domains.

Our analysis of the interlayer pairing includes the study of unusual magnetic response, disorder effects, phase diagrams for different band offsets, interlayer tunneling rates and external magnetic fields. Experimental evidence for the above nonlocal interface pairing would provide new perspectives in engineering the unconventional superconducting correlations in heterostructures including topologically nontrivial superconducting states.

This work was supported by the Russian Science Foundation (Grant No. 25-12-00042).

References

1. *M.H. Cohen and D.H. Douglass*, Phys. Rev. Lett. **19**, 118 (1967).
2. *K.B. Efetov and A.I. Larkin*, Zh. Eksp. Teor. Fiz. **68**, 155 (1975) [Sov. Phys. JETP **41**, 76 (1975)].
3. *A. Jindal, et al*., Nature (London) **613**, 48 (2023).

Effects of mean field and fluctuations in HTSC cuprates

S.G. Ovchinnikov[1,2], S.V. Nikolaev[2,1], V.I. Kuzmin[1],
M.M. Korshunov[1,2], E.I. Shneyder[1]

Kirensky Institute of Physics,
[1] Federal Research Center,
[2] Siberian Federal University, Krasnoyarsk

We will discuss mean field and fluctuations in cuprates. Within the generalized tight binding (GTB) approach in combination with the density function theory (LDA+GTB) within account the strong electron correlations and electron-phonon interaction we have calculated doping dependent electronic structure and constructed mean field theory of superconductivity with singlet $d_{x^2-y^2}$ pairing symmetry. This theory correctly reproduce doping dependence $T_c(x)$, $d_{x^2-y^2}$ pairing results from both magnetic and phonon contributions. Moreover this theory gives correct doping dependence of the isotope effect with minimum at optimal doping. It occurs that such mean field theory does not describe concentration dependence of the electronic structure, ARPES data and the Fermi surface. To get agreement with experimental data we have to consider fluctuations of the local magnetic order. We have developed cluster perturbation theory (CPT) with a periodic covering of the lattice by square $N\times N$ clusters. Exact diagonalization of the intracluster Hamiltonian gives us a set of the multielectron eigenstates that is used to construct the Hubbard X-operators for the given cluster. Hopping between clusters treated in the Hubbard I mean field type approximation.

For N=4 this approach results in the exact treatment of local correlations up to 9-th neighbours. We have obtained the pseudogap states and its concentration dependence. To describe dynamics of the charge and spin fluctuations we have developed cluster perturbation theory for two-particle Green functions. We have shown that pseudogap states are formed by fluctuations of the short range magnetic order.

Competition of polaronic and bipolaronic effects in the normal state of an electron-correlated system

E.I. Shneyder, S.V. Nikolaev, A.V. Dudarev,
M.V. Zotova, S.G. Ovchinnikov

Kirensky Institute of Physics, Federal Research Center KSC SB RAS, Krasnoyarsk, Russia,
Siberian Federal University, Krasnoyarsk, Russia,
Reshetnev Siberian State University of Science and Technology, 660037, Krasnoyarsk, Russia

Polaron effects in the properties of the normal state of systems with strong electron correlations and strong electron-phonon interactions are considered based on a model relevant to high-temperature copper oxides superconductors. It is shown that in the limit of strong Coulomb interaction, a competition of polaron and bipolaron effects arises, which forms the distinctive features of the normal state of the system.

The rich phase diagram of high-temperature superconductors (HTSC) is formed against the background of competing electron–electron and electron–phonon interactions. Therefore, it is of particular interest to study a realistic model of an HTSC system with simultaneously strong Coulomb and electron–lattice interactions in a wide range of parameters of the electronic and phonon subsystems. Here, the multiband two-dimensional pd-model is considered, extended to include lattice contributions coming from the modulation of both the on-site energy of electrons and their hopping parameter. Within the framework of the polaronic version of the generalized tight-binding method [1], the evolution of the electron band structure is determined with changes in the strength of the electron-lattice coupling and doping [2]. Using the Lang-Firsov transformation, we demonstrate that the distinctive features of the band structure, i.e. the Fermi surface and the density of states, are directly related to the competition of polaronic and bipolaronic transformations in the system [3]. To study the polaronic effects in the exchange interaction process, we use the technique of projection operators [4, 5] and obtain an analytical expression for the effective exchange parameter. It turns out that in the limit of strong electron correlations, strong electron-phonon interaction controls changes in the effective superexchange interaction and, as a consequence, the evolution of the pseudogap characteristics of the system.

The research was carried out within the state assignment of the Kirensky Institute of Physics.

Support by Russian Science Foundation (RSF project No. 24-12-00044) is acknowledged.

References

1. *I.A. Makarov, E.I. Shneyder, P.A. Kozlov, and S.G. Ovchinnikov*, Phys. Rev. B **92**, 155143 (2015).
2. *E.I. Shneyder, M.V. Zotova, A.V. Dudarev et al*., https://doi.org/10.48550/arXiv.2503.06018 (2025).
3. *E.I. Shneyder, S.V. Nikolaev, M.V. Zotova et al*., Phys. Rev. B **101**, 235114 (2020).
4. *K.A. Chao, J. Spalek and A.M. Oles*, J. Phys. C: Solid State Phys. **10,** L271 (1977).
5. *V.A. Gavrichkov, S.I. Polukeev and S.G. Ovchinnikov*, Phys. Rev. B **95**, 144424 (2017).

Odd frequency spin-triplet pairing in disordered electron liquid

V.A. Zyuzin, A.M. Finkel'stein

Landau Institute for Theoretical Physics

We studied a mechanism of spin-triplet odd-frequency superconducting pairing between electrons in strongly disordered conductors [1]. We showed that mixing the conventional superconducting fluctuations above the transition temperature or critical magnetic field together with the spin part of repulsive Coulomb interaction results in an effective interaction which mediates the s-wave spin-triplet odd-frequency pairing in the particle-particle (Cooper) channel. Diffusion processes such as diffusions and Cooperons lead to the pronounced frequency dependence of the effective interaction required for this type of pairing. Therefore, regular spin-singlet superconducting state in strongly disordered films may be accompanied by an intermediate phase characterized by spin-triplet odd-frequency pairing between electrons. We showed that the transition into this phase may occur through the first order phase transition. Therefore, domains with different spin projections of the spin-triplet order parameter are expected to occur. We argue that the spin-triplet odd-frequency paired phase corresponds to the insulating state experimentally found in highly disordered films of InO ([2] and many more) and TiN. These materials show a superconductor to insulator transition as a function of the magnetic field when the superconductivity is suppressed. At even higher magnetic fields a reentrance into a highly resistive conducting state occurs. The insulating state is experimentally found to show 2e-Little-Parks oscillations suggesting the existence of a phase coherence in it. Our suggested picture for the description of such an exotic insulating behavior is as follows: domains with different spin polarization of the spin-triplet odd-frequency pairing block the supercurrent, while phase coherence still results in the 2e-Little-Parks oscillations. Absence of a bulk supercurrent makes the system to be an insulator (a sort of super-insulator) at low temperatures.

References

1. *V.A. Zyuzin and A.M. Finkel'stein*, Phys. Rev. B **105**, 214523 (2022);
2. *V.F. Gantmakher, M.V. Golubkov, V.T. Dolgopolov, G.E. Tsydynzhapov, and A.A. Shashkin*, JETP Lett. **68**, 363 (1998).
3. *D. Gurovich, K.S. Tikhonov, D. Mahalu, and D. Shahar*, Phys. Rev. B **91**, 174505 (2015).

Oral

Higher-order condensates in multicomponent superconductors

Vadim Grinenko

Tsung-Dao Lee Institute, Shanghai Jiao Tong University, Shanghai

The muon-spin-rotation (μSR) experiments and the observation of a spontaneous Nernst effect indicate time-reversal symmetry breaking (BTRS) above the superconducting transition temperature T_c in $Ba_{1-x}K_xFe_2As_2$ at x ~ 0.8. Combined theoretical and experimental studies have pointed out that this BTRS state is caused by the formation of a new state of matter associated with the condensation of pairs of electron pairs. In this talk, I will summarise experimental observations supporting the appearance of a quartic metallic state and multicomponent superconductivity from incoherent Cooper pairs in the narrow doping range. I will present new experimental data, including spectroscopic evidence for pseudogap and ultrasound experiments that support multicomponent superconductivity in this compound.

When fermions form pairs in a condensed matter system, new states of matter, such as a superconductor, emerge. For more than 100 years, experimental and theoretical research has proven that the problem of electronic pair condensates is one of the most profound problems in physics. For example, it is attested by the large number of Nobel prizes awarded to this topic and its generalizations in adjacent fields. The theoretical description of superconductivity broadly relies on mean-field approximations. However, many researchers believe that the mean-field theories are insufficient to describe high-temperature superconductivity consistently. In this talk, I will present our recent experimental observation of unprecedented effects in the $Ba_{1-x}K_xFe_2As_2$ system, which goes beyond the predictions of mean-field theories. The superconducting state of this system at a high doping level breaks time-reversal symmetry [1, 2]. Besides superconducting pairing, the $Ba_{1-x}K_xFe_2As_2$ system allows the formation of an electron quadrupling state above the superconducting critical temperature T_c [3]. At low temperatures, this state is a new kind of superconducting state that is characterized by multicomponent imaginary order parameters associated with electrons residing within different bands. As a result, this state breaks U(1) gauge and Z_2 time-reversal symmetries. This yields a plethora of new phenomena revising textbook concepts: the generation of spontaneous magnetic fields [1-3], formation of superconducting domain walls [5], Abricosov (full quants) vortex splitting to fractional flux vortices [5-7], formation of CP_2-Skyrmions [5] and the fluctuation driven fermionic quadrupling condensate above superconducting critical temperature [3,4,8,9]. These observations are relevant not only for condensed matter physics but also it was proposed that similar phenomena can be found in color superconductivity of dense quark matter [10], and very recently, a related phenomenon was demonstrated in an optical-lattice emulator involving ultracold atoms [11]. Besides that, our observations have a broad application perspective. For example, flux fractionalization enables

base-N computational schemes in fluxonics, and a possible realization of universal topological quantum computations scheme based on general principles that integer charges bound to fractional flux in bulk superconductors are anyons [12].

References

1. *V. Grinenko et al*., Phys. Rev. B **95**, 214511 (2017).
2. *V. Grinenko et al*., Nat. Phys. **16**, 789–794 (2020).
3. *V. Grinenko et al*., Nat. Phys. **17**, 1254–1259 (2021).
4. *I. Shipulin et al*., Nat. Commun **14**, 6734 (2023).
5. *Y. Zheng, Q. Hu et al*., arXiv: 2407.18610.
6. *Y. Iguchi et al*., Science **380**, 1244-1247(2023).
7. *Q.Z. Zhou et al*., arXiv: 2408.05902.
8. *F. Bärtl et al*., arXiv: 2501.11936.
9. *C. Halcrow et al*., arXiv: 2404.03020.
10. *M. Eto et al*., Prog. Theor. Exp. Phys. 012D01 (2014).
11. *Y.G. Zheng et al.*, Nat. Phys. **21**, 208–213 (2025).
12. *F. Wilczek*, PRL **48** (17), 1144 (1982).

Doping Evolution of Na(Fe,Co)As Superconducting Gap Structure: Influence of Spin Fluctuations

S.A. Kuzmichev[1,2], A.D. Ilina[2], I.A. Nikitchenkov[1,2], I.V. Morozov[3], A.I. Shilov[2], Ye.O. Rakhmanov[2,3], T.E. Kuzmicheva[2]

[1] Lomonosov Moscow State University, Faculty of Physics, 119991, Moscow, Russia,
[2] Lebedev Physical Institute, Russian Academy of Sciences, 119991, Moscow, Russia,
[3] Lomonosov Moscow State University, Department of Chemistry, 119991, Moscow, Russia

Using incoherent multiple Andreev reflection effect (IMARE) spectroscopy, in Na(Fe,Co)As superconducting pnictides we detect an enhance of the *k*-space anisotropy of the superconducting (SC) order parameter in underdoped compositions as compared to overdoped ones. This points to a strong influence of spin fluctuations to the SC order parameter symmetry of Na(Fe,Co)As pnictides.

Alkali-metal Na(Fe,Co)As pnictides show superconductivity even in stoichiometric NaFeAs composition with $T_c \approx 10$ K, that can be increased by electron (Fe,Co) substitution reaching the maximum $T_c \approx 22$ K under optimal doping [1]. In underdoped and stoichiometric compositions, antiferromagnetic (AFM) and nematic phases develop above T_c. Due to the alkali metal, the NaFeAs-family pnictides rapidly degrade in presence of even trace amounts of water vapor and oxygen, thus strongly complicating any experimental probing of its properties.

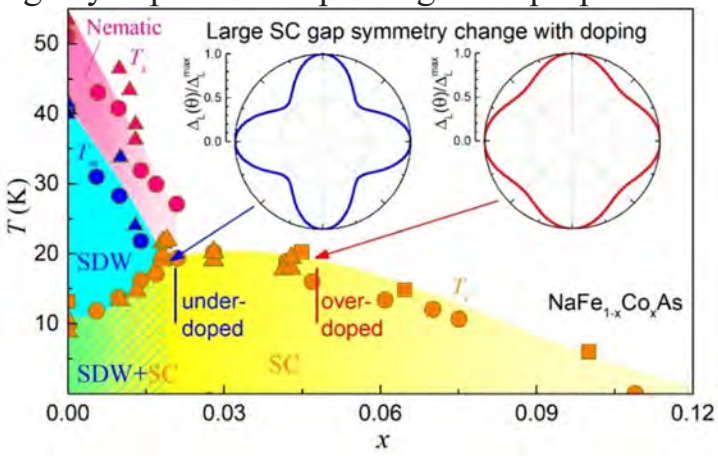

Fig. 1: Electron doping phase diagram of Na(Fe,Co)As pnictides, and a sketched change in the large gap angle distribution in the *k*-space with doping.

Single crystals of alkali metal based superconducting (SC) pnictides (the 111 family) $NaFe_{1-x}Co_xAs$ with x=0.021−0.045 and $T_c \approx 18-20$ K were grown using "self-flux" technique [2-4]. At T=4.2 K, Andreev junctions of SnS-type (*S* – superconductor, *n* – thin normal metal) were formed using planar "break-junction'' technique [5]. Here, we present a comprehensive study of the SC order parameter of $Na(Fe_{1-x}Co_x)As$ single crystals with underdoped (nominal x=0.021) and overdoped (x=0.045) compositions using IMARE spectroscopy of SnS-junctions (direct local probe).

Below T_c, we show a multiple-gap superconductivity and determine the magnitudes and characteristic ratios of the SC order parameters [2-4]. Considering the IMARE data within the classical models [6, 7], we conclude an observation of a moderate *k*-space anisotropy of the large SC gap Δ_L with nodeless extended s-wave symmetry and isotropic small SC gap Δ_S. For the large SC gap, we directly determined its extrema Δ_L^{in} and Δ_L^{out} being the minimum and the maximum Cooper pair coupling energies in dependence of the momentum direction. The SC gap anisotropy is estimated as $A_L \equiv 100$.

Temperature dependences of the SC order parameters $\Delta_L^{out}(T)$, $\Delta_L^{in}(T)$, and $\Delta_S(T)$ directly determined using IMARE spectroscopy are also presented.

The characteristic ratios $2\Delta_L^{out}(0)/k_BT_c \approx 6$ and $2\Delta_S(0)/k_BT_c \approx 1.5{-}2.0$ remain almost unchanged along the studied range of the doping phase diagram. With it, the ratio $2\Delta_L^{in}(0)/k_BT_c$ grows from ≈3.7 in underdoped compositions to ≈4.2 in overdoped ones. The latter corresponds to an increase in the Δ_L anisotropy in the vicinity of the AFM and nematic phases, from $A_L \approx 25\%$ in the overdoped region to ≈40% in the underdoped one with similar $T_c \approx 18$ K [4]. Within the framework of theoretical approach [8], the decrease in the inner SC gap edge (Δ_L^{in}) in underdoped compositions originates from a strengthen of spin fluctuations near the AFM phase. Our results favor the theoretical predictions [8] and indicate a strong influence of spin fluctuations to the SC order parameter symmetry of Na(Fe,Co)As pnictides.

The work is supported by RSF project no. 22-72-10082P.

References

1. *S.A. Kuzmichev, T.E. Kuzmicheva*, JETP Lett. **114**, 630 (2021).
2. *L.A. Morgun, et al*., Materials **16**, 6421 (2023).
3. *S.A. Kuzmichev*, *et al*., Eur. Phys. J. Plus **139**, 74 (2024).
4. *S.A. Kuzmichev*, *et al*., JETP Lett. 117, 612 (2023); **120**, 125 (2024).
5. *S.A. Kuzmichev, T.E. Kuzmicheva*, Low Temp. Phys. **42**, 1008 (2016).
6. *R. Kuemmel*, *et al*., Phys. Rev. B **42**, 3992 (1990).
7. *T.P. Devereaux, P. Fulde*, Phys. Rev. B **47**, 14638 (1993).
8. *T. Saito*, *et al*., Phys. Rev. B **88**, 045115 (2013).

Dynamic spin response within the effective Hubbard model for cuprates

V.I. Kuz'min[1], S.V. Nikolaev[1,2],
M.M. Korshunov[1,2], S.G. Ovchinnikov[1,2]

[1] Kirensky Institute of Physics, Federal Research Center KSC Siberian Branch Russian Academy of Sciences, 660036, Krasnoyarsk, Russia,
[2] Siberian Federal University, 660041, Krasnoyarsk, Russia

Inelastic neutron scattering data on cuprates show that their spin response doping evolution varies from one type of compound to another. We apply cluster perturbation theory to calculate the dynamic spin susceptibility of the effective Hubbard model for cuprates and show that by varying its parameters we can describe qualitatively the differences in the doping dependencies of the spin response in cuprates.

Undoped cuprates are AFM insulators, their spin dynamics correspond to the excitation of magnons and could be described by a linear spin-wave theory. When the delocalized holes are doped into the system, the AFM long-range order quickly disappears, and the spectra become more complicated. Often, the lower downward dispersing and higher upwards dispersing branches of an "hourglass" spectrum are observed. In the underdoped pseudogap region, several types of behavior have been found in different materials [1-3].

We apply the cluster perturbation theory to the effective Hubbard model of cuprates, which has been previously used to investigate the one- and two-particle properties of the Emery model [4], in order to study dependence of the dynamic spin susceptibility on the strength of Coulomb repulsion and the values of the nearest-neighbor hoppings. We demonstrate that by varying paremeters we can produce effects qualitatively similar to experimental features, such as the "hourglass"-like spectrum, or transition from AFM peak to incommensurate peak structure at low energies, as well as four-peak structure rotation with the increasing energy.

References

1. *O. J. Lipscombe et al.*, Phys. Rev. Lett. **102**, 167002 (2009).
2. *V. Hinkov et al*., Nat. Phys. **3**, 780 (2007).
3. *M. Chan et al*., Nat. Commun. **7**, 10819 (2016).
4. *V. I. Kuz'min et al*., Materials **16**, 4640 (2023).

The electronic mechanism for charge carrier pairing in real space in HTSC oxides based on $BaBiO_3$

A.P. Menushenkov

National Research Nuclear University MEPhI

Based on the analysis of the results of the experiment on the study of the time dependence of changes in the local electronic structure of $BaBiO_3$, conducted by us on an X-ray free-electron laser with femtosecond excitation through an optical gape, the substantiation for the electronic nature of the charge carriers pairing in real space, in contrast to the phonon (bipolaron) mechanism, is presented. The causes of the negative Anderson's potential U' are explained. It is shown that the electronic mechanism is primarily due to the local nature of the pairing of electrons and holes on neighboring octahedral complexes in the perovskite lattice, leading to Coulomb attraction between complexes filled with electron and hole pairs.

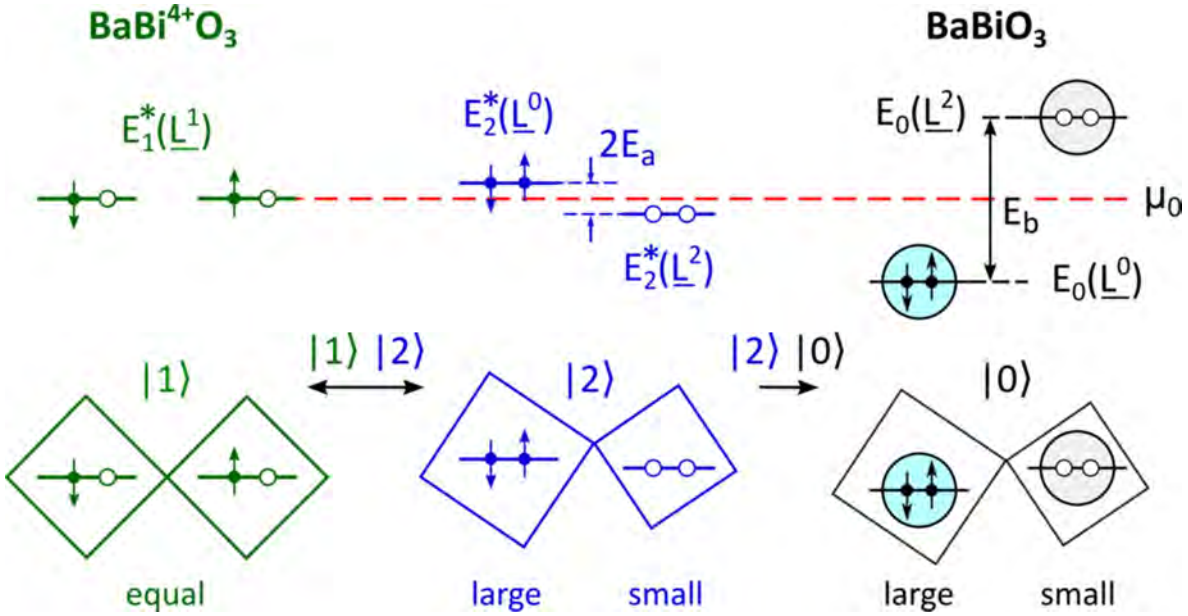

Fig. 1. The mechanism of transformation of the metastable single-particle state of the hypothetical compound $BaBi^{4+}O_3$ into the two-particle ground state of $BaBiO_3$.

Recently, by conducting an experiment on X-ray absorption spectroscopy with time (femtosecond) resolution on an X-ray free-electron laser, we obtained direct evidence of the existence of a paired state of local charge carriers in real space in the parent compound $BaBiO_3$ of the family of high-temperature superconductors (HTSC) (bismuthates) having a perovskite-like structure similar to the structure of cuprate HTSCs [1].

The analysis of the dynamics of the change in the state of the local electronic structure of $BaBiO_3$ after excitation by a resonant laser pulse through an optical gap, carried out in [2], made it possible to explain the mechanism of disproportionation of the Bi6*s*–O2*p*σ*-bond, realized exclusively due to the local pairing of electrons and holes on neighboring octahedral complexes (Fig. 1). As a result, a conclusion was

made about the possibility of an electronic rather than a phonon (bipolaron) mechanism of pairing of charge carriers in bismuthates [2]. The main arguments against implementing the phonon mechanism are the high binding energy of 1.5 eV and the very short pairing time, not exceeding 240 fs, unattainable for the phonon subsystem. In this report, we present additional arguments in favor of the electronic mechanism for charge carrier pairing.

We consider in more detail the two stages of the transition from the single-particle metastable state of the hypothetical compound $BaBi^{4+}O_3$ with a cubic structure, corresponding to the excited state of the system at the end of the first picosecond after excitation, to the ground two-particle state of $BaBiO_3$ with a monoclinically distorted structure and show that the pairing process is described only in the frame of electron-electron interaction.

We discuss the reason for the appearance of the negative Anderson's potential *U*' in bismuthates as a consequence of the emergence of Coulomb attraction between octahedral complexes carrying electron and hole pairs during local pairing of electrons and holes on neighboring octahedra in the perovskite lattice [3].

We show that the Coulomb barrier, which an electron (hole) overcomes at the first stage when moving to a neighboring octahedron, is determined by the lattice deformation energy $2E_a$ from a cubic to a monoclinic-distorted structure. However, the attraction effect *U*' between neighboring octahedral complexes with local pairs of electrons and holes, which occurs at the second stage of pairing, leads to a decrease in the energy of the system by the value of the optical gap $E_G = E_b + 2E_a$, compensates for the energy costs of the first stage and creates the binding energy E_b between local pairs of electrons and holes. Thus, we observe the manifestation of Anderson's concept of the negative potential *U*', caused by the electronic mechanism of pairing of charge carriers, the possibility of the implementation of which in bismuthates was predicted earlier in [4, 5].

References

1. *A.P. Menushenkov, et al*., Phys. Rev. Research **6**, 023307 (2024).
2. *A.P. Menushenkov*, JETP Letters **121**, 562 (2025).
3. *P.W. Anderson*, Phys. Rev. Lett. **34**, 953 (1975).
4. *C.M. Varma*, Phys. Rev. Lett. **61**, 2713 (1988).
5. *A. Taraphder, et al*., Phys. Rev. B **52**, 1368 (1995).

Superconductivity in Jahn-Teller magnets

Alexander Moskvin

Ural Federal University, Ekaterinburg, Russia

The search for new oxide superconductors undertaken by Bednorz and Muller was based on the idea of creating conducting oxides containing Jahn-Teller (JT) ions which are characterized by strong electron-lattice coupling with the formation of polarons whose BCS type pairing or BEC of bipolarons can lead to high-temperature superconductivity (HTSC). This idea is not considered today among the leading mechanisms of HTSC, nevertheless, almost all HTSC or similar exotic superconducting materials known today are JT magnets based on 3*d*- or 4*d*-ions (cuprates La_2CuO_4, nickelates like $RNiO_2$ and $La_3Ni_2O_7$, ferropnictides/chalcogenides, Sr_2RuO_4, RuO_2). In contrast to the idea of Bednorz and Muller, I argue the superconducting prospects of JT magnets are not due to the JT effect, but to their inherent instability with respect to so-called anti-JT-disproportionation.

Jahn-Teller (JT) magnets are compounds based on Jahn-Teller 3*d*- or 4*d*-ions with configurations of the $t_{2g}^{n_1}e_g^{n_2}$ type in a highly symmetrical octahedral, cubic, or tetrahedral environment and with ground state orbital E_g-doublet [1]. These compounds are based on tetra-complexes with the configuration d^1 (Ti^{3+}, V^{4+}), low-spin (LS) configuration d^3 (V^{2+}, Cr^{3+}, Mn^{4+}), and high-spin (HS) configuration d^6 (Fe^{2+}, Co^{3+}), octa-complexes with HS-configuration d^4 (Cr^{2+}, Mn^{3+}, Fe^{4+}, Ru^{4+}), low-spin configuration d^7 (Co^{2+}, Ni^{3+}, Pd^{3+}), as well as octa-complexes with configuration d^9 (Cu^{2+}, Ni^{1+}, Ag^{2+}).

The class of JT magnets includes a large number of promising materials such as manganites $RMnO_3$, ferrates $(Ca,Sr)FeO_3$, ruthenates RuO_2, $(Ca,Sr)RuO_3$, $(Ca,Sr)_2RuO_4$, a wide range of ferropnictides (FePn) and ferrochalcogenides (FeCh), 3D nickelates $RNiO_3$ and $R_3Ni_2O_7$, 3D-cuprate $KCuF_3$, 2D cuprates (La_2CuO_4, …) and nickelates $RNiO_2$, silver-based compounds (AgO, AgF_2) with a rich spectrum of unique properties from various types of magnetic and charge ordering to metal-insulator transitions and superconductivity which are the focus of modern condensed matter physics.

All JT configurations of *d*-ions include one e_g-electron or one e_g-hole over stable, fully or half-filled shells [2]. In this sense, they are similar to the configurations of the numerous family of ions with one n*s*-electron over filled shells, such as the 6*s*-electron in Hg^+, Tl^{2+}, Pb^{3+}, Bi^{4+}. These ionic configurations are unstable with respect to the disproportionation reaction. Thus, in $BaBiO_3$, instead of the nominal valence 4+, bismuth prefers the stable valence states Bi^{3+} and Bi^{5+} with fully filled shells. However, unlike ions with n*s*-electrons, for JT ions we deal with orbital degeneracy for e_g-electrons/holes, hence the possibility of competition between the Jahn-Teller effect leading to orbital ordering, and the anti-JT

disproportionation effect, leading to the formation of a system of *S*-type electron and hole centers with an orbitally nondegenerate ground state [1, 2], equivalent to a system of effective composite spin-singlet or spin-triplet bosons in a nonmagnetic or magnetic lattice with clear prospects to form a superconducting phase. This mechanism indicated an unconventional bosonic spin-triplet superconductivity in ruthenates, ferropnictides and ferrochalcogenides. Over the past years, new results have been obtained in the study of JT magnets based on both 3*d*- and 4*d*-ions, as well as new arguments both for and against spin-triplet superconductivity.

The disproportionation scenario of superconductivity was addressed earlier by many authors, however, by now it was not properly developed theoretically, and perhaps that is why it has not yet been a worthy competitor to the traditional BCS approach.

In my talk I would like to revive interest in superconductivity of JT magnets by presenting the anti-JT-disproportionation scenario for superconductivity in a wide class of JT magnets, including cuprates, FePn/Ch-systems, different nickelates, ruthenates, silver compounds, and show that all of them can be described within an unified approach.

The research was supported by the Ministry of Education and Science of the Russian Federation, project No. FEUZ-2023-0017.

References

1. *A.S. Moskvin*, Magnetochemistry, **9**, 224 (2023).
2. *A.S. Moskvin*, JETP Letters, **121**, 411-420 (2025).

Optical Studies of $K_{0.8}Fe_{1.7}(Se_{0.73}S_{0.27})_2$ Single Crystals

A.V. Muratov[1], E.O. Rakhmanov[2,1], A.I. Shilov[1],
I.V. Morozov[2], Yu.A. Aleshchenko[1]

[1] P.N. Lebedev Physical Institute of RAS, 119991 Moscow, Russia,
[2] Department of Chemistry, Lomonosov Moscow State University, 119991 Moscow, Russia

The optical properties of $K_{0.8}Fe_{1.7}(Se_{0.73}S_{0.27})_2$ superconducting single crystals with $T_c \approx 26$ K have been studied in the broad frequency range by IR Fourier-transform spectroscopy and spectroscopic ellipsometry at the temperatures of 4-300 K. The real part of conductivity $\sigma 1$ was obtained by the Kramers-Kronig transformation of $R(\omega)$. The Drude-Lorentz model was applied to describe the conductivity spectra at low temperatures and the model parameters (plasma frequencies, scattering rates and oscillator strengths) were obtained.

Many experiments with isovalent substitution of S for Se revealed a coexistence of superconductivity with a strong AFM order in $A_xFe_{2-y}Se_2$ (A = K, Rb, Cs, Tl) iron-selenide superconductors. It was found that the superconducting (SC) phase in these materials evolves from an insulating phase rather than an SDW metal as in the case of Fe pnictides. Actually, $A_xFe_{2-y}Se_2$ is an inhomogeneous, phase separated material consisting of the insulating $A_2Fe_4Se_5$ (245) phase and the SC AFe_2Se_2 (122) one typically grown in the boundaries of the 245 crystallites. The critical temperature T_c of the superconductors of KFe_2Se_2 family reaches up to 32-33 K and gradually decreases with isovalent substitution of S for Se.

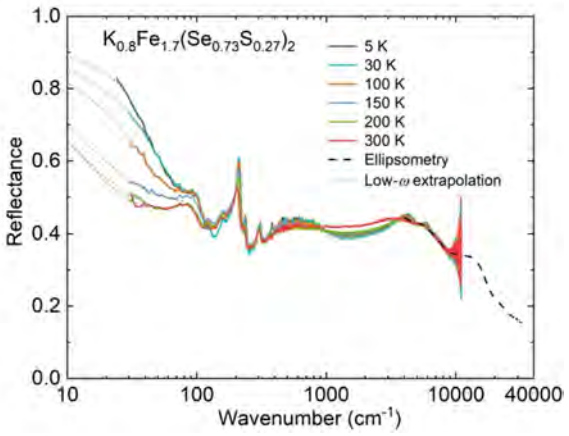

Fig. 1. The reflectance spectra of single crystals at various temperatures.

We have studied for the first time the optical properties of $K_{0.8}Fe_{1.7}(Se_{0.73}S_{0.27})_2$ single crystals with $T_c \approx 26$ K grown using self-flux technique [1]. The composition of the crystals was confirmed by EDX spectroscopy. Infrared spectra at near normal incidence were taken from the *ab* plane of single crystals using the IFS 125HR (Bruker) Fourier-transform spectrometer in the frequency range of 25-10000 cm^{-1} at temperatures of 4-300 K. An *in situ* aluminum overcoating technique was used to obtain the reflectance $R(\omega)$. The variable-angle spectroscopic ellipsometry (VASE, Woollam) was carried out in the range from 4000

to 30000 cm^{-1}. The real part of conductivity σ_1 was obtained by the Kramers-Kronig transformation of $R(\omega)$.

The reflectance spectra of $K_{0.8}Fe_{1.7}(Se_{0.73}S_{0.27})_2$ are shown in Fig. 1. The overall reflectance is rather low, which is characteristic of insulator. It is dominated by infrared-active phonons and interband features at higher energies. The low-frequency reflectance initially displays small temperature dependence but begins to increase below 200 K, with an abrupt increase close to T_c. In contrast to [2] the phonon mode at 212 cm^{-1} does not exhibit a Fano-like shape.

It should be noted that at room temperature there are no coherent (Drude) contribution to the optical conductivity σ_1 of $K_{0.8}Fe_{1.7}(Se_{0.73}S_{0.27})_2$. As temperature decreases, the Drude contribution arises. In this case, the Drude-Lorentz model is applicable. The calculated conductivity σ_1 at 30 K is shown in Fig. 2 together with its constituent contributions. In addition to the phonon modes, there are a number of broad interband transitions at 1000, 4400, 5900, 6500, 12785 и 35000 cm^{-1}. These transitions were observed previously in iron selenides [2-5] and were ascribed to spin-controlled interband transitions.

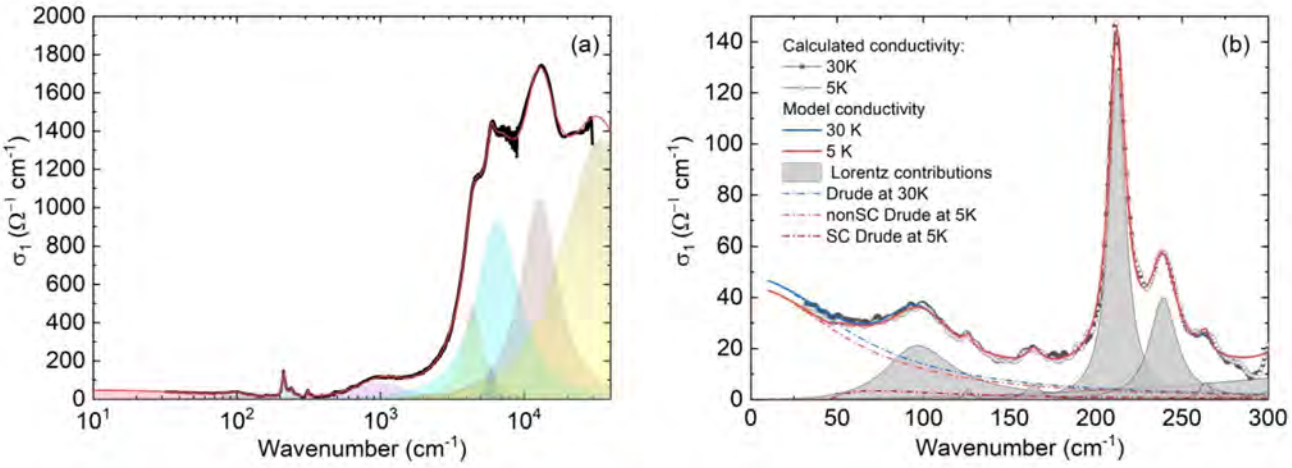

Fig. 2. (a) The real part of the optical conductivity of $K_{0.8}Fe_{1.7}(Se_{0.73}S_{0.27})_2$ at 30 K; (b) The real part of the optical conductivity in the low-frequency region of $K_{0.8}Fe_{1.7}(Se_{0.73}S_{0.27})_2$ single crystals at 30 and 5 K.

An example of the calculated conductivity in the low-frequency region at 30 and 5 K is shown in Fig. 2b. The dash-dotted lines depict Drude contributions. The Lorentz contributions are shown in gray. The model parameters (plasma frequencies, scattering rates and oscillator strengths) were obtained. For the Drude contribution at 30 K the optical conductivity, scattering rate, and plasma frequency are $\sigma_0 = 47$ Ω^{-1} cm^{-1}, $\gamma = 64$ cm^{-1}, and $\omega_{pl} = 425$ cm^{-1}, respectively.

As temperature decreases from 30 to 5 K, the conductivity decreases signaling the opening of the SC gap. According to our estimate, the SC phase constitutes not more than 25% of the sample volume. The work is supported by RSF project no. 22-72-10082P.

References

1. *T.E. Kuzmicheva, et al*., J. Supercond. Novel Magn. **38**, 120 (2025).
2. *R.H. Yuan et al*., Sci. Rep. **2**, 221 (2012).
3. *Z.G. Chen et al*., Phys Rev. B **83**, 220507(R) (2011).
4. *A. Charnukha et al*., Phys. Rev. B **85**, 100504(R) (2012).
5. *C.C. Homes et al*., Phys. Rev. B **85**, 180510(R) (2012).

Systems with strong long-range electron-phonon coupling and cuprates-like dispersion: single nature of pseudogap, charge ordering and superconducting phases and other peculiarities of two-liquid system of charge carriers

A.E. Myasnikova, R.R. Arutyunyan, S.V. Doronkina*,
A.H. Dzhantemirov, D.D. Vasilenko, A.S. Fukalov

Southern Federal University, Zorge str. 5, 344090 Rostov-on-Don, Russia,
*Rostov State Medical University, Nakhichevansky Lane 29, 344022 Rostov-on-Don, Russia

We show that ground and low-excited states of systems with strong long-range electron-phonon coupling and cuprates-like dispersion are two-liquid systems of charge carriers comprising Bose liquid of large bipolarons and Fermi liquid of delocalized carriers. We calculate observable properties of such systems: phase diagram, temperature of the superconducting transition in systems with different number of conducting planes in the unit cell, charge ordering wave vector, density of the superconducting component, spectra of resonance elastic X-ray scattering and angle-resolved photoemission spectroscopy, Hall and Seebeck coefficients. They agree with the properties of superconducting cuprates.

We develop two methods to obtain free energy of the two-liquid system of charge carriers emerging at their strong coupling with phonons and cuprates-like dispersion. The first method uses distribution function in systems where autolocalized and delocalized carriers can coexist [1]. The second method is like BCS approach with variationally determined distribution functions for autolocalized and delocalized carriers. Binding energy of the bipolaron as a function of its radius is obtained with the variation over the parameters of trial wave function except the bipolaron radius which is fixed; the coherent states representation is used for the state of the phonon field [2]. Variation of the free energy over the bipolaron size determines the equilibrium bipolaron size (or two sizes if an inhomogeneous system is more profitable energetically). Comparison of the obtained free energy with the free energy of pure Fermi liquid of delocalized carriers determines the region on the phase diagram doping-temperature where the bipolaron liquid is present. This region coincides with the region of presence of the pseudogap resulting from the impact of the potential of bipolarons on the stationary states of delocalized carriers [3].

The equilibrium bipolaron size determines the charge ordering wave vector; small coherence length of the charge ordering corresponds to local order in the bipolaron liquid. The momentum-space structure of the two-liquid system of charge carriers is also characterized by the momentum which is determined by the bipolaron size through the uncertainty relation and divides the momentum space into two parts, in one of which delocalized carriers are forbidden in presence of autolocalized ones. This momentum is visualized by the angle-resolved photoemission spectroscopy (ARPES) spectra as the “waterfall” wave vector; the “waterfall” results from different

energetic cost of the system relaxation after photoemission from the described different parts of the momentum space [4]. Calculated manifestation of the bipolaron liquid in the spectra of resonance elastic X-ray scattering (REXS) [2] and ARPES [4] agrees with the features observed in cuprates including the values of the charge ordering and "waterfall" wave vectors.

Both methods developed yield the same phase diagram in coordinates doping-temperature with presence of pseudogap, charge ordering and superconductivity in the same regions of the phase diagram as in cuprates [1]. Thus, we show that there exists a class of systems where pseudogap, charge ordering and superconductivity have single nature as was supposed earlier on the base of similar phase diagram in different cuprates [5]. Expression for the temperature of the superconducting transition obtained in the standard Bose liquid approach demonstrates its increase with the number of conducting planes in the unit cell until it exceeds three [1] as it takes place in cuprates. The density of the superfluid component of the bipolaron liquid decreases linearly with the doping at the overdoping [1] as in cuprates [6]. Calculated density of carriers in autolocalized and delocalized states is used to obtain Hall and Seebeck coefficients as functions of doping and temperature. The calculated charge ordering period and variety of its doping dependences for different system characteristics agree with those observed in cuprates. In the frames of BCS-like approach we reveal that two-liquid system of charge carriers at some doping and medium parameters demonstrates inhomogeneity, namely, coexistence of regions with and without charge ordering like one observed recently in cuprates [7] or regions with two different wave vectors of the charge ordering.

References

1. *A.E. Myasnikova, S.V. Doronkina, R.R. Arutyunyan and A.H. Dzhantemirov*, J. Phys.: Condens. Matter **36**, 325601 (2024).
2. *A.E. Myasnikova, T.F. Nazdracheva, A.V. Lutsenko, A.V. Dmitriev, A.H. Dzhantemirov, E.A. Zhileeva and D.V. Moseykin*, J. Phys.: Condens. Matter **31**, 235602 (2019).
3. *A.E. Myasnikova, S.V. Doronkina, A.H. Dzhantemirov and A.V. Lutsenko*, Physica E: Low-Dimensional Systems and Nanostructures **136**, 115052 (2022).
4. *A.E. Myasnikova, E.A. Zhileeva and D.V. Moseykin*, J. Phys.: Condens. Matter **30**, 125601 (2018).
5. *B. Loret et al*., Nat. Phys. **15**, 771 (2019).
6. *I. Božović, X. He, J. Wu and A. T. Bollinger*, Nature **536**, 309 (2016).
7. *C. C. Hsu et al*., Nat. Commun. **12**, 3893 (2021).

Laser ARPES on Pairing Symmetry and High-T_c Origin in High Temperature Superconductors

Xingjiang Zhou

Institute of Physics, Chinese Academy of Sciences, Beijing 100190, China

Using laser ARPES to study high temperature superconductors, we gained new insights on pairing symmetry and superconductivity mechanism of these superconductors.

We will report our recent progress in studying high temperature superconductors by laser-based angle-resolved photoemission spectroscopy (ARPES). A new approach is developed to make ARPES able to measure not only the superconducting gap size but also the gap sign [1]. The pairing symmetry is determined to be of the nodal s+-(G-M) form in the iron-based superconductor KFe_2As_2 which has only hole pockets [2]. Ubiquitous coexisting electron coupling with 70 meV and 40 meV modes is observed in cuprate superconductors [3]. The electronic origin of high-T_c maximization in trilayer cuprate superconductors is revealed [4]. We found orbital-dependent electron correlations in $La_3Ni_2O_7$ [5]. These results provide key insights in understanding superconductivity mechanism and also pave a way to further enhance T_c in these high temperature superconductors.

References

1. *Qiang Gao, L. Zhao, X. J. Zhou et al*., Nature Communications **15**, 4538 (2024).
2. *Dingsong Wu, Lin Zhao, X. J. Zhou et al*., Nature Physics **20**, 571 (2024).
3. *Hongtao Yan, X. J. Zhou et al*., PNAS **120**, e2219491120 (2023).
4. *Xiangyu Luo, X. J. Zhou et al*., Nature Physics **19**, 1841 (2023).
5. *Jiangang Yang, L. Zhao, X. J. Zhou et al*., Nature Communications **15**, 4373 (2024).

Posters

Electron-phonon interaction with forward scattering in FeSe monolayers on $SrTiO_3$

R. Babaian, E.Z. Kuchinskii

Institute of Electrophysics of the Ural Branch of the Russian Academy of Sciences

We present an exactly solvable model of forward electron scattering in a monolayer of FeSe on high-energy optical phonons of an $SrTiO_3$ substrate and perform its numerical analysis.

We present an exactly solvable model of electron-phonon interaction with forward electron scattering, which allows for the full summation of perturbative diagrams for the single-particle Green's function using the Ward identity.

We apply the model to the FeSe/$SrTiO_3$ system, where, according to several studies, the enhancement of the superconducting transition temperature relative to bulk FeSe may be driven by the coupling between FeSe electrons and high-energy optical phonons in the $SrTiO_3$ substrate.

We perform numerical calculations and compare our exact solution with the self-consistent Born approximation, which is commonly used in existing studies.

This work was supported by Russian Science Foundation (RSF) [grant number 25-12-00418].

SnS-andreev spectroscopy of superconducting polycrystalline pnictide with underdoped composition $BaFe_{2-x}Ni_xAs_2$ at x=0.07

A.D. Ilina[1], I.A. Nikitchenkov[1,2], S.A. Kuzmichev[2,1], K.S. Pervakov[1], V.A. Vlasenko[1], A.S. Medvedev[1], T.E. Kuzmicheva[1]

[1] P.N. Lebedev Physical Institute, Moscow, Russia
[2] Physical Faculty of Lomonosov Moscow State University, Moscow, Russia

The message is dedicated to the study of the superconducting gap structure of a polycrystalline pnictide $BaFe_{1.93}Ni_{0.07}As_2$, grown by a new method. Using the spectroscopy of incoherent multiple Andreev reflection effect, two microscopic superconducting order parameters were directly determined – a small superconducting gap and a large gap, which is presumably anisotropic in k-space, along with their characteristic ratios and temperature dependencies. The temperature dependencies of the gaps were calculated within the two-gap model of the Moskalenko and Suhl theory. A resonant interaction between the superconducting subsystem and a characteristic bosonic mode was discovered, and its energy was determined at temperatures much lower than T_c.

The studied polycrystalline samples with nominal composition $BaFe_{1.93}Ni_{0.07}As_2$ grown by a new method belong to the family of iron-based superconductors (SC) known as Ba-122. The transition to the SC-state occurs at a maximum critical temperature $T_c \approx 20$ K for $x \approx 0.1$ on the phase diagram [1].

The aim of the work was to determine the magnitudes of the SC gaps and their temperature dependencies and $T_c \approx 17$–18 K using the spectroscopy of incoherent multiple Andreev reflection effect (IMARE). We also aimed to study the temperature dependence of a reproducible feature at bias voltages $eV > 2\Delta_L$, presumably related to an interaction with spin exciton.

The contacts of SnS-type (SC–normal metal–SC) were formed at $T = 4.2$ K using the "break-junction" technique [2]. As a result of the study, we analyzed Andreev features observed in the $I(V)$ and $dI(V)/dV$ characteristics at $T = 4.2$ K, as well as their temperature evolution up to T_c. At $T = 4.2$ K, we found evidence of IMARE as predicted by theoretical models [3, 4].

For the isotropic small SC gap, we obtained the characteristic ratio $2\Delta_S(0)/k_BT_c \approx 2$. We identified the extrema of a presumably anisotropic large SC gap (minimum and maximum values of the Cooper pair binding energy in the k-space in the given bands [5]) with corresponding characteristic ratios of $2\Delta_L^{in}(0)/k_BT_c \approx 4$ and $2\Delta_L^{out}(0)/k_BT_c \approx 5.5$. These results are consistent with previously obtained data for $BaFe_{2-x}Ni_xAs_2$ single crystals with $x = 0.08$ and similar close $T_c = 18.3$ K [6]. The obtained temperature dependencies $\Delta_L^{in}(T)$, $\Delta_L^{out}(T)$, and $\Delta_S(T)$ are shown in Fig. 1. Assuming anisotropy of the larger SC gap, the temperature dependences of the order parameters were approximated using functions calculated within the framework of the two-band theoretical model by Moskalenko and Suhl [7,8], where the effective amplitude of the larger gap is taken as the average: $\Delta_L^{eff} = (\Delta_L^{out} + \Delta_L^{in})/2$.

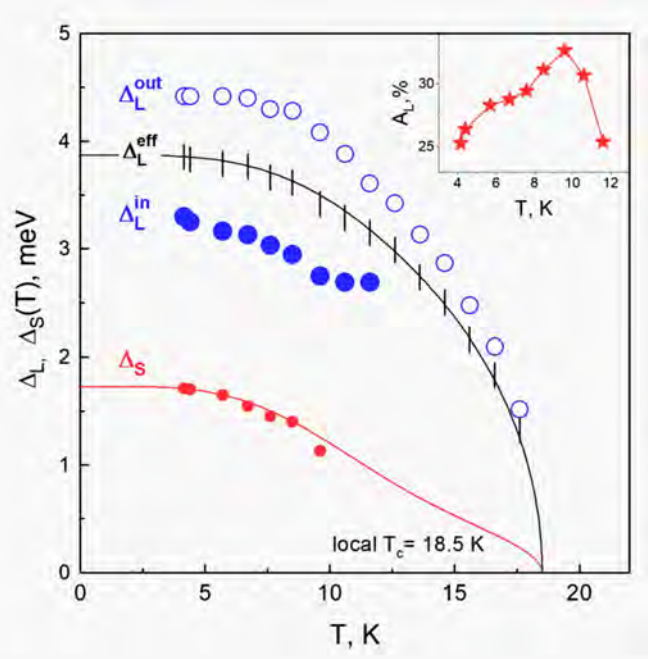

Fig. 1. The obtained temperature dependencies $\Delta_L^{in}(T)$, $\Delta_L^{out}(T)$, and $\Delta_S(T)$ (rounds) were approximated using functions calculated within the framework of the two-band theoretical model by Moskalenko and Suhl (solid lines) [7, 8], where the effective amplitude of the larger gap is taken as the average: $\Delta_L^{eff} = (\Delta_L^{out} + \Delta_L^{in})/2$ (vertical strokes). Inserted graph shows anisotropy of the larger SC gap $A_L = 100\% \cdot [1 - \Delta_L^{in}/\Delta_L^{out}] \approx 30 \pm 5$ %.

In addition to the gap-related features, below T_c we also observed a fine structure in the dynamic conductance spectra at $|eV| = [2\Delta + E_{res}]/n$, possibly associated with boson emission during IMARE or electron density of states renormalization on the coupling with a bosonic mode. For the first time in underdoped $BaFe_{2-x}Ni_xAs_2$, the boson energy $E_{res}(0) \approx 4.3$ meV and its temperature dependence were determined. As the temperature increased, $E_{res}(T)$ decreased slightly, not resemble the $\Delta(T)$ dependence, but showing the behavior similar to the spin-resonance peak energy in iron-based SCs [9].

References

1. *T.E. Kuzmicheva, et al*. JETP Letters **121**(5–6), 462–480 (2025).
2. *Kuzmichev, S.A., and T.E. Kuzmicheva*. Low Temperature Physics **42**(11), 1284–1310 (2016).
3. *U. Gunsenheimer, and A.D. Zaikin*. Physical Review B **50**, 6317 (1994).
4. *R. Kuemmel,* Physical Review B **42**, 3992 (1990).
5. *T.P. Devereaux, and P. Fulde*. Physical Review B **47**, 14638(R) (1993).
6. *A.V. Sadakov, et al.* JETP Letters **116**, 686 (2022).
7. *V.A. Moskalenko*, Physics of Metals and Metallography **8**, 25 (1959).
8. *H. Suhl, B.T. Matthias, and L.R. Walker.* Physical Review Letters **3**, 552 (1959).
9. *M.M. Korshunov, V.A. Shestakov, and Yu.N. Togushova*. Physical Review B **94**, 094517 (2016).

The role of spin-orbit coupling in the formation of the Fermi surface in multiorbital models of iron pnictides

D.A. Ivanov, M.M. Korshunov

Kirensky Institute of Physics, Federal Research Center KSC SB RAS, 660036 Krasnoyarsk, Russia,
Siberian Federal University, 660041 Krasnoyarsk, Russia

Here we study the role of spin-orbit coupling in the formation of the Fermi surface topology in three-, five-, and ten-orbital models of iron pnictides in the Brillouin zone, corresponding to two iron atoms per unit cell.

Here we study the role of spin-orbit coupling in the formation of the Fermi surface topology in three-, five-, and ten-orbital models of iron pnictides in the Brillouin zone, corresponding to two iron atoms per unit cell [1-5]. Several variants of spin-orbit coupling were considered in the three-orbital model. In the first of them, only the *z* component of the spin-orbit coupling is used [6], while in the second, all its components are taken into account at once. The model introduces constants of the spin-orbit coupling on one iron ion (λ) and between two iron ions (λ') in a unit cell that includes two iron atoms. The spin-orbit coupling constant shows how strong the interaction is between the spin of a particle and its orbital motion.

Without taking into account the spin-orbit coupling, the Fermi-contours near the (π, 0) and (0, π) points of the Brillouin zone intersect along the directions k_x and k_y. Once the spin-orbit coupling is finite, the intersections disappear so the contours of the Fermi surface sheets near the points (π, 0) and (0, π) become open instead of closed. Thus, in the three-orbital model, in both cases, the z-component and all components, considering the finite spin-orbit coupling between two iron ions the interatomic spin-orbit coupling leads to a topological transition of the Fermi surface.

In the five-orbital model, when considering only the intraionic part of the spin-orbit coupling (λ = 100 MeV, λ' = 0), there is a slight change in the volume of the central contour around the Γ-point, as well as the appearance of additional contours around M and symmetrical points on the Fermi surface. When considering only the interionic part of the spin-orbit coupling (λ = 0, λ' = 100 MeV), the topology of the contours of the Fermi surface around the point M and the points symmetrical to it is changed as follows: instead of coinciding contours of the Fermi surface in the X − M direction, we get four separate contours. Taking into account both components of the spin-orbit coupling (λ = λ' = 100 MeV) leads to the Fermi surface, which is a combined version of the two previous cases, and therefore there is a change in the shape of the contours around the Γ-point and the appearance of additional contours around the M-point and points symmetrical to it on the Fermi surface. Thus, in the case of the five-orbit model, it is the interionic contribution of the spin-orbit coupling that leads to changes in the topology of the Fermi surface.

In Figure, the Fermi surface in the case of a ten-orbital model is shown for the case when only the intra-ionic part of the spin-orbit coupling with the constant λ is finite.

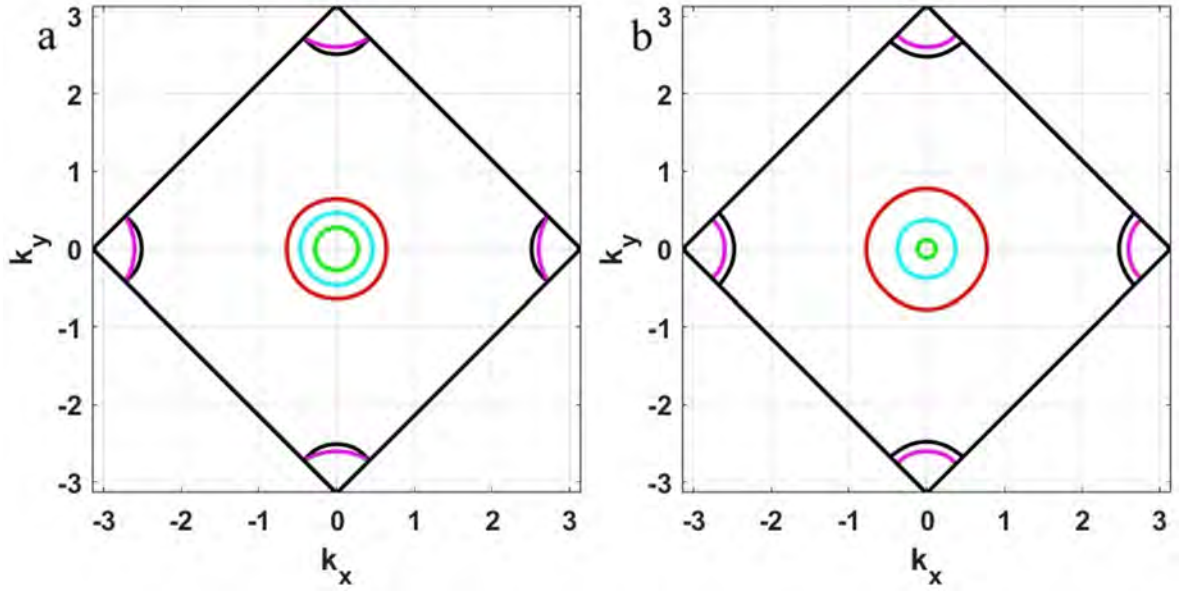

Figure 1. Fermi surface in the ten-orbital model in the Brillouin zone, corresponding to two iron atoms per unit cell, in the presence of spin-orbit coupling: a) λ = 0, μ = – 0.0126 eV; b) λ = 100 meV, μ = 0.0057 eV.

Evidently, the change in the topology of the Fermi surface near the M-point appears even if there is only an intra-ion spin-orbit coupling. This is a significant difference from the results for the three- and five-orbit models, where a similar effect occurs only in the presence of effective inter-ionic spin-orbit coupling.

References

1. *Korshunov M.M., Togushova Y.N.* Journal of Siberian Federal University. Mathematics & Physics **11**(4), 430–437 (2018).
2. *Ivanov D.A., Togushova Y.N., Korshunov M.M.* Journal of Siberian Federal University. Mathematics & Physics **16**(6), 795-803 (2023).
3. *Graser S. et al.* New J. Phys. **11**, 025016 (2009).
4. *Ivanov D.A., Korshunov M.M.* Superconductivity: Fundamental and Applied Research, № 4, 12-18 (2024).
5. *Eschrig H., Koepernik K.* Phys. Rev. B **80**, 104503 (2009).
6. *Eremin I., Manske D., Bennemann K.H.* Phys. Rev. B **65**, 220502 (2002).

Simulation of the NbN film heating process by a current pulse

N.D. Kuzmichev, E.V. Danilova, M.A. Vasyutin, D.A. Shilkin

Ogarev Mordovian State University, Saransk, 430005, Russia

Numerical simulation of heating of a niobium nitride film by a current pulse at low temperatures in its longitudinal section based on a two-dimensional equation of thermal conductivity is performed.

When examining the volt-ampere characteristic film, it is necessary to ensure a good heat sink. This problem is often solved by using pressure contacts made of beryllium bronze and a copper base (thermostat), as well as passing a current pulse through the film. The high heat absorption by the contacts and the thermostat is due to an increase in the thermal conductivity of copper by more than an order of magnitude at temperatures from 5 to 50 K [1, 2]. The NbN sample (film) was examined, which has a length of Ly = 9 mm, a width of w = 5 mm and a thickness of d = 400 nm. Experimentally measuring the maximum heating temperature of a film during the passage time of a current pulse is difficult and expensive. Therefore, it is easier to perform numerical simulation of the heating process. Numerical modeling was performed in the integrated Microsoft Visual Studio environment. A program was written in C++ that solves a two-dimensional equation of thermal conductivity. The equation is:

$$\partial T / \partial t = a^2 (\partial^2 T / \partial x^2 + \partial^2 T / \partial y^2) + f(x, y, z), \quad (1)$$

where $a^2 = 4.3 \cdot 10^{-2}$ cm^2/s is the thermal conductivity coefficient of the film at 20 K, T is the film temperature, t is time, x and y are coordinates (Fig. 1), the value of $f(x,y,t) = P(x,y,t)/(c_{NbN} \cdot \rho_{NbN})$, $P(x,y,t)$ is the volumetric power density of the heat source (films), c_{NbN} = 17 J/(kg·K) is the specific heat capacity of the film at T = 14 K, ρ_{NbN} = 8400 kg/m^3 is the film density [1]. The current increases linearly over time t_0 from 0 to I_{max}. The value of $P(x,y,t)$ is determined by the Joule-Lenz law and does not depend on coordinates:

$$P(x, y, t) = \rho j_0^2 t^2, \ x < d, \ t < t_0; 0, x > d, t > t_0.$$

Here, $\rho \approx 440$ μΩ·cm is the resistivity of the film in the normal state, $j_0 = I_{max}/(dwt_0)$, t_0 = 0.25 ms, I_{max} = 1.12 A. The NbN film is in a resistive state at T = 14 K. At the left end, we set a problem of the third kind, since the left boundary of the film through contacts is in heat exchange with the medium according to Newton's law, with a temperature of 14 K (Fig. 1): $\partial T(0, y, t) / \partial x = H(y)[T(0, y, t) - 14]$.

The heat transfer coefficient H depends on y, i.e. $H = H(y)$:

$$H(y) = H_0, 3a + 3b < y \le 3a + 4b = L_y;$$

$$0, 2a + 3b < y \le 3a + 3b; H_0, 2a + 2b < y \le 2a + 3b; \ 0, \ a + 2b < y \le 2a + 2b;$$

$$H_0, a + b < y \le a + 2b; \ 0, b < y \le a + b; \ H_0, y \le b.$$

Here a is the width of the contact area, b is the width of the contact. In the contact area $H = 0$, in the contact area $H = H_0 = 50$ μm^{-1}. The right boundary condition (the right boundary of the substrate) has the form: $T(L_x, y, t) = T_0 = 14$ K, here L_x is the thickness of the substrate together with the film. The upper and lower boundary conditions will be written as $\partial T(x,0,t)/\partial x = \partial T(x,L_y,t)/\partial x = 0$.

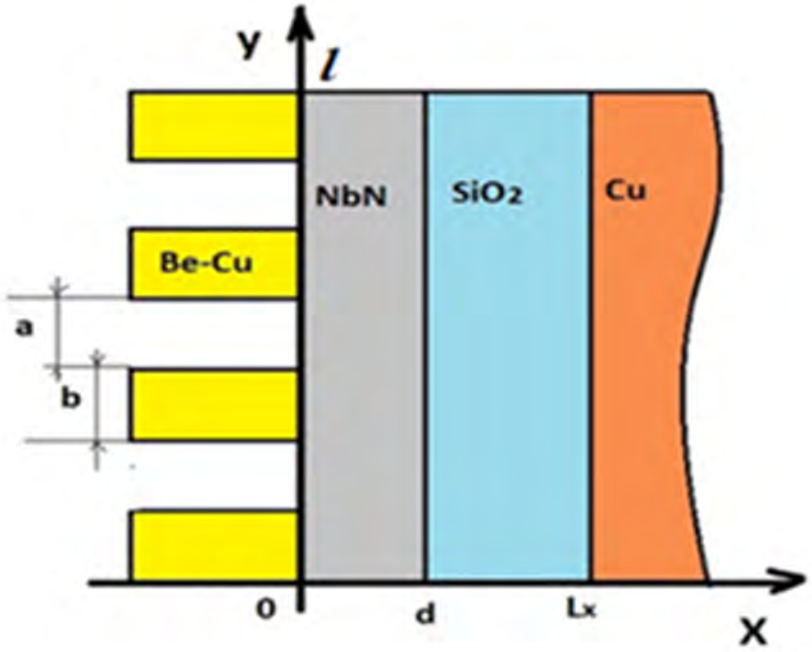

This corresponds to the absence of heat exchange. As a result, the initial boundary conditions for equation (1) have the form:

$$T(x,y,0) = 0;\ \partial T(0,y,t)/\partial x = H(y)[T(0,y,t) - T_0;$$
$$T(L_x,y,t) = T_0;\ \partial T(x,0,t)/\partial y = 0;\ \partial T(x,L_y,z,t)/\partial y = 0. \quad (2)$$

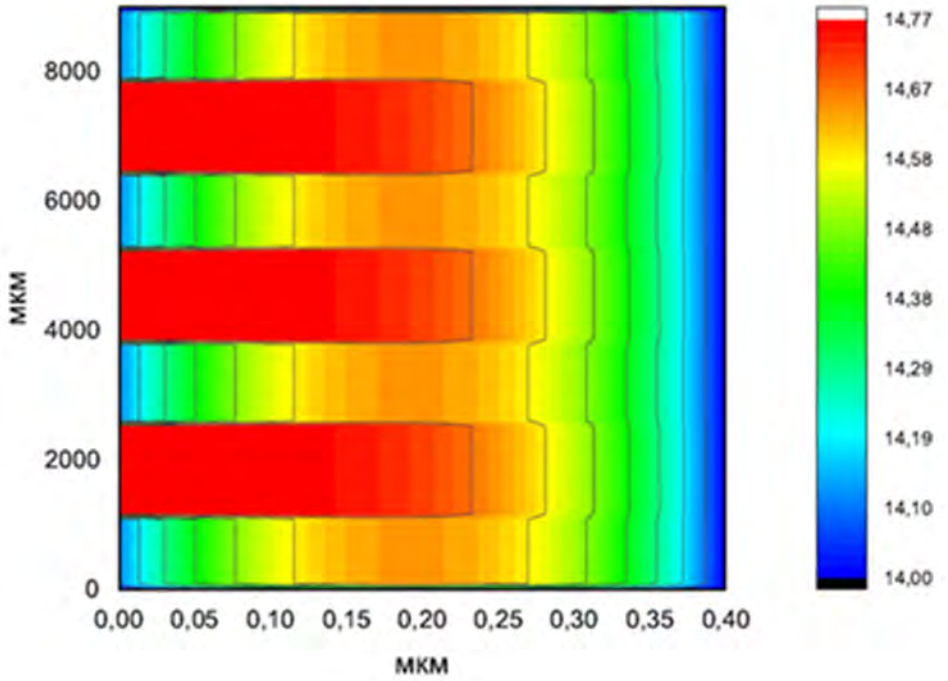

To approximate the differential equation (1) by finite-difference relations, we introduce a space-time grid with coordinates: $x_i=(i-1)\cdot h_x$, $y_i=(j-1)\cdot h_y$, $t_n=n\cdot\tau$. Here h_x,

h_y are the grid steps in x, y coordinates, respectively, τ is the time step; i =1, 2, …, N_x, j=1, 2, …, N_y, n = 0, 1, 2…, K. Here N_x = 91, N_y = 401. The number K varied depending on depends on the magnitude of the step t (50 μs, 100 μs) and the final moment of time. A local one-dimensional scheme of A.A. Samarsky [3] was used for the solution, which is absolutely stable. The calculation results are shown in Fig. 2.

Figure 2 shows the temperature distribution inside the cross-section of the film at a time of 250 μs after the start of the pulse. The pulse increases linearly for 250 μs. From the results shown in Figure 2, it can be seen that the maximum heating temperature is inside the film and its highest value is reached at the end of the pulse. After the pulse is stopped at the 3rd ms, the film cools significantly to 14.03 K. It can be seen from Fig. 2 of the results that the maximum heating temperature of the film increases slightly by ≈ 0.8 K.

The change in the maximum temperature inside the niobium nitride film during 20 ms. It can be seen from the graph that the temperature reaches its maximum, as expected, at the moment when the pulse is completed, namely 14.8 K at 250 μs. In the contact area, the heating is 0.2 lower than in the non-contact area.

The boundary condition at $x = d$ was not taken into account, since the thermal conductivity coefficients of the film and the substrate are close in value ($a^2 \sim 10^{-2}$ cm^2/s).

The calculation of the contact temperature jumps for the thermal resistance of the Kapitsa $R_K \sim 10^{-4}$ m^{2}K/W at a heat flux density $q \approx 5 \cdot 10^{-2}$ W/m^2 [4] leads to a value of several hundredths of a Kelvin. This is an order of magnitude less than the resulting temperature increase, which confirms the validity of the right boundary condition.

References

1. Tables of physical quantities. Guide. Edited by Academician I.K. Kikoina (M., Atomizdat, 1976). – 1008 p.
2. *A. Misnar*. Thermal conductivity of solids, liquids, gases and their compositions (Moscow: Mir, 1968). – 464 p.
3. *V.F. Formalev, D.L. Reviznikov*. Numerical methods (FIZMATLIT, M., 2006). – 406 p.
4. *V.M. Popov*. Heat exchange in the contact zone of detachable and non-removable joints (Moscow: Publishing House of Energy, 1971). – 216 p.

Superconducting state of iron pnictides in a ten-Orbital model with a realistic Fermi surface

E.A. Larionov, M.M. Korshunov

Kirensky Institute of Physics, Federal Research Center KSC SB RAS, 660036 Krasnoyarsk, Russia,
Federal Research Center «Krasnoyarsk Science Center SB RAS», Siberian Federal University

Reveal how the presence of additional Fermi pockets observed experimentally affects the superconducting state.

Interest in high-temperature superconductivity in iron-based compounds is driven both by the practical applications of these materials and by unresolved theoretical challenges in modeling such systems. One key issue is the discrepancy between density functional theory (DFT) calculations and experimental observations in hole-doped iron compounds: DFT fails to predict additional Fermi contours that are clearly present in experiments (see Fig. 1). This study analyzes the influence of these extra Fermi surface elements on the symmetry of the superconducting state. Calculations were performed using a realistic 10-orbital model derived from Ref. [1], with parameters adjusted to reproduce the experimentally observed Fermi surface from Ref. [2]. The spin susceptibility $\chi(q, \omega)$ was computed as a spin correlation function within the random phase approximation (RPA), incorporating multiorbital on-site Coulomb interactions. The interaction parameters included: Intraorbital (U) and interorbital (U') Hubbard repulsion, Hund's coupling (J), Interorbital pair hopping (J') [3]. The Cooper vertex was calculated, and the superconducting gap equation was solved. The role of the additional Fermi contours in shaping both the susceptibility and the superconducting state is discussed.

Figure 1. Fermi surface of a hole-doped iron-based compound. Additional Fermi contours are highlighted in red.

Acknowledgments

The study was supported by the Russian Science Foundation grant N 25-22-20043, https://rscf.ru/project/25-22-20043/, grant of the Krasnoyarsk Regional Science Foundation.

References

1. *Eschrig H., Koepernik K.* Physical Review B **80**(104503), 6-7 (2009).
2. *Kordyuk A.A., Zabolotnyy V.B., Evtushinsky D.V., Yaresko A.N., Büchner B., Borisenko S.V.* Journal of superconductivity and novel magnetism **26**, 2837-2841 (2013).
3. *M.M. Korshunov*. Physics-Uspekhi **184**, 882–888 (2014).

Physical nature of the pseudogap phase and anomalous transfer of spectral weight in underdoped cuprates

K. Mitsen, O. Ivanenko

P.N. Lebedev Physical Institute

It is shown that many anomalies observed in underdoped cuprates, including anomalous spectral weight transfer and a large pseudogap, appear to have a common nature due to both the cluster structure of the underdoped phase and the specific mechanism of superconducting pairing. The combined action of these factors leads to the fact that at a temperature T lying in a certain temperature range T_c.

In this work, we have shown that a number of unusual properties distinguishing underdoped cuprates from conventional superconductors appear to be of a common nature and result from the cluster structure of the underdoped phase and the specific mechanism of superconducting pairing in cuprates. This pairing mechanism is assumed to be mediated by the virtual scattering of electrons into unoccupied localized pair states formed on pairs of neighboring Cu cations under doping and is reminiscent of the Little-Ginsburg mechanism.

The cluster structure of the underdoped phase in combination with the special mechanism of superconductivity of cuprates leads to the fact that in a certain temperature range $T_c<T<T^*$ finite isolated clusters can exist in both superconducting and normal states, switching between these states randomly due to fluctuations of pair states occupation with electrons.

In this case, we can consider that below T_c the cluster is almost always in a superconducting state, and above T^* – in a normal state, and the interval $T_c<T<T^*$ can be identified with the region of existence of the so-called pseudogap phase. The temperatures T_c and T^* for $YBa_2Cu_3O_{6+d}$ were calculated depending on the doping level. The calculation results are in good agreement with experiment without any fitting parameters.

In the same temperature range, the contribution to optical conductivity from a sequence of randomly arising superfluid density pulses from each cluster can be represented as a random process with a correlation time $t_{corr}\sim10^{-15}$ sec, which corresponds to the effective spectrum width $\Delta\omega_{eff}\sim1$ eV and explains the apparent SW transfer from the high-frequency region.

In the vicinity of T_c, fluctuation induced s-n switching of finite clusters are apparently the cause of another group of phenomena: the anomalous Nernst effect, giant diamagnetism (above T_c) and reversibility of magnetization curves (below T_c).

Thus, the approach under consideration allows us to explain many anomalous properties of underdoped cuprates. This fact can be considered as an indirect confirmation of the validity of the proposed model of HTSC cuprates.

Superconductivity of the materials undergoing anharmonicity sign inversion

Zh.Kh. Murlieva, D.K. Palchaev, S.Kh. Gadzhimagomedov

Dagestan State University, Makhachkala, Russia; e-mail: zhariyat@mail.ru

Based on experimental data for a large number of nonmetals, we find that the phonon thermal resistance correlates linearly with the product of the thermal expansion coefficient per temperature at each equilibrium state. This fact allows us to understand the noticeable increase in thermal conductivity of loose-packed materials near the temperature of inversion of the sign of thermal expansion, since the contribution of the phonon component becomes negative. For HTSCs, as well as for many weakly packed structures, there is an inversion of the TEC sign below the transition temperature and directly at the transition. This allows us to express the criteria for the increase in thermal conductivity of superconductors below the superconducting transition temperature.

In [1] the problem of establishing the nature of the increase in thermal conductivity of superconductors below the superconducting transition temperature (T_c) is outlined. The literature review shows that to date there is no the unambiguous interpretation of this experimentally observed fact. According to the recognized concepts, the thermal resistance $W(T)$ (the inverse of thermal conductivity) is directly proportional to the square of the coefficient of thermal expansion (TEC), i.e., to the thermal deformation of the lattice determined by the anharmonicity of atomic vibrations. Such representations do not take into account the peculiarities of thermal conductivity behavior at inversion of anharmonicity sign. In HTSCs, in which there are no generalized charge excitations, the heat resistance is determined mainly by the contribution of the deformation potential of phonon scattering on phonons (W_p). Based on experimental data for a large number of nonmetals, we have found that the ratio W_p to the thermodynamic complex, which is the product of TEC per temperature, is a constant W^* at each equilibrium state. The value W^* is the characteristic (limiting) for each material thermal resistance, which in the case of sign inversion is different for the region of positive and negative values of TEC. Then in the region of negative TEC we should expect a decrease of W below the value determined by the contribution from scattering at the boundaries, i.e., an increase in thermal conductivity. On samples of monocrystalline silicon of different sizes we have shown that $W(T)$ falls sharply at the temperature of inversion of the TEC sign, and then decreases with the violation of a smooth course.

Note that in any conductor the lattice deformation leads to both the excitation of charges and their relaxation. At the same time, in loosely packed structures, deformations associated with the removal and approach of atoms, resulting from doping, lead to the transition from a dielectric to the state of a conductor and even a superconductor. Taking into account the self-consistency of the lattice deformation with the changes occurring in the electronic subsystem, the issues related to the

inversion of the sign of anharmonicity become particularly relevant in the creation of materials with a given conductivity and superconductivity.

For HTSCs, as well as for many weakly packed structures, the inversion of the sign of the TEC below T_c and directly at the transition point is characteristic, for example, for magnesium diboride. Based on these facts, the report substantiates the following criteria for the transition of materials to the «thermal superconductivity» state: in the absence of the boundary effect, the values of the strain potential should be close to zero, or it acquires a negative sign. Such criteria have were formulated earlier by us also for the case of electronic superconductivity, including in a magnetic field.

This work was supported by State assignment FZNZ-2025-0003.

References

1. *V.L. Ginzburg*, JETP Letters **49**(1), 50-51 (2010).

Relation of anomalies of temperature dependences of resistance with thermal deformation of the YBCO lattice

D.K. Palchaev[1], A.E. Rabadanova[1], V.S. Efimchenko[2], S.Kh.Gadzhimagomedov[1], Zh.Kh. Murlieva[1], S.V. Simonov[2]

[1] Dagestan State University, Makhachkala, Russia; e-mail: dairpalchav@mail.ru,
[2] Institute of Solid State Physics, of RAS, Chernogolovka, 142432, Russia

The results of direct measurements of $\rho(T)$ and temperature deformation of lattice parameters of microcrystalline sample YBCO in normal and superconducting states are presented. The temperature dependences of the derivatives of resistivity at the superconducting transition, show a jump with a positive deviation from zero. The lattice deformation occurs with a decrease in volume up to T_c and a sharp increase at this temperature, in the absence of a magnetic field. The changes in the deformation of the lattice parameters at T_c occur with inversion of sign. It is shown that in the normal state there is a linear correlation between the temperature coefficients of electrical resistivity and thermal deformation of the lattice parameters with a correlation coefficient of at least 0.98. The results of these studies allow us to present a possible scenario of the material transition to the superconducting state.

On the basis of the study of correlation of temperature dependences of resistance and thermal expansion coefficient (TEC), the nature of the formation of the deformational potential of electron scattering on phonons in materials whose conductivity varies from values characteristic of classical metals to HTSC has been established. This allows us to quantitatively describe the temperature dependence of the phonon resistance ($\rho(T)$) of classical conductors from ~0 K to their melting temperature. This result can be explained equally well both within the Drude-Bloch and Maxwell's concepts. Although in them the resistance is inversely and directly proportional respectively to the relaxation time of charge excitations. In metals, $\rho(T)$ is linearly related to the product of TEC – $\alpha_V = dV(T)/V(T)dT$ on the temperature. In intermetallides and HTSC there is a direct or inverse correlation of temperature coefficients of electrical resistance (TCR) – $\alpha_\rho = d\rho(T)/\rho(T)dT$ and TEC within the limits of existence of any of the considered phases. Knowledge of the nature of the established deformation potential allows us to assume its determining role in the formation of the superconductivity effect in the framework of the BCS theory.

We report the results of direct measurements of $\rho(T)$ and thermal strain of lattice parameters of a microcrystalline $YBa_2Cu_3O_{7-\delta}$ (YBCO) sample, with two pre-dominant superconducting phases (DCPs), in normal and superconducting co-states. The temperature dependences of the resistivity derivatives for each of these phases at 90.5 K and 87 K, respectively, show jumps with positive deviation from zero. The lattice deformation occurs with a decrease in volume up to T_c=90.5 K and T_c=87 K and of sharp it increase (striction) at these temperatures, in the absence of a magnetic field. The TEC changes of all lattice parameters at T_c for DCPs occur with sign inversion. It is shown that there is a linear correlation between the temperature coefficients of electrical resistivity (TCR) and TEC below (forward) and above (reverse) the transition temperature to the pseudogap state (~160 K) with a correlation coefficient of at least 0.98. As a result of

doping with oxygen atoms, the YBCO lattice is deformed with weakening of directionality and saturation of covalent bonding (with the local of charge excitations). This is evidenced by the transition of YBCO from a dielectric to a conductor state. The generalization of local charge excitations throughout the volume obviously occurs as a result of the observed lattice compression at approach to T_c up to the volume value corresponding to 0K. High values of the lattice elasticity at such a volume and the principle of detailed equilibrium promote pairing of charge excitations generalized over the volume – ordering in the electronic subsystem. The fact of this ordering follows from the fact that the value of the entropy difference in T_c is zero, so the work on the observed growth (jump) of the volume at this temperature occurs at the expense of a decrease in internal energy. The ordering in the electronic subsystem is accompanied by the appearance of a superconducting gap at the Fermi level as a result of a corresponding sharp decrease in the value of the Fermi wave vector associated with the volume change.

This work was supported by State assignment FZNZ-2025-0003.

Features of Josephson vortex system in a flux-flow regime in electron doped HTSC

M. Popov[1], T. Charikova[1], V. Neverov[1], N. Shelushinina[1], A. Ivanov[2]

[1] M.N. Mikheev Institute of Metal Physics, Ural Branch, Russian Academy of Sciences, 18, S. Kovalevskoy St., Ekaterinburg, 620108, Russia,
[2] National Research Nuclear University MEPhI, Moscow, 115409, Russia

The current-voltage (I-V) properties along the c axis on $Nd_{2-x}Ce_xCuO_4/SrTiO_3$ epitaxial films (110) with x = 0.145, 0.15 were investigated. For all the samples it has been established that the I-V characteristics exhibit several resistive branches. The power dependence of the tunneling I-V characteristics $U \sim I^{0.75}$ indicates the non-monotonicity of the d-wave order parameter in electron-doped HTSCs.

The current-voltage (*I–V*) properties along the c axis on $Nd_{2-x}Ce_xCuO_4/SrTiO_3$ epitaxial films (110) with x = 0.145, 0.15 were investigated. For all the samples it has been established that the *I–V* characteristics exhibit several resistive branches, which correspond to the resistive states of individual Josephson junctions [1, 2]. The results confirm the idea of a tunneling mechanism between the CuO_2 layers (superconductor – insulator – superconductor junction) for the investigated $Nd_{2-x}Ce_xCuO_4$ compound. The power dependence of the tunneling *I–V* characteristics $U \sim I^{0.75}$ indicates the non-monotonicity of the d-wave order parameter in electron-doped HTSCs, which is associated with the features of the Fermi surface in the region of optimal doping (x = 0.15) and with the coexistence of superconductivity and fluctuations of antiferromagnetic spin excitations [3].

The *c*-axis flux-flow magnetoresistance on the magnetic field parallel to CuO_2 layers shows a well-defined step structure (Fig. 1).

It is shown that in the region of a free flow of Josephson vortices, the structure is periodic with a period of $\Delta B \sim \Phi_0/(\lambda_{ab}\lambda_c)$. It is essential that the magnetic penetration depths in the ab-plane (λ_{ab}) and along the *c*-axis (λ_c) determine the sizes of the Josephson vortices in the Lawrence-Doniach model for an anisotropic layered superconductor [4].

The work was carried out within the framework of the state assignment of the Ministry of Science and Higher Education of the Russian Federation for the IMP UB RAS using the equipment of the Collaborative Access Center «Testing Center of Nanotechnology and Advanced Materials» of the IMP UB RAS.

References

1. *R. Kleiner, et al*., Phys. Rev. Lett. **68**, 2394–2397 (1992).
2. *A.A. Yurgens*, Supercond. Sci. Technol., **13**, R85–R100 (2000).
3. *T. B. Charikova, et al.*, Solid State Communications **394**, 115723 (2024).
4. *W.E. Lawrence and S. Doniach*, Theory of Layer-Structure Superconductors (Keigaku, Tokyo, 1971).

Multilayer multicomponent superconducting systems based on FeAs

I.R. Shein, N.S. Pervakov, I.A. Nekrasov

Institute of Electrophysics, Ural Branch of RAS, 620016, Yekaterinburg, Russia,
Lebedev Phisical Institute RAS, 119991, Moscow, Russia

We discuss the features of the electronic band structure, charge configurations, phase stability and interatomic interactions obtained by methods of the first-principles band theory. In particular, the oxygen-free compounds $MCa_2Fe_4As_4F_2$ (where M = K, Rb, Cs) and compounds with oxygen $Ba_3Sc_2A_2As_2O_5$, $Ba_4Sc_2A_2As_2O_6$ and $Ba_4Sc_3A_2As_2O_8$ (where A = Fe, Ni) are considered. It is shown that the substitution of Fe atoms for Ni atoms leads to a significant rearrangement of electronic configurations and changes in physical properties.

The discovery of superconducting properties in a large number of FeAs-based layered phases with sufficiently large critical transition temperatures has initiated many works, in which both theoretical and experimental results of various properties of these superconductors are presented. In the present communication we discuss the features of the electronic band structure, charge configurations, phase stability and interatomic interactions obtained by methods of the first-principles band theory. In particular, the oxygen-free compounds $MCa_2Fe_4As_4F_2$ (where M = K, Rb, Cs) and compounds with oxygen $Ba_3Sc_2A_2As_2O_5$, $Ba_4Sc_2A_2As_2O_6$ and $Ba_4Sc_3A_2As_2O_8$ (where A = Fe, Ni) are considered. It is shown that the substitution of Fe atoms for Ni atoms leads to a significant rearrangement of electronic configurations and changes in physical properties.

The work was supported by the RNF project № 25-12-00418.

(RTS) SUPERCONDUCTIVITY AT HIGH PRESSURES. ROUTES TO «ROOM» TEMPERATURE SUPERCONDUCTIVITY AT ATMOSPHERIC PRESSURE

Plenary

Progress in approaching room temperature superconductivity in hydrides

Viktor Struzhkin[1,2], Dmitrii Semenok[3],
Di Zhou[3], Ivan Troyan[4], Ho-kwang Mao[1,2,3]

[1] Center for High Pressure Science and Technology Advanced Research (HPSTAR), Shanghai,
[2] Shanghai Key Laboratory of Material Frontiers Research in Extreme Environments (MFree), Shanghai Advanced Research in Physical Sciences (SHARPS), Pudong, Shanghai 201203, China,
[3] Center for High Pressure Science and Technology Advanced Research (HPSTAR), Beijing,
[4] Shubnikov Institute of Crystallography, RAS, Moscow

The experimental evidence of high T_c values in superhydrides is derived mostly from resistivity studies under very high pressure. In our report we present an overview of some of the recent Meissner effect studies in this new family of superconductors, as well as critical considerations of the technique in the literature. We will also present our measurements of magnetic susceptibility by improved techniques in several superconducting superhydrides, including LaH_x (x~12) with T_c near 270-280 K and La-Sc ternary hydride with record high critical temperatures.

The discovery of near-room-temperature superconductivity in hydrogen-rich ("superhydride") materials has sparked tremendous excitement in the scientific community, offering the tantalizing possibility of revolutionary advances in energy transmission, magnetic levitation, and quantum computing. However, the initial reports of high critical temperatures (T_c) in these systems–particularly in lanthanum hydrides (LaH_x) and ternary hydrides–have been met with both enthusiasm and skepticism, as the evidence for superconductivity has relied heavily on resistivity measurements under extreme pressures, with limited direct confirmation via the Meissner effect. Given the profound implications of room-temperature superconductivity, it is crucial to rigorously verify these claims through complementary magnetic susceptibility measurements, which provide definitive proof of superconductivity through the expulsion of magnetic fields.

In this work, we present a comprehensive overview of Meissner effect studies in superconducting superhydrides, critically assessing the methodologies employed in the literature and their limitations. We report advanced magnetic susceptibility measurements on several high-T_c hydrides, including LaH_x (*x* ~ 12) with (T_c) near 270–280 K and a La-Sc ternary hydride exhibiting record-breaking critical

temperatures. Our experimental approach employs two innovative techniques: (1) a "single-coil" method for sensitive detection of the Meissner response and (2) a "Lenz lens" technique for probing high-frequency magnetic susceptibility in the RF range (tens to hundreds of MHz). Furthermore, we extend the single-coil method to estimate the lower critical field (H_{c1}) in $LaH_{10\pm x}$, revealing exceptionally high values that suggest an extremely short magnetic penetration depth–consistent with strong superconductivity.

While these findings provide compelling support for superconductivity in superhydrides, further refinement of these techniques is necessary to resolve outstanding questions regarding their validity and sensitivity under high-pressure conditions. Future studies will focus on optimizing measurement protocols, expanding the range of probed hydride compositions, and exploring the interplay between crystal structure, stoichiometry, and superconducting properties. Success in these endeavors will not only solidify the case for room-temperature superconductivity in hydrides but also pave the way for the development of next-generation superconducting technologies operating under practical conditions.

Invited

Superconductivity in Hydrides at Nearly Room Temperature

Ivan Troyan[1], Dmitrii Semenok[2], Andrei Sadakov[3], Anna Ivanova[1], Kirill Pervakov[3], Vladimir Pudalov[3], Viktor Struzhkin[4]

[1] A.V. Shubnikov Institute of Crystallography of the Kurchatov Complex of Crystallography and Photonics, Moscow 119333, Russia
[2] Center for High Pressure Science & Technology Advanced Research, Beijing, 100193, China
[3] V.L. Ginzburg Center, P.N. Lebedev Physical Institute, Moscow, Russia
[4]Center for High Pressure Science and Technology Advanced Research (HPSTAR), Shanghai

The discovery of superconductivity at megabar pressures in hydrogen sulfide (H3S), then in metal polyhydrides, starting with binary (LaH_{10}, etc.) and ending with ternary (including $(La,Y)H_{10}$, etc.), revolutionized the field of condensed matter physics. These discoveries not only set a record for the critical superconducting temperature, T_c=250-260K. More importantly, they demonstrate the capabilities of the electron-phonon pairing mechanism and refute a number of previously proposed limitations on the electron-phonon coupling constant. This talk reviews the major experimental findings in the field of hydride superconductivity [1-5], such as (i) the isotope effect, (ii) temperature- and magnetic field resistivity dependences, (iii) upper critical field temperature dependence, (iv) the influence of magnetic and non-magnetic impurities on T_c, and (v) magnetic field shielding. The available experimental data for all hydrides provides evidence for the singlet-type pairing, electron-phonon pairing mechanism, and strong coupling regime. The normal state properties of hydrides were found to be non-trivial and quite different from the conventional Fermi liquid behavior.

References

1. *D.V. Semenok, I.A. Troyan, A.V. Sadakov, et al*., Adv. Materials **34**, 2204038 (2022).
2. *I.A. Troyan, D.V. Semenok, A.G. Ivanova, A.V. Sadakov, Di Zhou, A.G. Kvashnin, I.A. Kruglov, O.A. Sobolevskiy, M.V. Lyubutina, D.S. Perekalin, T.Helm, S.W. Tozer, M. Bykov, A.F. Goncharov, V.M. Pudalov, I.S. Lyubutin*, Adv. Science **10** (30), 2303622 (2023).
3. *D.V. Semenok, I.A. Troyan, A.G. Ivanova, A.G. Kvashnin, I.A. Kruglov, M.Hanfland, A.V. Sadakov, O.A. Sobolevskiy, K.S. Pervakov, I.S. Lyubutin, K.V. Glazyrin, N.Giordano, D.N. Karimov, A.L. Vasiliev, R.Akashi, V.M. Pudalov, A.R. Oganov*, Materials Today **48**, 18-28 (2021).
4. *I.A. Troyan, D.V. Semenok, A.V. Sadakov, I.S. Lyubutin, V.M. Pudalov*, ZhETF **166**, 74 (2024).
5. *D.V. Semenok, A.V. Sadakov, D. Zhou, et al.*, Mater. Today Phys. **49**, 101595 (2024).
6. *D.V. Semenok, I.A. Troyan, Di Zhou, A.V. Sadakov, K.S. Pervakov, O.A. Sobolevskiy, A.G. Ivanova, M.Galasso, F.G. Alabarse, W. Chen, C. Xi, T. Helm, S. Luther, V.M. Pudalov, V.V. Struzhkin*, Adv. Funct. Materials (2025). https://doi.org/10.1002/adfm.202504748.

Oral

Superconductivity in Ca-Y-H at high pressures

M.A. Grebeniuk, G.M. Shutov, D.O. Poletaev, A.R. Oganov

Skolkovo Institute of Science and Technology,
Skolkovo, 30c1 Bolshoi boulevard, Moscow, 121205, Russia

This study explores calcium-yttrium-hydrogen ternary hydrides as candidates for near-room-temperature superconductivity under high-pressure conditions. Using evolutionary structure prediction (USPEX) and density functional theory (DFT), we identify thermodynamically stable phases such as P-6m2–$CaYH_{18}$, which exhibits critical temperatures T_c of 324–348 K at 400 GPa (λ =3.25, where λ is the electron-phonon coupling constant). Hydrogen-rich polyhedral frameworks (e.g., interconnected CaH_9 and YH_9 units) enhance T_c by strengthening phonon-mediated electron interactions. At 350 GPa, P-6m2–$CaYH_{18}$ achieves λ =3.461, yielding T_c=313–336 K. Other stable configurations, including Imm2–CaY_3H_{36} (T_c=258–279 K at 300 GPa) and Imm2–Ca_3YH_{36} (T_c=263–286 K at 300 GPa), further highlight the role of structural motifs in optimizing superconducting properties. These results underscore the potential of ternary hydride design for achieving ambient-condition superconductivity through extreme-pressure engineering.

Superconductivity at ambient conditions remains one of the most intriguing frontiers in condensed matter physics. Since the discovery of superconductivity in Hg by Kamerlingh Onnes in 1911, researchers have pursued materials exhibiting zero electrical resistance at technologically accessible temperatures. Recent breakthroughs in hydrogen-rich superconductors, such as H3S (203 K at 155 GPa) and LaH10 (250 K at 160 GPa), have reignited interest in compressed hydrides as potential room-temperature superconductors. However, binary systems often require high pressures (>150 GPa) to achieve near-ambient Tc, motivating systematic exploration of ternary compositions that might stabilize hydrogen-rich materials at lower pressures.

This work addresses this challenge through computational screening of the Ca–Y–H ternary system, leveraging evolutionary crystal structure prediction (USPEX) combined with first-principles density functional theory (DFT). Our methodological pipeline integrates:

Structure prediction: Evolutionary algorithm searches in USPEX identify low-energy configurations across pressure range 100–400 GPa.

Thermodynamic analysis: Convex hull construction quantifies phase stability, including zero-point vibrational energy corrections from finite-displacement phonon calculations (Phonopy).

Electronic characterization: Band structures and density of states (DOS) are calculated using projector-augmented wave potentials in VASP with PBE and AM05 functionals.

Superconductivity assessment: Electron-phonon coupling (λ) and critical temperatures are computed via density functional perturbation theory (Quantum ESPRESSO), followed by isotropic Migdal-Eliashberg formalism for clathrate-like phases.

Key discoveries include three dynamically stable ternary architectures emerging above 300 GPa:

P-6m2–CaYH18: This arrangement features interconnected CaH9 and YH9 polyhedra. With λ=3.287 at 300 GPa, Eliashberg solutions yield T_c=293–314 K, increasing to 324–348 K at 400 GPa despite slight λ reduction (λ=3.25).

Imm2–CaY3H36 shows moderate T_c=258–279 K (λ=2.631) at 300 GPa.

Pmm2–Ca3YH36 achieves T_c=263–286 K (λ=2.389) at 300 GPa. Pressure-dependent trends reveal critical insights:

Synergistic cation effects: Mixed Ca/Y lattices outperform binary hydrides by optimizing charge transfer – yttrium stabilizes complex polyhedral geometries at CaH_9.

Our results establish Ca–Y–H as a model system for exploring ternary hydride superconductivity, demonstrating that multi-component alloying enables fine-tuning of electronic structure and phonon spectra toward practical room-temperature operation. Future experimental validation of these predicted phases could accelerate development of next-generation superconducting materials for lossless power transmission and quantum computing applications.

Direct prediction of Eliashberg spectral function with Euclidean neural networks

A.G. Kvashnin, M.M. Lukanov, M. Grebenyuk

Skolkovo Institute of Science and Technology,
Bolshoi Blv. 30, Building 1, Moscow 121205, Russian Federation

Application of density functional theory for calculations of Eliashberg spectral function of metal hydrides under pressure is time consuming and computationally expensive. Here we use the Euclidean neural networks to predict the Eliashberg spectral functions of hydrides in the Ca-Y-H system.

Hydrogen-rich hydrides attract great attention due to recent theoretical [1] and then experimental discovery of record high-temperature superconductivity in H_3S (T_C = 203 K at 155 GPa [2]). Since that time many different hydride systems were computationally predicted and experimentally synthesized [3–7].

Computationally new hydrides are studied using density functional theory which is the traditional and standard instrument for investigating. The most computationally expensive part is the calculation of the Eliashberg spectral function, which requires significant computational resources. This significantly limits the possibility of large-scale screening of new high-temperature hydrides among predicted ones or during the computational search for new crystal structures. Another drawback is the impossibility of calculating the Eliashberg spectral function for noncrystalline structures for detailed study of changes in a 2F during phase transition etc.

Here we use the Euclidean neural networks (ENNs) trained on the computational data of known Eliashberg spectral function of binary hydrides to predict the new ones of structures containing hundreds of atoms. The calculation of the Eliashberg function is crucial for determining the impact of phonon contribution to superconductivity. It is noticeable that the Eliashberg function can be obtained both on experimental and theoretical levels, allowing us to explicitly interpret the theoretical models. But the calculation procedure is very time and computer resource consuming, especially if we use methods of quantum chemistry on ab initio level. To solve this problem, approaches based on machine learning methods can be applied for approximation ab initio calculation by means of parametrized functions. Neural networks are a wide range of such parametrized functions, the architecture of which is selected based on specific tasks. Euclidean neural networks (E3NN) [8] are a powerful tool for representing molecular and crystal structures, taking into account the symmetry considerations and equivariancy of some characteristics (for example, velocities, atom forces and others). We used them to predict the Eliashberg function in this work. Using E3NN, we created a framework for predicting the Eliashberg function of binary yttrium hydrides with further determination of superconductivity characteristics.

References

1. *Duan D. et al.* Scientific Reports **4**, 6968 (2014).
2. *Drozdov A.P. et al.* Nature **525**(7567), 73–76 (2015).

3. *Semenok D.V. et al.* Curr. Opin. Solid State Mater. Sci. **7**, 100808 (2020).
4. *Semenok D.V. et al.* Materials Today **48**, 18–28 (2021).
5. *Semenok D.V. et al.* Mat. Today **33**, 36–44 (2020).
6. *Troyan I.A. et al.* Advanced Materials **33**(15), 2006832 (2021).
7. *Boeri L. et al.* J. Phys.: Condens. Matter. **34**, 183002 (2022).
8. *Chen Z. et al.* Advanced Science **8**(12), 2004214 (2021).

Simulation of formation of LaH_{10} under pressure by deep learning potentials

A.G. Kvashnin, V.S. Baidyshev

Skolkovo Institute of Science and Technology, Bolshoi Blv. 30, Building 1, Moscow 121205, Russian Federation

Here we use deep neural network potential to simulate the formation of high-temperature superconductor LaH_{10} during the laser heating. Heating (melting) and cooling (crystallization) of crystal structures in the La-H system is studied. Different hydrogen concentrations are considered to define the optimal conditions for formation of single crystal LaH_{10} at the pressure of 200 GPa.

Hydrogen-rich hydrides attract great attention due to recent theoretical [1] and then experimental discovery of record high-temperature superconductivity in H_3S (T_C = 203 K at 155 GPa [2]). Since that time many different hydride systems were computationally predicted and experimentally synthesized [3–7].

Computationally new hydrides are studied using density functional theory which is the traditional and standard instrument for investigating. However, it is computationally expensive, which significantly limits the possibility of large-scale screening of new high-temperature hydrides or for investigations of new more complex compositions, like ternary or quaternary hydrides.

This limitation can be overcome by using machine learning techniques, namely machine learning of interatomic potentials, to perform large-scale simulations of different properties of hydrides under pressure, except superconductivity.

Here we use deep neural network potential to simulate the formation of high-temperature superconductor LaH_{10} during the laser heating. Heating (melting) and cooling (crystallization) of crystal structures in the La-H system is studied. Different hydrogen concentrations are considered to define the optimal conditions for formation of single crystal LaH_{10} at the pressure of 200 GPa. Training of deep neural network (DNN) potential was performed by using the DP-GEN package [8], which was previously successfully used for training of the potentials and simulations [9].

References

1. *Duan D. et al.* Scientific Reports **4**, 6968 (2014).
2. *Drozdov A.P. et al.* Nature **525**(7567), 73–76 (2015).
3. *Semenok D.V. et al.* Curr. Opin. Solid State Mater. Sci. **7**, 100808 (2020).
4. *Semenok D.V. et al.* Materials Today **48**, 18–28 (2021).
5. *Semenok D.V. et al.* Mat. Today **33**, 36–44 (2020).
6. *Troyan I.A. et al*. Advanced Materials **33**(15), 2006832 (2021).
7. *Boeri L. et al*. J. Phys.: Condens. Matter. **34**, 183002 (2022).
8. *Zhang Y. et al*. Computer Physics Communications **253**, 107206 (2020).
9. *Baidyshev V.S., Tantardini C., Kvashnin A.G*. Sci. Rep. Nature Publishing Group **14**(1), 28678 (2024).

Vortex Phase Transitions in Bismuth Hydride BiH_2 at 169 GPa

A.V. Sadakov[1], V.A. Vlasenko[1], D.V. Semenok[2], Di Zhou[2], I.A. Troyan[3]

[1] P.N. Lebedev Physical Institute, Russian Academy of Sciences, Moscow 119991, Russia,
[2] Center for High Pressure Science and Technology Advanced Research, Bldg. #8E, ZPark, 10 Xibeiwang East Rd, Haidian District, Beijing, 100193, China,
[3] A.V. Shubnikov Institute of Crystallography of the Kurchatov Complex of Crystallography and Photonics (KKKiF), 59 Leninsky Prospekt, 119333 Moscow, Russia

Bismuth hydride BiH_2 is a representative of the new high-temperature superconducting (HTS) materials from the class of binary superhydrides. To date, only a few experimental studies exist on this compound, which demonstrate its transition to the superconducting state. We therefore present the first comprehensive study of the vortex state in bismuth superhydride and determine the key parameters of the vortex phase transition.

Magnetotransport measurements were performed on superconducting bismuth superhydride in magnetic fields up to 5 Tesla within the temperature range from T_c = 42 K (zero-resistance criterion) down to 5 K. The measurements were conducted using the Cryogenics CFMS-16 system. The sample temperature was monitored using a Cernox™ thermometer mounted on the pressure chamber in close proximity to the diamond anvils. Resistance data and current-voltage characteristics were analyzed according to the vortex glass (VG) theory. The so-called vortex glass melting line was determined, and the critical exponents of this phase transition were evaluated. Based on the comparison of the obtained data with theory, conclusions were drawn regarding the dimensionality of the vortex state in this system. A phase diagram was constructed, and comparisons were made with other representatives of the superhydride class.

(SQ) PROPERTIES OF SUPERCONDUCTORS AND QUANTUM/TOPOLOGICAL MATERIALS

Plenary

Inverse melting of the vortex lattice in a superconducting thin film

Pratap Raychaudhuri

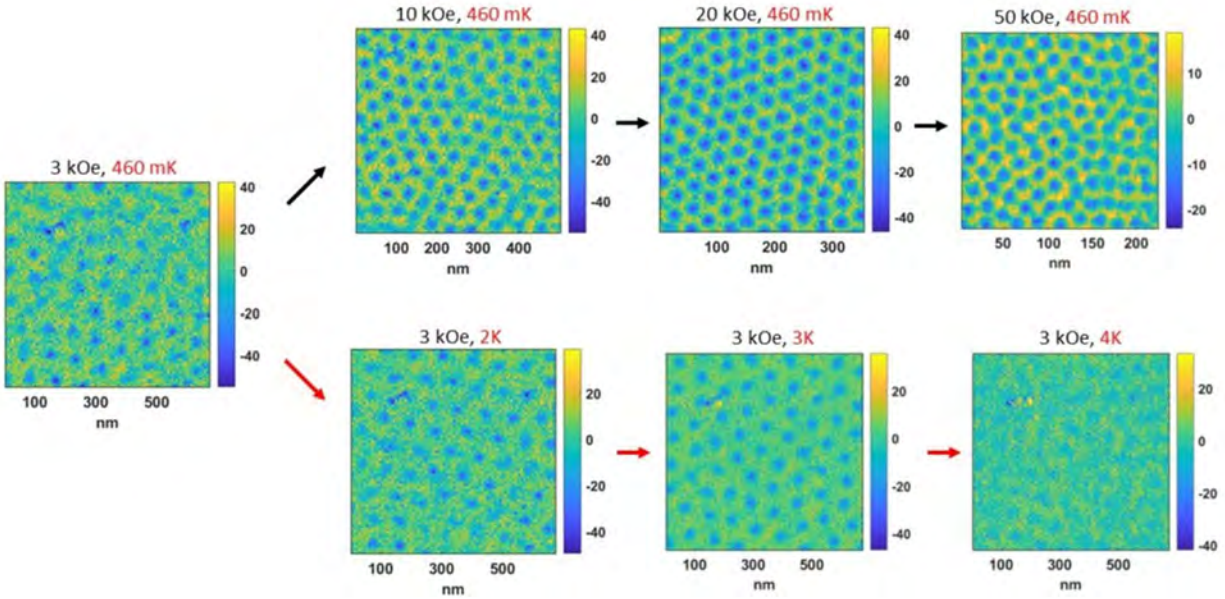

When the temperature is increased, solids melt into a liquid at a characteristic temperature. However, there are rare situations where an increase in temperature can induce a transformation from a liquid to a solid. This phenomenon, inverse melting, is only observed in a handful of systems. Here, analyzing real space images of the vortex state using a scanning tunneling microscope, I will show the observation of inverse melting of the vortex lattice in a 20 nm thick Re_6Zr thin film where the vortices transform from an inhomogeneous liquid to a solid and then back to a liquid when temperature or magnetic field increased. These transformations leave distinct signatures on the magneto-transport properties of the superconductor.

References

1. *R. Duhan, et al.,* Nat. Commun. **16**, 2100 (2025).

Can the noble metals (Au, Ag, and Cu) be superconductors?

Giovanni Alberto Ummarino

Dep. of Applied Science and Technology, Politecnico di Torino,
Corso Duca degli Abruzzi 24, 10129 Torino, Italy,
Dep. of Semiconductor Quantum Electronics, National Research Nuclear University MEPhI,
Moscow Engineering Physics Institute, Kashira Hwy 31, 115409 Moskva, Russia

On the other hand, quantum confinement in thin films has been consistently shown to induce a significant enhancement of the superconducting critical temperature in several superconductors. It is, therefore, an important fundamental question whether ultrathin film confinement may induce observable superconductivity in nonsuperconducting metals. We present a generalization, in the Eliashberg framework, of a BCS theory of superconductivity in good metals under thinfilm confinement. By numerically solving these new Eliashberg-type equations, we find the dependence of the superconducting critical temperature on the film thickness L. This parameter-free theory predicts a maximum increase in the critical temperature for a specific value of the film thickness, which is a function of the number of free carriers in the material. Exploiting this fact, we predict that ultrathin films of gold, silver, and copper of suitable thickness could be superconductors at low but experimentally accessible temperatures. We demonstrate that this is a fine-tuning problem where the thickness must assume a very precise value, close to half a nanometer.

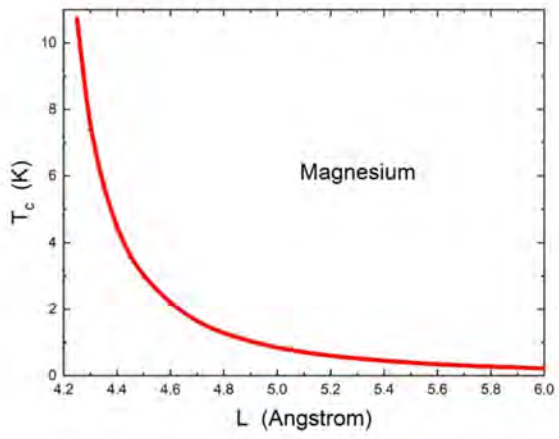

Finally we applied the same method to magnesium and found a significantly higher critical temperature than that of noble metals.

References

1. *Giovanni Alberto Ummarino and Alessio Zaccone*, Physical Review Materials **8**, L101801 (2024).
2. *Giovanni Alberto Ummarino and Alessio Zaccone*, Condensed Matter **10**, 17 (2025).

Invited

Fermi Surface Topology and High-Order van Hove Singularities in $Sr_3Ru_2O_7$

D. Efremov

Topological transitions of the Fermi surface, known as Lifshitz transitions, can give rise to van Hove singularities (VHSs). These occur when the electronic density of states diverges. These singularities are a key driver of electronic instabilities and correlated phases in quantum materials. In this talk, we explore how VHSs manifest in three systems: single-layer ruthenate (Sr_2RuO_4), bilayer ($Sr_3Ru_2O_7$) and twisted graphene-based moiré superlattices.

In twisted bilayer and trilayer graphene, VHSs can be engineered by adjusting the twist angle, resulting in both conventional and higher-order singularities. These features lead to strong correlations and emergent phases, such as superconductivity and correlated insulators. It is believed that the proximity of the Fermi level to a VHS enhances the superconducting critical temperature in Sr_2RuO_4. In $Sr_3Ru_2O_7$, tuning through a VHS using a magnetic field gives rise to a metamagnetic quantum critical endpoint and electronic nematicity. This makes it a canonical example of quantum critical behaviour driven by Fermi surface topology.

Gapless and gapped vortex bound states in higher-order topological superconductors

A.D. Fedoseev, A.O. Zlotnikov

Kirensky Institute of Physics, Federal Research Center KSC SB RAS

We demonstrate the coexistence of zero-energy vortex modes and Majorana corner modes in a 2D second-order topological superconductor. The model describes an interface between a normal layer supporting the topological insulating phase and a superconducting layer. We show that the gapless vortex modes can appear in the superconducting state with a vortex if the bulk energy spectrum of the normal state has Dirac cones. The number of pairs of such vortex modes corresponds to the number of Dirac cones. If the normal layer is in the state of a topological insulator, then the vortex modes become gapped.

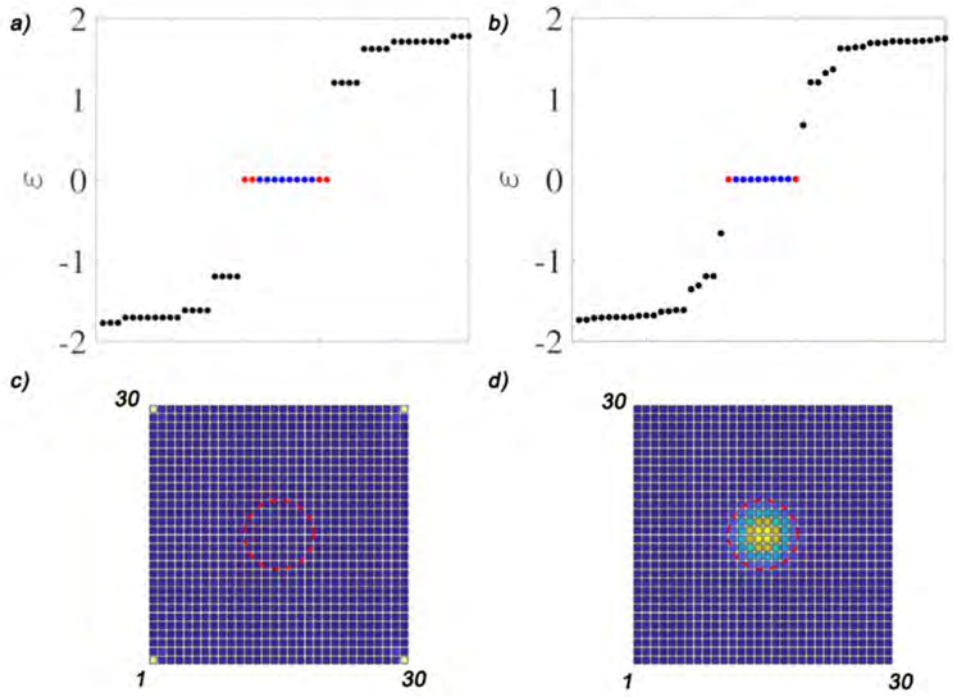

The concept of higher-order topological insulators (HOTIs) gained significant attention in 2017 [1, 2], though analogous phenomena had been predicted earlier in systems such as ^{3}He-B [3] and 3D first-order topological insulators (FOTI) under a magnetic field [4]. Shortly afterward, the framework of higher-order topology was extended to superconductors, leading to the proposal of higher-order topological superconductors (HOTSCs) [5].

In higher-order topological systems, both bulk and edge states are gapped, while topologically protected gapless excitations emerge at higher-order boundaries– specifically, at corners in 2D systems and at corners/hinges in 3D systems. Notably, in 2D HOTSCs, these states manifest as Majorana corner modes (MCMs), which

exhibit zero energy and obey non-Abelian exchange statistics, making them promising candidates for quantum computation via braiding protocols [6]. Proposed realizations of HOTSCs include hybrid structures combining FOTIs with superconductors, first-order topological superconductors (FOTSCs) under a magnetic field, nanowire-based systems (such as Rashba nanowires and magnetic chains), superconductor-altermagnet/noncollinear magnet heterostructures, and $FeTe_{0.55}Se_{0.45}$ (see reviews [7, 8]).

In FOTSCs, a well-established correspondence exists between Majorana zero modes localized at boundaries and those bound to vortex cores [9]. However, this edge-vortex correspondence may break down in HOTSCs. While HOTSCs inherently possess a gapped edge spectrum – suggesting gapped vortex modes from the FOTSC perspective – recent studies have demonstrated the coexistence of MCMs and zero-energy vortex modes in certain HOTSCs [10, 11].

In this work, we study the interplay between gapped/gapless vortex modes (VMs) and MCMs in a 2D HOTSC model comprising a spin-orbit-coupled normal layer interfaced with a superconducting layer. Typically, such a normal layer is modeled as a topological insulator with a gapped bulk and gapless edges, where superconducting pairing induces a Dirac mass at the edges, stabilizing the HOTSC phase [12]. VMs are gapped in such a case. Here, however, we focus on scenarios where the normal layer hosts one or two Dirac cones in the bulk spectrum. Superconducting pairing opens a gap in both bulk and edge spectra, yet unlike the previous case, this regime supports either single-pair or double-pair zero-energy VMs alongside MCMs. The double-pair case features two pairs of zero-energy states per vortex core, whereas the single-pair case hosts only one such pair. The number of pairs of such VMs corresponds to the number of Dirac cones. We demonstrate that the reason for formation of zero-energy VMs in our model is the same as on the superconducting surface of FOTI [13]. The found zero-energy VMs remain robust across a broad parameter space, including variations in chemical potential, spin-orbit coupling, and pairing amplitudes. However, we explicitly show how they become gapped upon tuning other parameters, such as an energy offset for different orbitals, next-nearest-neighbor hopping parameter, and anisotropic (along x and y axes) nearest-neighbor hopping parameters on a square lattice.

Figures (a) and (b) display the energy spectra of a square-shaped HOTSC with a vortex located at the center, illustrating double-pair (a) and single-pair (b) vortex modes (red dots), alongside Majorana corner modes (blue dots). The spatial profiles of MCMs and VMs are shown in panels (c) and (d), respectively.

We further examine how VMs interact with edges and MCMs when the vortex approaches the boundary. Key findings include: (i) VMs can be gapped by sufficient defects (e.g., system edges); (ii) hybridization between vortex and corner modes opens a gap for the excitation energy of both modes; (iii) the vortex core itself – even without zero-energy modes – breaks time-reversal symmetry, destabilizing Majorana corner Kramers pairs and inducing their hybridization when the vortex gets near a corner. The key results have been presented in Ref. [14].

The influence of orbital and Zeeman effects under a magnetic field on zero-energy modes will be also discussed for the present model.

The work was supported by Russian Science Foundation (project No. 24-22-20088, https://rscf.ru/en/project/24-22-20088/) and Krasnoyarsk Regional Fund of Science.

References

1. *W.A. Benalcazar, B.A. Bernevig, and T.L. Hughes*, Science **357**, 61 (2017).
2. *F. Schindler, A.M. Cook, M.G. Vergniory et al*., Science Advances **4**, eaat0346 (2018).
3. *G.E. Volovik*, Jetp. Lett. **91**, 201 (2010).
4. *M. Sitte, A. Rosch, E. Altman, and L. Fritz*, Phys. Rev. Lett. **108**, 126807 (2012).
5. *J. Langbehn, Y. Peng, L. Trifunovic et al*., Phys. Rev. Lett. **119**, 246401 (2017).
6. *T.E. Pahomi, M. Sigrist, and A.A. Soluyanov*, Phys. Rev. Research **2**, 032068(R) (2020).
7. *A.O. Zlotnikov, M.S. Shustin, and A.D. Fedoseev*, J. Supercond. Nov. Magn. **34**, 3053 (2021).
8. *Y.-B. Yang, J.-H. Wang, K. Li, and Y. Xu*, J. Phys.: Condens. Matter **36**, 283002 (2024).
9. *J. Alicea, Y. Oreg, G. Refael et al*., Nature Physics **7**, 412 (2011).
10. *M. Kheirkhah, Z. Yan, and F. Marsiglio*, Phys. Rev. B **103**, L140502 (2021).
11. *Z. Zhang, Z. Wu, C. Fang et al*., Nature Communications **15**, 7971 (2024).
12. *S.V. Aksenov, A.D. Fedoseev, M.S. Shustin, and A.O. Zlotnikov*, Phys. Rev. B **107**, 125401 (2023).
13. *A.L. Rakhmanov, A.V. Rozhkov, and F. Nori*, Phys. Rev. B **84**, 075141 (2011).
14. *A.D. Fedoseev, A.O. Zlotnikov*, arXiv: 2411.14831, accepted to Phys. Rev. B (2025).

Superconducting proximity effects in nodal and nodeless altermagnets

Lun-Hui Hu

Zhejiang University

The recent discovery of altermagnets, a groundbreaking class of antiferromagnets with nonrelativistic spin-split bands, has opened a frontier in quantum materials research. In this talk, we discuss how these exotic states reshape superconducting proximity effects, revealing phenomena with profound implications for quantum technologies. Focusing on 2D altermagnet/superconductor junctions, we present two paradigmatic cases. (i) Nodal Altermagnets (e.g., d-wave RuO_2): Here, spin-split Fermi surfaces with symmetry-protected nodes induce oscillating spin-singlet Cooper pairs with finite momentum, which is a spatial interference phenomenon reminiscent of Fulde-Ferrell-Larkin-Ovchinnikov states. (ii) Nodeless Altermagnets (100% spin-valley polarized): Remarkably, the absence of nodes triggers a complete suppression of spin-singlet pairs, instead stabilizing robust spin-triplet superconductivity, which is a rare feat without conventional magnetic frustration. We further demonstrate how 0-pi phase transitions in these systems are governed by distinct quantum knobs.

Observation of the Leggett collective plasma oscillation and the spin exciton in two-gap superconductors using SNS-Andreev spectroscopy

S.A. Kuzmichev[1,2], T.E. Kuzmicheva[2], M.M. Korshunov[3], B.M. Bulychev[4], S.I. Krasnosvobodtsev[2], N.D. Zhigadlo[5], I.V. Morozov[4]

[1] Faculty of Physics, Lomonosov Moscow State University, 1, Leninskiye Gory 119991, Moscow, Russia
[2] Lebedev Physical Institute of the RAS, 53, Leninsky Ave., 119991 Moscow, Russia
[3] Kirensky Institute of Physics, SB RAS, 60, Akademgorodok, 660036, Krasnoyarsk, Russia
[4] Department of Chemistry, Lomonosov Moscow State University, 1, Leninskiye Gory 119991, Moscow, Russia
[5] Crystmat company, 11 Zschokkestrasse, 8037 Zuric, Switzerland

In this talk we summarize the pioneer experimental observation of two collective resonant effects realized in two-gap superconductors (SC) and enhanced by the tunneling. We revisit the Leggett plasma mode (caused by small fluctuations of the phase difference between two SC condensates) in $(Mg,Al)B_2$ superconductor firstly observed by Prof. Ya.G. Ponomarev et al. in 2002, and consider the spin exciton (originated from a presence of a spin-resonance peak in the imaginary part of dynamic spin susceptibility) in SC oxypnictides of the 1111 family observed by us since 2017. We compare and discuss the features of the experimental observation of these effects in the Andreev spectra of planar "break-junctions''.

MgB_2 becomes the first-ever-known two-gap SC, where two weakly interacting SC condensates with the distinct coupling energies ($2\Delta_\sigma$ and $2\Delta_\pi$) develop in the SC state below T_c. As early as in 1966 A.J. Leggett predicted that collective plasma oscillation caused by small fluctuations of the phase difference between two SC condensates ("internal Josephson effect in the k-space"), develop in two-gap superconductors [1]. The main result of the pioneer work [1] re-derived by Sharapov *et al*. [2] specially for MgB_2 is that the square of the massless term of the oscillation frequency $\omega_0^2 = \omega_L^2$ ($k \to 0$) at T=0 is proportional to $\Delta_\sigma(0)\cdot\Delta_\pi(0)$. For the first time, Leggett plasmon in MgB_2 was experimentally detected in our laboratory by supervision of Prof. Ya.G. Ponomarev in 2002 [3, 4].

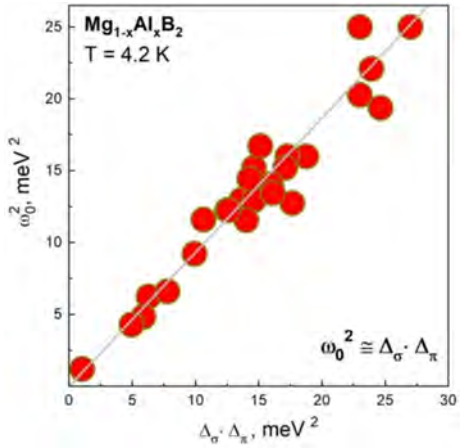

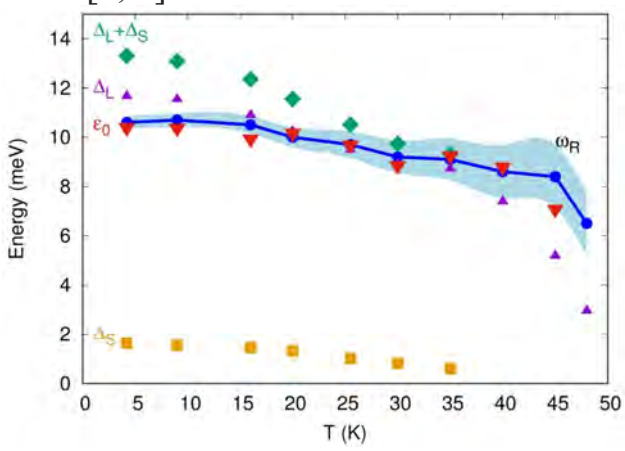

For the iron-based superconductors, the Fermi surface consists of hole barrels near the Gamma point and electron barrels near the M point of the Brillouin zone, which are coupled by a nesting vector Q. As a result, within the framework of 5-orbital spm-model, the imaginary part of the dynamic spin susceptibility Im[χ(Q,ω)] shows a spin-resonance peak at position $\omega_R(0)<[\Delta_L(0)+\Delta_S(0)]$ [5].

At 4.2 K, using a planar "break-junction'' technique we formed Josephson SIS and Andreev SnS nanojunctions (*S* is superconductor, *n* – thin normal metal, *I* – insulator). In *I*(*V*) and *dI*(*V*)/*dV* characteristics of the tunneling junctions, we reproducibly observed a fine structure caused by a resonant interaction of Josephson supercurrent with a bosonic mode (in SIS regime) or emission of bosons during multiple Andreev reflections (in SnS regime), and determined the energy of the bosonic mode [6].

Here we revisit our experimental results on Leggett plasma mode detection in disordered MgB_2 and electron doped (Mg,Al)B_2 compounds in a wide range of critical temperatures $T_c \approx 13.5-40$,K. In average, ω_0 does not exceed the small SC gap $2\Delta\pi(0)$ value and reaches $\omega_0 \approx 4-5$ meV in MgB_2 with $T_c \approx 40$ K. Summarizing the data obtained by Josephson and Andreev spectroscopies, we demonstrate almost linear $\omega_0^2(\Delta_\sigma \cdot \Delta_\pi)$ dependence and an absence of a "dirty limit'' transition within this T_c range [3, 4] and present here an experimental temperature dependence of the Leggett plasma mode $\omega_0(T)$.

In the *dI*(*V*)/*dV*-spectra of SnS-junctions formed in Gd(O,F)FeAs and (Sm,Th)OFeAs oxypnictides (the 1111 family) with various doping degree and maximum $T_c \approx 50$ K [7-10], as well as in $(K,Na)_xFe_{2-y}Se_2$ selenides with $T_c \approx 26$ K, the observed fine structure was attributed to an interaction with a spin exciton. In particular, multiple emission of up to 4 bosons was detected in (Sm,Th)OFeAs [9]. At $T_{ll}T_c$, the spin exciton energy epsilon0 was not exceed the indirect SC gap $\Delta_L(0)+\Delta_S(0)$ in the oxypnictides, and $2\Delta(0)$ in single-gap selenides. In the 1111-compounds, under doping variation, epsilon0 was scaled with T_c together with $\Delta_L(0)$ and $\Delta_S(0)$ [7, 9].

The experimental temperature dependence $\varepsilon_0(T)$ agrees well with the $\omega_R(T)$ dependence calculated within the spm model [10].

The work is supported by RSF project no. 22-72-10082P. The authors are forever grateful to Prof. Ya.G. Ponomarev, S.N. Tchesnokov and E.P. Khlybov. We also thank L.G. Sevastyanova, O.V. Kravchenko and K.P. Burdina for the provided MgB_2 and (Mg,Al)B_2 samples during 2001-2007. We thank P.I. Arseev and N.K. Fedorov for several fruitful discussions during 2009-2013.

References

1. *J. Leggett*, Prog. Theor. Phys. **36**, 901 (1966).
2. *G. Sharapov*, *et al*., Eur. Phys. J. B **30**, 45 (2002).
3. *G. Ponomarev*, *et al*., Bulletin of the V. Tarasov Center of Chemotronics of Glass **2**, 139 (2002); arXiv: cond-mat/2301.02929 (2023); Proceedings of the 1st international conference «Fundamental problems of HTS» (FPS), 234 (2004).

4. *G. Ponomarev*, *et al*., arXiv: cond-mat/0303640 (2003); Solid State Comm. **129**, 85 (2004); JETP Lett. **85**, 46 (2007).
5. *M. Korshunov et al*., Phys. Rev. B **94**, 094517 (2016).
6. *A. Kuzmichev, T.E. Kuzmicheva*, Low. Temp. Phys. **42**, 1008 (2016).
7. *T.E. Kuzmicheva*, *et al*., Physics-Uspekhi **57**, 819 (2014); Phys. Rev. B **95**, 094507 (2017).
8. *S.A. Kuzmichev, T.E. Kuzmicheva*, JETP Lett. **105**, 671 (2022).
9. *S.A. Kuzmichev*, *et al*., EPL **119**, 17007 (2017).
10. *M.M. Korshunov*, *et al*., Materials **15**, 6120 (2022).

Effect of substitution on the structural and superconducting properties of $Ba(Ag_{1.8-x}TM_x)Bi_2$ (TM=Cu, Au)

I.V. Morozov[1], E.O. Rakhmanov[1,2], A.I. Shilov[1,2],
T.E. Kuzmicheva[2], S.A. Kuzmichev[2], A.Yu. Levakhova[2],
V.A. Grinenko[3], S.Yu. Gavrilkin[2]

[1] Lomonosov Moscow State University, Dept. of Chemistry, 119991, Moscow, Russia,
[2] V.L. Ginzburg Centre for High-Temperature Superconductivity and Quantum Materials P.N. Lebedev Physical Institute of the Russian Academy of Sciences (LPI RAS), 53, Leninsky Ave., 119991 Moscow, RUSSIA,
[3] Tsung-Dao Lee Institute, 1 Lisuo Road, Pudong New Area, 201210, Shanghai, China

Recently, a new superconductor $BaAg_{1.8}Bi_2$ with a previously unknown variant of the monoclinically distorted structure $CaBe_2Ge_2$ was obtained and its superconducting properties were studied [1, 2]. This is a type II superconductor with a relatively high critical temperature of 5.4 K for bismuthides of composition 122. It turned out that this structural type allows partial substitution of gold and copper in the d-metal position. In this report, we will show how such a substitution affects the structural and superconducting properties.

Recently, a new superconductor $BaAg_{1.8}Bi_2$ with a previously unknown variant of the monoclinically distorted structure $CaBe_2Ge_2$ was obtained and its superconducting properties were studied [1, 2]. This is a type II superconductor with a relatively high critical temperature of 5.4 K for bismuthides of composition 122. It turned out that this structural type allows partial substitution of gold and copper in the d-metal position. In addition, substitution of barium by an alkali metal is also possible. Single-crystal X-ray diffraction studies showed that Cu and Au atoms preferentially replace silver atoms decorating a flat square network of bismuth atoms in a fluorite-like layer. Specific susceptibility measurements showed that substitution by copper and especially by gold suppresses superconductivity, while substitution by an alkali metal (Rb) leads to an increase in the superconducting transition temperature. The report will discuss the reasons for such an influence of substitution on superconducting properties.

References

1. *Shilov, Andrey I., et al.* Crystals **14**(2), 155 (2024).
2. *Sadakov, A.V., et al*. JETP Letters **121**(1), 72-77 (2025).

Peculiarities of the electronic structure of multilayer high-T_c pnictides

I.A. Nekrasov, I.R. Shein, K.A. Pervakov

Institute of Electrophysics, Ural Branch, Russian Academy of Sciences, Yekaterinburg, 620016, Russia,
Lebedev Physical Institute, Russian Academy of Sciences, Moscow, 119991, Russia

The interest in the family of high-temperature superconducting iron-based pnictides and chalcogenides discovered in 2008 prompted the search for new families of chemical and/or structural analogs of these systems. One such family is materials with complete substitution of Fe by other chemical elements. Another direction for creating such materials is to change the types of atoms between FeAs layers or even to introduce additional layers of rather diverse geometry and chemical composition. It has also been found that it is possible to grow superconducting materials consisting of layers belonging to different families of high-T_c pnictides. In this paper we present a review of the electronic spectra of various recently synthesized High-T_c systems such as 1144, 12442, 32225, 42226, 43228 and their comparative analysis.

This work was supported by the RNF project No. 25-12-00418.

Spatially-resolved dynamics of the amplitude Schmid-Higgs mode in disordered superconductors

P.A. Nosov, E.S. Andriyakhina, I.S. Burmistrov

Department of Physics, Harvard University, Cambridge, Massachusetts 02138, USA,
Freie Universitat Berlin, Dahlem Center for Complex Quantum Systems and Fachbereich Physik, Arnimallee 14, Berlin, 14195, Germany,
L.D. Landau Institute for Theoretical Physics, acad. Semenova av. 1-a, Chernogolovka, 142432, Russia

We investigate the spatially-resolved dynamics of the collective amplitude Schmid-Higgs (SH) mode in disordered s-wave superconductors and fermionic superfluids. By analyzing the analytic structure of the zero-temperature SH susceptibility in the complex frequency plane, we find that when the coherence length greatly exceeds the mean free path: (i) the SH response at fixed wave vectors exhibits late-time oscillations decaying as $1/t^2$ with frequency 2Δ, where Δ is the superconducting gap; (ii) sub-diffusive oscillations with a dynamical exponent $z=4$ emerge at late times and large distances; and (iii) spatial oscillations at fixed frequency decay exponentially, with a period that diverges as the frequency approaches 2Δ from above. When the coherence length is comparable to the mean free path, additional exponentially-decaying oscillations at fixed wave vectors appear with frequency above 2Δ. Furthermore, we show that the SH mode induces an extra peak in the third-harmonic generation current at finite wave-vectors. The frequency of this peak is shifted from the conventional resonance at Δ, thereby providing an unambiguous signature of order parameter amplitude dynamics.

We investigate the spatially-resolved dynamics of the collective amplitude Schmid-Higgs (SH) mode in disordered s-wave superconductors and fermionic superfluids. By analyzing the analytic structure of the zero-temperature SH susceptibility in the complex frequency plane, we find that when the coherence length greatly exceeds the mean free path: (i) the SH response at fixed wave vectors exhibits late-time oscillations decaying as $1/t^2$ with frequency 2Δ, where Δ is the superconducting gap; (ii) sub-diffusive oscillations with a dynamical exponent $z=4$ emerge at late times and large distances; and (iii) spatial oscillations at fixed frequency decay exponentially, with a period that diverges as the frequency approaches 2Δ from above. When the coherence length is comparable to the mean free path, additional exponentially-decaying oscillations at fixed wave vectors appear with frequency above 2Δ. Furthermore, we show that the SH mode induces an extra peak in the third-harmonic generation current at finite wave-vectors. The frequency of this peak is shifted from the conventional resonance at Δ, thereby providing an unambiguous signature of order parameter amplitude dynamics. The results are published in [1].

References

1. *P.A. Nosov, E.S. Andriyakhina, I.S. Burmistrov*, arxiv: 2409.11647.

Electronic states emerging at magnetic domain walls on the surface of semiconductors with band structure topology

I.P. Rusinov, V.N. Men'shov, E.V. Chulkov

The Lebedev Physical Institute of the Russian Academy of Sciences Moscow, Russia,
The Lebedev Physical Institute of the Russian Academy of Sciences Moscow, Russia,
Saint-Petersburg State University, Saint-Petersburg, Russia

We demonstrate that electron scattering at a magnetic domain wall on the surface of magnetic topological insulators, as well as magnetic semiconductors with Rashba splitting, can lead to the emergence of both topologically protected and trivial one-dimensional electronic states.

The band topology of materials with strong spin-orbit coupling, combined with various types of magnetic ordering, forms a rich platform for studying unusual quantum phenomena with potential applications in spintronic devices. In this work, we demonstrate that electron scattering at a magnetic domain wall on the surface of magnetic topological insulators, as well as magnetic semiconductors with Rashba splitting, can lead to the emergence of both topologically protected and trivial one-dimensional electronic states.

The modification of the surface electronic structure under the influence of magnetization with complex textures is studied using both analytical and numerical methods. One-dimensional states arising at Ising, Bloch, and Néel domain walls are described. In the case of a magnetic topological insulator, it is shown that the domain wall generates a bound state with a linear spectrum within the exchange gap. The velocity, spin polarization, and spatial localization of this state depend on the mutual orientation of magnetizations in the domains. Notably, on a surface with a strong Rashba effect, the domain wall induces the formation of a one-dimensional resonant state, whose characteristics are similar to those of the bound state in the topological insulator case, with the key difference being a slight spectral broadening.

It should be noted that in the case of a magnetic topological insulator, in addition to the topologically protected state with linear dispersion, there may exist Volkov-Pankratov gap states, the number and characteristics of which depend on the type and width of the domain wall. Similarly, on a surface with a strong Rashba effect, in addition to the gapless resonant state, gapped resonant states may appear on a wide domain wall.

We qualitatively assess the contribution of one-dimensional electron states at domain walls to magnetoresistance and the anomalous Hall effect in the intrinsic antiferromagnetic topological insulator $MnBi_2Te_4$ and in the diluted magnetic semiconductor with giant Rashba splitting $Bi_{1-x}(V,Mn)_xTeI$.

The realization of stable spin-polarized electronic states associated with domain walls of various configurations opens a new approach to creating data storage, writing, and reading devices based on materials with topological band structure features.

Disorder in $FeSe_{1-x}S_x$ ($0 \leq x \leq 1$) superconducting crystals

Aifeng Wang, Lijun Wu, Qianheng Du, Muntaser Naamneh, Walber Hugo Brito, AM Milinda Abeykoon, Wojciech Radoslaw Pudelko, Jasmin Jandke, Yu Liu, Nicholas C. Plumb, Gabriel Kotliar, Vladimir Dobrosavljevic, Milan Radovic, Yimei Zhu, Valentin Ivanovski, Qianheng Du, Andreas Baum, Eli Stavitskii, Nenad Lazarevic, Klaus Attenkofer, Zoran Popovic, Cedomir Petrovic

Condensed Matter Physics and Materials Science Department, Brookhaven National Laboratory, Upton, New York 11973, United States,
Department of Physics, Ben-Gurion University of the Negev, Beer-Sheva 84105, Israel,
Departamento de Física, Universidade Federal de Minas Gerais, 30123-970 Belo Horizonte, Minas Gerais, Brazil,
National Synchrotron Light Source II, Brookhaven National Laboratory, Upton, New York 11973, United States,
Swiss Light Source, Paul Scherrer Institut, CH-5232 Villigen, Switzerland,
Department of Physics and National High Magnetic Field Laboratory, Florida State University, Tallahassee, Florida 32306, United States,
Center for Solid State Physics and New Materials, Institute of Physics Belgrade, University of Belgrade, 11080 Belgrade, Serbia,
Vinca Institute of Nuclear Sciences, University of Belgrade, Belgrade 11001, Serbia,
Walther Meissner Institut, Bayerische Akademie der Wissenschaften, 85748 Garching, Germany

Here we show that changes in superconducing Tc in S-doped FeSe are correlated with disorder, as seen in average and local structure as well as in thereby induced scattering rates. High-temperature resisitivity for strong disorder exceeds Mott limit and provides an example of violation of Mooij law, which is dominant when disorder is added in Drude/Matthiassen's regime in all materials.

Connections among crystal chemistry, disorder and critical temperature T_c have been at the forefront of superconductivity, one of the most widely studied phenomena in physics, chemistry and materials science alike. In Fe-based superconductors T_c correlates with the average anion height above the Fe plane, i.e. with the geometry of the $FeAs_4$ or FeCh4 (Ch = Te, Se, S) tetrahedron. By synthesizing $FeSe_{1-x}S_x$ ($0 \leq x \leq 1$) single crystal alloys with atomic defects we find that their T_c is not correlated with the anion height of other Fe superconductors. Instead, changes in $T_c(x)$ and tetragonal-to-orthorombic (nematic) transition $T_s(x)$ on cooling are correlated with Bragg plane and Fe vibrations disorder in direction orthogonal to Fe planes and thereby induced scattering rates $(1/\tau)(x)$ [1, 2]. The disorder stems from deformed $Fe(Se,S)_4$ tetrahedra with different Fe-Se and Fe-S bond distances. Moreover, high-temperature metallic resistivity in the region of strong disorder exceeds Mott limit and provides an example of the strong violation of Matthiesen's rule and Mooij law which is known to be a dominant when adding moderate disorder past the Drude/Matthiassen's regime in all materials [2]. Scattering mechanism of Mott limit-exceeding resistivity is unrelated to phonons and arises for strong Se/S atom disorder in tetrahedral surrounding of Fe. Observations point to intricate connection between nanostructure details and unconventional scattering mechanism, possibly related to charge-nematic or magnetic spin fluctuations [2, 3].

References

1. *Aifeng Wang et al*., Inorg. Chem. **61**, 11036 (2022).
2. *Aifeng Wang et al*., Nano Lett. **22**, 6900 (2022).
3. *Yu Liu et al*., Nanoscale Horizons **10**, 59 (2023).

Josephson Tunneling and Thermoelectric Transport in Exfoliated Cuprate Flakes

Ding Zhang

Department of Physics, Tsinghua University, Beijing, China

The recent decade has seen impressive progresses in techniques for handling delicate two-dimensional materials. Here, we apply these techniques to study bismuth-based cuprate compounds that are archetypes of high temperature superconductors.

We revisit the Josephson effect in *c*-axis twisted cuprates by employing the van der Waals stacking technique and fabricate junctions out of mechanically exfoliated thin flakes of both $Bi_2Sr_2CaCu_2O_{8+x}$ (Bi-2212) [1][2] and $Bi_2Sr_{2-x}La_xCuO_{6+y}$ (Bi-2201) [3]. In these junctions with their atomically structures clarified, we still observe pronounced Josephson tunneling across the twisted boundary at different twist angles. The latest progresses include the observation of ac Josephson effect with both integer and fractional Shapiro steps, as well as the on-demand realization of superconducting diode effect. We discuss implications of these results in the context of the recent proposal of exotic pairing in the twisted cuprates.

We also develop a method to measure the thermoelectric properties of ultrathin Bi-2212 flakes (1.5 to 2 unit-cell thick). We realize samples from optimal doping to the extremely underdoped situation with unprecedentedly high homogeneity. The samples show prominent Nernst effect both in the vortex liquid regime and the superconducting fluctuation regime. By combining the thermoelectric and magneto-transport results, we are able to extract the vortex entropy. Interestingly, the vortex entropy decreases exponentially with reduced doping. These results challenge the current understanding of vortex dynamics [4].

References

1. *Y. Zhu, M. Liao, Q. Zhang, H.-Y. Xie, F. Meng, Y. Liu, Z. Bai, S. Ji, J. Zhang, K. Jiang, R. Zhong, J. Schneeloch, G. Gu, L. Gu, X. Ma, D. Zhang, and Q.-K. Xue*, Phys. Rev. X **11**, 031011 (2021).
2. *Y. Zhu, H. Wang, Z. Wang, S. Hu, G. Gu, J. Zhu, D. Zhang, and Q.-K. Xue*, Phys. Rev. B **108**, 174508 (2023), Editors' Suggestion.
3. *H. Wang, Y. Zhu, Z. Bai, Z. Wang, S. Hu, H.-Y. Xie, X. Hu, J. Cui, M. Huang, J. Chen, Y. Ding, L. Zhao, X. Li, Q. Zhang, L. Gu, X. J. Zhou, J. Zhu, D. Zhang, and Q.-K. Xue*, Nat. Commun. **14,** 5201 (2023).
4. *S. Hu, J. Qiao, G. Gu, Q.-K. Xue, and D. Zhang*, Nat. Commun. **15**, 4818 (2024).

Josephson current and imperfections in a planar topological junction

Yuriy Makhlin

Condensed-matter physics, HSE

Current experiments demonstrate physics which may be associated with Majorana zero modes and other low-energy states in planar topological Josephson junctions. This includes vanishing critical current at integer flux values under applied magnetic field. These modes are expected to show peculiar properties and may be used in prospective topological quantum computations. We analyze the influence of imperfections on the supercurrent measured in long Josephson junctions, including inhomogeneities of the junction shape and width in linear and Corbino geometry, as well as of the ends of a linear junction.

Oral

Flux-flow instability in superconducting single-crystal TiN films caused by heated electrons

E. Baeva[1,2], N. Titova[1], S. Saha[3], A. Boltasseva[3], S. Bogdanov[4,5,6], S. Evlashin[7], V. Shalaev[3], G. Goltsman[1,2], and A. Kolbatova[2]

[1] HSE University, 101000 Moscow, Russia,
[2] Moscow Pedagogical State University, 119435 Moscow, Russia,
[3] Birck Nanotechnology Center and Elmore Family School of Electrical and Computer Engineering, Purdue University, IN 47907 West Lafayette, USA,
[4] Department of Electrical and Computer Engineering, University of Illinois at Urbana-Champaign, IL 61801 Urbana, USA ,
[5] Holonyak Micro and Nanotechnology Lab, University of Illinois at Urbana-Champaign, IL 61801 Urbana, USA,
[6] Illinois Quantum Information Science and Technology Center, University of Illinois at Urbana-Champaign, IL 61801 Urbana, USA ,
[7] Skolkovo Institute of Science and Technology, Moscow, Russia

We study flux-flow instability (FFI) in a single-crystalline superconducting titanium nitride (TiN) film exhibiting negligible volume pinning. From the maximum velocity of the flux flow, we extract the inelastic energy relaxation time t_E by various dynamics FFI models. Comparing our results with t_E obtained from other experimental methods, we conclude that energy relaxation into the vortex core occurs not due to quasiparticles jumping out of the vortex core but due to a change in the quasiparticle's temperature.

Vortex dynamics in superconducting films and devices is an important subject for both fundamental research and practical applications of superconductivity [1]. Investigating the limiting value of the vortex velocity v^* is essential for the generation of ultrasound, magnons, microwave radiation, and estimation of the energy relaxation time t_E [1]. When the time for vortex passage becomes less than t_E, quasiparticles in the vortex core, are unable to relax and flux-flow instability (FFI) occurs. Depending on the relaxation mechanism, two models can be used to describe FFI in weakly-pinned superconductors: the Larkin-Ovchinnikov (LO) model and the Kunchur model. In the LO model [1], it is assumed that the electron-electron relaxation occurs more slowly than electron-phonon relaxation ($t_{ee} >> t_{eph}$), leading to dissipation of vortex energy occurs through the escape of quasiparticles from the vortex core. The LO model has been recently shown to facilitate the search for materials potentially suitable for superconducting microstrip single-photon detectors (SMSPDs) [2]. By measuring v^*, it is possible to obtain the value of t_E via the LO model, and therefore evaluate the evolution of the hot spot that occurs when a photon is absorbed by SMSPD. However, superconducting films commonly used in SMSPD are strongly disordered and, hence, ($t_{ee} << t_{eph}$) regime should be considered. Meanwhile, the Kuchur model, which is the opposite of the LO model, is typically not considered when calculating.

In this study, we investigated the phenomenon of flux-flow instability in a 12-nm thick single-crystal titanium nitride (TiN) film with negligible vortex pinning. Based on previous research [3], we found that the condition occurs in TiN at the critical temperature, making it difficult to choose a theoretical model to explain FFI. We measured the critical current density in TiN wires of various widths, we identified the onset of the flux-flow instability. From these measurements, and obtained different estimates of the vortex velocity and t_E, depending on the theoretical approach used. By comparing the estimated values of t_E to the electron-phonon relaxation time t_{eph}, we conclude that energy dissipation within the vortex core is in agrees to the Kuchur model i.e. is described by increase in the temperature of quasiparticle temperature.

This work was supported by the RSF grant № 24-72-10105.

References

1. *O.V. Dobrovolskiy*, Encyclopedia of Condensed Matter Physics (Elsevier, 2024), p. 735–754.
2. *Y.P. Korneeva et al.*, Supercond. Sci. Technol. **34**(8), 084001 (2021).
3. *E. Baeva et al.*, Phys. Rev. B **110**, 104519 (2024).

Theory of subgap states in helical magnetic atom chains on the surface of a superconductor

A.A. Bespalov, A.O. Baranov

Institute for Physics of Microstructures, Russian Academy of Sciences, 603950 Nizhny Novgorod, GSP-105, Russia,
National Research Lobachevsky State University of Nizhny Novgorod, 603022 Nizhny Novgorod, Russia

Within the formalism of the Bogoliubov-de Gennes equations, we develop a theory of subgap states in helical magnetic atom chains placed on the surface of a superconductor. The surface is modeled as a rigid wall for electrons. We find that single surface Yu-Shiba-Rusinov states and Majorana modes at the edges of the chain are more localized than their counterparts induced by magnetic atoms in the bulk of a superconductor. The energy of the topological edge mode is proportional to the inverse square of the length of the chain. We also study the topological phase diagram of the system and find that for a planar spin helix up to three Majorana modes can coexist on one edge of the chain.

One of the proposals to implement Majorana fermions in condensed matter systems is based on combining conventional superconductivity with a Zeeman field with helical structure [1, 2]. Such structure may appear due to different reasons in magnetic atom chains in contact with a superconductor. There is evidence that both spiral magnetic order and Majorana edge modes have been observed in Fe atom chains on top of superconducting Re [3, 4]. Previous analytical studies of such systems considered models where the magnetic atoms were placed in the bulk of the superconductor, which does not reflect the geometry of real experiments. More realistic models with magnetic atoms on the surface of a superconductor have been studied numerically (see [5, 6] and some other papers), and the obtained results are mostly material-specific. The present works aims to develop an analytical theory of subgap states in magnetic atom chains on the surface of a superconductor to highlight qualitative differences between such states in the bulk and surface geometries.

We consider a magnetic atom chain with helical magnetic order placed on top of an s-wave superconductor, which occupies the region $z>0$. We calculate the subgap quasiparticle spectrum using the Bogoliubov-de Gennes equations, assuming that the sample surface is a rigid wall for electrons. A magnetic impurity in the bulk is typically modeled as an s-wave scatterer. However, near the surface spherically symmetric scattering is suppressed, and we have to consider scattering with angular momentum $l=1$. We find that for a single impurity the local density of states ν corresponding to a Yu-Shiba-Rusinov state is proportional to z^2/r^4 (with superimposed Friedel-like oscillations) near the surface, where r is the distance from the impurity. This implies that the measured density of states should be proportional to r^{-4} – note that for a bulk Yu-Shiba-Rusinov state, the falloff law is $\nu \propto r^{-2}$.

In a chain, Yu-Shiba-Rusinov states hybridize and form two Shiba bands. At the edges of the chain, Majorana zero modes (MZMs) can appear. To study their structure, in the limit of large distance between the magnetic atoms we derive a discrete model (similar to [7]), which is formally equivalent to a Kitaev chain. The pairing and hopping amplitudes between sites (atoms) are inversely proportional to the square of the distance between them when this distance is much smaller than the coherence length ξ. As a result, the wave function of a MZM falls off as s^{-2}, where s is the distance from the edge of the chain (however, when s is larger than ξ, the falloff law is exponential). In a finite chain with length L the energy of the topological edge mode composed of two Majoranas is proportional to L^{-2}. Thus, MZMs are more localized, and the energy of the topological mode in a finite chain is generally lower for a chain on the surface of a superconductor as compared to a chain in the bulk [7].

A necessary condition for the existence of MZMs is the presence of a gap in the spectrum of an infinite chain. We demonstrate that this condition is almost certainly satisfied for a planar spin helix. Such spin configuration is also interesting from another point of view: our system then possesses an effective time reversal symmetry (the Bogoliubov-de Gennes equations have real coefficients) and belongs to the Altland-Zirnbauer symmetry class BDI [8]. One-dimensional gapped systems belonging to this class are characterized by an integer topological invariant. We calculated this invariant and found that its absolute value can be as high as three. This means that up to three stable MZMs can coexist on one edge of the chain, provided that the atomic spins are coplanar.

References

1. *M. Kjaergaard, K. Wölms, and K. Flensberg*, Phys. Rev. B **85**, 020503(R) (2012).
2. *I. Martin and A.F. Morpurgo*, Phys. Rev. B **85**, 144505 (2012).
3. *H. Kim, A. Palacio-Morales, T. Posske, L. Rózsa, K. Palotás, L. Szunyogh, M. Thorwart, and R. Wiesendanger*, Sci. Adv. **4**, eaar5251 (2018).
4. *L. Schneider, S. Brinker, M. Steinbrecher, J. Hermenau, T. Posske, M. dos Santos Dias, S. Lounis, R. Wiesendanger, and J. Wiebe*, Nat. Commun. **11**, 4707 (2020).
5. *R. Hess, H.F. Legg, D. Loss, and J. Klinovaja*, Phys. Rev. B **106**, 104503 (2022).
6. *A. Lászlóffy, B. Nyári, G. Csire, L. Szunyogh, and B. Újfalussy*, Phys. Rev. B **108**, 134513 (2023).
7. *A.A. Bespalov*, Phys. Rev. B **106**, 134503 (2022).
8. *C.-K. Chiu, J.C.Y. Teo, A.P. Schnyder, and S. Ryu*, Rev. Mod. Phys. **88**, 035005 (2016).

Density of electronic states, resistivity and superconducting transition temperature in density-wave compounds with imperfect nesting

P.D. Grigoriev[1], A.V. Tsvetkova[2], Ya.I. Rodionov[3]

[1] L.D. Landau Institute of Theoretical Physics, RAS, Chernogolovka, 143423, Russia,
[2] National University of Science and Technology MISIS, Moscow, 119049 Russia,
[3] Institute for Theoretical and Applied Electrodynamics, Russian Academy of Sciences, Moscow, 125412 Russia

We study the effects of imperfect nesting in the density wave (DW) state on various electronic properties within a simple 2D tight-binding model. The discussed model reflects the main features of quasi-1D metals where the DW emerges. We show that a DW with imperfect nesting leads to unusual singularities in the quasiparticle density of states and to a power-law renormalization of the superconducting critical temperature. Our results are derived at arbitrary large antinesting and may help to understand the phase diagram of the wide class of density-wave superconductors. We also compute the conductivity tensor in a wide temperature range, including the DW transition, and obtain a satisfactory agreement with the experimental data on rare-earth trichalcogenides and many other DW materials.

We study the effects of imperfect nesting in a density wave (DW) state on various electronic properties within a strongly anisotropic 2D tight-binding model. The discussed model reflects the main features of quasi-1D metals where the DW emerges. We show that a DW with imperfect nesting leads to unusual singularities in the quasiparticle density of states and to a power-law renormalization of the superconducting critical temperature. Our results are derived at arbitrary large antinesting and may help to understand the phase diagram of the wide class of density-wave superconductors. We also compute the conductivity tensor in a wide temperature range, including the DW transition, and obtain a satisfactory agreement with the experimental data on rare-earth trichalcogenides and many other DW materials.

The interplay between superconductivity (SC) and charge or spin density wave (DW) appears in various strongly-correlated electron systems, including most high-Tc cuprate and iron-based superconductors, $NbSe_2$ [1, 2] and other transition-metal and rare-earth di- and poly-chalcogenides, various organic superconductors and many other materials (for reviews see, e.g., [3–6]).

The DW in metals creates a spatial modulation of the charge or spin density of conducting electrons with the wave vector $\boldsymbol{Q}$ and opens a gap Δ at the Fermi level in the electronic spectrum, which reduces the electron energy [7]. Depending on the electron dispersion $\epsilon(\boldsymbol{k})$ in this metal, two different DW states are possible. When $\epsilon(\boldsymbol{k}) + \epsilon(\boldsymbol{k} + \boldsymbol{Q}) < \Delta$ for all $\boldsymbol{k}$ on the Fermi surface (FS), then the entire FS is covered by the DW gap Δ and the metal becomes a semiconductor in a DW state. In this case a uniform SC on a DW background is hardly possible, but SC may appear via a spatial

segregation with DW, as happens in various materials [8–10]. This SC heterogeneity is visualized by scanning tunneling microscopy [8, 11], by the local diamagnetic probe [12, 13], or detected and analyzed using the resistivity anisotropy measurements [14–20].

The spatially uniform DW-SC coexistence may appear in the case of imperfect FS nesting when $\epsilon(\boldsymbol{k})+\epsilon(\boldsymbol{k}+\boldsymbol{Q}) > \Delta$ for some $\boldsymbol{k}$ at the FS. In this case the metallic conductivity survives in a DW state till $T \to 0$, being anisotropically reduced, e.g., as in various rare-earth three-chalcogenides [21] and many other materials [3– 7]. One could expect an exponential decrease of the superconducting transition temperature T_c in the presence of the DW background even in the imperfect-nesting case, because according to the BCS theory in the weak-coupling regime $T_c \sim \omega_D \exp(-1/gv_F)$ exponentially depends on the electron density of states (DoS) at the Fermi level v_F multiplied by the coupling constant g, with the Debye frequency ω_D in the pre-exponential factor. As the DW opens a gap, at least in some parts of FS, the DoS v_F is reduced by the DW, leading to destructive SC-DW interference [22, 23]. However, usually, one observes a more complicated SC-DW interplay: the superconducting transition temperature T_c is the highest at the quantum critical point (QCP) where the density wave (DW) gets suppressed by some external parameter, such as doping level, pressure, cooling rate [14, 15], disorder [2], etc. The T_c dome-like shape near the DW QCP results from the enhancement of electron-electron (e-e) interaction $g \to g_*(\boldsymbol{Q})$ in the Cooper channel by the critical DW fluctuations, which can be described as the SC vertex renormalization in the language of Feynman diagram technique [24, 25]. Note that this vertex renormalization changes its momentum dependence and may favor the unconventional superconductivity [26–28].

According to the theoretical calculations [24–27] the SC coupling enhancement $g \to g_*(\boldsymbol{Q})$ is not very strong, especially far from the DW QCP, when the DW order parameter Δ is larger than the SC energy gap. On the contrary, the gapped FS area in the DW state is, usually, rather large, as visualized by ARPES measurements in various compounds. How the observed increase of T_c in the presence of the DW, implying the increase of product gv_F, is then possible?

In this work [29] we consider only the second scenario of the uniform DW in the case of imperfect nesting. What is stronger, the SC coupling renormalization $g \to g_*(\boldsymbol{Q})$ or the DoS reduction $v_F \to v_{F*}$ by the DW? The answer to this question dramatically affects the SC transition temperature in the weak-coupling regime.

References

1. *Chao-Sheng Lian, Chen Si, and Wenhui Duan*. Nano Lett., **18**(5): 2924–2929, April 2018.
2. *Kyuil Cho, Kon´czykowski, S. Teknowijoyo, M.A. Tanatar, J. Guss, P.B. Gartin, J.M. Wilde, A. Kreyssig, R.J. McQueeney, A.I. Goldman, V. Mishra, P.J. Hirschfeld, and R. Prozorov*. Nat. Commun., **9**(1): 2796, July 2018.
3. *A.M. Gabovich, A.I. Voitenko, J.F. Annett, and M. Ausloos*. Supercond. Sci. Technol., **14**(4): R1–R27, March 2001.
4. *M. Gabovich, A.I. Voitenko, and M. Ausloos*. Phys. Rep., **367**(6): 583–709, September 2002.

5. *Pierre Monceau*. Phys., **61**(4): 325–581, August 2012.
6. *Jean-Paul Pouget and Enric Canadell*. Reports on Progress in Physics, **87**(2): 026501, January 2012.
7. *George Gru*. Density Waves in Solids. Addison-Wesley Pub. Co., Advanced Book Program, 1994.
8. *V. Kresin, Y. Ovchinnikov, and S. Wolf*. Phys. Rep., **431**(5): 231–259, September 2006.
9. *Arjun Narayanan, Andhika Kiswandhi*, *David Graf, James Brooks, and Paul Chaikin*. Rev. Lett., **112**(14): 146402, April 2014.
10. *Campi, A. Bianconi, N. Poccia, G. Bianconi, L. Barba,G. Arrighetti, D. Innocenti, J. Karpinski, N.D. Zhigadlo, S.M. Kazakov, M. Burghammer, M.V. Zimmermann, M. Sprung, and A. Ricci*. Nature, **525**(7569): 359–362, Sep 2015.
11. *Jennifer E.* Reports on Progress in Physics, **74**(12): 124513, Nov 2011.
12. *Ienari Iguchi, Tetsuji Yamaguchi, and Akira Sugimoto*. Nature, **412**(6845): 420–423, July 2001.
13. *Akira Sugimoto, Ienari Iguchi, Takashi Miyake, and Hisashi*. Japanese Journal of Applied Physics, **41**: L497, May 2002.
14. *A. Gerasimenko, S.V. Sanduleanu, V.A. Prudko- glyad, A.V. Kornilov, J. Yamada, J.S. Qualls, and V.M. Pudalov*. Phys. Rev. B, **89**(5): 054518, February 2014.
15. *Shingo Yonezawa, Claire A. Marrache-Kikuchi, Klaus Bechgaard, and Denis Jerome*. Phys. Rev. B, **97**(1): 014521, January 2018.
16. *A. Sinchenko, P.D. Grigoriev, A.P. Orlov, A.V. Frolov, A. Shakin, D.A. Chareev, O.S. Volkova, and N. Vasiliev*. Phys. Rev. B, **95**(16): 165120, April 2017.
17. *S. Seidov, K.K. Kesharpu, P.I. Karpov, and P.D. Grigoriev*. Phys. Rev. B, **98**(1): 014515, July 2018.
18. *Vladislav D. Kochev, Kaushal K. Kesharpu, and Pavel D. Grigoriev*. Rev. B, **103**: 014519, Jan 2021.
19. *Vladislav D. Kochev, Seidali S. Seidov, and Pavel D. Grigoriev*. Magnetochemistry, **9**(7), 2023.
20. *Pavel Grigoriev, Vladislav D. Kochev, Andrey P. Orlov, Aleksei V. Frolov, and Alexander A. Sinchenko*. Materials, **16**(5), 2023.
21. *A. Sinchenko, P.D. Grigoriev, P. Lejay, and P. Monceau*. Phys. Rev. Lett., **112**: 036601, Jan 2014.
22. *Levin, D.L. Mills, and S.L. Cunningham*. Phys. Rev. B, **10**: 3821–3831, Nov 1974.
23. *A. Balseiro and L.M. Falicov*. Phys. Rev. B, **20**: 4457–4464, Dec 1979.
24. *A. Bychkov, L.P. Gor'kov, and I.E. Dzyaloshinskii*. Sov. Phys. JETP, **23**: 489, 1966.
25. *Yuxuan Wang and Andrey Chubukov*. Rev. B, **88**: 024516, Jul 2013.
26. *Tanaka and K. Kuroki*. Phys. Rev. B, **70**: 060502, Aug 2004.
27. *C. Nickel, R. Duprat, C. Bourbonnais, and N. Dupuis*. Phys. Rev. Lett., **95**: 247001, Dec 2005.
28. *P. Gor'kov and P.D. Grigoriev*. Phys. Rev. B, **75**(2):020507(R), January 2007.
29. *V. Tsvetkova, Ya.I. Rodionov, and P.D. Grigoriev*. Density of electronic states in density-wave compounds with imperfect nesting, arXiv: 2501.00341, Phys. Rev. B (in press, 2025).

Interference of non-equilibrium quasiparticle excitations in a superconductor

A.S. Gursky[1], V.A. Ievleva[1,2], E.F. Pozdnyakova[1,3], D.L. Shapovalov[4], E.A. Sedov[5], A.M. Chekushkin[3], M.A. Markina[3], M.A. Tarasov[3], K.Yu. Arutyunov[3]

[1] National Research University Higher School of Economics
[2] P.N. Lebedev Physical Institute of the Russian Academy of Sciences
[3] V.A. Kotelnikov Institute of Radio Engineering and Electronics of the Russian Academy of Sciences
[4] P.L. Kapitsa Institute for Physical Problems of the Russian Academy of Sciences
[5] Moscow Institute of Physics and Technology

The paper experimentally investigated the coherent component of the current of non-equilibrium quasiparticles injected through a tunnel barrier into a superconductor made of normal metal into a superconducting "fork". Nanostructures can be considered as solid-state analogs of a two-beam optical interferometer. Quasiperiodic dependences of the tunnel current on an external perpendicular magnetic field were obtained, qualitatively indicating the detection of the desired effect. The observation is of fundamental importance: the interference of electrons in a non-equilibrium state was demonstrated.

Relaxation of non-equilibrium quasiparticle excitations in a superconductor, as a rule, requires the presence of an inelastic scattering channel. At sufficiently low temperatures, due to the absence of a phonon mechanism, relaxation times (lengths) can reach extremely large scales. For example, in aluminum, the corresponding scales are in the ~10 μm range [1, 2]. The main hypothesis of the present work, which requires confirmation, is the possibility of experimentally recording the interference of non-equilibrium quasiparticles in a superconductor.

In this work, we studied hybrid nanostructures in the form of a T-shaped electrode made of a normal metal (copper) – a tunnel dielectric layer (aluminum oxide) – a superconducting fork (aluminum), which are solid-state analogs of a two-beam optical interferometer (Fig. 1). Unpaired electrons are injected into the superconductor with energies eV exceeding the superconducting gap. Due to the Aharonov-Bohm magnetic effect, the quasiparticles receive a phase shift proportional to the ratio of the magnetic flux Φ through the area of the loop and the quantum of the magnetic flux $\Phi_0=h/e$. The discovered dependences of the tunnel current I on the perpendicular magnetic field B (Fig. 2) can be associated with the detection of the sought-after effect. The corresponding current-magnetic characteristics I(V=const, B) demonstrate a quasi-Fraunhofer shape: the central maximum at $|B| \leq 1$ mT and weakly distinguishable maxima of higher orders. The dotted curve in Fig. 2 corresponds to a typical distribution of light intensity of a two-slit optical interferometr. The monotonic component of the tunnel current can be associated with partial suppression of the superconducting gap by the magnetic field. The observed effect indicates a new phenomenon: interference of charge carriers in a non-equilibrium state.

The work was supported by the Russian Science Foundation, project 23-72-00018 «Study of non-equilibrium and boundary phenomena in superconducting hybrid nanostructures».

References

1. *Y. Arutyunov, H.P. Auraneva, A.S. Vasenko*, Physical Review B **83**(10), 104509 (2011).
2. *K.Yu. Arutyunov, et al*., Journal of Physics: Condensed Matter **30**, 343001 (2018).

Absence of «fractional ac Josephson effect» in superconducting junctions

M.S. Kalenkov, A.D. Zaikin

I.E. Tamm Department of Theoretical Physics,
P.N. Lebedev Physical Institute, 119991 Moscow, Russia

We develop a microscopic theory of the nonequilibrium Josephson effect in SIS junctions. The scattering matrix of the barrier is assumed to be arbitrary and may include magnetic effects. Using the formalism of the quasiclassical theory of superconductivity, we derive a formally exact expression for the Josephson current under an arbitrary time-dependent voltage. In the limit of a time-independent bias, we obtain a 2π-periodic electric current as a function of the Josephson phase φ, for any form of the scattering matrix. Our result unambiguously rules out the so-called "fractional ac Josephson effect," which implies a 4π-periodic current-phase relation.

In conclusion, while the Andreev bound state picture remains extremely useful in equilibrium, its naive application to nonstationary regimes may lead to qualitatively incorrect conclusions, such as the appearance of a 4π-periodic Josephson effect [5]. A full microscopic treatment is essential to avoid such artifacts.

References

1. *M.S. Kalenkov, A.D. Zaikin*, Phys. Rev. B **110**, 134521 (2024).
2. *D. Averin and A. Bardas*, Phys. Rev. Lett. **75**, 1831 (1995).
3. *D. Averin and A. Bardas*, Phys. Rev. B **53**, R1705 (1996).
4. *A.V. Galaktionov and A.D. Zaikin*, Phys. Rev. B **107**, 214507 (2023).
5. *J. Michelsen, V.S. Shumeiko, and G. Wendin*, Phys. Rev. B **77**, 184506 (2008).

Thermopower and Hall effect in correlated metals and doped Mott-Hubbard insulators: DMFT approximation

E.Z. Kuchinskii, N.A. Kuleeva, M.V. Sadovskii

Institute for Electrophysics, Russian Academy of Sciences, Ural Branch,
Amundsen str. 106, Ekaterinburg 620016, Russia

We present comparative theoretical investigation of thermoelectric power and Hall effect in the Hubbard model within the DMFT approximation for correlated metal and Mott insulator (considered as prototype cuprate superconductor) for different concentrations of current carriers.

We present comparative theoretical investigation of thermoelectric power and Hall effect in the Hubbard model for correlated metal and Mott insulator (considered as prototype cuprate superconductor) for different concentrations of current carriers. Analysis is performed within standard DMFT approximation. For Mott insulator we consider the typical case of partial filling of the lower Hubbard band (hole doping). We calculate the dependence of the Hall coefficient and thermopower on doping level and determine the critical concentration of carriers corresponding to sign change of these quantities A significant temperature dependence of the Hall coefficient and an anomalous dependence of thermopower on temperature (significantly different from linear typical for the usual metals) is obtained. The role of disorder scattering is analyzed on qualitative level. We also perform a comparison of our theoretical results with some known experiments on doping dependence of Hall number in the normal state of YBCO and Nd-LSCO, demonstrating rather satisfactory agreement of theory and experiment. Violation of electron – hole symmetry leads to the appearance of the relatively large interval of band – fillings (close to the half – filling) where thermopower and Hall effects have different signs. We propose a certain scheme allowing to determine the number of carriers from ARPES data and perform semi – quantitative estimate of both thermopower and Hall coefficient using the usual DFT calculations of electronic spectrum.

Electronic structure of the CuO monolayer in the paramagnetic phase considering the Coulomb interactions

I.A. Makarov[1], A.A. Slobodchikov[2], I.A. Nekrasov[2,3],
Yu.S. Orlov[1], L.V. Begunovich[4], M.M. Korshunov[1], S.G. Ovchinnikov[1]

[1] Kirensky Institute of Physics, Federal Research Center KSC SB RAS, 660036, Krasnoyarsk, Russia,
[2] Institute of Electrophysics of the Ural Branch of the Russian Academy of Sciences, 620016, Ekaterinburg, Russia,
[3] P.N. Lebedev Physical Institute of the Russian Academy of Sciences, 119991, Moscow, Russia,
[4] Federal Research Center «Krasnoyarsk Science Center of the Siberian Branch of the Russian Academy of Sciences», 660036, Krasnoyarsk, Russia

It is believed that the main properties of HTSC cuprates are formed in CuO_2 planes. In relatively recent studies [1-3], another type of copper-oxygen layers, CuO monolayers, was synthesized. The crystal structure of CuO monolayers differs from the structure of CuO_2 planes but they have many common characteristics such as atomic composition, electronic configuration, the presence of structural elements in the form of copper atoms separated by oxygen atoms. The similarities between these two systems hint at the possibility of the existence of high-temperature superconductivity in CuO monolayers. Strong electronic correlations (SEC) can play an important role in these compounds. Therefore, the study of the electronic structure of the CuO monolayer taking into account the intra- and interatomic Coulomb interactions is an actual task.

To describe the electronic system of CuO monolayer we use the eight-band p-d model including the copper d_{x2-y2}-, d_{3z2-r2}-, d_{xy}-, d_{xz}-, d_{yz}- and the oxygen p_x-, p_y-, p_z-orbitals. The on-site energies and hopping integrals up to fourth nearest neighbors are obtained within *ab initio* calculations. Five types of Coulomb interactions are taken into account: intra-atomic intra-orbital U_d and inter-orbital V_d interactions, Hund's exchange J_d on copper atoms, intra-atomic interactions on oxygen atoms U_p and interatomic interactions between copper and oxygen atoms V_{pd}. In this work, we will vary the Coulomb parameters to explore all possible types of electronic structure that may exist in the CuO monolayer.

SEC and multiparticle effects are taken into account within the generalized tight-binding (GTB) method [4]. In this method, the entire crystal lattice is divided into separate clusters, the electronic structure is formed by quasiparticle excitations between many-body cluster eigenstates. A transformation in the k-space is firstly proposed to orthogonalize three 2p-orbitals of oxygen atom in the neighboring CuO clusters, whereby the atomic orbitals p_x, p_y, p_z is replaced by the molecular orbitals α, β, γ. It is convenient to work in the hole representation against the background of the completely filled with electrons copper d- and oxygen p-orbitals. The local part of the Hamiltonian for the orbital λ at the site f without hybridization with other orbitals and without Coulomb interactions in the hole representation has the form

$$H_{f\lambda}^{(h)} = \varepsilon_0 - (\varepsilon_\lambda + \widetilde{U}) h_{\lambda f}^{\dagger} h_{\lambda f},$$

where $h_{\lambda f\sigma}$ is the hole annihilation operator, $h_{\lambda f\sigma} = c_{\lambda f\bar{\sigma}}^{\dagger}$ ($c_{\lambda f\bar{\sigma}}^{\dagger}$ is the creation operator of an electron). It is seen that the energy of local state with the unoccupied orbital λ (or one hole) is defined as the energy of completely filled shells ε_0 reduced by the on-site energy ε_λ of an electron removed from the corresponding orbital λ together with all interactions U' in which it participates.

The orbital nature of the excitations forming the conductivity band and the top of the valence band is determined by the orbital nature of the ground zero-, single- and two-hole cluster eigenstates. The probability density distribution of holes over copper and oxygen orbitals in the multiparticle CuO cluster eigenstates is calculated using the exact diagonalization. A map of the orbital type with the maximal probability density distribution of holes in the ground cluster eigenstates is calculated in the space of intra-atomic Coulomb parameters on copper atoms $U'_d=\{U_d,V_d,J_d\}$ and the intra-atomic Coulomb interactions on oxygen atoms $U'_p=\{U_p,V_{pd}\}$. There are two main regions in this map: the region of predominance of the U'_d parameters (holes in the ground states are on d-orbitals) and the region of predominance of the U'_p parameters (the ground state are formed by p-orbitals). Also there is a narrow intermediate region of the mixed pd-states between the regions of d- and p-states.

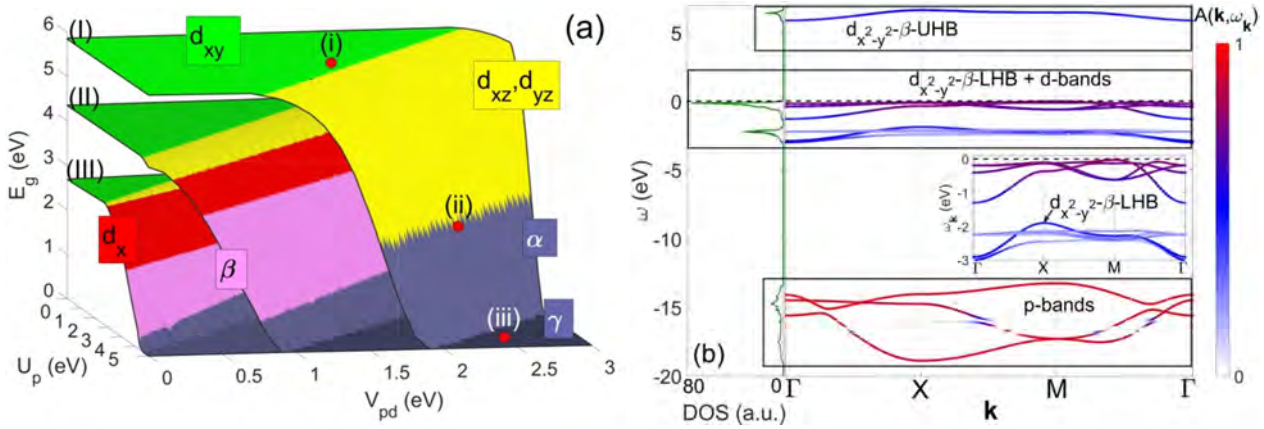

Fig. 1. (a) Dependencies of the band gap E_g for the CuO monolayer in the parameter space U_p-V_{pd} for three fixed sets: (I) U_d=9, V_d=7, J_d=1; (II) U_d=6, V_d=5, J_d=0.5; (III) U_d=4, V_d=3.2, J_d=0.4 eV. The uniformly colored areas of the surfaces with orbital label show the regions of the Coulomb parameters for which this orbital makes a predominant contribution to the states at the top of the valence band. The points (i), (ii) and (iii) show the values of the parameters U_p and V_{pd} at which the band structure will be discussed. (b) Band structure and density of states (DOS) of quasiparticle excitations of the CuO monolayer at U_d=9, V_d=7, J_d=1, U_p=3, V_{pd}=1.5 eV.

The electronic structure is calculated using the equations of motion method for Green's functions within the multiband Hubbard model. The band structure calculations within the model without Coulomb interactions indicates that the CuO monolayer is in a metallic state. The states at the Fermi level are formed by the copper d_{x2-y2}- and oxygen β-orbital, the appearance of d_{xz}- and d_{yz}-states at the Fermi level is possible under the influence of small external influences such as doping or pressure. Taking into account the Coulomb interaction leads to splitting of the band

of the d_{x2-y2} and β-orbitals on the upper and lower Hubbard subbands, the Fermi level falls into band gap between these subbands. The surface of the band gap magnitude supplemented by the orbital type forming the top of the valence band is constructed in the parameter space U_p-V_{pd} (Fig.1a). At Coulomb parameters on oxygen typical for cuprates, the p-states lie deep in the valence band (Fig.1b), the p-d hybridization is weak due to the large gap between the d- and p-states. The band of the d_{xy}-orbitals has the strongest dispersion due to largest d-d hoppings among d-orbitals. As a result, the d_{xy}-band forms the top of the valence band (Fig.1a, green plateau at the surface (I)). The increase in the Coulomb parameters U_p and V_{pd} leads to that the top of the valence band acquires the character of the d_{xz}-d_{yz}-orbitals (Fig.1a, yellow color) and then the p-bands reach to the top of the valence band (Fig.1a, dark blue region). The oxygen p-bands close the band gap and make predominant contribution to the spectral weight of the states near the Fermi level with further increasing the Coulomb interactions U'_p, (Fig.1a, dark blue plateau). Thus, a metallic state is formed again at large Coulomb interactions U'_p.

The study was supported by the grant of the Russian Science Foundation № 25-22-20043, https://rscf.ru/project/25-22-20043/, the grant of the Krasnoyarsk Regional Fund of Science.

References

1. *E. Kano, D.G. Kvashnin, S. Sakai et al*., Nanoscale **9**, 3980 (2017).
2. *K. Yin, Y.-Y. Zhang, Y. Zhou et al*., 2D Mater. **4**, 011001 (2017).
3. *D.G. Kvashnin, A.G. Kvashnin, E. Kano et al*., J. Phys. Chem. C **123**, 17459 (2019).
4. *S.G. Ovchinnikov and I.S. Sandalov*, Physica C **161**, 607 (1989).

Optical conductivity of $(Na_{0.33}K_{0.33}Rb_{0.33})_{0.8}Fe_2Se_2$ single crystals

A.V. Muratov[1], E.O. Rakhmanov[2,1], A.I. Shilov[1],
I.V. Morozov[2], Yu.A. Aleshchenko[1]

[1] P.N. Lebedev Physical Institute of RAS, 119991 Moscow, Russia,
[2] Department of Chemistry, Lomonosov Moscow State University, 119991 Moscow, Russia

The optical properties of $(Na_{0.33}K_{0.33}Rb_{0.33})_{0.8}Fe_2Se_2$ superconducting single crystals with $T_c \approx 30$ K have been studied at the temperatures of 4-300 K in the broad frequency range by IR Fourier-transform spectroscopy and spectroscopic ellipsometry. The real part of the optical conductivity σ_1 was obtained by the Kramers-Kronig transformation of the reflectance $R(\omega)$. The Drude-Lorentz model was applied to describe the conductivity spectra $\sigma_1(\omega)$ at low temperatures and the model parameters (plasma frequencies, scattering rates and oscillator strengths) were obtained.

The Fe-selenide $A_xFe_{2-y}Se_2$ (A = alkaline metal or Tl) system represents a natural composite in which the 122 metallic phase is formed on the border of the 245 antiferromagnetic stripes [1]. At some compositions of the system, this metallic phase exhibits the superconducting (SC) properties with the critical temperature T_c up to 32-33 K.

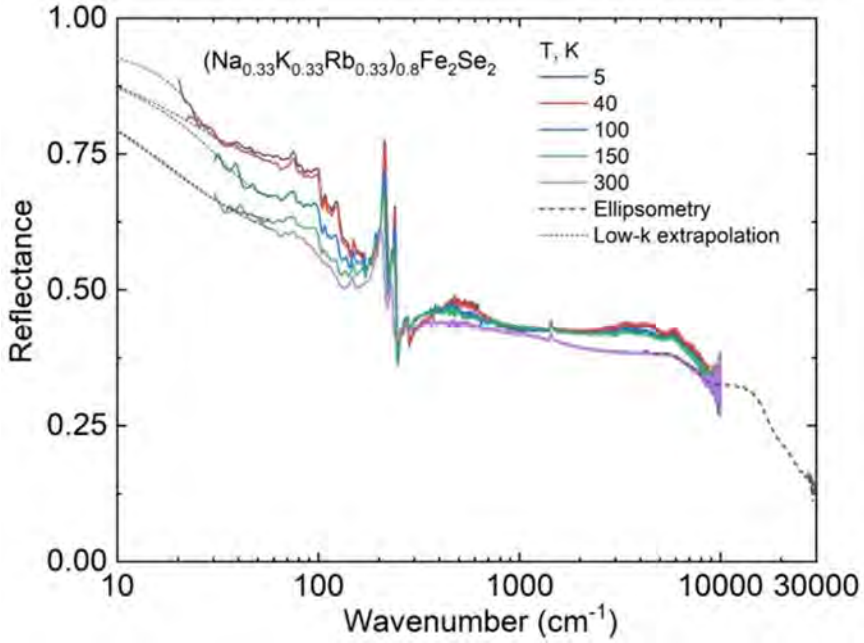

Fig. 1. The reflectance spectra of $(Na_{0.33}K_{0.33}Rb_{0.33})_{0.8}Fe_2Se_2$ single crystals at various temperatures.

We have studied for the first time the optical properties of $(Na_{0.33}K_{0.33}Rb_{0.33})_{0.8}Fe_2Se_2$ single crystals grown using self-flux technique. The composition of the crystals was confirmed by EDX spectroscopy. The critical temperature of the SC transition $T_c \approx 30$ K was determined from the magnetic susceptibility measurements. Infrared spectra at near normal incidence were taken

from the *ab* plane of single crystals using the IFS 125HR (Bruker) Fourier-transform spectrometer in the frequency range of 25-10000 cm^{-1} at temperatures of 4-300 K. An *in situ* aluminum overcoating technique was used to obtain the reflectance $R(\omega)$. The variable-angle spectroscopic ellipsometry (VASE, Woollam) was carried out in the range from 4000 to 30000 cm^{-1}. The reflectance calculated from the directly obtained by ellipsometry refractive indexes and extinction coefficients was used to bind the experimentally measured reflectance from the high-frequency side. The low-frequency extrapolation was based on the Drude model. The real part of conductivity σ_1 was obtained by the Kramers-Kronig transformation of $R(\omega)$.

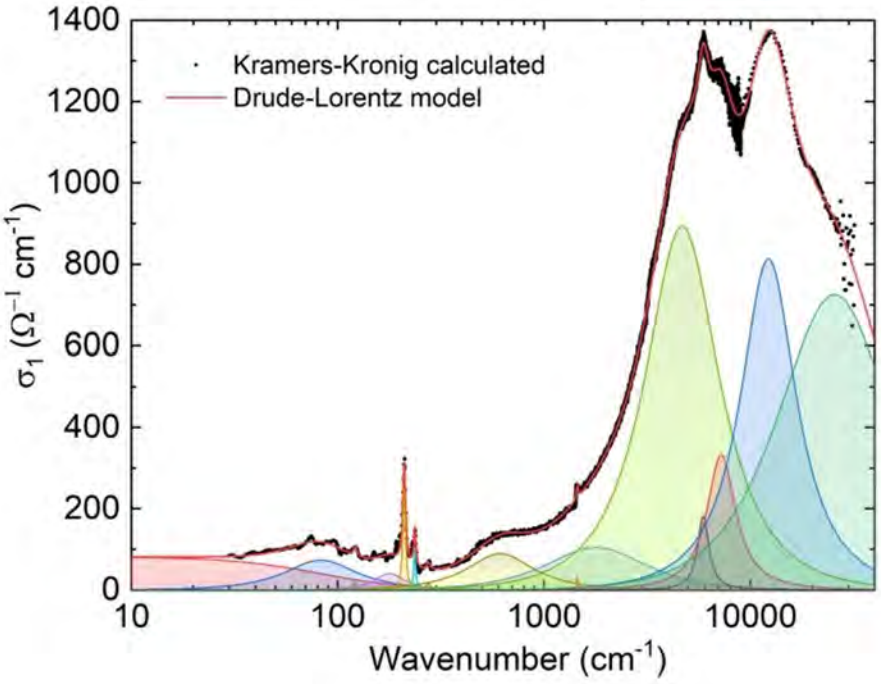

Fig. 2. The real part of the optical conductivity of $(Na_{0.33}K_{0.33}Rb_{0.33})_{0.8}Fe_2Se_2$ at 40 K and the results of Drude-Lorentz analysis.

The reflectance spectra of $(Na_{0.33}K_{0.33}Rb_{0.33})_{0.8}Fe_2Se_2$ single crystals are shown in Fig. 1. The overall reflectance is rather low, which is characteristic of insulator. It is dominated by infrared-active phonons and interband transitions. A lot of phonon contributions are particularly noteworthy given that in tetragonal 122 structure (*I*4/*mmm*) only two in-plane IR-active E_u modes are allowed. This is explained by the formation of a $\sqrt{5}\,x\,\sqrt{5}\,x1$ superlattice pattern due to the Fe vacancy ordering resulting in larger 245 (*I*4/*m*) unit cell [2]. The low-frequency reflectance initially displays small temperature dependence but begins to increase below 150 K.

Figure 2 shows optical conductivity spectrum $\sigma_1(\omega)$ for $(Na_{0.33}K_{0.33}Rb_{0.33})_{0.8}Fe_2Se_2$ at 40 K. It should be noted that at room temperature there are no coherent (Drude) contribution to the optical conductivity σ_1 of $(Na_{0.33}K_{0.33}Rb_{0.33})_{0.8}Fe_2Se_2$. As temperature decreases, the Drude contribution arises. In this case, the Drude-Lorentz model is applicable. Besides the spin-controlled high-frequency interband transitions at 1800, 4670, 5910, 7220, 12250 and 25680 cm^{-1} inherent for iron selenides [3-6] there are some low-frequency transitions at 80, 180 and 615 cm^{-1}. The low-frequency transitions were also observed previously in the spectra of $RbFe_2Se_2$ [5].

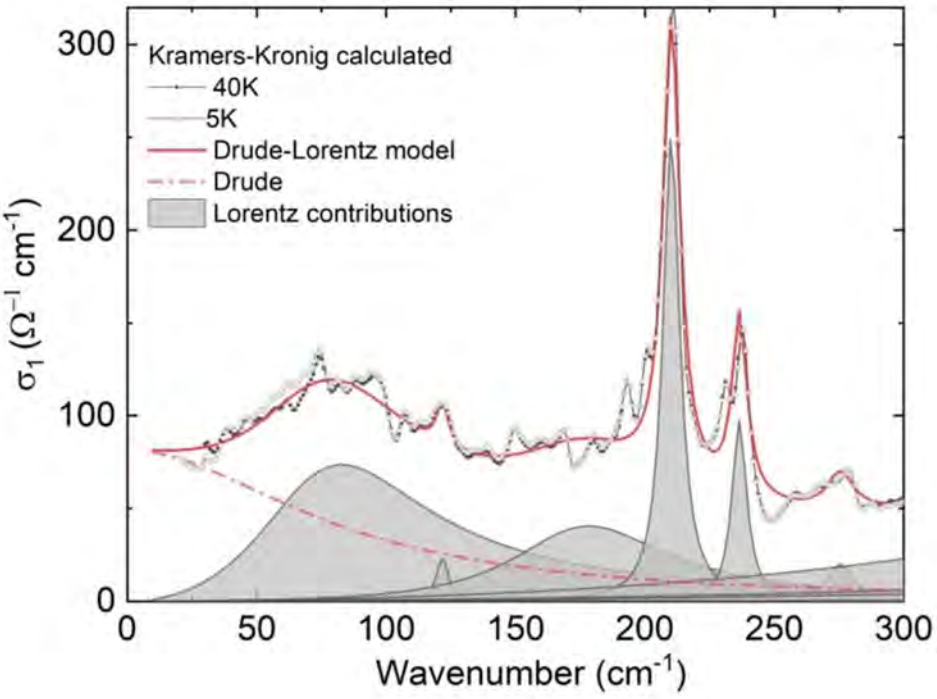

Fig. 3. The real part of the optical conductivity in the low-frequency region of $(Na_{0.33}K_{0.33}Rb_{0.33})_{0.8}Fe_2Se_2$ single crystals at 40 and 5 K.

In Fig. 3 are shown the conductivity spectra $\sigma_1(\omega)$ of $(Na_{0.33}K_{0.33}Rb_{0.33})_{0.8}Fe_2Se_2$ single crystals at 40 and 5 K in the expanded low-frequency region. The dash-dotted line depicts Drude contribution. The Lorentz contributions are shown in gray. It is seen that the spectra at 5 and 40 K are nearly indistinguishable. It can be explained by the small fraction of the SC phase in the samples under study. The model parameters (plasma frequencies, scattering rates and oscillator strengths) were obtained. For the Drude contribution at 40 K the optical conductivity, scattering rate, and plasma frequency for $(Na_{0.33}K_{0.33}Rb_{0.33})_{0.8}Fe_2Se_2$ are $\sigma_0 = 81\ \Omega^{-1}\ cm^{-1}$, $\gamma = 82.5\ cm^{-1}$, and $\omega_{pl} = 634\ cm^{-1}$, respectively.

The work is supported by RSF project no. 22-72-10082P.

References

1. *Q. Si, R. Yu and E. Abrahams*, Nat. Rev. Mater., **1**, 16017 (2016).
2. *W. Bao, et al*., Chin. Phys. Lett. **28**, 086104 (2011).
3. *R.H. Yuan et al*., Sci. Rep. **2**, 221 (2012).
4. *Z.G. Chen et al*., Phys Rev. B **83**, 220507(R) (2011).
5. *A. Charnukha et al*., Phys. Rev. B **85**, 100504(R) (2012).
6. *C.C. Homes et al*., Phys. Rev. B **85**, 180510(R) (2012).

Vortex state in a topological superconductor RbZnBi

A.R. Prishchepa, A.V. Sadakov, A.I. Shilov

P.N. Lebedev Physical Institute, Russian Academy of Sciences

The compound RbZnBi, according to quantum mechanical calculations, may be a non-trivial topological material exhibiting superconducting properties [1-2]. Compounds of this class are extremely interesting for fundamental research. It also can find applications in spintronics and quantum computing [3].

Samples of RbZnBi were prepared using the following method. Metallic Rb, Zn, and Bi were placed in an alumina crucible in a molar ratio of 1.5:1:1. The crucible was sealed in a protective niobium container to prevent the interaction of alkali metal vapors with the walls of the quartz ampoule and to avoid shifting the composition of the melt from the initial one. To protect the container from oxidation at high temperatures, it was placed in a vacuum-sealed quartz ampoule. The resulting assembly was then placed in a muffle furnace and heated to a temperature of 800 °C over 9 hours, after which it was held at this temperature for 24 hours and then cooled at a rate of 2 °C/h to a final temperature of 400 °C, after which the furnace was turned off.

We conducted systematic studies of the vortex state using two experimental facilities. One was a dilution refrigerator in the temperature range from 100 mK to 1 K in magnetic fields from 0 to 1 T. The other was the CFMS-16 cryostat in the temperature range from 1.6 to 5 K in magnetic fields from 0 to 16 T. Measurements of IV-characteristics were made while varying the magnetic field at fixed temperatures. Additionally, resistive measurements were conducted in magnetic fields.

The obtained experimental data were approximated within the framework of the vortex glass theory [4]. An experimental phase diagram was obtained.

At temperatures close to , a phase transition from the vortex liquid state to the vortex glass state was detected, and its dimensionality was investigated.

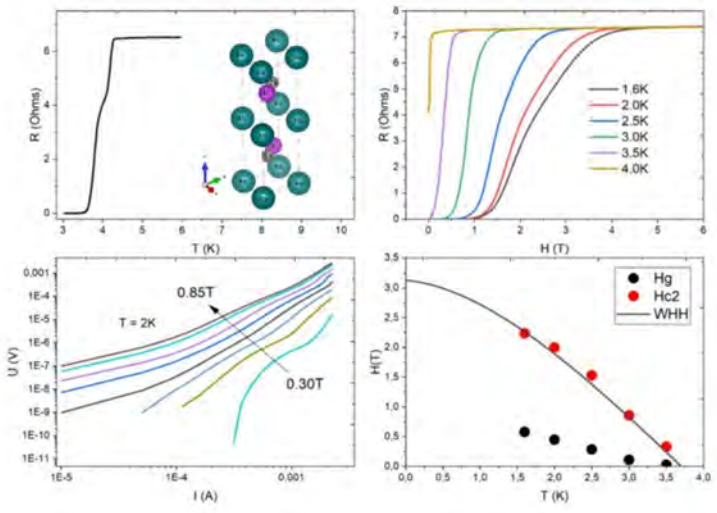

According to the experimental data, no dissipationless transition was detected at temperatures up to 350 mK and fields from 0.5 to 1 T. This fact indicates that the vortex system does not transition into a vortex glass state similar to highly anisotropic cuprates [5].

References

1. *Song, J.; Kim, S.; Kim, Y.; Fu, H.; Koo, J.; Wang, Z.; Lee, G.; Lee, J.; Oh, S. H.; Bang, J.,* Phys. Rev. X **11**, 021065 (2021).
2. *Hyunggeun Lee, Myung Joon Han, and Kee Joo Chang,* ACS Omega **9**(27), 29820-29828 (2024).
3. *Xiao-Liang Qi, Shou-Cheng Zhang,* Rev. Mod. Phys. **83**, 1057 (2011).
4. *M.P.A. Fisher,* Phys. Rev. Lett. **62**, 1415 (1989).
5. *Z. Sefrioui, D. Arias, M. Varela, J.E. Villegas, M.A. López de la Torre, C. León, G.D. Loos, and J. Santamaría,* Phys. Rev. B **60**, 15423 (1999).

Vortex matter and strong pinning in underdoped PrFeAs(O,F) with regularly distributed atomic-sized defects

A.V. Sadakov[1], V.A. Vlasenko[1], A.Yu. Levakhova[1],
N.D. Zhigadlo[2], E.M. Fomina[1], I.V. Zhuvagin[1]

[1] P.N. Lebedev Physical Institute, Russian Academy of Sciences, Moscow 119991, Russia,
[2] Laboratory for Solid State Physics, ETH Zurich, CH-8093 Zurich, Switzerland

We present a comprehensive investigation of the field-dependent critical current density and pinning force, combined with a detailed analysis of the nanostructural defect landscape in single crystal of underdoped PrFeAs(O,F) superconductor. Our study demonstrates that for both in-plane and out-of-plane magnetic field orientations critical current density exhibits a strong pinning regime in intermediate fields across the entire temperature range. Scanning transmission electron microscope studies reveal that O/F substitutional defects form a periodic arrangement of alternating fluorine and oxygen atoms within the lattice.

The behavior of the critical current density was systematically studied as a function of temperature, magnetic field strength, and field orientation with respect to the crystal planes. It was demonstrated that the critical current density exhibits remarkably similar trends for both magnetic field orientations, revealing distinct regimes: single-vortex pinning, strong collective pinning, a second magnetization peak associated with the onset of vortex elasticity, and a crossover from elastic to plastic deformations of the vortex lattice.

Point defects provide the dominant contribution to the pinning. Quantitative analysis estimates the concentration of these defects to be 0.59/cell. HR STEM studies further identified these point defects as localized regions of oxygen-to-fluorine substitution, forming a periodic arrangement of alternating fluorine and oxygen atoms within the lattice.

Non-equilibrium superconductivity in nanowires InAs/Al

E.V. Shpagina, V.S. Khrapai

Osipyan Institute of Solid State Physics, Russian Academy of Sciences, 142432 Chernogolovka, Russian Federation,
National Research University Higher School of Economics, 20 Myasnitskaya Street, 101000 Moscow, Russian Federation

We examine superconducting Al/InAs nanowire islands in non-equilibrium near collapse, focusing on the order parameter. Two approaches create non-equilibrium: transport current or phonon heating via a mesoscopic heater. The two-temperature model describes transport current-induced critical power (P_C) with equilibrium energy distribution function and minor non-equilibrium (tiny hysteresis), while heater-induced collapse requires different analysis. We calculate the collision integral with all phonon processes to estimate P_C. The phonon absorption is suppressed below a some current limit, but for some samples showing increased P_C with an increase to this limit current.

We investigate the properties of superconducting islands formed by epitaxial Al/InAs nanowires, which are a type of semiconductor-superconductor-semiconductor structure that is in a state of strong non-equilibrium near the collapse of superconductivity. We are interested in the order parameter, which reduces to problem of finding the energy distribution function of the superconductor. In the calculation, a type of non-equilibrium additive to the equilibrium energy distribution function is proposed.

There are two ways for creating a non-equilibrium state in a superconductor: passing a large transport current through the nanowire or heating the nanowire to a critical temperature. For the second way, we have developed a mesoscopic heater that touches one end of the nanowire. When current is passed through the heater, electrons cannot pass from the heater to the nanowire, but phonons can, creating a flow of non-equilibrium phonons into the superconductor.

As was found in experiments with transport current, electrons trapped in a superconducting island spend more time in electron-phonon relaxation [1]. As a result, the electronic subsystem heats up to a critical temperature. A two-temperature heating model is used as a basic proposal for the superconductivity collapse model [1-3]. It separates the heating of the electronic and phonon subsystems, and the Joule power released at the moment of superconductivity collapse obeys from the heat balance equation $I_C V_C \sim T_e^5 - T_{ph}^5$. Here, T_{ph} is the constant bath temperature, $T_e = T_C$ is the electron temperature in the island, increasing to T_C with increasing transport current to I_C. The model well describes the collapse of superconductivity caused by transport current. Regarding the issue of the energy distribution function in the island, we assume it to be close to equilibrium. The presence of a small fraction of non-equilibrium quasiparticles in the island is confirmed by the fact that the

transition of the island between the superconducting and the normal state relative to the direction of the transport current sweep has a tiny hysteresis. We consider non-equilibrium as a small addition to the Fermi-Dirac equilibrium function in the form of a step. Which allows us to describe the hysteresis and gives the bistability of the order parameter relative to T_e similar to [4] with the hysteresis relative to the applied voltage.

However, the two-temperature model is not applicable to the case of a mesoscopic heater, as observed when measuring the critical power from simultaneous heating by transport and heater current. Measurements of the noise temperature [5] of the nanowire show that heating due to the heater current destroys superconductivity at a heater temperature equal to T_C. To estimate the critical power, we calculate the collision integral. In a non-equilibrium addition to the thermalized energy distribution function, we take into account all possible phonon absorption and emission processes. We also investigate the collapse of superconductivity in a magnetic field parallel to a nanowire. In fields of less than 20 mT, we observe a feature in the small currents of the heater. There is a clear limit to the heater current below which the island's ability to absorb a flow of non-equilibrium phonons is suppressed. And for several samples, an increase in critical power is observed with increasing heater current up to this limit current, which can be interpreted in terms of the Eliashberg effect.

Our experiments with Al/InAs nanowires have revealed a diverse range of non-equilibrium phenomena in the superconducting state that cannot be fully explained by simple models based on electron-phonon thermalization.

References

1. *E.V. Shpagina, E.S. Tikhonov, D. Ruhstorfer, G. Koblmueller, V.S. Khrapai*, Phys. Rev. B **109**, L140501 (2024).
2. *A. Ibabe, M. G´omez, G.O. Steffensen, T. Kanne, J. Nygard, A. L. Yeyati, and E.J.H. Lee*, Nature Communications **14**, 2873 (2023).
3. *A. Ibabe, G.O. Steffensen, I. Casal, M. Gomez, T. Kanne, J. Nygard, A.L. Yeyati, E.J.H. Lee*, Nano Lett. **24**, 6488 (2024).
4. *I. Snyman and Yu.V. Nazarov*, Physical Review B **79**, 014510 (2009).
5. *E.S. Tikhonov, D.V. Shovkun, and V.S. Khrapai*, Phys. Rev. Lett. **117**, 147001 (2016).

Theoretical analysis of interplay between WSe_2 moire bilayer geometry and its electronic structure

M.A. Vysotin, V.I. Kuz'min, S.G. Ovchinnikov

Kirensky Institute of Physics, Federal Research Center KSC SB RAS, Krasnoyarsk, 660036 Russia

The moire superlattices of transition metal dichalcogenides are one of the most prospective Hubbard model simulators and are able to reproduce a wide variety of phenomena, including correlated phases and superconductivity. In this work, the interplay between the electronic structure and geometrical parameters of t-WSe_2 moire, a prominent twisted bilayer system, is investigated through density functional calculations. The impact of computational procedures of finding the equilibrium geometry on the band structure is studied. The possibility of switching between hexagonal and trigonal topology of the valence band maximum via in-plane strain is shown.

In the last decade, the moire superlattices of transition metal dichalcogenides have been proven to be a versatile instrument for studying novel electronic properties in low-dimensional materials [1]. The wide spectrum of phenomena that could be investigated with such systems include flat bands, spin-valley locking, correlated phases and unconventional superconductivity. While some parameters of the system cannot be directly adjusted experimentally, for example the out-of-plane displacement field cannot be changes without shifting the level of doping, adequate theoretical models are of great importance for further studies.
The peculiarities of moire electronic properties come form a spatial modulation of the carrier potential inside of one TMD monolayer by the proximity of the atoms from the other monolayer [2]. However, since full relaxation of the bilayer structure is a computationally-demanding task, several studies are limited to relaxation of only the interlayer distance. In those cases the layers remain planar and do not acquire a long-wave corrugation, which may cause effects comparable to the potential modulation by the adjacent layer. Therefore, the applicability of such a simplification is yet to be investigated. In this work, we employ density functional calculations of twisted WSe_2 bilayer moires to study how the changes in the layer geometry affect the electronic structure of the system.

The calculations of twisted WSe_2 moires with different angles show a common trend for bigger corrugation amplitude for smaller angles with undulation in each layer up to 0.21 A for the angle of 5.6°. Compared to the planar bilayer structure, the fully-relaxed 5.6° moire exhibit different topology of the upper subbands of the valence band maximum: during the geometry optimization the trigonal-type dispersion switches to hexagonal-like. The same behavior can be observed if in-plane strain is applied to the moire bilayers of different angles. Besides some changes in the widths of the subbands, the general trend is that the set of hexagonal-like subbands are shifted upwards upon simultaneous extension of the WSe_2 layers. This effect gives an opportunity for strain engineering of the electronic properties, which may

greatly enhance the potential of such systems for application in sensors and other fields.

References

1. *Wang T., Yuan N.F.Q., Fu L.* Physical Review X **11**(2), 021024 (2021).
2. *Xiao Y., Liu J., Fu L.* Matter **3**(4), 1142-1161 (2020).

Superconducting photocurrents induced by structured electromagnetic radiation

O.B. Zuev, M.V. Kovalenko, A.S. Melnikov

Moscow Institute of Physics and Technology (National Research University), Dolgoprudny, Russia,
Landau Institute for Theoretical Physics RAS, Chernogolovka, Russia,
Institute for Physics of Microstructures RAS, Nizhny Novgorod, Russia

We develop a phenomenological theory describing the interaction between a superconducting condensate and a Bessel beam of structured light carrying orbital angular momentum. Extending previous approaches based on the time-dependent Ginzburg-Landau theory and Maxwell's equations, we calculate the photo-induced current at zero frequency and at the second harmonic. Contributions include the inverse Faraday effect, photon drag of Cooper pairs, and the ponderomotive force. Using the London equations, we determine the compensating Meissner currents and the resulting magnetic field at the superconductor's surface. The results are presented for both a half-space and a thin-film geometry.

The interaction of electromagnetic radiation with various forms of condensed matter– such as metals, semiconductors, and plasma–has been extensively studied and remains a topic of ongoing interest. The aim of the present work is to develop a phenomenological theory describing the interaction of the superconducting condensate with a Bessel beam of structured (twisted) light possessing a nonzero projection of the angular momentum m. Issues related to the interaction of light with matter have been extensively discussed previously for metals, semiconductors, and plasma. In particular, in the recent work [1], the authors calculated the contributions to the current induced by a Bessel beam in a semiconductor layer. In the context of superconductors, one of the first works in this area was [2], where the interaction of a superconductor with a plane wave was considered. Our work is a direct continuation and generalization of [2] to the case of Bessel beams.

Using the time-dependent Ginzburg-Landau theory and Maxwell's equations in a superconductor, we have calculated the photo-induced current at zero frequency, as well as the current at the second harmonic. The photocurrent at zero frequency contains such typical contributions as the inverse Faraday effect, the effect of Cooper pairs dragged by photons, and the ponderomotive force.

Using the London equations, we have also computed the compensating Meissner currents at zero frequency. Taking these currents into account, we have calculated the magnetic field at the surface of the superconductor, which is an experimentally measurable quantity. The results for a superconducting half-space have been extended to the case of a thin film.

This work was supported by the Russian Science Foundation (Grant No. 25-12-00042).

References

1. *A.A. Gunyaga, M.V. Durnev, and S.A. Tarasenko*, Phys. Rev. B **108**, 115402 (2023).
2. *S.V. Mironov, A.S. Mel'nikov, and A.I. Buzdin*, Phys. Rev. Lett. **132**, 096001 (2024).

Posters

R&D on superconducting NbTi coaxial cables for quantum computers

I.M. Abukhanov, M.V. Alekseev, A.G. Silaev, M.M. Potapenko,
M.V. Krylova, D.V. Sokolovsky, A.S. Tsapleva, S.A. Shevakova,
U.A. Markina, V.I. Tkachenko

VNIINM, MIREA

Superconducting coaxial NbTi cables 0.8-2.5 mm in diameter are important elements for quantum computers construction. Using of the superconducting NbTi alloy in coaxial cables provides low energy losses while signal transmission and low thermal conductivity, which decreases heat gain and therefore enhances duration of the qubit quantum state. Such coaxial cables can be applied in any devices where low energy losses and low thermal conductivity are important.

In the report the results of R&D on superconducting coaxial cables for quantum computers are presented. The results of manufacture regimes development, mechanical properties and structure investigations of NbTi wire (inner conductor) and NbTi capillary tube (outer conductor) are shown.

Today, superconductors are finding more and more applications in many areas of science and technology, including transport and energy infrastructure, medicine, various equipment for physical and chemical research, as well as in experimental installations for thermonuclear fusion. The properties of superconducting materials also make it possible to find applications, for example, in magnetic suspension trains, transformers, generators, motors and energy storage devices, as well as in devices based on the phenomenon of nuclear magnetic resonance. In the near future, superconductors may become widespread in many other areas, one of which is computing technology, in particular, developments in the field of quantum computers. [1]. The main potential advantage of quantum computers over modern computers is a significantly higher computing speed, which opens up new opportunities for physical modeling, cryptography, research in the field of artificial intelligence, etc.

As for the components of such devices, one of the most important elements of a quantum computer can be cables based on superconducting materials, in particular, coaxial type, since they have greater noise immunity and relatively low energy losses.

The main problem of cables of this type, in particular, based on superconducting materials, is the complexity of manufacturing components of such cables. During the manufacturing process, semi-finished products are subjected to multiple drawing, that is, to high degrees of deformation. In addition, they are also subjected to intermediate heat treatment between drawing processes. Therefore, it is necessary to establish the degree of influence of deformation and heat treatment on

the mechanical characteristics of semi-finished coaxial cables at each stage of drawing.

In accordance with this, the purpose of this work is to study the influence of deformation and intermediate heat treatment on the mechanical properties and structure of Nb-Ti semi-finished coaxial cables.

The paper presents data on the mechanical properties and structure of Nb-Ti semi-finished products, and analyzes the influence of deformation and heat treatment on the obtained properties and structure of Nb-Ti semi-finished products.

Domain wall superconductivity in van der Waals structures with ferroelectric ordering

D.S. Annenkov, A.A. Kopasov, A.S. Mel'nikov

L.D. Landau Institute for Theoretical Physics RAS, 142432 Chernogolovka, Russia,
Moscow Institute of Physics and Technology (National Research University), Dolgoprudnyi, 141701 Moscow Region, Russia,
National University of Science and Technology «MISIS», Moscow 119049, Russia,
Institute for Physics of Microstructures, Russian Academy of Sciences, 603950 Nizhny Novgorod, GSP-105 Russia

We suggest a model describing the interplay of ferroelectric and superconducting order parameters in van der Waals structures. The model assumes the presence of the interlayer superconducting correlations affected by the relative shifts of the energy bands caused by spontaneous polarization oriented perpendicular to the layers. Accounting for the interlayer tunneling we study the superconductivity nucleation at the ferroelectric domain walls and the depairing effect of an external magnetic field parallel to the layers both for spin-singlet and spin-triplet interlayer Cooper pairs.

Recently there has been huge interest in the physics of low-dimensional van der Waals structures, and one possible reason for this interest is the possibility of controlling various types of ordering (superconductivity, ferroelectricity) through the electric field effect. This work demonstrates that the structure of superconducting correlations in van der Waals systems significantly depend on the nonlocal nature of electron attraction, which can lead to the formation of Cooper pairs composed of electrons localized in different layers of a hybrid structure [1–5]. These issues are explored for a model bilayer system in the presence of tunneling and relative shifts of the energy bands in the layers caused by spontaneous polarization oriented perpendicular to the layers [6].

We found that for a stepwise relative band shift, there exist superconducting states, which are localized at such a domain wall and have critical temperature higher than uniform superconducting state. It is shown, that the tunneling between the layers strongly modifies the system phase diagram suppressing the domain wall superconductivity. We also show that the in-plane magnetic field can suppress the tunneling between the layers providing a specific depairing mechanism for interlayer pairing. Joint impact of the orbital and the Zeeman pair breaking effects is discussed for spin-siglet and spin-triplet interlayer supeconducting correlations.

The obtained results are discussed in the context of recent experimental data on the coexistence of ferroelectricity and superconductivity in van der Waals bilayers [7, 8].

This work has been supported by the Russian Science Foundation (Grant No. 25-12-00042).

References

1. *M.H. Cohen and D.H. Douglass*, *Jr*., Phys. Rev. Lett. **19**, 118 (1967).
2. *K.B. Efetov and A.I. Larkin*, JETP **41**, 76 (1975).
3. *M.V. Hosseini and M. Zareyan*, Phys. Rev. Lett. **108**, 147001 (2012).
4. *C.-X. Liu*, Phys. Rev. Lett. 118, 087001 (2017).
5. *M. Alidoust, M. Willatzen, and A.-P. Jauho*, Phys. Rev. B **99**, 155413 (2019).
6. *A.A. Kopasov and A.S. Mel'nikov*, Phys. Rev. B **110**, 094503 (2024).
7. *A. Jindal, A. Saha, Z. Li et al*., Nature **613**, 4852 (2023).
8. *Z. Li, A. Jindal, A. Strasser, Y. He, W. Zheng, D. Graf, T. Taniguchi, K. Watanabe, L. Balicas et al*., Phys. Rev. Lett. **133**, 216002 (2024).

Induced superconductivity in organic polymer

K.Yu. Arutyunov[1,2], V.V. Zavialov[2,1], V.V. Artemov[3], A.L. Vasiliev[3,4], A.R. Yusupov[5], A.F. Galiev[5], D.D. Karamov[6], A.N. Lachinov[5,6]

[1] National Research University Higher School of Economics, 101000, Moscow, Russia,
[2] P.L. Kapitza Institute for Physical Problems RAS,119334, Moscow, Russia,
[3] Federal research center «Crystallography and photonics» RAS, 119333, Moscow, Russia,
[4] National research center «Kurchatov institute», 123182, Moscow, Russia,
[5] Bashkir state pedagogic university, 450008, Ufa, Russia,
[6] Instutute of physics of molecules and crystals RAS, 450054, Ufa, Russia

Polydiphenylenephthalide (PDF) belongs to the class of carbocyclic organic electroactive polymers, which exhibit electric conductive properties when an external electrostatic field and/or mechanical stress is applied. Being sandwiched between two massive superconductors, a thin film of PDP demonstrates features that can be explained by the effect of induced superconductivity. An extensive microscopic analysis reveals no signs of trivial metal-to-metal shortcuts. The mechanism of the effect is still under debates.

Polydiphenylenephthalide (PDP) in the ground state is the wide-band dielectric, but can exhibit high electric conductivity under the influence of external parameters as mechanical stress and/or electric field [1]. The effect is interpreted as stimulation of metallic state [2].

In a number of experiments, it has been demonstrated that sandwiches superconductor – PDP – superconductor with sufficiently thin layer of the polymer (let say, below 400 nm) reveal $R(T)$ and $V(I)$ dependencies typical for a superconductor [3-5]. The same effect has been demonstrated with varios electrode materials (Sn, Pb, In). Tin and lead films were fabricated using thermal evaporation, while cold rolling has been used for indium samples. Magnetic filed, parallel to the S-PDP-S sandwich plane, effectively quench superconductivity. The critical current I_c expectedly decreases with increase of parallel magnetic filed B, while no regular (e.g. Fraunhofer-type) structure $I_c(B)$ has been observed, which otherwise might indicate the existence of Josephson loops with commensurate areas. Numerous SEM an TEM studies to reveal trivial metal-to-metal shortcuts failed. Previous AFM studies of PDP film on top of a normal metal demonstrated no structural (topological) defects on polymer surface, while STM analysis of the same samples revealed microscopic domains with higher local conductivity, induced by the proximity with metal. All these observations allow one to suggest that a non-trivial universal phenomenon is involved. However, so far universally accepted model of the phenomena does not exist.

This work was supported by the «Mirror Laboratories» project «Quantum effects in low-dimensional hybrid nanostructures» of the HSE University and M. Akmullah Bashkir State Pedagogical University.

References

1. *N. Lachinov, et al*., JETP **102**(4), 640 (2006).
2. *N. Lachinov, N.V. Vorob'eva*, Physics – Uspekhi **49**(12), 1238 (2006).
3. *N. Ionov, A. N. Lachinov, R. Rench*, JTP Lett. **28**(14), 69 (2002).
4. *Yu. Arutyunov, et al*., Beilstein J. Nanotechnology **13**, 1551, (2022).
5. *Yu. Arutyunov, et al*., Physics of the Solid State **64**(12), 603 (2022).
6. *M. Kornilov, A.N. Lachinov*, JTP Lett. **26**(21), 37 (2000).
7. *M. Kornilov, et al*., Izvestia UNC RAN **1**, 41 (2024).

Novel high-entropy superconductor $(Na_{0.2}K_{0.2}Rb_{0.2}Sr_{0.2}Ba_{0.2})Fe_2As_2$

A.D. Denishchenko, V.A. Vlasenko, K.S. Pervakov

P.N. Lebedev Physical Institute, Russian Academy of Sciences, Moscow

A polycrystalline high-entropy superconductor of the 122 family $(Na_{0.2}K_{0.2}Rb_{0.2}Sr_{0.2}Ba_{0.2})Fe_2As_2$ was synthesized using the mechanical alloying method, the phase composition confirmed by X-ray diffraction analysis. The superconducting transition temperature is 10.8 K. According to magnetic measurements, only one superconducting phase is present in the sample.

Currently, the "high-entropy" approach to the synthesis of new compounds is rapidly developing. Its main concept is to create multicomponent solid solutions with high configurational entropy. Compounds with configurational entropy ($S_{conf} > 1.5R$) that are formed from five or more elements with equimolar or near-equimolar atomic ratios in the one crystallographic position are called high-entropy compounds (HECs) [1–3]. During research on HECs, many unique properties were identified in these compounds, which were not the sum of the properties of the "basic" compounds that make up the high-entropy compound, but rather their individual properties. The presence of such properties is associated with the emergence of four main HEC effects: the high-entropy effect, the crystal lattice distortion effect, the delayed diffusion effect, and the "cocktail" effect [1, 4].

A polycrystalline sample of a high-entropy superconductor (HES) of the 122 family was synthesized by mechanical alloying from the starting metals: Na (99.9%), K (99.5%), Rb (99.9%), Ba (99.8%), Sr (99.9%), Fe (99.9%), As (6N), and Fe_2As. The Fe_2As precursor was pre-synthesized from simple substances Fe (99.9%) and As (6N), for which the sample was sealed in a quartz ampoule and heated up to 900°C and held for 24 hours. Mechanical alloying was carried out in a CryoMill vibrational mill. After processing, the finely dispersed powder was pressed into pellets, which were then loaded into alumina crucibles. The crucibles with the pellets were sealed in steel containers and heat treated. Heat treatment was carried out in two stages with intermediate homogenization. The first annealing was carried out at a temperature of 700°C with a holding time of 4 hours at a heating rate of 700°C/hour, and cooling was carried out with the furnace turned off. The second annealing was carried out using thermal shock: heating to 700°C with a holding time of 3 hours, followed by relaxation to 600°C and a holding time of 12 hours. All operations, except for mechanical alloying and annealing, were carried out in a glove box with an argon atmosphere (O_2 and H_2O content less than 0.5 ppm).

X-ray diffraction analysis of the obtained samples was performed by a Bruker D2 Phaser diffractometer using CuKα radiation in the angle range $2\Theta = 10–80°$ in an argon-filled sealed cuvette. Dynamic magnetic susceptibility measurements were performed on a PPMS-9 (Quantum Design) instrument in a zero constant magnetic field ($H_{DC} = 0$ T) with a modulation amplitude of $H_{AC} = 5$ Oe and a frequency of $\nu = 377$ Hz.

X-ray diffraction analysis was performed to evaluate the phase composition of the obtained sample. According to its results, two phases were found in the studied sample: a solid solution of high-entropy superconductor composition $(Na_{0.2}K_{0.2}Rb_{0.2}Sr_{0.2}Ba_{0.2})Fe_2As_2$ and an impurity phase FeAs. The structure model obtained in the Vesta Crystallography program and the experimental diffraction pattern are shown in Figure 1(a and b). The resulting diffraction pattern contains no reflections corresponding to possible parent 122 phases that could form from the initial components, indicating the formation of a single solid solution with a random distribution of alkali and alkaline-earth elements in the Wyckoff *2a* position. The parameters of the unit cell of the resulting solid solution $(Na_{0.2}K_{0.2}Rb_{0.2}Sr_{0.2}Ba_{0.2})Fe_2As_2$ were determined using the relationship between Miller indices and interplanar space for tetragonal crystal system from crystallographic planes *(002)* and *(103)*. The obtained lattice parameters were a = 3.8742 Å, c = 13.6184 Å.

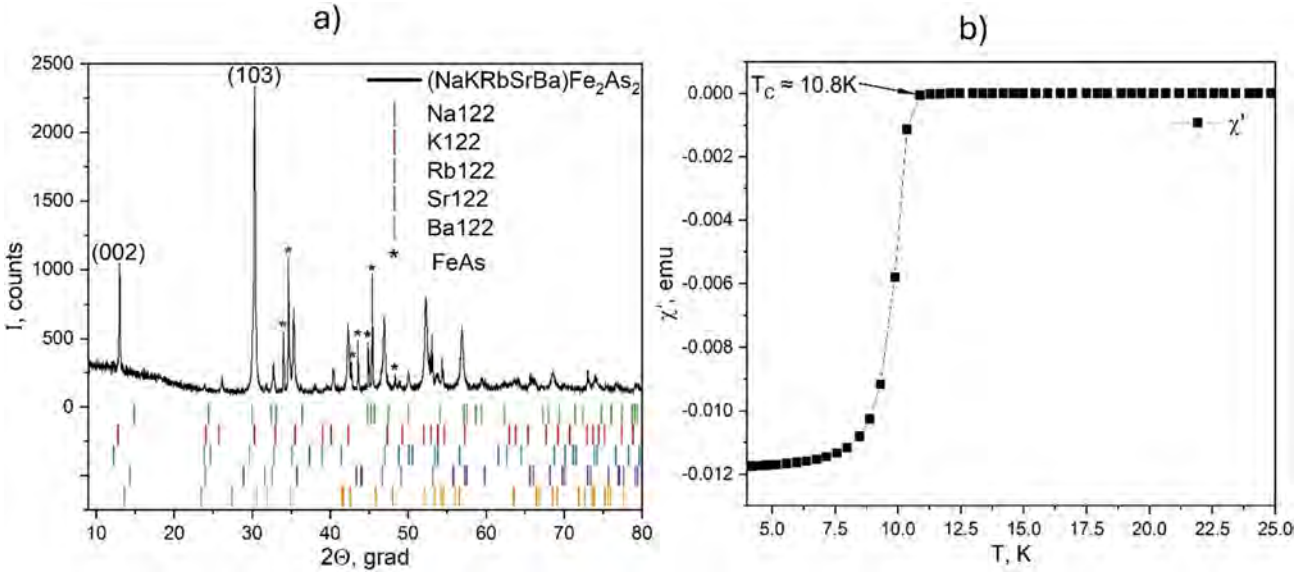

Figure 1. a) X-ray diffraction patterns of $(Na_{0.2}K_{0.2}Rb_{0.2}Sr_{0.2}Ba_{0.2})Fe_2As_2$ solid solutions; b) Temperature dependences of in-phase (χ') part of AC magnetic susceptibility.

Magnetic studies were carried out with a PPMS-9 Quantum Designed to investigate superconducting properties. The figure shows a plot of the temperature dependence of dynamic magnetic susceptibility for $(Na_{0.2}K_{0.2}Rb_{0.2}Sr_{0.2}Ba_{0.2})Fe_2As_2$. The χ'(T) curve of the synthesized sample clearly shows a sharp transition to the superconducting state at $T_C \approx 10.8$ K. The superconducting transition signal reaches a plateau with pronounced signal shielding, indicating the high homogeneity of the resulting superconducting phase.

This work was supported by the RSF project #23-12-00307 and performed using LPI Shared Facility Center equipment.

References

1. *W.-L. Hsu, C.-W. Tsai, A.-C. Yeh, J.-W. Yeh*, Clarifying the four core effects of high-entropy materials, Nat Rev Chem **8**, 471 (2024). https://doi.org/10.1038/s41570-024-00602-5.
2. *D.B. Miracle, O.N. Senkov*, A critical review of high entropy alloys and related concepts, Acta Materialia **122**, 448 (2017). https://doi.org/10.1016/j.actamat.2016.08.081.
3. *B. Cantor, I.T.H. Chang, P. Knight, A.J.B. Vincent*, Microstructural development in equiatomic multicomponent alloys, Materials Science and Engineering: A **375–377**, 213 (2004). https://doi.org/10.1016/j.msea.2003.10.257.
4. *A. Amiri, R. Shahbazian-Yassar*, Recent progress of high-entropy materials for energy storage and conversion, J. Mater. Chem. A **9**, 782 (2021). https://doi.org/10.1039/D0TA09578H.

Synthesis and growth of single crystals of a new topologically nontrivial compound $CaSn_2As_2$

M.A. Feshina, A.S. Medvedev, V.A. Vlasenko,
K.S. Pervakov, A.I. Shilov

RSF grant No. 25-72-31027, LPI Shared Facility Center

The paper [1] presents calculations of the electronic structure of the compound $CaSn_2As_2$. These calculations demonstrate that, when spin-orbit interaction is taken into account, this material is topologically nontrivial and can exhibit the properties of a topological insulator. Currently, there is an absence of research focusing on the synthesis, growth of single crystals, and the study of the physical properties of this compound. This underscores the significance of acquiring this compound for research purposes. In this study, the synthesis of the charge for the growth of single crystals of the compound Ca122 was conducted, and the growth of single crystals of this compound was subsequently achieved. The elemental composition of the single crystal surface was investigated, and it was found that the composition of the single crystal within an error coincides with the target composition. Diffraction patterns in the [001], [010], and [100] directions were obtained. The crystal structure of the compound $CaSn_2As_2$ was determined to be in trigonal syngony in the space group $R\bar{3}m$ with cell parameters a = 4.1503(13) Å and c = 26.049(11) Å, and with R = 6.18%, wR = 14.23%.

In the study presented in [1], electronic structure calculations of the compound $CaSn_2As_2$ were performed. These calculations showed that this material is topologically non-trivial when the spin-orbit interaction is taken into account and exhibits properties corresponding to those of a topological insulator, in accordancy to the properties exhibited by other compounds of this family previously studied in [2, 3]. Currently, there is no data on research focused on the synthesis, single crystal growth, and physical properties of this compound, which underlines the importance of obtaining this compound for further study.

In this research, a starting material mixture for crystal growth of a topologically non-trivial material with a nominal composition of $CaSn_2As_2$ (Ca122) was prepared by mechanical alloying. Single crystals of the compound were grown from the obtained powder in several stages, and their investigations were carried out.

The first stage of the process is the synthesis of the SnAs precursor. The elements tin (99.99%) and arsenic (99.999%) in the metallic form were sealed in a quartz ampoule in a 1:1 ratio and then annealed at a temperature of 620°C. The obtained SnAs compound was then mixed with metal Ca (99.999%) in a ratio of 2:1, the resulting mixture was then grinded in a vibrating mill, after which the powder was pressed into pellets and then heated in a quartz ampoule for 168 hours.

The growth of $CaSn_2As_2$ was carried out by means of a modified Bridgman method from the self-flux of the native SnAs component in a molar ratio of Ca122 and SnAs powders equal to 1:2. The mixed powders were embedded into corundum crucibles, which were then loaded into a quartz ampoule. The process of growth was divided into multiple stages, beginning with heating to 1150°C, followed by holding

at this temperature for 12 hours. Then it was gradually cooled down to 900°C, and ultimately, rapidly cooled down to room temperature. The ampoule was opened in an argon box to prevent oxidation of the obtained material. This revealed crystal aggregations in the flux. Following mechanical cleaning of the flux, single crystals of maximum size equal to 2 mm were found out (Fig. 1A).

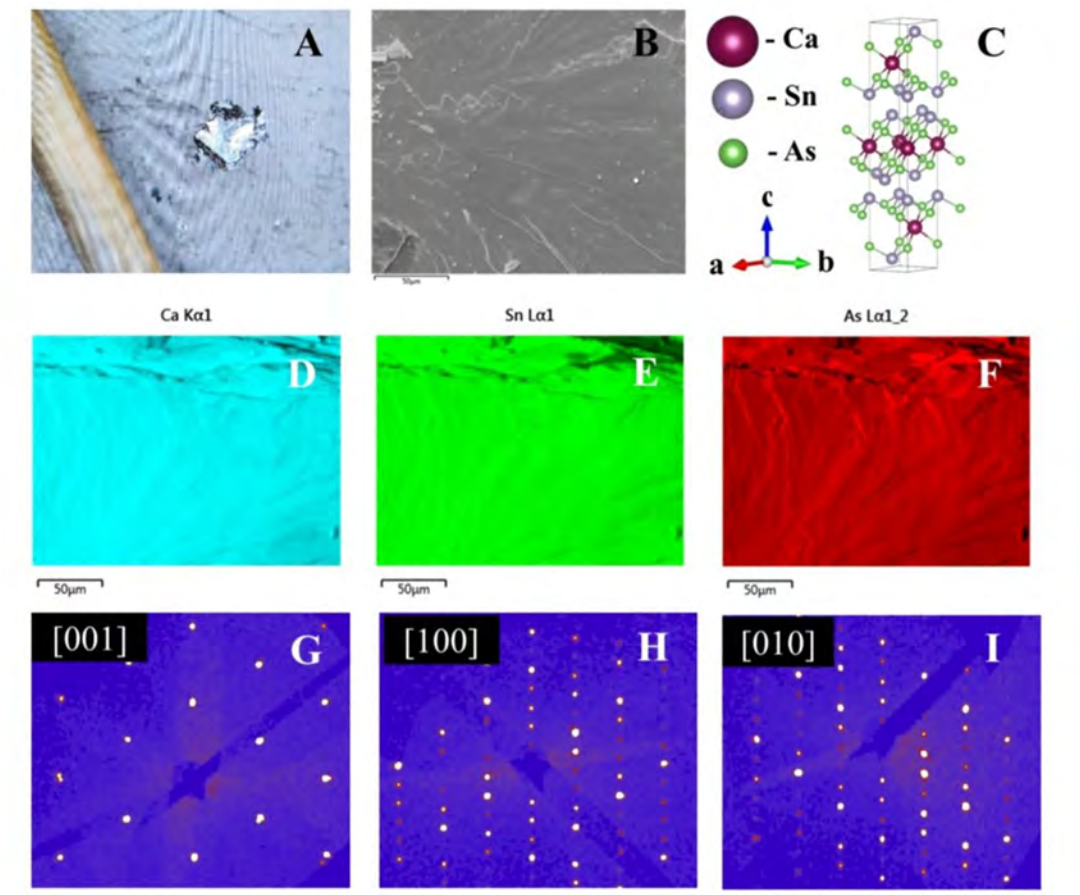

The surface of single crystals was investigated using a SEM and energy-dispersive spectroscopy, which revealed the presence of terraces, that indicates the layered structure of the compound (Fig. 1B). The distribution maps of Ca, Sn, and As on the surface demonstrate an even distribution of all elements (Fig. 1G-E). The molar ratio of elements was calculated from the total spectrum of the map, revealing an approximate value of $Ca_{0.97(2)}Sn_{1.99(4)}As_{2.04(4)}$. This result, within the established error limits, corresponds to the required composition.

The crystal structure of the sample (Fig. 1C) was established by X-ray diffraction analysis of a single crystal measuring 0.1 × 0.1 mm^2. Diffraction patterns in the [001], [010], and [100] directions are presented in Fig. 1J-I. The crystal structure of the $CaSn_2As_2$ compound was determined to be in trigonal symmetry in the space group $R\bar{3}m$, with cell parameters a = 4.1503(13) Å and c = 26.049(11) Å, and with R = 6.18%, wR = 14.23%. The obtained structure is consistent with the structures of other compounds in this family [2, 4, 5] and matches the structure calculated in [1], suggesting the successful synthesis of the desired compound.

References

1. *Inzani K. et al.* Physical Review Research **3**(1), 013069 (2021).
2. *Rong L.Y. et al*. Scientific Reports **7**(1), 61-72 (2017).
3. *Li H. et al*. Physical Review X **9**(4), 041039 (2019).
4. *Huan-Cheng Chen et al*. Chinese Phys. Lett. **37**, 047201 (2020).
5. *Goto Y. et al*. Journal of the Physical Society of Japan **86**, 123701 (2017).

Synthesis of stoichiometric superconductors $KCa_2Fe_4As_4F_2$ and $RbCa_2Fe_4As_4F_2$

A.A. Gippius, V.A. Vlasenko, S.Yu. Gavrilkin, K.S. Pervakov

P.N. Lebedev Physical Institute of the Russian Academy of Sciences

Polycrystalline samples of composition $KCa_2Fe_4As_4F_2$ and $RbCa_2Fe_4As_4F_2$ were synthesized using mechanical alloying. The composition was characterized by powder X-ray diffraction, the unit cell parameters were refined by Le Bail method in the space group I4/mmm. It is found that the obtained sample $KCa_2Fe_4As_4F_2$ has unit cell parameters a = 3.8656(4) Å, c = 30.997(4) Å, and for the sample $RbCa_2Fe_4As_4F_2$ a = 3.86978(18) Å, c = 31.6396(14) Å. Magnetic properties and transport measurements were also carried out. The superconducting transition temperatures are 33K and 30K for $KCa_2Fe_4As_4F_2$ and $RbCa_2Fe_4As_4F_2$, respectively.

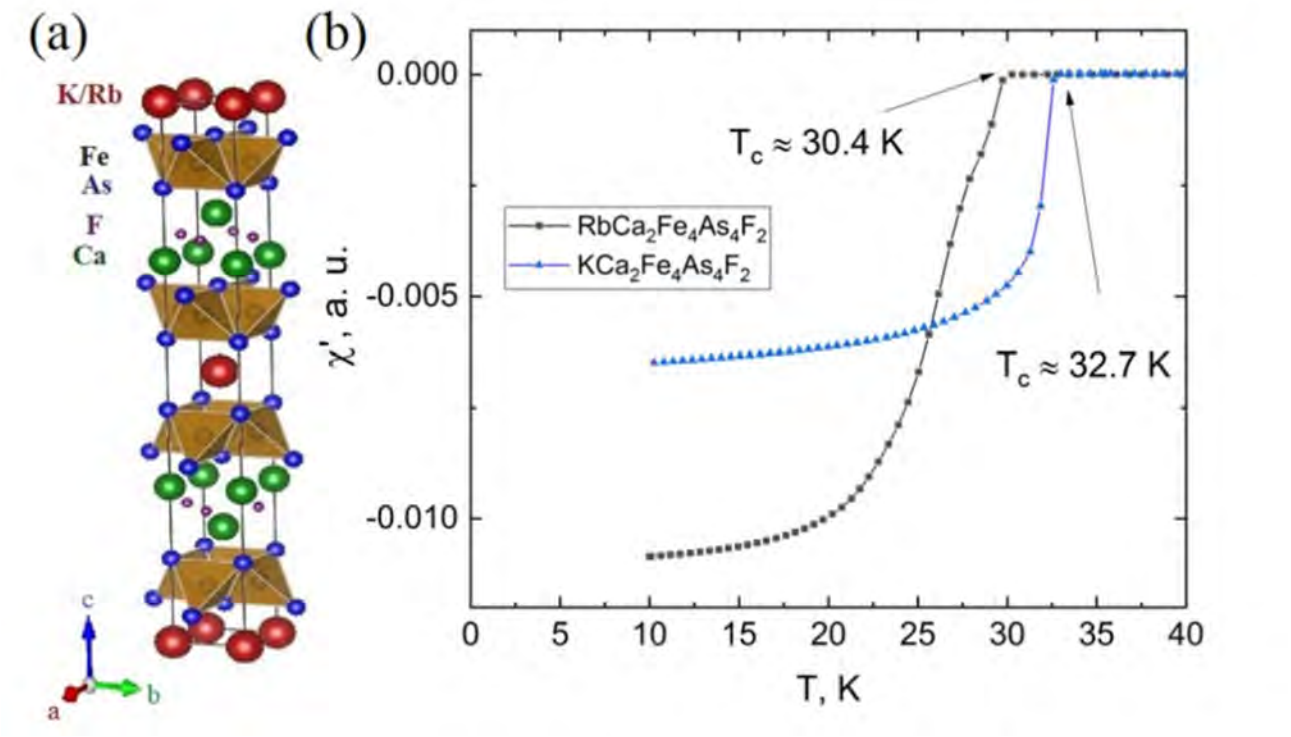

Fig. 1. (a) Crystal structure of pnictides of the 12442 family (b).

Pnictides of the 122 family, crystallizing in the $ThCr_2Si_2$ structural type, have been known for a relatively long time [1], but in 2008, the interest of the scientific community for these compounds significantly increased due to the discovery of high-temperature superconductors in this family [2]. In 2016, a new family of pnictides – 12442, was discovered, whose structure can be visualized as a crystallographic junction of the structures of two families, 1111 CaFeAsF and 122 with an alkali metal KFe_2As_2 (Fig. 1, a) [3]. This family is interesting because it demonstrates high-temperature superconductivity (about 30K) at stoichiometric composition.

In the presented work, polycrystalline samples of composition $KCa_2Fe_4As_4F_2$ and $RbCa_2Fe_4As_4F_2$ were synthesized using mechanical alloying from alkali metal, Ca, As, FeAs and FeF_3. Using classic solid-state reaction method with numerous heat treatment of components was unsuitable because of the possibility of the forming CaFeAsF, KFe_2As_2 and CaF_2 and takes too much time. On the other side, using of mechanical alloying allowed to mix all components and it takes about only 30 minutes to increase particles contact area.

All components were placed in 35 ml stainless steel milling jar with 20 mm steel milling ball in a glove box with an argon atmosphere. The mixture was ground in cryomill during 30 minutes. Then the resulting powder was pressed into pellets (diameter 12 mm), placed in an alumina crucible and sealed in a stainless steel container. It was welded in an argon welding machine, heated in a muffle furnace and quenched in water.

An excess of alkali metal as well as sintering temperature were found as the key parameters for the target product yeild: an optimal excesses are 3.1 and 11.7 mol % for $KCa_2Fe_4As_4F_2$ and $RbCa_2Fe_4As_4F_2$, respectively, the sintering temperature for $KCa_2Fe_4As_4F_2$ was 930-950^{o}C, for $RbCa_2Fe_4As_4F_2$ – 800-820^{o}C. Another important parameter of the synthesis was quenching: both samples were quenched in iced water. Deviation from the optimal parameters led to the decomposition of the target compound 12442 to 1111 and 122 compounds.

The composition was characterized by powder X-ray diffraction, the unit cell parameters were refined by Le Bail method in the space group *I4/mmm*. It is found that the obtained sample $KCa_2Fe_4As_4F_2$ has unit cell parameters a=3.8656(4)Å, c=30.997(4)Å, and for the sample $RbCa_2Fe_4As_4F_2$ a=3.86978(18)Å, c=31.6396(14)Å.

Magnetic properties (Fig. 1, b) and transport measurements were also carried out [4]. The superconducting transition temperatures are 33K and 30K for $KCa_2Fe_4As_4F_2$ and $RbCa_2Fe_4As_4F_2$, respectively. Up to date, the work on the synthesis of a polycrystalline sample of $CsCa_2Fe_4As_4F_2$, as well as on the crystal growth of representatives of this family is in progress.

This work was supported by RSF grants 23-12-00307.

References

1. *P. Klüfers, A. Mewis*, Z. Naturf. B **32**(7), 753-756 (1978).
2. *Paul C. Canfield, Sergey L. Bud'ko*, Annu. Rev. Condens. Matter Phys. **1**, 27-50 (2010).
3. *A.V. Sadakov, A.A. Gippius, A.T. Daniyarkhodzhaev, et al*., JETP Letters **119**(2), 111-117 (2024).
4. *I.V. Zhuvagin, V.A. Vlasenko, A.T. Daniyarkhodzhaev, et al*., JETP Letters **120**(4), 277-283 (2024).

Properties of graphene placed on an array of superconducting islands

V. Ievleva, A. Kuntsevich, V. Prudkoglyad, A. Prishchepa

Lebedev Physical Institute, Higher School of Economics, Department of Physics

Starting from 2012 [1] there have been several publications where an array of superconducting islands was placed on graphene to form a graphene josephson junction array. Below the critical temperature of separated islands there take place a BKT transition [2] when the graphene resistance disappears due to proximity effect, superconductor to insulator transition (SIT) near the neutrality point of graphene and re-entrace of superconductivity in magnetic field greater than critical [3]. Importantly, electrically controlled SIT makes graphene josephson junction array a possible superconducting transistor, so this system is interesting both for fundamental research and practical investigation.

The most commonly used superconductor for creating the graphene josephson junction array is tin [1, 3, 4]. Unlike most of the metals, tin has high wettability to the graphene and can be evaporated on graphene directly without any sublayer.

In this research, we propose a technological route of fabricating rhenium graphene josephson junction arrays, where graphene is placed atop of islands through dry hot transfer method. Rhenium is a chemically inert superconductor and does not oxidize in the air [5], therefore, it is possible to create a transparent interface between rhenium islands and graphene transferred on top of it. Besides, the critical temperature (T_c) of micron sized islands is usually suppressed comparing to the T_c of bulk material, while the T_c of rhenium amorphous thin films reaches 6-7 K [5], which is several times grater than the T_c of rhenium crystal (1.7 K) [6] and this makes rhenium highly compatible with nanolithography.

We fabricate an array of rhenium islands in a matrix of hexagonal boron nitride by electron beam lithography, SF6 plasma etching and electron beam evaporation and transfer graphene under hBN atop. The encapsulated graphene on superconducting islands is expected to demonstrate greater critical temperature and is compatible with local gating technology. Through a series of experiments, we show that the system is fundamentally meta stable.

References

1. *Allain, A., Han, Z. & Bouchiat, V*. Nature Mater, **11**, 590–594 (2012).
2. *Feigel'man, M.V., Skvortsov, M.A. & Tikhonov, K.S.* Jetp Lett. **88**, 747–751 (2008).
3. *Z. Han, A. Allain, H. Arjmandi-Tash et al*., Nature Physics **10**(5), 380–386 (2014).
4. *Sun, Y., Xiao, H., Zhang, M. et al.,* Nature Communications **9**, 2159 (2018).
5. *D.P. Pappas, et al*., Appl. Phys. Lett. **30** April 2018; 112 (18): 182601.
6. *N.E. Alekseevskii, M.N. Mikheeva, and N.A. Tulina*, Soviet Physics JETP 5.4 (1967).

Local magnetization and SNS-Andreev spectroscopy of layered iron-free pnictide superconductor $BaPd_2As_2$

E.M. Ivanova, A.T. Daniyarkhodzhaev, A.S. Usoltsev, L.A. Morgun, A.V. Sadakov, B.I. Massalimov, S.Yu. Gavrilkin

P.N. Lebedev Physical Institute, Russian Academy of Sciences, 119991, Moscow, Russia

It's been almost 20 years since the discovery of high temperature superconductivity in iron-based compounds [1]. Nevertheless, the interest of scientific community towards these materials didn't fade away due to their remarkable features. Among all classes of iron-based superconductors, the most thoroughly studied one is AFe_2As_2 (A = alkaline-earth or rare-earth), also known as 122-system. The reason for this is high transition temperature and wide range of doping by both holes and electrons.

It was discovered that similar compounds with formula AT_2Pn_2 (A = alkaline-earth or rare-earth; T = transition metals; Pn = P, As or Sb) and $ThCr_2Si_2$-type structure (I4/mmm) also exhibit superconductivity [2]. While many of them undergo a superconducting transition at fairly low temperatures, compounds $LaRu_2As_2$, $SrPt_2As_2$, $LaRu_2P_2$ and $BaPd_2As_2$ have a relatively high critical temperature of 7.8 K, 5.2 K, 4.1K and 3.8 K respectively. Even though $BaPd_2As_2$, subject of this paper, is well-studied [3,4], experimental evidence of specific type of gap symmetry in this compound is still lacking.

The purpose of this work was to try and shed light on symmetry of superconducting order parameter in $BaPd_2As_2$. To achieve this, single crystals of $BaPd_2As_2$ with sharp superconductor transition at T_c=3.7 K were studied by means of local magnetization with a two-dimensional electron gas-based micro Hall sensor with an active area of 50×50 μm^2 in order to measure lower critical field in temperatures down to 10 mK. Several models were used to fit the temperature dependence and determine possible gap symmetry: isotropic and anisotropic s-wave, d-wave and s-wave with two gaps. We found that experimental results clearly deviate from conventional s-wave curve, while anisotropic s-wave and two-gap models reproduce results pretty well.

The goal of the next step was to directly investigate the value of the superconducting gap. Samples were also studied by means of break-junction technique on clean cryogenic cleavage. Intrinsic multiple Andreev reflections effect (IMARE) spectroscopy was preformed to obtain value and structure of the energy gap. We cleaved the sample, scanned over a hundred of contacts with varying sample banks distance and examined temperature behavior of the spectra. Our data shows a single energy gap with a value Δ=0.64 mEv, which means that characteristic $2\Delta/T_c$ ratio equals 4.12, that is much larger than for conventional superconductors. That value is close to iron based Ba-122 and suggests strong electron-boson interaction.

References

1. *Kamihara, Yoichi, et al*. Journal of the American Chemical Society **130**(11), 3296-3297 (2008).
2. *Jeitschko, W.; Glaum, R.; Boonk, L.* J. Solid State Chem. **69**, 93-100 (1987).
3. *Guo, Qi, et al*. Europhysics Letters **113**(1), 17002 (2016).
4. *Abdel-Hafiez, Mahmoud, et al.* Physical Review B **97**(13), 134508 (2018).

Three-Gap Superconductivity in LiFeAs

S.A. Kuzmichev[1,2], I.V. Morozov[3], A.I. Shilov[2],
A.I. Boltalin[3], T.E. Kuzmicheva[2]

[1] Lomonosov Moscow State University, Faculty of Physics, 119991, Moscow, Russia,
[2] Lebedev Physical Institute, Russian Academy of Sciences, 119991, Moscow, Russia,
[3] Lomonosov Moscow State University, Department of Chemistry, 119991, Moscow, Russia

Using incoherent multiple Andreev reflection effect (IMARE) spectroscopy, we unambiguously show three distinct superconducting (SC) order parameters in LiFeAs pnictides, with an extended *s*-wave symmetry. We present IMARE data on the SC gaps temperature dependence, their characteristic ratios and the level of anisotropy as well.

Alkali-metal LiFeAs pnictides show optimal SC properties in the stoichiometric composition with $T_c \approx 17$ K, whereas any electron substitution rapidly decrease the critical temperature [1]. With it, LiFeAs is fully nonmagnetic and shows no Fermi surface nesting [2]. Due to the alkali metal, the LiFeAs-family pnictides rapidly degrade in presence of even trace amounts of water vapor and oxygen, thus strongly complicating any experimental probing of its properties.

Single crystals of alkali metal based LiFeAs pnictides (the 111 family) were grown using "self-flux" technique [3-5]. At $T = 4.2$ K, Andreev junctions of SnS-type (s – superconductor, n – thin normal metal) were formed using planar "break-junction'' technique [6]. Here, we present a comprehensive study of the SC order parameter of LiFeAs single crystals using IMARE spectroscopy of SnS-junctions (direct local probe).

Below T_c, we show a multiple-gap superconductivity and determine the magnitudes and characteristic ratios of the three SC order parameters: the largest one Δ_Γ, the middle SC gap Δ_L, and the small SC gap Δ_S [3-5]. Considering the IMARE data within the classical models [7, 8], we conclude an observation of a minor *k*-space anisotropy with nodeless extended *s*-wave symmetry. Experimentally, we directly determined the extrema Δ^{in} and Δ^{out} of each anisotropic SC order parameter being the minimum and the maximum Cooper pair coupling energies in dependence of the momentum direction in the related bands. The SC gap anisotropy is estimated as $A \equiv 100 \times (1 - \Delta_L^{in} / \Delta_L^{out}) \cdot 100\%$. The resulting values are $A_\Gamma \approx 10\%$, $A_L \approx (30-35)\%$, and $A_S \approx 37\%$. Such complex SC gap Andreev structure is reproducibly observed in the obtained $dI(V)/dV$ spectra of SnS-junctions formed in different LiFeAs from the same batch. We show a bulk nature of the determined energy parameters $\Delta_i^{in,out}(0)$ and no correlation with the normal resistance of the junction. Turning to ARPES data [2], one may suppose that Δ_Γ develops at the inner hole barrel at the Γ point of the first Brillouin zone, Δ_S develops at the outer hole barrel, whereas Δ_L – in the electron bands near the M point.

Temperature dependences of the gap edges $\Delta_i^{out}(T)$ and $\Delta_i^{in}(T)$ ($i = \Gamma, L, S$) directly determined using IMARE spectroscopy are also presented. We estimate a moderate interband interaction between the three SC condensates in the *k*-space.

The characteristic ratios are $2\Delta_\Gamma(0)/k_BT_c \approx 7.0-8.2$, $2\Delta_L(0)/k_BT_c \approx 3.0-5.0$, and $2\Delta_S(0)/k_BT_c \approx 1.2-2.1$ (the ranges correspond to the *k*-space anisotropy degree). These values remain almost unchanged along the studied range of the local critical temperature $T_c^{local} \approx 15.0-17.5$ K.

Fig. 1. Characteristic ratio of the extrema of three SC gaps anisotropic in the *k*-space in LiFeAs versus the local critical temperature of the junction.

References

1. *S.A. Kuzmichev, T.E. Kuzmicheva*, JETP Lett. **114**, 630 (2021).
2. *S.V. Borisenko*, *et al*., Symmetry **4**, 251 (2012).
3. *I. Morozov*, *et al*., Cryst. Growth & Design **10**, 4428 (2010).
4. *T.E. Kuzmicheva*, *et al*., JETP Lett. **111**, 350 (2020).
5. *S. Kuzmichev*, *et al*., SN Appl. Sci. **4**, 189 (2022).
6. *S.A. Kuzmichev, T.E. Kuzmicheva*, Low Temp. Phys. **42**, 1008 (2016).
7. *R. Kuemmel*, *et al*., Phys. Rev. B **42**, 3992 (1990).
8. *T.P. Devereaux, P. Fulde*, Phys. Rev. B **47**, 14638 (1993).

Comparison of the Superconducting Properties of the Iron Selenides with Isovalent Substitution

T.E. Kuzmicheva[1], S.A. Kuzmichev[2,1], A.D. Ilina[1],
I.A. Nikitchenkov[2,1], E.O. Rakhmanov[3,1], A.I. Shilov[1],
I.V. Morozov[3]

P.N. Lebedev Physical Institute, 119991 Moscow, Russia,
Faculty of Physics, Lomonosov Moscow State University, 119991 Moscow, Russia,
Department of chemistry, Lomonosov Moscow State University, 119991 Moscow, Russia

$A_xFe_{2-y}Se_2$ (A is alkali metal) iron selenides are natural composites, where thin crystallites of the superconducting (SC) phase grow on the boundaries of bulk antiferromagnetic (AFM) dielectric crystals. Using incoherent multiple Andreev reflection effect (IMARE) spectroscopy, we unambiguously show a single-gap superconductivity of iron selenides with various type of composition, directly determine the magnitude and the temperature dependence of the SC gap $\Delta(T)$. We show a minor strengthen of the Cooper pairing in the ternary $(Na,K,Rb)_xFe_{2-y}Se_2$ compound as compared to ferroselenides with (Na,K) and (Se,S) isovalent substitution.

Selenides $A_xFe_{2-y}Se_2$ (A – Na, K, Rb, the so-called 122-Se family) are natural composites containing at least two coexisting phases: about 80 of the crystal volume is occupied by crystals of the AFM dielectric phase $A_{0.8}Fe_{1.6}Se_2$, and about 20 – by crystallites of the metallic $A_{0.3}Fe_2Se_2$ phase which becomes superconducting below T_c. It is known that different types of isovalent substitution differently affect the critical temperature T_c: thus, even a small substitution of an alkali metal causes a jump-like T_c change [1], while under (Se,S) substitution, T_c forms a "semi-dome'' [2]. Due to natural phase separation and rapid degradation of the SC properties in open air (in several minutes), $A_xFe_{2-y}Se_2$ selenides remain extremely understudied to date.

In particular, for the compositions considered in the work, $(K_{0.8}Na_{0.2})_{0.9}Fe_{1.7}Se_2$ (hereafter KNFS), $(K_{0.3}Na_{0.3}Rb_{0.3})_{0.8}Fe_{1.7}Se_2$ (NKRFS), and $K_{0.8}Fe_{1.7}(Se_{0.73}S_{0.27})_2$ (KFSS), the topology of the Fermi surface remains unknown, and there are also no data from other groups on the amount of SC condensates formed below T_c.

Using the "self-flux" method, we grew large (up to 8-10 mm) KNFS, KFSS, and NKRFS crystals with three types of isovalent substitution and the range of critical temperatures $T_c \approx 25-34$ K [3-5]. Using the planar mechanically controlled "break-junction" technique [6], various types of tunnel structures were created in the crystals, including Andreev SnS contacts and tunneling ScS contacts (where S is a superconductor, c – constriction, and n – thin normal metal).

Using IMARE spectroscopy of SnS-junctions, the magnitude of the SC gap and its BCS-like temperature dependence were directly determined. We show a bulk

nature of the detected SC gap, the reproducibility of its magnitude and independence on the geometric parameters of the SnS-contact (i.e. area and the normal resistance).

The obtained temperature dependences of the excess Andreev current $I_{exc}(T) \equiv I(T, eV) - I(T_c, eV) \propto \Delta(T)$, taken at a constant bias eV gg 2Delta, are well described by a single – band BCS – shapeddependence, which agrees with the theoretical predictions [7] for the IMARE regime. Using tunnel spectroscopy of ScS contacts, the temperature dependence of the supercurrent $I_c(T)$ was obtained, that could be roughly related to the Cooperpairs concentration. The experimental data [4] can be fitted with the Ambegaokar–Baratoff formula $I_c(T) \propto \Delta(T) \cdot \tanh[\Delta(T)/2k_BT]$ using the experimental $\Delta(T)$ dependence directly measured by IMARE spectroscopy.

The data obtained by three methods ($\Delta(T)$, $I_{exc}(T)$, $I_c(T)$) indicate the consistency of the results of the used spectroscopic techniques and unambiguously indicate the implementation of single-gap superconductivity of the studied ferroselenides.

In KNFS and KFSS, the characteristic ratio was $2\Delta(0)/k_BT_c \approx 4.1-4.6$, whereas in NKRFS this value was a bit larger: $2\Delta(0)/k_BT_c \approx 4.4-5.0$. All the values exceed the weak-coupling BCS-limit 3.5, thus indicating strong coupling in the electron bands.

The similarity of the SC-gap structure and the value of the characteristic ratio allows us to conclude a similar mechanism of Cooper pairing realized in KNFS and KFSS. The observed constancy of the $2\Delta(0)/k_BT_c^{local}$ characteristic ratio, i.e. scaling between $2\Delta(0)$ and T_c indicates a single evolution of the properties of the SC subsystem of KNFS and KFSS selenides with a critical temperature. Contrary, a minor strengthen of the Cooper pairing in the ternary NKRFS compound develops, as compared to ferroselenides with (Na,K) and (Se,S) isovalent substitution.

The work supported by the RSF project no. 22-72-10082P.

$KCa_2Fe_4As_4F_2$ single crystal: microstructure, vortex matter and Andreev spectroscopy

A.Yu. Levakhova[1], A.V. Sadakov[1],
A.S. Usoltsev[1], V.A. Vlasenko[1], Junyi Ge[2]

[1] V.L. Ginzburg Centre for High-Temperature Superconductivity and Quantum Materials P.N. Lebedev Physical Institute of the RAS, Moscow, Russia,
[2] Shanghai University, Shanghai, China

The single crystals of the new iron – based superconducting layered 12442 family are studied in this work. HRTEM studies (HAADF and EDX mapping Chemi STEM) show planar defects in the structure. We show, that these defects are monolayers of CaFeAsF and KFe_2As_2. Andreev reflection spectroscopy experiment reveal several distinct temperature dependent energy gap structures. One of these gap structures have local transition temperature of T_c=28 K (1111) and the other one has T_c=34K (12442). We argue that in 12442 system there are at least two different pinning mechanisms. The strong pinning prevails at higher-temperatures and the weak prevails at low-temperatures in our system.

The single crystals of the new iron – based superconducting layered 12442 family are studied in this work [1]. The 12442 ($KCa_2Fe_4As_4F_2$) compound is self-doped, it has a narrow crystallization range and is formed from two phases 1111 (CaFeAsF) and 122 (KFe_2As_2) [2]. Single crystals of the $KCa_2Fe_4As_4F_2$ were grown by "self-flux" method (KAs) [2]. The XRD measurements confirm the high quality of the crystal with sharp (00l) reflections and minimum trace of the second phase. Magnetic susceptibility measurements show superconducting transition at about 34 K. HRTEM studies (HAADF and EDX mapping Chemi STEM) show planar defects in the structure. We show, that these defects are monolayers of CaFeAsF and KFe_2As_2. Andreev reflection spectroscopy experiment reveal several distinct temperature dependent energy gap structures. One of these gap structures have local transition temperature of T_c=28 K (1111) and the other one has T_c=34K (12442). The critical current density J_c and the nature of the pinning mechanism in these samples were examined. It was found that the second magnetization peak at 24, 26, 28 K can be related to pinning of Abrikosov vortices on planar defects. At higher magnetic fields, the critical current follows a power law behavior $J_c \propto H^{-a}$ with 0.3-04± 0.1 at higher temperatures (up to 20 K), and following increasing to 1,2-1,5 ± 0.1 at low temperatures. The theory predicts that exponent values $a \propto H^{-5/8}$ and lower, indicates strong vortex pinning. We argue that in 12442 system there are at least two different pinning mechanisms. The strong pinning prevails at higher-temperatures and the weak prevails at low-temperatures in our system.

This research was supported by Russian Science Foundation (№ 23-12-00307).

References

1. *Z.C. Wang, et al*., J. Am. Chem. Soc., **138**(25), 7856-7859 (2016).
2. *T. Wang, et al*., J. Phys. Chem. C., **123**(22), 13929-7859 (2019).
3. *A.Y. Degtyarenko, et al*., Nanomaterials., **12**(21), 3801 (2022).
4. *L.X. Gao, et al*., Supercond. Sci. Technol., **35**(5), 055013 (2022).
5. *P.V. Lopez, et al*., Sci Rep, **12**, 20359 (2022).

Tunneling Spectroscopy of Na(Fe,Co)As and Ba(Fe,Ni)$_2$As$_2$ Pnictides with Variable Electron Doping in the Normal State

I.A. Nikitchenkov[1,2], S.A. Kuzmichev[1,2], K.S. Pervakov[2],
V.A. Vlasenko[2], I.V. Morozov[3], A.I. Shilov[2],
Ye.O. Rakhmanov[3,2], A.D. Ilina[2,4], T.E. Kuzmicheva[2]

[1] Faculty of Physics, M.V. Lomonosov Moscow State University, Moscow, Russia,
[2] P.N. Lebedev Physical Institute of the Russian Academy of Sciences, Moscow, Russia,
[3] Department of Chemistry, M.V. Lomonosov Moscow State University, 119991 Moscow, Russia,
[4] Moscow Institute of Physics and Technology, Dolgoprudny, Russia

Tunneling spectroscopy was applied to Na(Fe,Co)As and Ba(Fe,Ni)$_2$As$_2$ single crystals of underdoped and overdoped compositions (T_c = 12–22 K). The $dI(V)/dV$ spectra of tunneling junctions formed in both compounds show a robust, temperature-independent nonlinearity that retains well above T_c, shifts systematically with electron doping and supposed to disappear near the strongly overdoped regime. The feature does not directly relate to the SC properties, and cannot be caused by overheating effect or geometric resonances. The observed non-linearity in dI/dV is probably attributed to doping-induced renormalization of the normal-state electronic density of states, possibly driven by nematic fluctuations or specific band-structure topology of the 122/111 family pnictides.

Ba(Fe,Ni)$_2$As$_2$ (the 122 family) and Na(Fe,Co)As compounds (the 111 family) share a layered crystal structure in which superconducting FeAs blocks alternate with Ba- or Na-planes along the *c*-axis. In the stoichiometric state both materials possess long-range antiferromagnetic order (AFM). Electron doping gradually suppresses AFM and gives rise to a dome-shaped superconducting phase with maximum critical temperature T_c of 21 K for Ba(Fe,Ni)$_2$As$_2$ and 22 K for Na(Fe,Co)As [1, 2]. Unlike the 122 family, 111 pnictides display low-T_c superconductivity already in stoichiometric NaFeAs. The Fermi-surface of each compound consists of hole pockets near the Γ-point (which often treated as a single effective pocket) and electron cylinders near the *M*-point of the Brillouin zone.

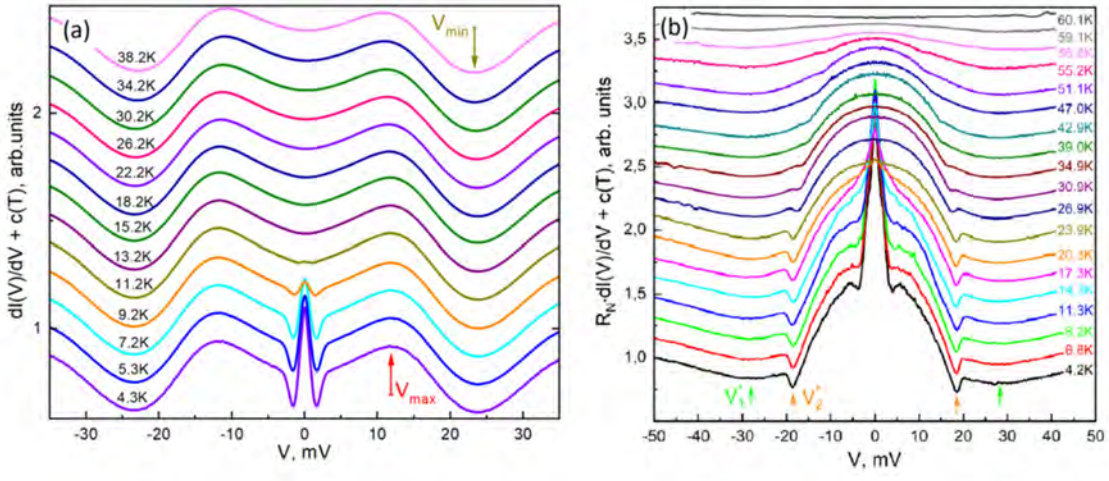

We studied $BaFe_{2-x}Ni_xAs_2$ single crystals with under- and overdoped compositions (x = 0.06–0.14, T_c = 12–21 K) together with nominally underdoped $NaFe_{0.979}Co_{0.021}As$ ($T_c \approx 22$ K). At T = 4.2 K, break-junctions of the superconductor–constriction–superconductor (ScS) type were formed, with a semiballistic quasiparticle transport [3]. The goal was to analyze the current–voltage characteristics (CVCs) and dynamic-conductance spectra $dI(V)/dV$ of the contacts in both superconducting and normal states.

Below T_c we observed incoherent multiple Andreev reflections (IMARE), which generate an excess current at any bias eV, accompanied by enhanced Andreev conductance at zero bias and gap minima for any temperatures up to T_c [4]. In addition, both CVCs and $dI(V)/dV$ exhibited a non-IMARE nonlinearity that persisted in the superconducting and the normal state.

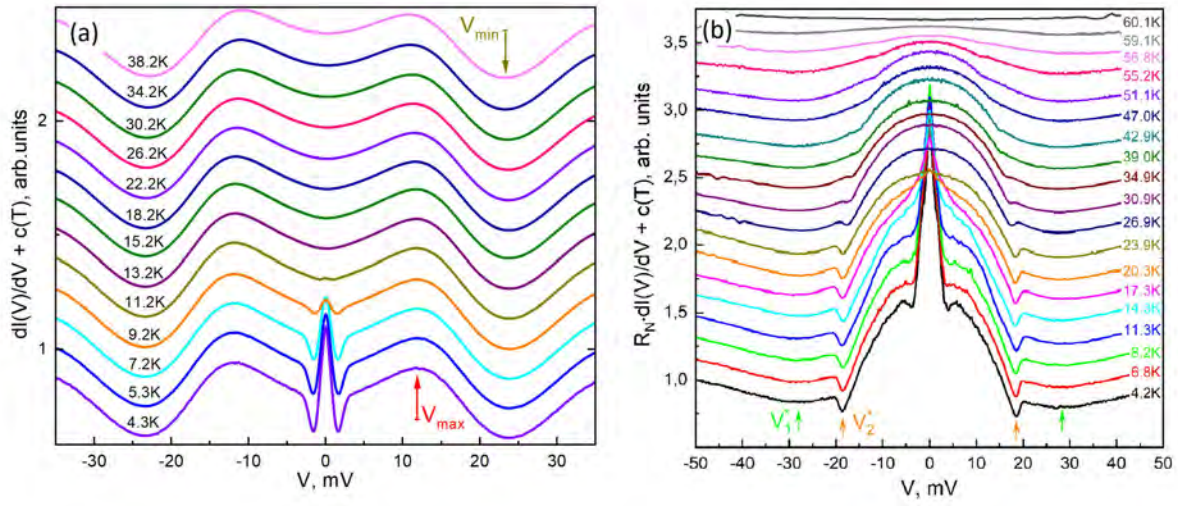

For $BaFe_{2-x}Ni_xAs_x$, a representative shape of this $dI(V)/dV$ nonlinearity is shown in Fig. 1a. The positions and form of the features are almost temperature-independent between 4.3 K and 50 K and remain similar across different doping levels and T_c values. Moving along the doping phase diagram, the energy positions of the maximum and minimum shift: in the overdoped region (away from the AFM and nematic phases) both V_{max} and V_{min} decrease. Linear extrapolation towards higher Ni content predicts that the features should vanish and the $dI(V)/dV$ spectrum should become linear in a strongly overdoped, non-superconducting composition with $x \approx 0.22$ [5]. Because the nonlinearity is observed in both, superconducting and normal state, and does not changed at T_c, these normal-state features are seemingly not directly linked to the superconducting properties.

In the normal state of $NaFe_{0.979}Co_{0.021}As$ the $dI(V)/dV$ spectra display minima at $V_1^* \approx 26.6$ mV and $V_2^* \approx 21.2$ mV (arrows in Fig. 1b). Unlike the above mentioned 122-family compounds, the 111-family pnictide shows an additional $dI(V)/dV$ peak at low biases eV. Noteworthily, such nonlinearity was not typical for overdoped Na(Fe,Co)As at all.

These normal-state features reproducibly observed for all tunneling contacts, independent of their normal resistance R_n, and cannot be explained by local overheating effect. We demonstrated that the nonlinear $dI(V)/dV$ shape cannot

originate from geometric resonances or a specific crystal microstructure (e.g., twinning), contrary, characterizes bulk electronic properties of the material [5].

The tunneling spectrum of NcN contact (N – thick normal metal) is known to depend on the electronic density of states N(E) near the Fermi level [6]. The observed effect may thus arise from peculiarities of $N(E_F)$[1] const caused by the band-structure topology of the 122/111 family pnictides, the presence of nematic fluctuations with the associated splitting of d_{xz}/d_{yz} iron-orbital bands [7], or a renormalization of N(E) due to coupling to characteristic bosonic modes [8]. Remarkably, the temperature $T \approx 60$ K of $dI(V)/dV$-spectrum flattering in $NaFe_{0.979}Co_{0.021}As$ [9] agrees well with the temperature of nematic transition determined in [10]. This favors a possible nematicity-driven origin of the observed effect in $NaFe_{0.979}Co_{0.021}As$.

References

1. *Xingye Lu.* Phase Diagram and Magnetic Excitations of $BaFe_{2-x}Ni_xAs_2$: A Neutron Scattering Study. – Springer Theses, 2017.
2. *E. Kuzmicheva & S.A. Kuzmichev*, JETP Lett. **114**, 685 (2021).
3. *A. Kuzmichev & T.E. Kuzmicheva*, Low Temp. Phys. **42**, 1284 (2016).
4. *Kuemmel et al*., Phys. Rev. B **42**, 3992 (1990).
5. *A. Nikitchenkov, S.A. Kuzmichev*, *A.D. Ilina et al*., JETP **166**, 834 (2024).
6. *Giaever & K. Megerle*, Phys. Rev. **112**, 1101 (1961).
7. *Shimojima, T. Sonobe, W. Malaeb et al*., Phys. Rev. B **89**, 045101 (2014).
8. *M. Svistunov, M.A. Belogolovskii, O.I. Chernyak*, Sov. Phys. Usp. **30**, 31 (1987).
9. *A. Nikitchenkov, S.A. Kuzmichev, A.D. Ilina, et al*., Solid State Phys. **67**, 1226 (2025).
10. *Q. Deng, et al*., Phys. Rev. B **91**, 020508(R) (2015).

High-performance amorphous superconducting rhenium films by e-beam evaporation

E.V. Tarkaeva, V.A. Ievleva, A.R. Prishcepa,
E. Zhukova, A.Yu. Kuntsevich

Lebedev Physical Institute, Moscow Institute of Physics and Technology

In this work, we report the deposition of elementary rhenium thin films using electron beam evaporation onto substrates maintained at room temperature. Structural characterization shows that the films are amorphous. The films are superconducting, with a critical temperature above 6 K–the highest reported for rhenium–as well as high critical currents and critical fields. Optical spectroscopy studies confirm a conventional BCS-like superconducting behavior, characterized by a zero-temperature energy gap of approximately 2 meV and a subgap optical conductivity. The fabricated films demonstrate stability and compatibility with standard photolithographic processes, including photoresist lift-off.

The development of superconducting devices requires materials with transition temperatures exceeding 4.2 K. While bulk rhenium exhibits a relatively low Tc of 1.7 K, thin rhenium films can achieve significantly higher transition temperatures–up to 6 K. This enhancement makes rhenium a promising candidate for practical applications in superconducting electronics, particularly in quantum computing and sensitive detectors. However, the high melting point of rhenium poses a major challenge in thin-film deposition, as excessive heating can damage underlying structures or degrade lithographic masks. To ensure compatibility with standard lift-off processes, deposition techniques must carefully balance temperature control and film quality. Electron-beam evaporation offers a viable solution, though precise parameter optimization is required to achieve optimal superconducting properties.

We demonstrate the fabrication of thin rhenium films (tens of nanometers thick) using electron-beam evaporation in a MEB PLASSYS 400 system. These films exhibit high critical temperatures (T_c > 6 K), strong critical magnetic fields, and high critical currents, making them suitable for demanding superconducting applications. Furthermore, they demonstrate excellent stability, with reproducible resistance-temperature characteristics even after multiple thermal cycles.

Another key advantage of rhenium is its chemical inertness–unlike many superconductors, it does not oxidize under ambient conditions. This property makes it an ideal bottom electrode material for hybrid nanostructures: delicate devices (such as 2D materials or topological insulator layers) can be transferred onto pre-patterned rhenium films without interfacial degradation. The absence of native oxides ensures clean electrical contacts, while rhenium's high Tc preserves superconductivity in the electrode even at elevated operating temperatures. Structural characterization via X-ray diffraction confirms the amorphous nature of the films, while optical studies support that their superconducting behavior follows the Bardeen-Cooper-Schrieffer (BCS) theory.

Anomalous magnetic flux flow in superconducting niobium nitride films

M.A. Vasyutin, N.D. Kuzmichev, D.A. Shilkin

Ogarev Mordovia State University, Saransk, Russia, 430005

Linear sections that do not change slope in a certain region of magnetic fields have been discovered in I-V characteristics of superconducting films NbN. This is explained by the strong interaction of vortices in the collective pinning model and the movement of a part of the vortex system relative to the strongly pinned vortices.

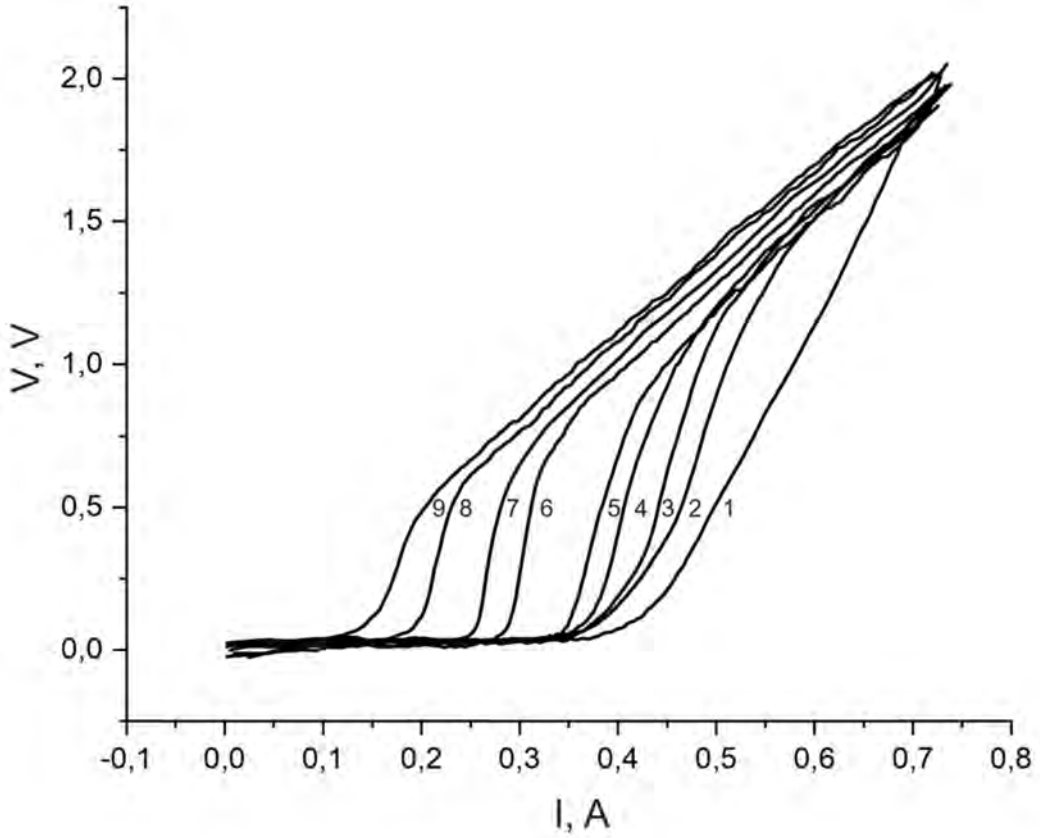

Fig. 1. The current-voltage curves of NbN sample with T_c = 16.3 K at a temperature of 15.4 K in magnetic field strength of: 1 – 0.5 kOe, 2 – 2.5 kOe, 3 – 3.75 kOe, 4 – 5 kOe, 5 – 6.25 kOe, 6 – 8.75 kOe, 7 – 10 kOe, 8 – 12.5 kOe, 9 – 15 kOe.

I-V characteristics of superconducting NbN films were obtained at temperatures below T_c in constant magnetic fields. The preparation of films and experimental details is given in articles [1-4]. In the temperature range from 0.7 T_c to 0.95 T_c for constant magnetic fields with a strength of up to H = 80 kOe, regions of linear I–V characteristics with differential resistance independent of the magnetic field were observed (especially noticeable on curves 1 and 2 on Fig. 1). The resistive state of the films in this case is not described by the usual flow of magnetic flux. The presence of such sections of the current-voltage characteristic is explained by the additional constant force acting on the vortex lattice. The origin of this force may be related to collective lattice pinning on atomic-scale inhomogeneities always present

in niobium nitride and to strong intervortex interactions. In this case, movement of a weakly fixed part of the vortex lattice in an environment of strongly pinned vortices is possible. The decrease in the linear part with increasing H is associated with a decrease in the distance between the vortices. As the field strength approaches 12 kOe, when the number of vortices becomes equal to the number of centers of strong pinning, a greater force is required to displace the entire vortex lattice as a whole. This leads to a more rapid occurrence of the Larkin-Ovchinnikov instability.

References

1. *M.A. Vasyutin, N.D. Kuzmichev, D.A. Shilkin*, Phys. Solid State **58,** *2,* 236 (2016).
2. *M.A. Vasyutin, N.D. Kuzmichev, D.A. Shilkin*, Phys. Solid State **60,** *11,* 2287 (2018).
3. *M.A. Vasyutin, N.D. Kuzmichev, D.A. Shilkin*, Phys. Met. Metallogr. **121,** *10,* 955 (2020).
4. *D.M. Gokhfeld, N.E. Savitskaya, S.I. Popkov, N.D. Kuzmichev, M.A. Vasyutin, D.A. Balaev*, JETP **134,** *6,* 707 (2022).

(SM) SUPERCONDUCTIVITY AND MAGNETISM

Invited

Superconducting proximity effect for topological semimetals

E. Deviatov

Institute of Solid State Physics of the Russian Academy of Sciences, 142432 Chernogolovka, Russia

We present experimental results on charge transport in different proximity devices, which are formed as junctions between a superconductor and a thick single crystal flake of topological semimetal. We demonstrate surface-state transferred Josephson current between two 5 μm spaced superconducting indium leads, a. c. Josephson effect with fractional Shapiro step under microwave irradiation, reentrant proximity-induced superconductivity, Josephson spin-valve realization in the magnetic nodal-line topological semimetals, coalescence of Andreev bound states on the surface of a chiral topological semimetal, and surface superconductivity in a three-dimensional Dirac semimetals.

Like other topological materials, topological semimetals acquire topologically protected surface states due to the bulk-boundary correspondence. Dirac semimetals are characterized by gapless bulk spectrum with band touching in some distinct Dirac points. In Weyl semimetals every touching point splits into two Weyl nodes with opposite chiralities. Fermi arc surface states are connecting projections of these nodes on the surface Brillouin zone, so the topological surface states are chiral for Weyl materials [1].

For topological semimetals, the main problem of transport investigations is to reveal the surface states contribution in the material with gapless bulk spectrum. As a possible scenario, one can consider the superconducting proximity effect. In proximity with a superconductor, topological surface (or edge) states are able to carry supercurrent over extremely large distances, while the coherence length is much smaller for the bulk carriers. Also, in proximity to a superconductor, topological materials exhibit nontrivial physics due to the spin-momentum locking, that can in various cases result in topological superconductivity and existence of Majorana modes.

Here, we present experimental results on charge transport in different proximity devices, which are formed as junctions between a superconductor and a thick single crystal flake of topological semimetal. We demonstrate surface-state transferred Josephson current between two 5 μm spaced superconducting indium leads, a. c. Josephson effect with fractional Shapiro step under microwave irradiation, reentrant proximity-induced superconductivity, Josephson spin-valve realization in the magnetic nodal-line topological semimetals, coalescence of Andreev bound states on the surface of a chiral topological semimetal, and surface superconductivity in a three-dimensional Dirac semimetals. Also, we perform first experimental investigations of electron transport across a single planar junction between the superconducting electrode and recently discovered altermagnetic materials.

We gratefully acknowledge financial support by the Russian Science Foundation, project RSF-24-22-00060, https://rscf.ru/project/24-22-00060/.

References

1. *N.P. Armitage, E.J. Mele, and A. Vishwanath*, Rev. Mod. Phys. **90**, 15001 (2018).

NMR spectroscopy of transition metal pnictide and gallide superconductors and related compounds

A.A. Gippius[1,2], A.V. Tkachev[2], S.V. Zhurenko[2], N.E. Gervits[2], A.V. Gunbin[2], Y.A. Ovchenkov[1], I.G. Puzanova[1], A.A. Gippius[1,2], I.V. Morozov[1], V.Yu. Verchenko[1], A.V. Shevelkov[1]

[1] M.V. Lomonosov Moscow State University, Moscow, Russia,
[2] P.N. Lebedev Physical Institute of RAS, Moscow, Russia

Specific examples of using NMR spectroscopy in the study of various classes of superconductors are discussed, including classical BCS and unconventional superconductors: cuprate, heavy-fermion, iron-containing and intermetallic superconductors. The results of recent experimental studies of $FeSe_{0.675}Te_{0.3}S_{0.025}$ and $FeSe_{0.7}Te_{0.3}$ crystals, novel $Ba(Cr_{1-x}Co_x)_2As_2$ compounds and a new family of gallium-based intermetallic superconductors $Mo_4Ga_{20}Sb$ and $Mo_8Ga_{41}Sb$ will be discussed in more detail.

We consider specific examples of using NMR spectroscopy in the study of various classes of superconductors. The main focus will be put on the capabilities of the NMR method for determining the pairing mechanism and characteristics of the superconducting gap, both in classical BCS and unconventional superconductors: cuprate, heavy-fermion, iron-containing and intermetallic superconductors. The results of recent experimental studies of $FeSe_{0.675}Te_{0.3}S_{0.025}$ and $FeSe_{0.7}Te_{0.3}$ compounds which are close to the nematicity change point in Fe(Se,Te) system, novel $Ba(Cr_{1-x}Co_x)_2As_2$ compounds, and a new family of gallium-based intermetallic superconductors $Mo_4Ga_{20}Sb$ and $Mo_8Ga_{41}Sb$ will be discussed in more detail.

In particular, ^{77}Se NMR data obtained on $FeSe_{0.675}Te_{0.3}S_{0.025}$ compounds showed a noticeable line broadening below the structural transition and an anomaly in the temperature dependence of the relaxation rate, which was not observed in FeSe. Our results confirm existence of the nematicity change point (NCP) in Fe(Se,Te) at a low Te content and make the phase diagram of quasi-binary Fe(Se,Te) compounds generally consistent with the phase diagram of FeSe under pressure.

In the $FeSe_{0.7}Te_{0.3}$ crystals, a structural phase transition occurs in two stages. At higher temperatures, the electronic subsystem undergoes a rearrangement, leading to a significant increase in elastoresistance. ^{77}Se NMR data show an abrupt change in the relaxation rate during this transition. The final transition occurs at a temperature several degrees below and is also accompanied by anomalies in the electronic properties. Thus, in the Fe(Se,Te) series, similarly to the behavior of pure FeSe under pressure, the type of transition changes and intermediate state appear before the structural transition is suppressed.

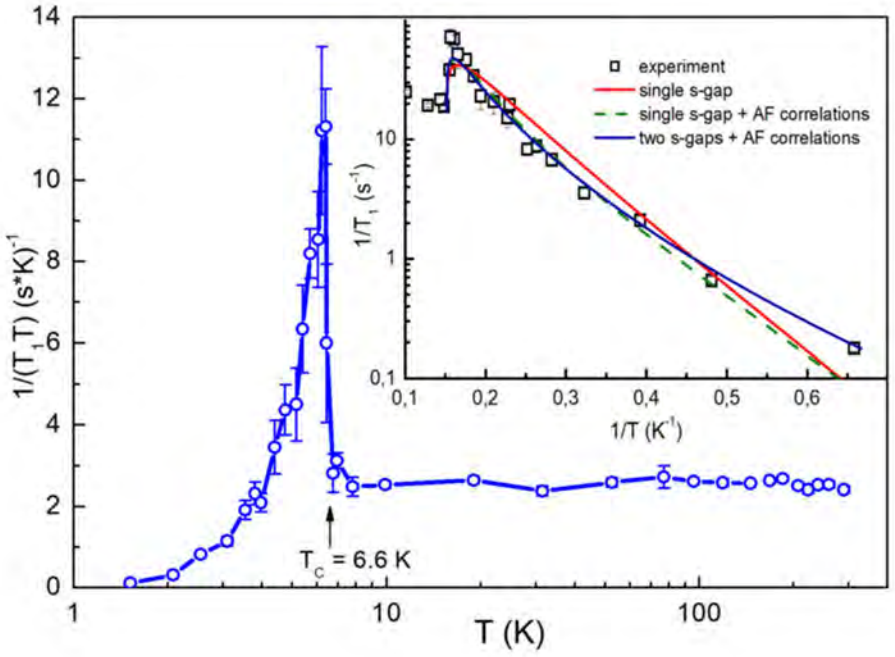

Molybdenum gallide superconductor $Mo_4Ga_{20}Sb$ with T_c = 6.6 K represents a family of novel intermetallic superconductors $Mo_4Ga_{20}X$ (X = S, Se, Te and Sb) of the Mo_4Ga_{21} structure type which attracts significant scientific interest due to unusual properties of their superconducting state and enhanced electron-phonon coupling [1]. In particular, the specific heat of $Mo_4Ga_{20}Sb$ follows the BCS-derived α-model [2] with the enhanced value of $\alpha = \Delta(0)/(k_B T_c) = 1.825$ and $\Delta C_e/(\gamma T_c) = 1.53$ [3].

We performed an extensive study of the intermetallic superconductor $Mo_4Ga_{20}Sb$ by means of NMR and NQR spectroscopy on ^{69}Ga and ^{71}Ga nuclei to gain novel information about its normal state and superconducting properties including pairing mechanism and gap values. We succeeded to observe the complete ^{69,71}Ga NQR spectrum of $Mo_4Ga_{20}Sb$ at 4.2 K, which consists of four pairs of lines corresponding to the four nonequivalent crystallographic positions of gallium in the crystal structure. We found that above T_c the nuclear spin lattice relaxation $1/T_1$ of ^{69}Ga isotope in the Ga1 position follows the Korringa law $K^2T_1T = const$ characteristic for the systems with good metallic conductivity. Below T_c, we observed a pronounced intensive Hebel-Slichter peak (Fig.1) evidencing for the *s*-wave superconductivity without points or zeroing lines in the *k*-space (full gap *s*-wave superconductivity). We demonstrated that the best coincidence with the experimental data is achieved assuming two *s*-wave superconducting gaps of 13 K and 6 K with relative weights of 0.8 and 0.2, respectively, taking into account antiferromagnetic correlations (Inset in Fig.1). The obtained weighted average value of 11.6 K is consistent with the literature estimate of Δ = 12.05 K [3].

A comprehensive study of the intermetallic superconductor Mo_8Ga_{41} was conducted by means of HRPXRD, *ab-initio* calculations, NMR and NQR spectroscopy on ^{69}Ga and ^{71}Ga nuclei, as well as tunneling spectroscopy. All

experimental methods used demonstrated the presence of an inherent surface superconducting phase in addition to the bulk superconducting phase. For the latter, the *s*-wave type single-gap superconducting behavior was observed with a slightly increased $2\Delta_0/k_BT_c = 3.89$ in agreement with the known enhanced electron-phonon coupling in this compound [4]. From nuclear spin-lattice relaxation experiment, the estimated superconducting gap value of the surface phase was $2\Delta_0^* = 22.2$ K, which corresponds to the $T_c^* \approx 6.3$ K in the weak-coupling BCS limit. Meanwhile, the tunneling spectroscopy reveals similar values of $T_c^* \sim 6.0 - 7.3$ K for this surface phase. Thus, the known evidence of the Mo_8Ga_{41} multi-gap behavior [5, 6] can be explained by the influence of the inherent surface superconducting phase.

The report presents experimental results obtained in the Condensed Matter NMR Laboratory of the Department of Low Temperature Physics and Superconductivity of Moscow State University and the Solid State NMR Laboratory of the Lebedev Physical Institute.

References

1. *V.Yu. Verchenko, A.V. Shevelkov*, Dalton Trans. **50**, 5109–5114 (2021).
2. *H. Padamsee, J.E. Neighbor, C.A. Shifman*, J. Low Temp. Phys. **12**, 387 (1973).
3. *V.Yu. Verchenko et al*., Chemistry of Materials **32**, 6730 (2020).
4. *V.Yu. Verchenko et al*., Phys. Rev. B **93**, 064501 (2016).
5. *Y. Zhou et al*., Phys. Rev. B **102**, 134512 (2020).
6. *A. Sirohi et al*., Phys. Rev. B **99**, 054503 (2019).

Pure Nematic Transition Inside the Superconducting Dome of Iron Chalcogenide Superconductor $FeSe_{1-x}Te_x$

K.Y. Liang, R.Z. Zhang, Z.F. Lin, B.R. Chen, P.H. Zhang,
K.Z. Yao, Q.S. He, Q.Z. Zhou, H.X. Yao, K. Jin, Y.H. Wang

Fudan University

Nematicity and magnetism are prevalent orders in high transition temperature (T_c) superconductors. Quantum fluctuation of nematicity and spin are both plausible candidates for mediating unconventional Cooper pairing. Identifying the sole effect of a nematic quantum critical point (QCP) on the superconducting dome without any interference of spin fluctuations is therefore highly desirable. The iron chalcogenide superconductor FeSe exhibits pure nematicity without any magnetic ordering. A nematic quantum transition can be induced by Te substitution but experimental study of the nematic transition is so far limited to its normal state. By performing local susceptometry on composition-spread $FeSe_{1-x}Te_x$ films using scanning SQUID microscopy, we investigate the superfluid density (ρ_s) across the pure nematic transition in extremely fine steps of $\Delta x = 0.0008$. The temperature dependence of ρ_s changes from the form of anisotropic pairing on the nematic side to an isotropic one across the critical doping (x_c). The power-law dependence of gap anisotropy on $x - x_c$ provides evidence for nematic quantum criticality under the superconducting dome. The low-temperature ρ_s scales linearly with Tc in the nematic phase, whereas the gap amplitude, which is maximal at x_c, determines the T_c for $x > x_c$. Our result establishes a pure nematic QCP in $FeSe_{1-x}Te_x$, separating two superconducting orders with distinct pairing boosted by nematic quantum fluctuations.

A quantum critical point (QCP) refers to the point where a symmetry-breaking phase of matter is continuously suppressed to zero by tuning non-thermal parameter at zero temperature. Strong quantum fluctuation of the order parameter exists around a QCP. Symmetry breaking orders of both charge and spin are ubiquitous in the parent compounds of high transition temperature (T_c) superconductors. These orders can be gradually suppressed by chemical doping for example, which also leads to the emergence of superconducting dome. The close proximity of the highest T_c point to potential QCP is a tantalizing clue to establish their causal relationship. In iron-based superconductors (FeSCs), for example, superconductivity reaches maximum when the electronic nematic order, which reduces the C_4 crystalline symmetry to a C_2 electronic ordering, is suppressed by chemical doping or pressure to a putative QCP. In cuprate superconductors, recent studies also signifies a nematic QCP near the verge of the pseudogap state. It has been theoretically proposed that strong nematic fluctuation near such a QCP can be responsible for superconducting pairing. Experimentally elucidating the existence and the role of the nematic QCP beneath the superconducting dome is thus crucial for understanding the microscopic origin of high-T_c superconductivity.

Since the appearance of the superconducting dome obscures a potential QCP of the original symmetry-breaking phase, it is generally difficult to access the QCP to identify the effect of quantum fluctuations on superconductivity. Furthermore, there are typically more than one symmetry breaking order in the parent compound of most high T_c materials. For cuprate superconductors, the coexistence of nematicity with spin density wave order poses significant challenges in isolating the influence of nematic transition. Similar situation occurs in FeSCs, where the nematic phase is always overlapped with an itinerant antiferromagnetism (AFM) order, making the putative nematic QCP and the AFM QCP indistinguishable (Fig. 1a). In particular, although a sharp peak of London penetration is observed near the critical doping of several iron pnictide superconductors, which is attributed to the enhancement of quasiparticle mass due to the quantum critical fluctuations, it is yet unknown whether this anomaly corresponds to a nematic QCP or an AFM QCP.

The iron chalcogenide superconductor $FeSe_{1-x}Te_x$ (FST) is a unique system whose nematic phase is decoupled from any magnetic ordering at ambient pressure. Isovalent substituting Se with Te monotonically suppresses the nematic order, leading to a putative nematic QCP at x_c (0.5 for bulk sample and 0.2-0.4 for thin films), as evidenced by the divergent nematic susceptibility observed in the normal state (Fig. 1b). Moreover, the absence of significant spin fluctuations near x_c has been revealed by nuclear magnetic resonance measurements. These advantages render FST an ideal material platform to study the nonmagnetic nematic QCP in high-T_c superconductors. However, direct evidence for the nematic QCP inside the superconducting dome is still lacking so far. This is largely because conventional technique to probe normal state nematic criticality such as elastoresistivity is no longer effective in the superconducting state due to vanishing resistance. Applying a strong magnetic field can suppress the superconducting phase to expose the 'bare' nematic QCP, but this may induce a different QCP or shift the zero-field QCP.

One key parameter characterizing the superconducting state is the superfluid density (, where is the Cooper pair density and its effective mass), which encodes the phase rigidity of the pairing condensate. The temperature (T) dependence of is associated with the quasiparticle energy spectrum that depends on the superconducting gap structure. Importantly, it is found that the gap anisotropy of orthogonal FST is intimately related to its nematic order through various scenarios, e.g., the mixture of s- and d– wave components in the A_{1g} symmetry in the nematic phase, the nematic pairing due to orbital-selective correlations or spin fluctuations in the nematic phase, pairing in the presence of nematic orbital ordering, the strong gap anisotropy due to the shrink of electron pocket below the nematic transition. Hence, the temperature dependence of superfluid density can be regarded as a good tool for reflecting the nematic order inside the superconducting dome.

Here we perform local measurements on composition-spread FST films via scanning superconducting quantum interference device (sSQUID) microscopy. The continuous variation of Te content from 0 to 1 on a single substrate in conjunction with the micron spatial resolution of sSQUID enables us to explore across the pure

nematic transition in unprecedently fine steps, $\Delta x = 0.0008$. By analyzing the data for different compositions, we find the superconducting gap structure of FST undergoes a transition from anisotropic symmetry to isotropic symmetry at $x_c \sim 0.23$. Close to x_c, the gap anisotropy obeys a power-law dependence on Te content, evidencing the nematic quantum criticality in the superconducting state. The averaged gap value reaches maximum at x_c, strongly supports the scenario that pairing interaction is strengthened by the nematic fluctuations associated with the QCP. On the other hand, we find that the Te content at which peaks derivates from x_c as temperature decreases, possibly due to the suppression of phase coherence by the pinned nematic fluctuations beyond the QCP. Combing T_c, and gap data together, we find that the pure nematic QCP divides the superconducting dome into two regions, where T_c is dominated by the phase rigidity and the pairing potential for $x < x_c$ and $x > x_c$, respectively.

Visualization of skyrmion-superconducting vortex pairs in a chiral magnet-superconductor heterostructure

Xianggang Qiu

Institute of Physics, Chinese Academy of Sciences

Magnetic skyrmions, the topological states possessing chiral magnetic structure with non-trivial topology, have been widely investigated as a promising candidate for spintronic devices. They can also couple with superconducting vortices to form skyrmion-vortex pairs, hosting Majorana zero mode which is a potential candidate for topological quantum computing. A lot of theoretical proposals have been put forward on constructing skyrmion-vortex pairs in heterostructures of chiral magnet and superconductor. Nevertheless, how to generate skyrmion-vortex pairs in a controllable way experimentally remains a significant challenge. We have designed a heterostructure of chiral magnet and superconductor $[Ta/Ir/CoFeB/MgO]_7/Nb$ in which zero field Néel-type skyrmions can be stabilized and the superconducting vortices can couple with the skyrmions when Nb is in the superconducting state. We have directly observed the formation of skyrmion-superconducting vortex pairs which is dependent on the direction of the applied magnetic field. Our results provide an effective method to manipulate the quantum states of skyrmions with the help of superconducting vortices, which can be used to explore new routines to control the skyrmions for spintronics devices. [1].

Magnetic skyrmions are small swirling topological defects induced by chiral magnetic interactions or broken inversion symmetry cite. There are two typical types of magnetic skyrmions: Néel-type and Bloch-type skyrmions, which correspond to different symmetries of chiral Dzyaloshinskii–Moriya interactions. Skyrmions can be defined by the topological number (or winding number)

$$N = \frac{14}{\pi}\int \mathbf{M}\cdot\left(\frac{\partial \mathbf{M}}{\partial x}\times\frac{\partial \mathbf{M}}{\partial y}\right)dxdy,$$

which is a measure of the winding of the normalized local magnetization **M** [1]. Their stabilization and dynamics depend strongly on their topological properties. Owing to their topological property, small size, and high mobility, skyrmions can be manipulated by a very small current density. Skyrmions have been therefore proposed as promising candidates for the next generation, low-power spintronic devices, such as non-volatile information storage and logic devices.

We have designed a kind of chiral magnet-superconductor heterostructure (MIS) of $[Ta/Ir/CoFeB/MgO]_7/Nb$ on Si substrate. The proximity effect has been suppressed by inserting an insulator layer between the chiral magnet and superconductor, so that skyrmion and vortex interact via stray field only. It is found that in our heterostructures, Néel-type skyrmions can be stabilized at zero field after their nucleation at high fields. Formation of SVPs has been directly observed by magnetic force microscopy (MFM). When a negative magnetic field is applied, the superconducting vortices prefer to locate at the centers of the skyrmions, forming SVPs with enlarged radii. While in a positive field, superconducting vortices are

expelled away from the skyrmions. Such isolated SVPs can be an ideal platform to explore Majorana zero mode for topological computation as well as applications based on the manipulation of skyrmions.

After the zero-field skyrmions have been formed in the chiral magnet layer at 10 K which is above the superconducting transition temperature T_c, a perpendicular magnetic field is applied at the desired strength, and then the sample is cooled down below T_c to 5 K (field cooling (FC)). Fig. 1 (a-c) are the MFM images taken at calibrated magnetic fields of zero, –3 Oe, 1 Oe with FC processes, respectively. A characteristic region is marked by a white dashed rectangle in Fig. 1(a-c) which represents the same scanning area.

Compared with the MFM image for the same scanning area at 10 K, it can be found that besides the isolated skyrmions appear as small yellow dots at fixed positions, there are two other kinds of bright dots with larger radii marked by green squares and red circles, respectively. We can find the following: (1) When a negative perpendicular magnetic field (H_{perp} = –3 Oe, along $-z$ direction and parallel to the skyrmions core) is applied, both the numbers of green squares and red circles increase. The additional green squares are generated from skyrmions at the same position. Meanwhile, the additional red circles emerge from the blue background. When a positive external magnetic field H_{perp} = 1 Oe, along $+z$ direction is applied, the green squares turn into skyrmions at the same positions. In the mean time, the red circles are replaced by a triangular array of dark circles. By comparing with the MFM images of Nb film, we can attribute the red circles and dark dots to superconducting vortices. The dark circles are actually the anti-vortices arising from the reversal of the direction of the magnetic field. It is noticed that the vortices in green square always appear at the fixed positions under individual FC processes of different negative fields, in contrast to the random distribution of vortices in bare Nb film.

The formation of SVPs has been directly observed which is dependent on the direction of the applied magnetic field. The superconducting vortices are located at the centers of the skyrmions under a negative magnetic field, forming SVPs with enlarged radii. While in a positive field, superconducting vortices are expelled away from the skyrmions. The extremely small field operations of manipulating the skyrmion state provide a practical routine for controllable manipulation of skyrmion by means of magnetic field. And the dissipationless superconducting current in this kind of heterostructure can provide a great advantage in spintronics devices based on current-driven skyrmion motion.

References

1. *Y.J. Xie et al*., Physical Review Letters **133**, 166706 (2024). Editor's suggestion.

Spin dynamics and dark particles in a weak-coupled quantum Ising ladder with $\mathbf{D}_8^{(1)}$ spectrum

Jianda Wu

Shanghai Jiao Tong University

When two quantum critical transverse-field Ising chains (TFIC) are weakly coupled, the weak inter-chain coupling can drive the system to emerge as an integrable model with eight particles, organized by the $D_8^{(1)}$ Lie algebra. Realizing the quantum criticality of the TFIC is a key step to access the exotic integrable system. In my talk, after briefly exposing the quantum criticality of the TFIC, I will begin my journey with an inelastic neutron scattering experiment on $CoNb_2O_6$, which claims observation of evidence of E_8 physics in the material. Despite a ten-year gap, recent THz spectroscopy on the same material reignited our interest, leading us to challenge the E_8 paradigm and propose the $D_8^{(1)}$ picture. I will discuss why the $D_8^{(1)}$ physics provides a comprehensive understanding for the experimental observations. Along the course, we also surprisingly found long-life-time dark particle, a special kind of many-body magnetic excitation, in the integrable system which accommodates the $D_8^{(1)}$ physics. We will discuss how the dark particles are able to be prepared via another exotic soliton excitations in the system, and further propose a thermal activation detection of the lightest dark particle.

Oral

Effect of fluctuations on the Microwave Response in FeSeS near the nematic QCP

I.I. Gimazov[1], D.A. Chareev[2], A.N. Vasiliev[3], Yu.I. Talanov[1]

[1] Zavoisky Physical-Technical Institute, 420029, Kazan, Russian Federation; e-mail: gimazov@kfti.knc.ru
[2] Institute of Experimental Mineralogy, Russian Academy of Sciences, 142432, Chernogolovka, Moscow District, Russian Federation,
[3] Lomonosov Moscow State University, 119991, Moscow, Russian Federation

This study investigates the relationship between nematicity and superconductivity in $FeSe_{1-x}S_x$ (x=0-0.21) single crystals using resistivity, susceptibility, and microwave absorption (MWA). Comparison of resistivity and microwave absorption data for all concentrations demonstrated small discrepancies, which can be attributed to magnetic fluctuations of isotropic and anisotropic nature. Near the nematic quantum critical point (x=0.16), a magnetic field increases MWA amplitude below the structural transition, suggesting changes in electronic structure rather than magnetic order.

One of the recent advances in the study of high-temperature superconductors has been the discovery of electron correlations with a dedicated direction (nematic state), whose fluctuations may play a key role in the formation of superconductivity. However, the presence of a large number of phases, with different type of magnetic and charge order of high-temperature superconductors makes it difficult to distinguish the role of nematic fluctuations. Promising objects for studying the relationship between the nematic phase and superconductivity are iron chalcogenides, which, unlike iron pnictides, lack both magnetic and charge order phases. Moreover, hydrostatic pressure has a significant effect on the nematic state of these materials: with increasing pressure, the nematic phase is suppressed, and as it disappears, spin density waves appear.

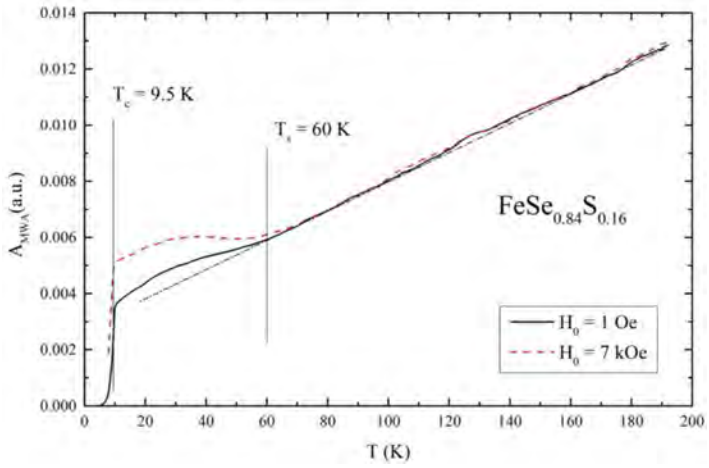

Fig. 1. Temperature dependences of microwave absorption for the $FeSe_{0.84}S_{0.16}$ sample obtained in a magnetic field of 1 Oe and 7 kOe. The dash-dotted line shows the linear behavior. Vertical lines correspond to the temperatures of superconducting and structural transitions.

Of particular interest are iron chalcogenides under the action of chemical pressure. For example, replacement of selenium by sulfur leads to suppression and disappearance of the nematic state. With further increase of sulfur content, the magnetic phase does not occur. It is assumed that the sulfur concentration at which the nematic phase disappears (x = 0.17) corresponds to the nematic quantum critical point (Nematic QCP). The study of the phase diagram near this point is particularly interesting because of the amplification of fluctuations of various order parameters at the quantum critical point.

In this work, $FeSe_{1-x}S_x$ single crystals (x=0, 0.050, 0.075, 0.160, 0.021) [1] were chosen as objects of study. Characterization of the obtained samples was carried out by measuring resistivity and magnetic susceptibility. A modified EPR spectrometer was used as the main experimental tool, which registers the temperature dependence of microwave absorption (MWA). Comparison of resistivity and microwave absorption data for all concentrations demonstrated small discrepancies between the $A_{\mathrm{MWA}}(T)$ and $(\mu_0\omega_0\rho/2)^{1/2}(T)$ curves, which can be attributed to magnetic fluctuations of isotropic and anisotropic nature [2]. In addition, similar measurements were performed in a magnetic field of 7 kOe. Analysis of the resistivity data showed no significant changes below the T_s structural transition temperature when exposed to an external magnetic field. With using high frequencies method (9.4 GHz) for the sample with sulfur concentration x=0.16, an increase in the MWA amplitude below T_s is observed (Fig. 1). When considering these data, it is necessary to take into account that the MWA method is sensitive to magnetic and electronic excitations, so the orbital nature of the nematic phase is not considered. Measurements of the Shubnikov-de Haas oscillation in $FeSe_{1-x}S_x$ have shown suppression of spin fluctuations near the nematic QCP [3]. On this basis, it can be assumed that the observed increase in the MWA amplitude with increasing external magnetic field for the $FeSe_{0.84}S_{0.16}$ sample can be attributed to changes in the electronic structure.

This work was funded by the Russian Science Foundation (No. 21-72-20153-P).

References

1. *Chareev D. et al*., Cryst. Eng. Commun. **15**, 1989 (2013).
2. *Gimazov I. et al*., JETP **129**, 81 (2019).
3. *Coldea A.I. et al*., Quantum Mater. **4**, 2 (2019).

Enhanced superconductivity coexisting with antiferromagnetism in the FeTe-$NbSe_2$ system

E. Kislov[1], N.V. Selezneva[1], N.V. Baranov[1,2]

[1] Ural Federal University, Institute of Natural Sciences and Mathematics, Yekaterinburg, Russia,
[2] Institute of Metal Physics of Ural Branch of Russian Academy of Sciences, Yekaterinburg, Russia

Alloyage of $Fe_{1.1}Te$ with $(NbSe_2)y$ ($0 \leq y \leq 1.2$) is found to lead to an increase in the superconducting onset transition temperature up to $T_c \sim 12$ K, as well as to the phase segregation and a change in the crystal lattice parameters of the formed phases. The superconducting state in the samples coexists with antiferromagnetic ordering. The observation of atypically hard superconductivity in the entire range of $NbSe_2$ concentrations can be explained by the significant inhomogeneity of the samples and the influence of interface effects.

Unlike iron selenide FeSe, which in bulk form has a superconducting transition temperature $T_c = 8$ K, isostructural iron telluride FeTe does not exhibit a transition to the superconducting state and has antiferromagnetic ordering below $T_N = 70$ K, however, substitutions in the metal and chalcogen sublattices can significantly affect its properties. The dependence of the superconducting transition temperature on Se content x in the $FeTe_{1-x}Se_x$ system has a dome-shaped form with a maximum $T_c = 15$ K at $x = 0.5$. In this regard, studies with simultaneous substitutions in both the chalcogen and metallic sublattices would be of interest to overcome this limitation. In the present work we investigate the possibilities of increasing the transition temperature by alloyage of non-superconducting antiferromagnetic $Fe_{1.1}Te$ with superconducting niobium diselenide $NbSe_2$ with $T_c \sim 7$ K.

Samples of the $Fe_{1.1}Te+y\cdot[NbSe_2]$ system have been synthesized for the first time using the melting method, studied using x-ray diffraction analysis and electrical and magnetic measurements. It is shown that the phase segregation and a decrease in the crystal lattice parameters of both FeTe- and $NbSe_2$-based phases occurs with the increase of $NbSe_2$ concentration. Based on the temperature dependences of electrical resistance and magnetic susceptibility measurements, it is found that all samples demonstrate a superconducting transition at a temperature of $T \sim 12$ K, which contrasts with substitutions only on the chalcogen or metallic sublattices. The coexistence of a superconducting transition and antiferromagnetism is observed throughout the full doping interval. The lack of a strong diamagnetic response in all alloyed samples necessitates the exploration of alternative mechanisms of the superconductivity manifestation aside from the partial substitution on the chalcogen sublattice of FeTe in this system. Considering the data on the increase in the superconducting transition temperature in iron selenide on a niobium-doped $SrTiO_3$ substrate, as well as when FeSe films are coated with niobium, the presence of niobium atoms in our samples can have a positive effect on the superconducting properties. Apparently, the effect of robust superconducting state can be achieved due

to the significant heterogeneity of the samples, where the FeTe- and $NbSe_2$-based regions containing selenium and tellurium, respectively, coexist. These regions contribute to both the superconducting transition and the antiferromagnetic ordering. Such components compatibility is not achieved with all materials and one of the key tasks is to establish its criteria. In this case, presumably, it is compatibility in the crystal lattices parameters of the FeTe and $NbSe_2$ phases – the values of the parameters with a high degree of accuracy must coincide in at least one crystallographic direction. Thus, the obtained results show a way to modify the superconducting properties of iron chalcogenides Fe*Ch* based on the compositional effect and the selection of a compatible material, which allows to improve the properties of the initial compound and stabilize the superconducting transition.

This work was supported by the Russian Science Foundation (Grant No. 22-13-00158).

Signatures of surface magnetic disorder in single-crystal superconducting titanium nitride films

A. Kolbatova[1], E. Baeva[1,2], A. Lomakin[1], N. Titova[1], A. Semenov[1], S. Saha[3], A. Boltasseva[3], S. Bogdanov[4,5,6], V. Shalaev[3], G. Goltsman[1,2], V. Khrapai[2]

[1] Moscow Pedagogical State University, 119435 Moscow, Russia,
[2] HSE University, 101000 Moscow, Russia,
[3] Birck Nanotechnology Center and Elmore Family School of Electrical and Computer Engineering, Purdue University, IN 47907 West Lafayette, USA,
[4] Department of Electrical and Computer Engineering, University of Illinois at Urbana-Champaign, IL 61801 Urbana, USA,
[5] Holonyak Micro and Nanotechnology Lab, University of Illinois at Urbana-Champaign, IL 61801 Urbana, USA,
[6] Illinois Quantum Information Science and Technology Center, University of Illinois at Urbana-Champaign, IL 61801 Urbana, USA

We investigate the superconducting properties, electron transport, and phase-breaking mechanisms of epitaxial titanium nitride (TiN) samples with various thicknesses. Our analysis reveals correlations between the superconducting transition width, material parameters, and device dimensions, attributing the inhomogeneity to surface magnetic disorder. Additionally, we measure the electron dephasing rate via magnetoresistance from the superconducting transition temperature T_c to ~3 – 4T_c. Spin-flip scattering associated with magnetic disorder near the oxidized surface is identified as the dominant source of phase breaking in thin TiN films. These findings provide valuable insights into microscopic inhomogeneities present in thin superconducting films and loss mechanisms in superconducting quantum devices.

Titanium nitride (TiN) has shown great potential as a superconductor for use in quantum circuits due its low losses and long quantum coherence time compared to other superconducting materials [1, 2]. In our recent study, we investigated the transport properties of single-crystal superconducting TiN films and found exceptional electronic parameters, such as the surface scattering-limited electron mean free path, the critical temperature (T_c) close to the bulk value, and a weak magnetic disorder residing in the surface layer, with a characteristic magnetic defect density of $n_s \sim 10^{12}$ cm^{-2} [3]. We also explored the other fundamentals aspects of these films, focusing on the impact of minute surface magnetic disorder on superconducting properties.

We investigated the effect of various fluctuation mechanisms on the DC resistance of epitaxial TiN films [4]. We observed a sharp decrease in T_c and a broadening of the superconducting transition with decreasing film thickness and width of the TiN samples. The TiN samples we studied showed a relatively steep resistive transition (RT), with a transition width $\Delta T/T_c \sim 0.002-0.025$, depending on film thickness and device dimensions. This value is significantly larger than expected for conventional superconducting fluctuations ($\Delta T/T_c \ll 10^{-3}$). The shape and width of

the resistive transition can be perfectly described by the well-known effective medium theory, which allows us to understand the origin of the inhomogeneity in the superconducting properties of TiN films (see inset in Figure 1). We propose that this inhomogeneity may have both dynamic and static components. The dynamic mechanism is associated with spontaneous fluctuations in electron temperature (T-fluctuations), while the static mechanism is due to a random spatial distribution of surface magnetic disorder. Our analysis revealed clear correlations between the transition width and material parameters as well as device size for both mechanisms (see Figure 1). While T-fluctuations may contribute significantly to the observed transition width, our findings suggest that the dominant contribution comes from magnetic disorder.

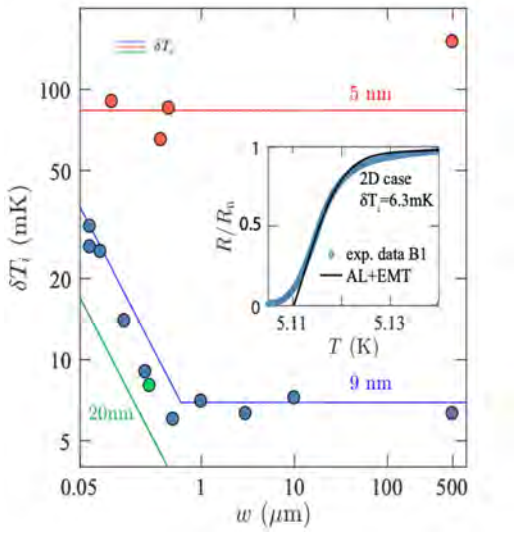

Figure 1. Main: The width of the transition, denoted by T_i, depends on the width, w, of the TiN samples with different thicknesses. The symbols represent the best fit of the experimental data using the EMT model, while the solid lines show the standard deviation of the critical temperature, accounting for magnetic disorder. Inset: The temperature dependence of the normalized resistance R/Rn in comparison with the EMT approximation for 9-nm thick sample.

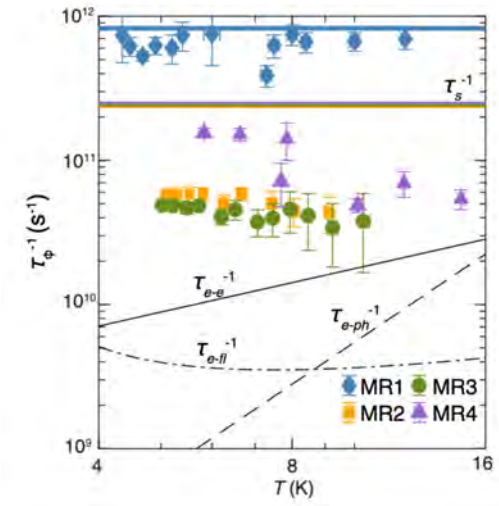

Figure 2. The phase-breaking rates and the relative contributions of inelastic and magnetic scattering processes in epitaxial TiN films.

We also studied the electron dephasing rate measured via magnetoresistance over a temperature range from T_c to ~3 – 4T_c for epitaxial TiN films of various thicknesses. We found that electron dephasing occurs on a picosecond time scale and is nearly independent of temperature (see Figure 2). This differs from inelastic scattering processes due to electron-phonon and electron-electron interactions, which occur on the nanosecond time scale near the superconducting transition, as shown by noise thermometry and spectroscopy measurements in Ref. [5]. We suggest that spin-flip scattering could serve as an additional process for electron dephasing in epitaxial TiN films. This scattering is associated with the magnetic disorder near the surface of the naturally oxidized films.

Our findings suggest that naturally oxidized surfaces play a significant role in electron dephasing. Recent studies emphasize the critical role of magnetic impurities localized within the native oxide of materials, which drive two-level systems (TLS) loss [6]. These impurities are also identified as a major source of RF dissipation in niobium oxides [7]. In particular, 2D superconducting quantum systems, using TiN-capped niobium films exposed to air and forming a native oxide layer, exhibit slightly improved qubit relaxation times, however these times are still limited to approximately 100 us [8]. Similar signatures of surface magnetic disorder are observed in the evolution of the superconducting properties in Nb films as their thickness decreases [9], and in studies of the temperature dependence of of unprotected Nb films, where a tendency toward saturation in is seen at low temperatures [10]. A similar trend is also observed in thin copper (Cu) films [11]. In the case of Nb and Cu films passivated with a silicon layer, slower values of and a more pronounced power-law dependence on temperature (~$T^{-2.5}$ for Nb [10] and ~T^{-3} for Cu [11]) are observed. These findings suggest that this magnetic disorder may be a significant source of RF dissipation in superconducting thin- film-based devices, and may also provide insight into the microscopic origins of inhomogeneity in these films.

This work was supported by the RSF grant № 24-72-10105.

References

1. *H. Deng et al.*, Phys. Rev. Applied **19**, 024013 (2023).
2. *M. Bal et al.*, njp Quantum Information **10**, 43 (2024).
3. *N. Saveskul et al.*, Phys. Rev. Applied **12**, 054001 (2019).
4. *E. Baeva et al.*, Supercond. Sci. Technol. **37**, 105017 (2024).
5. *E. Baeva et al.*, Phys. Rev. B **110**, 104519 (2024).
6. *S.E. de Graaf et al.,* Nature Communications **9**, 1143 (2018).
7. *T. Proslier et al.,* Applied Physics Letters **92**, 212505 (2008).
8. *M. Bal et al.,* npj Quantum Information **10**, 43 (2024).
9. *A.S. Samsonova*, *et al.,* IEEE Transactions on Applied Superconductivity **31**, 1 (2021).
10. *A. Lomakin*, *et al.*, St. Petersburg State: Polytechnical University Journal. Physics and Mathematics **15**, 64 (2022).
11. *J. Vranken*, *et al.,* Phys. Rev. B **37**, 8502 (1988).

Compounds with Giant Magnetoelectric Effect as a Possible New Class of Materials for Obtaining High-Temperature Superconductors

V.G. Orlov, G.S. Sergeev

National Research Center «Kurchatov Institute», 123182 Moscow, Russia

We carried out calculations of the electronic band structure and parameters of Bond Critical Points in the charge density distribution for a number of compounds with a giant linear magnetoelectric effect, such as $TbPO_4$ and $HoAl_3B_4O_{12}$. Taking into account the correlation that we have identified earlier between the critical temperature T_c of HTSC and the Laplacian of the charge density at the Bond Critical Point with the largest charge density value, compounds with a giant linear magnetoelectric effect seem promising for obtaining HTSCs with very high T_c.

In our recent papers [1, 2], we showed that the semiconducting compounds La_2CuO_4 and $YBa_2Cu_3O_6$, that are the parent materials for a number of families of unconventional high-temperature superconductors (HTSCs), have two properties that can stimulate the emergence of superconductivity in the metallic phase obtained by doping the parent compound.

The first property, that we previously identified in bismuth and antimony chalcogenides, iron pnictides, cuprates and related unconventional superconductors [3, 4], is a specific chemical bonding mechanism, which is different from covalent, ionic and metallic [5, 6]. This mechanism of chemical bonding is characterized by: 1) positive values of the Laplacian of the charge density $\Delta\rho_b$ at all critical points of the bond type (BCPs) [5, 6] in the distribution of the charge density in the crystal, 2) high values of the charge density ρ_b in BCPs, and 3) the number of BCPs per nonequivalent atoms in compounds exceeding the valences of the atoms.

The second property [1] is determined by the symmetry of crystal structures, described by space groups, for which there are magnetic crystal classes that allow the presence of a linear magnetoelectric effect (LMEE) [7]. In compounds with LMEE, both local magnetic fields and electric polarization are present in absence of external magnetic and electric fields. The source of local magnetic fields can be the dipole magnetic fields of magnetic ions and electric dipoles due to the allowed LMEE. In [1] it was suggested that the simultaneous presence of local magnetic fields and electric polarization in a sample may be thermodynamically unfavorable. So when charge carriers appear in the sample as a result of doping the parent compound, a specific type of chemical bonding leads to the appearance of more favorable superconducting state.

In this work, we carried out calculations of the electronic band structure and parameters of BCPs in the charge density distribution for a number of compounds with a giant LMEE, such as $TbPO_4$ [8] and $HoAl_3B_4O_{12}$ [9]. Taking into account the correlation that we have identified [3] between the critical temperature T_c of HTSC

and the Laplacian of the charge density $\Delta\rho_b$ at the BCP with the largest ρ_b, compounds with a giant LMEE seem promising for obtaining HTSCs with very high T_c.

References

1. *V.G. Orlov and G.S. Sergeev*, J. Supercond. Nov. Magn., **38**, 61 (2025).
2. *V.G. Orlov and G.S. Sergeev*, J. Exp. Theor. Phys. **137**, 95 (2023).
3. *V.G. Orlov and G.S. Sergeev*, Physica B **536**, 839 (2018).
4. *V.G. Orlov, G.S. Sergeev and E.A. Kravchenko*, J. Magn. Magn. Mater. **475**, 627 (2019).
5. *Gatti*, Z. Kristallogr. **220**, 399 (2005).
6. Ed. by C.F. Matta, R.J. Royd, The Quantum Theory of Atoms in Molecules. From Solid State to DNA and Drug Design. WILEY-VCH,Verlag GmbH&Co. KGaA, Weinheim (2007).
7. *A.S. Borovik-Romanov, H. Grimmer*, Chapter 1.5, Magnetic properties, International Tables for Crystallography, Vol. D. International Union of Crystallography, 105-149 (2006).
8. *G.T. Rado, J.M. Ferrari, and W.G. Maisch*, Phys. Rev. B **29**, 4041 (1984).
9. *K.-C. Liang, R.P. Chaudhury, B. Lorenz et al.* Phys. Rev. B **83**, 180417 (R) (2011).

Magnetic pinning and record critical current enhancement in iron-doped YBaCuO

K.S. Pigalskiy, A.A. Vishnev, N.N. Efimov,
P.N. Vasilyev, A.V. Shabatin, L.I. Trakhtenberg

Semenov Federal Research Center for Chemical Physics RAS, Moscow, Russia,
Kurnakov Institute of General and Inorganic Chemistry RAS, Moscow, Russia,
Frumkin Institute of Physical Chemistry and Electrochemistry RAS, Moscow, Russia,
Lomonosov Moscow State University, Moscow, Russia

The dependences of the intragranular critical current density (J_c) and the thermodynamic critical field (H_c) on the iron content in HTSC $Y_{1-x}Fe_xBa_2Cu_3O_y$ ($0 \le x \le 0.08$) are analyzed. The $J_c(x)$ dependence has a pronounced maximum at an optimal doping level of $x_{opt} \sim 0.04$. The value of x_{opt} is weakly dependent on the external magnetic field and temperature. A significant increase in the J_c value at $x \sim x_{opt}$ has been observed, reaching two orders of magnitude at temperatures around 77 K. The values of H_c and the paramagnetic contribution to the magnetic susceptibility from the spins of Fe ions have been determined. It has been found that H_c decreases monotonically with increasing x, by an amount that does not exceed 30% over the entire range of x. This behavior is not consistent with the features of $J_c(x)$ dependencies. It has also been found that the magnetic moment of Fe ions remains unchanged after the transition of the sample to the superconducting state. It has been concluded that the dominant interaction responsible for the pinning of vortices is the magnetic interaction between a vortex system and a nanoscale system of magnetic impurities.

For a series of $Y_{1-x}Fe_xBa_2Cu_3O_y$ samples ($0 \le x \le 0.08$), the effect of magnetic impurities on superconducting (SC) characteristics, including the density of the intragranular critical current (J_c) and the thermodynamic critical field (H_c), was studied. In order to achieve a homogeneous distribution of a small amount of dopant over the sample volume, synthesis was carried out using the nitrate-citrate variant of sol-gel technology at the initial stage. The synthesis procedure, temperature, and duration of annealing are described in [1]. The data from X-ray and electron microscopic studies, as well as the values of the transition temperatures to the SC state (T_c) are also presented. Magnetic susceptibility at $T > T_c$ and magnetization (M) hysteresis in increasing and decreasing external magnetic fields (H) up to 6 T at $T < T_c$ were measured for the samples obtained. The values of J_c are calculated from the magnetization hysteresis width within the framework of the Bean critical state model. For doped samples, there is a well-defined maximum in the $J_c(H)$ dependence (peak effect), which shifts to smaller fields as the Fe content and temperature increase. A nonmonotonic change in J_c was revealed with a change in the degree of doping. Figure 1a shows the dependence of $J_c(x)$ on a semilogarithmic scale for $H = 1$ T over a temperature range of 40–85 K. If the effect of doping on J_c is small at low temperatures, as the temperature increases, the changes in J_c become significant. A pronounced maximum in J_c is observed at an optimal doping level of

$x_{opt} \sim 0.04$, at which the effect of J_c increasing reaches two orders of magnitude. For other values of the external field and, correspondingly, for other periods of the vortex lattice, the presence of a sharp maximum in the $J_c(x)$ dependence persists at the same concentration of substitutional atoms.

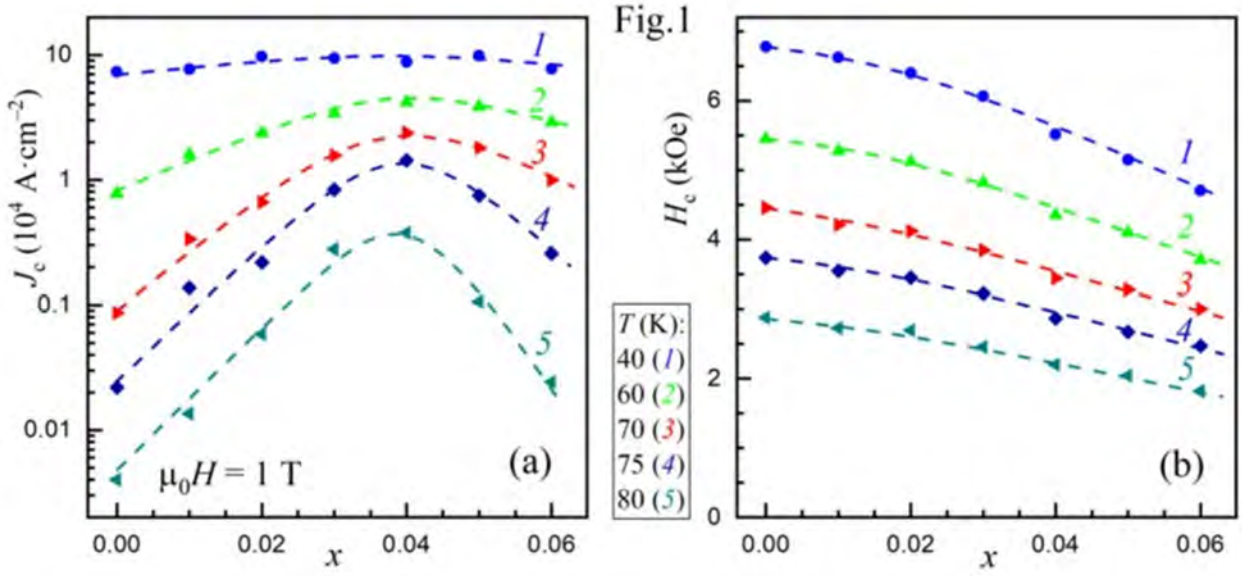

The revealed features of the behavior of $J_c(x)$ dependencies are in certain contradiction with the obtained equilibrium characteristics of the SC state. Indeed, the commonly accepted pinning mechanism is associated with a decrease in the energy of a vortex due to the overlapping of its core with an area where the SC order parameter has a reduced value near a defect. To determine the equilibrium characteristics, an analysis of the average magnetization lines M_{ev} was carried out. As a result, the values of the thermodynamic critical field and the paramagnetic contribution to the magnetic properties of the SC state were calculated. Figure 1b shows the dependence of H_c on Fe content at the same temperatures as in Fig. 1a. As x increases, there is a monotonic decrease in H_c, which does not exceed 30% within the studied range of x. Estimates suggest that such a reduction in H_c may be linked to a decrease in the volume of the SC phase, due to the formation of a normal region with dimensions comparable to coherence lengths $\xi_{ab}\xi_{ab}\xi_c$ near each defect. Another result of the $M_{ev}(H)$ analysis is that the magnetic moment of Fe^{3+} ions remains unchanged during the transition of the sample to the SC state.

The absence of any features in the $H_c(x)$ curves near x_{opt} indicates that there is an additional mechanism responsible for a significant increase in pinning at an optimal impurity concentration. The existence of such a mechanism with a magnetic nature was predicted in [2]. Estimates show that at $x_{opt} = 0.04$, the average distance between defects is $d_{opt} = 1.6$ nm and turns out to be close to the coherence length in the *ab* plane. Another characteristic length, which is close to d_{opt}, is the scale of the RKKY-type exchange interaction. A hypothesis is proposed regarding the implementation of ferromagnetic exchange between Fe^{3+} spins when they are located at distances corresponding to the optimal impurity concentration for pinning. As

shown in [3], nanoscale regions with ferromagnetic interactions may prove to be more effective pinning centers than normal phase regions.

References

1. *K.S. Pigalskiy, A.A. Vishnev, N.N. Efimov, A.V. Shabatin, L.I. Trakhtenberg*, Ceram. Int. https://doi.org/10.1016/j.ceramint.2024.12.523
2. *K.S. Pigalskiy, L.I. Trakhtenberg*, J. Magn. Magn. Mater. **497**, 165916 (2020).
3. *M.A. Sebastian, N.A. Pierce, I. Maartense, G. Kozlowski, T.J. Haugan*, IEEE Trans. Appl. Supercond. **31**, 8000607 (2021).

Iron-based superconductors of the 245 family: phase composition and morphology

E.O. Rakhmanov[1,3], A.I. Shilov[1], T.E. Kuzmicheva[1],
S.A. Kuzmichev[1,2], I.V. Morozov[3]

[1] V.L. Ginzburg Centre for High-Temperature Superconductivity and Quantum Materials, P.N. Lebedev Physical Institute of the Russian Academy of Sciences, 119991 Moscow, Russia,
[2] Faculty of Physics, M.V. Lomonosov Moscow State University, 119991, Moscow, Russia,
[3] Department of Chemistry, M.V. Lomonosov Moscow State University, 119991, Moscow, Russia

Iron-based superconductors of the 245 family have a complex phase composition. The ironchalcogenide 245 family $A_xFe_{2-y}Se_2$ with A = Na, K, Rb, Cs, Tl consists of an antiferromagnetic and a superconducting (SC) phase. This structure explains the difficulty of reproducibly obtaining superconducting samples. Thus, one of the interesting directions is the synthesis of samples containing Na, which can help stabilize the SC phase. Here, we report successful crystal growth, phase relations, comprehensive study of superconducting properties for $(Na;K;Rb)_{0.8}Fe_2Se_2$.

Iron-containing selenide superconductors $A_{1-x}Fe_{2-y}Se_2$ (A – K, Rb, Cs, Tl) ("122Se") were discovered in 2010. Despite the structural relationship with the ferroarsenide family 122, they are usually distinguished into a separate family due to a number of features, the most important of which is the phase separation into an antiferromagnetically ordered phase of the composition $A_{0.8}Fe_{1.6}Se_2$ ("245"), which is the main one, and a superconducting (SC) phase of the approximate composition $A_{0.2}Fe_2Se_2$, the mole fraction of which is usually no more than 15%, and which can exist only in the presence of the main phase 245, in the form of a micron-sized layer between 245 crystallites. It is known that the 245 and SC phases coexisting in the 122Se composite crystallize in the tetragonal syngony with noticeably different parameters. It can be assumed that this is one of the main reasons for the experimental problems associated with obtaining superconducting 122Se samples: the presence of superconductivity depends on the quenching mode, during which spinodal decomposition of the high-temperature disordered phase into a 122Se composite consisting of 245 and SC phases occurs. In our work, the task was to test the possibility of stabilizing the SC phase by introducing sodium cations into the system. Na+ cations, unlike larger alkali metals, cannot effectively stabilize Fe-containing superconductors of the 122 family. However, they can partially replace larger cations, which will affect the size of the unit cells. To identify the role of sodium in the formation of the SC phase, three compositions were synthesized: $(Na_{0.5}K_{0.5})_{0.8}Fe_2Se_2$, $(K_{0.5}Rb_{0.5})Fe_2Se_2$ and $(Na_{0.3}K_{0.3}Rb_{0.3})_{0.8}Fe_2Se_2$. The crystals were obtained in three stages by crystallization from the melt of their own components. Some of the samples were additionally quenched in ice water and liquid nitrogen. The structure, composition and morphology of the obtained samples were studied by X-ray diffraction, EPMA and electron microscopy. The SC properties were studied by Andreev spectroscopy. It was shown that the obtained samples exhibit characteristic phase separation (Fig. 1A, B). The best SC characteristics were demonstrated by the $(Na_{0.3}K_{0.3}Rb_{0.3})_{0.8}Fe_2Se_2$ sample (Fig. 1C).

Posters

Mesons in a quantum Ising ladder

Yunjing Gao, Yunfeng Jiang, Jianda Wu

Tsung-Dao Lee Institute, Shanghai Jiao Tong University

When two transverse-field Ising chains (TFICs) with magnetic order are coupled, the original free excitations become confined, giving rise to meson-like bound states. In this work, we study such bound states systematically. The mesons are characterized by their fermion number parity and chain-exchanging properties, which lead to distinct sets of mesonic states. The meson masses are determined by solving the Bethe-Salpter equation. An interesting observation is the additional degeneracy in the chain-exchanging odd sectors. Beyond the two particle approximation, we exploit the truncated free fermionic space approach to calculate the spectrum numerically. Corrections to the meson masses are obtained, and the degeneracy is further confirmed. The characterization and degeneracy can be connected to the situation when each chain is tuned to be quantum critical, where the system is described by the $Ising_2^h$ integrable model, a sine-Gordon theory with Z_2 orbifold. Here we establish a clear correspondence between the particles in the bosonized form and their fermionic counterparts. Near this point, the stability of these particles is analyzed using the form factor perturbation scheme, where four particles are always present. Additionally, we calculate the evolution of the dominant dynamical structure factor for local spin operators, providing further insight into the low-energy excitations and their role in the system's behavior. The two-particle confinement framework as well as the parity classifications may inspire the study for other coupled bi-partite systems.

Pinning enhancement in YBCO by magnetic nanoparticles: No royal roads

D.M. Gokhfeld, S.V. Semenov, M.I. Petrov

Kirensky Institute of Physics, Krasnoyarsk Scientific Center, Siberian Branch, Russian Academy of Sciences

The effects of ultra-small ε-Fe_2O_3 nanoparticles on the electrical properties, microstructure, magnetization and critical current density of $YBa_2Cu_3O_{7-d}$ were investigated. Samples were prepared using the solid state reaction method. The X-ray diffraction, four-point-probe electrical resistance, scanning electron microscopy and magnetization measurements were used to characterize the samples.

The additives of ultra-small ε–Fe_2O_3 nanoparticles in $YBa_2Cu_3O_{7-d}$ can increase the critical current density only after short heating.

Prolonged annealing at a temperature of 930 °C, which is common for solid-phase synthesis, leads to a significant suppression of the superconducting properties on the surface of the granules. What is about the effect of ultra-small NiO nanoparticles?

This work was supported by the Russian Science Foundation, project № 24-22-00053, https://rscf.ru/project/24-22-00053/.

High frequency dynamic response of Abrikosov vortices: time-dependent Ginzburg-Landau approach

R.I. Kinzibaev[1], A.S. Mel'nikov[1,2]

[1] Moscow Institute for Physics and Technology, Dolgoprudny 141700, Russia,
[2] Institute for Physics of Microstructures, Russian Academy of Sciences 603600, Nizhny Novgorod, GSP-105, Russia

Introduction

Starting from the seminal paper [1] the problem of vortex mass in the equation of motion of flux lines has been addressed in the variety of experimental and theoretical works. The importance of this issue for the physics of vortex matter is obvious as the frequency-dependent vortex response to the external current determines the microwave impedance and Ohmic losses of superconducting materials and devices in magnetic fields. Vortex dynamics is also essential for understanding how a moving vortex interacts with various pinning centers and boundaries.

Results

The aim of this work is to derive the dynamic equation describing the high-frequency vortex dynamics in a thin superconducting film under the influence of an alternating current. Our starting point is the time-dependent Ginzburg–Landau (TDGL) theory. Despite of the obvious restrictions on the range of validity of this model it is well known to provide instructive insights for a great variety of dynamic phenomena in superconductors.

Based on the perturbation approach described in [2], we derive the following equation of motion for the vortex line:

$$\left[\eta_{\mathrm{Rel}} + \frac{2l_E^2}{R_V^2}\cdot\frac{1}{1-i\omega l_E^2/D}\right]\mathbf{v}(\omega) = \frac{8eTD}{\sigma\pi\Delta_\infty^2}[\mathbf{j}_s(\omega),\mathbf{e}_z],$$

where: $\eta_{\mathrm{Rel}} \approx 0.279$ is the relaxation contribution to the vortex viscosity, $R_V \sim \xi$ is the characteristic vortex radius and the temperature-dependent coherence length, l_E is the electric field penetration depth, D is the diffusion coefficient, $\mathbf{j}_s$ is the transport supercurrent, $\mathbf{v}$ is the vortex velocity, σ is the normal state conductivity, Δ_∞ is the gap value far from the vortex core.

Based on the analysis of this equation, several important conclusions can be drawn:

1. A linear expansion of the kernel

$$\left(1-i\omega\frac{l_E^2}{D}\right)^{-1}$$

in powers of frequency leads to the appearance of an “effective negative mass” for the vortex which means that the correct description of the vortex dynamics requires the consideration of the full kernel given above.

2. The form of the kernel indicates that the vortex motion exhibits a retardation effect characterized by a relaxation time l_E^2 / D.

3. At high frequencies, the kernel contribution becomes inversely proportional to frequency. In the time domain this term gives us an effective elastic force resulting from the back-action of the charge imbalance potential.

Furthermore, using a standard relation for the averaged electric field induced by the vortex motion

$$\mathbf{E} = \frac{1}{c}[\mathbf{B}, \mathbf{v}_L],$$

we derive the frequency-dependent supercurrent–electric field relation:

$$\mathbf{j}_s = \sigma \mathbf{E} \left[\frac{\Phi_H}{4\pi l_E^2 B} \eta_{\text{Rel}} + \frac{\Phi_H}{2\pi R_V^2 B} \frac{1}{i\omega l_E^2 / D} \right],$$

where Φ_H is the magnetic flux quantum. This expression describes the complex impedance of the superconducting film arising due to vortex motion and highlights the contributions from both the relaxation processes and the retardation effects at finite frequencies.

Conclusion

Thus, the approach presented here provides an analytical description of the relaxation processes in the viscous dynamics of a single vortex under a weak alternating current and reveals important features of the high-frequency impedance of superconducting systems.

This work has been supported by the Russian Science Foundation (Grant No. 25-12-00042).

References

1. *J.I. Gittelman and B. Rosenblum*, Phys. Rev. Lett. **16**, 734, (1966).
2. *N. Kopnin*, Theory of Nonequilibrium Superconductivity (Oxford Science, London, 2001).

Characterization and synthesis of superconductors of $CaAFe_4As_4$ composition (A = K, Rb, Cs)

A.S. Medvedev, V.A. Vlasenko, K.S. Pervakov

P.N. Lebedev Institute of Physics, Russian Academy of Sciences,
V.L. Ginzburg Center for High Temperature Superconductivity and Quantum Materials

High-quality polycrystalline samples of stoichiometric iron-based superconductors $CaKFe_4As_4$, $CaRbFe_4As_4$ and $CaCsFe_4As_4$ were obtained by mechanical alloying. The phase composition of the synthesized materials was confirmed by X-ray phase analysis. The superconducting transition temperatures were 35.0 K ($CaRbFe_4As_4$), 31.1 K ($CaCsFe_4As_4$), 35.0 K ($SrRbFe_4As_4$) and 36.1 K ($SrCsFe_4As_4$). According to the results of magnetic measurements, it was found that only one superconducting phase is present in the samples.

Optimization of superconducting properties in compounds of the AFe_2As_2 (122) family, where A is an element from the group of alkaline-earth metals, requires doping. It is necessary to achieve high superconducting transition temperatures. However, this approach significantly complicates the synthesis of the material, since it requires precise control of the chemical composition and homogeneity of the distribution of elements. In contrast to this, stoichiometric compounds of the 1144 family do not require doping and have higher transition temperature to the superconducting state ($T_c \approx 31$-36 K), are of considerable interest [1].

Although compounds of this type, such as $CaKFe_4As_4$, $CaRbFe_4As_4$, and $CaCsFe_4As_4$, have been synthesized previously [2, 3], the lack of high-quality samples makes it difficult to fully investigate their physical properties. The aim of this work is to synthesize samples of these materials with minimal impurity phases and characterize them.

$CaKFe_4As_4$, $CaRbFe_4As_4$ and $CaCsFe_4As_4$ powders were synthesized by mechanical alloying method from the starting elements Ca, K (or Rb, Cs), Fe and As with purity of 99.9% (for Ca, Cs, Rb, Fe) and 99.9999% (for As) taken in stoichiometric ratios. The components were loaded into a grinding bowl and subjected to high-energy milling in a vibrating mill. The obtained powder was pressed into pellets, which were placed in crucibles and sealed in steel containers. The heat treatment was carried out at 880 °C, 900 °C and 950 °C for $CaKFe_4As_4$, $CaRbFe_4As_4$ and $CaCsFe_4As_4$, respectively. All synthesis steps, except for the mechanical alloying and annealing steps, were carried out under argon atmosphere inside a glove box.

The phase composition was confirmed by powder X-ray diffraction (Fig. 1 A). The lattice cell parameters were refined by Le Bayle method and are found to be for $CaRbFe_4As_4$ (Fig. 1 A): a = 3.87520(17) Å and c = 13.0992(7) Å, Rp = 7,86 %, wRp = 10,40% and $CaKFe_4As_4$: a = 3.8526(6) Å and c = 12.817(2) Å, Rp = 6,385 %, wRp =

8,53%. Figure 1 (B) shows the $CaCsFe_4As_4$ sample with the lowest, by far, amount of impurities.

Fig. 1B shows plots of the dependence of magnetic susceptibility on temperature at zero field, where the onset of the superconducting transition for all three samples is clearly distinguishable.

Fig. 1. (A) Diffractograms and (B) magnetic susceptibility temperature dependence of the $CaKFe_4As_4$ $CaRbFe_4As_4$ and $CaCsFe_4As_4$ compounds.

In summary, in this work, single-phase polycrystalline samples of $CaKFe_4As_4$, $CaRbFe_4As_4$, and $CaCsFe_4As_4$ with superconducting transition temperatures of 34,7 K, 35,2 K and 31,3 K respectively, were synthesized and characterized.

The work was financially supported by the RSF grant № 23-12-00307, using the equipment of the LPI shared facility center.

References

1. *Singh S.J. et al*. Superconductor Science and Technology **33**(2), 025003 (2019).
2. *Iyo A. et al*. Journal of the American Chemical Society **138**, 3410-3415 (2016).
3. *Stillwell R.L. et al*. Physical Review B **100**, 045152 (2019).

Cuprate superconducting thin films for heterostructures with strong spin-orbit interaction interface

I.E. Moscal[1], V.A. Baydikova[1,2], Y.V. Kislinskii[1], K.E. Nagornykh[1,3], K.Y. Constantinian[1], G.A. Ovsyannikov[1], A.M. Petrzhik[1], A.V. Shadrin[1,3]

[1] Kotelnikov Institute of Radio Engineering and Electronics Russian Academy of Sciences, 125009, Moscow, Mokhovaya 11-7, Russia; e-mail: ivan.moscal@yandex.ru
[2] Russian Technological University – MIREA, 119454, Moscow, Russia
[3] Moscow Institute of Physics and Technology (National Research University), Dolgoprudny 141701, Moscow region, Russia

We present results on fabrication and characterization of cuprate superconducting on $NdGaO_3$ substrate, using $YBa_2Cu_3O_{7-\delta}$ thin films with an interface exhibiting strong spin-orbit interaction. For this we utilize epitaxially grown strontium iridate films patterned into mesa-structures in combination with $YBa_2Cu_3O_{7-\delta}$ Strontium iridates.

Cuprate superconducting thin films for heterostructures with strong spin-orbit interaction interface.

We present results on fabrication and characterization of cuprate superconducting on $NdGaO_3$ substrate, using $YBa_2Cu_3O_{7-\delta}$ thin films with an interface exhibiting strong spin-orbit interaction. For this we utilize epitaxially grown strontium iridate films [1, 2] patterned into mesa-structures in combination with $YBa_2Cu_3O_{7-\delta}$. Strontium iridates $Sr_{(n+1)}IrnO_{(3n+1)}$ belong to Ruddlesden-Popper series exhibiting a change from a three-dimensional correlated semi-metal $SrIrO_3$ ($n\rightarrow\infty$) to a two-dimensional Mott insulator Sr_2IrO_4 (n=1) and as the superconductor $YBa_2Cu_3O_{7-\delta}$ had perovskite crystal structure. In this work, we discuss the structural features of $YBa_2Cu_3O_{7-\delta}$ thin films grown by dc cathode sputtering on $NdGaO_3$ along with XRD data of cuptate/iridate heterostructures. We discuss the features of electron transport flowing through the interface, taking into account that insulating Sr_2IrO_4 is a canted antiferromagnet with weak ferromagnetism of 10^{-2} μ_B per Ir, while well conducting $SrIrO_3$ is a paramagnetic material, likely being Dirac semi-metal. We show that electron transport properties of cuprate/iridate interfaces in heterostructures are promising for application aiming at the development of spin-dependent superconducting devices.

This work was supported by the Russian Science Foundation, project No. 23-49-10006.

References

1. *A.M. Petrzhik, K.Y. Constantinian, G.A. Ovsyannikov, et al*. Phys. Rev. B **100**, 024501 (2019).
2. *Y.V. Kislinskii, K.Y. Constantinian, I.E. Moskal, et al.* Rus. Microelectronics **52**, S53 (2023).

Magnetic and superconducting properties of $EuRbFe_4As_4$

Alena Levakhova, Nailya Safina, Andrey Sadakov, Vladimir Pudalov

V.L. Ginzburg Centre for High-Temperature Superconductivity and Quantum Materials
P.N. Lebedev Physical Institute of the RAS, 53, Leninsky ave., 119991 Moscow, Russia

For a long time, it was believed that magnetism should suppress superconductivity because magnetic atoms have a large magnetic moment. In practice, in magnetic compounds we see coexistence of superconductivity and magnetism. Among the new class of iron-containing superconductors, the compound $EuRbFe_4As_4$, in which superconductivity and magnetism are realized at the same time, has unique properties [1]. The crystal structure of $EuRbFe_4As_4$ is a building block of two blocks: $EuFe_2As_2$ and $RbFe_2As_2$ alternating along the crystallographic c-axis. The $EuFe_2As_2$ compound is non-superconducting, while $RbFe_2As_2$ has a superconducting transition temperature of ~ 2.6 K. Eu atoms have ferromagnetic ordering inside the layer and antiferromagnetic between the layers. The rotation angle between the layers has been calculated and is 90◦ [2, 3]. $EuRbFe_4As_4$ single crystals were prepared from the melt of the native RbAs component ('self-flux') [4]. Synthesis of a compound with such a stoichiometric composition is rather complicated, since phase 1144 competes with phase 122. The slightest fluctuations during synthesis lead to structural instabilities. The temperature dependences of the magnetic susceptibility show a superconducting transition at $T_c \approx 36$ K corresponding to the compound $EuRbFe_4As_4$ and magnetic ordering of Eu^{2+} atoms in the ab plane at $T_m \approx 15$ K.

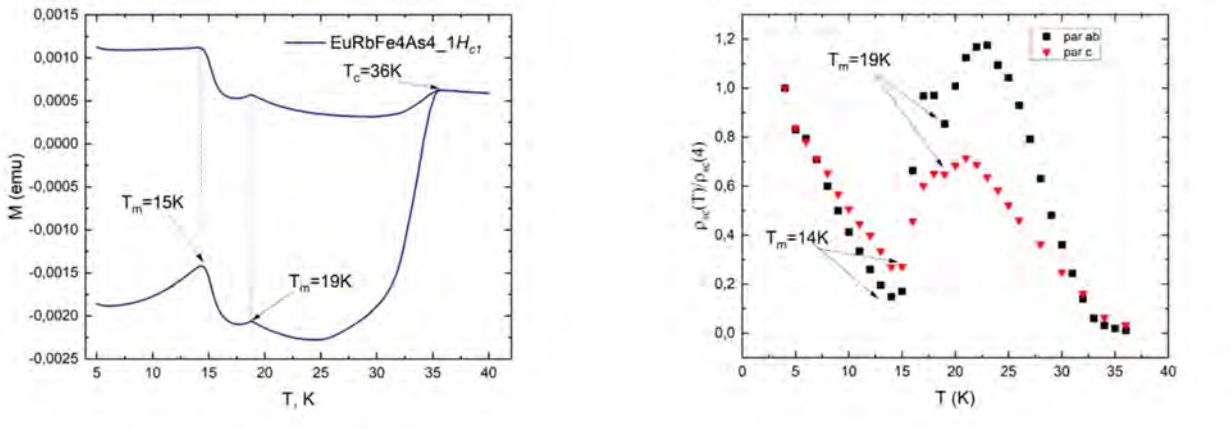

a) b)

Fig. 1. – a) Temperature dependences of magnetization M(T), b) Temperature dependences of the density function of the superconducting condensate.

Figure 1 shows the magnetization dependence of the second sample, which, in addition to the feature at 15 K, shows an additional peak at 19 K, indicating the presence of $EuFe_2As_2$ impurities. Such inclusions represent planar defects and can

serve as pinning centers of Abrikosov vortices [4]. The first critical field H_{c1} (T) was also investigated for two orientations H // ab and H // c. The reduced density function of the superconducting condensate was obtained and analyzed, which shows a feature at 15 K, which confirms the influence of antiferromagnetic ordering on the superconducting properties. At present, a model is being selected to describe the obtained dependences in order to determine the gap structure.

References

1. *Iyo A. et al.* Journal of the American Chemical Society **138**(10), 3410–3415 (2016).
2. *Kim T.K. et al.* Physical Review B **103**(17), 174517 (2021).
3. *Kim T.K. et al.* Uspekhi Fizicheskikh Nauk Journal **65**(7), 740-747 (2021).
4. *Degtyarenko A.Y. et al.* Nanomaterials **12**(21), 3801 (2021).

Investigation of critical current in micron wide NbN single photon detectors

M.D. Soldatenkova[1,2], E.M. Baeva[1,2], S.S. Svyatodukh[1,2], A.V. Semenov[2], A.I. Kolbatova[1,2], G.N. Goltsman[1,2]

[1] HSE University, 20 Myasnitskaya Str., Moscow, 101000, Russia,
[2] Moscow Pedagogical State University, 1/1 Malaya Pirogovskaya Str., Moscow, 119991, Russia

Here we report on a study of factors that limit the critical current in superconducting strips of various widths made from thin NbN films. We focus on the experimental dependence of the critical current on the external magnetic field at T = 4.2 K. Our observations suggest spatially inhomogeneous energy gap. It can be the main limiting factor for the current density in disordered NbN films. These findings have implications for superconducting single-photon detectors based on micron-sized wires operating at low temperatures.

Superconducting single-photon detectors (SSPD) [1] are an integral component in quantum optics experiments. Such detectors are used in a wide range of technical applications: quantum communications and quantum computing [2], light detection and ranging systems – LIDAR [3] and deep space communication [4]. Superconducting single-photon detectors based on micron-sized superconducting wires (SMSPD) are subjects of interest to the scientific community due to the advantages. According to the theoretical prediction of D.Y. Vodolazov [5], superconducting single–photon detector with a width of about several microns can detect a single infrared or optical photon if the ratio $I_c/I_{dep} > 0.7$ is maintained, where I_{dep} is the depairing current for a specific material and structure and I_c is the critical current. An experimental demonstration of single photon detection in micron-wide NbN strips was shown in ref. [6]. However, the critical current I_c rarely reaches the maximum possible current I_{dep} in the experiment due to different defects occurring in the strip [7] (meander bends, edge roughness, changes in the strip width – transition from a wide part to a narrow one). Another reason for limiting the critical current is the influence of material disorder. Nevertheless, superconducting disordered materials with a high normal state resistivity such as niobium nitride are successful for single-photon detection [8, 9]. In this work we investigate the factors limiting the critical current to optimize superconducting devices at low temperatures. The samples under this study are made from the thin NbN film. The samples are patterned into bridges of different width w. We estimate normal-state sheet resistance as $R_s^{\max} = \frac{R_{\max}}{N}$, where $R_{\max}$ is normal-state resistance at 20 K, $N=l/w$ is the number of squares in the sample, where l is the length of the strip. Parameters of the samples S_1, S_2, S_3, such as d, w, l, $R_s^{\max}$ are listed in Table.

Table. Parameters of the studied samples

	$d(nm)$	$w(\mu m)$	$l(\mu m)$	$T_c(K)$	$R_s^{max}(\Omega/\square)$	RRR	$I_c^{4.2\,K}(\mu A)$	$I_c^{4.2\,K}/I_{dep}^{4.2\,K}$
S_1	3.7	1	75	8.16	1407	0.72	39.2	0.49
S_2	3.9	2	75	7.2	515	0.7	87.2	0.57
S_3	4.2	7	75	8.9	1300	0.7	392	0.52

Here we focus on the experimental dependence of the critical current on external magnetic field. We measured the critical current for three samples and compared our data with the estimated depairing current according to the following expression [10]:

$$I_{dep}(T) = (0.74 w \Delta(0)^{3/2} / eR_s^{max}\sqrt{\hbar D})\left(1-\left(\frac{T}{T_c}\right)^2\right)^{3/2},$$

where $\Delta(0) = 1.764kT_c$ – superconducting gap energy, e – electron charge, D = 0.5 cm^2/s – diffusion coefficient for NbN film [17], T = 4.2 K – bath temperature, T_c is the critical temperature that was determined as the point at which the sample lost half of its resistance in the normal state. It is important to note that the result of our estimation is far from the condition in ref. [4].

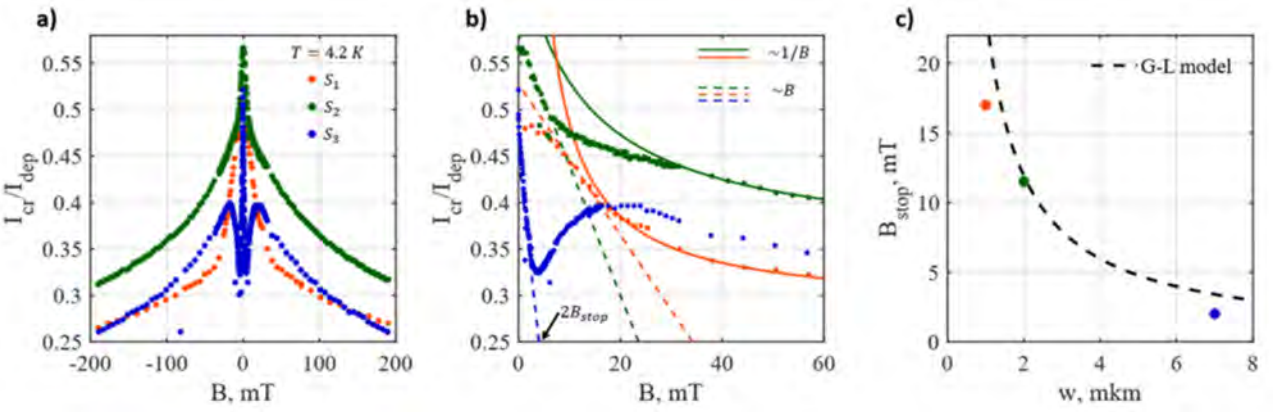

Figure 1. Dependencies of the I_{cr}/I_{dep} on the magnetic field in wide (a) and narrow (b) ranges. Experimental results are shown by red, green, and blue markers for samples S_1, S_2, S_3, respectively. In (b), solid and dashed lines are described dependences ~B and ~1/B. The arrow indicates the magnitude of the magnetic field corresponding to $2B_{stop}$. c) Dependence of magnetic field B_{stop} corresponding to the penetration of the first vortex on width of the strips. Dashed line – Ginzburg-Landau model.

Analysis of the behavior of the critical current in a magnetic field is one of the methods for identifying defects and inhomogeneities in a superconducting film [18]. To investigate the critical current, we measure current-voltage characteristics in an external magnetic field up to 200 mT at T=4.2 K. Our experimental results are presented in figure 1. The experimental data for samples and are plotted in red, green and blue, respectively. The linear behavior of the critical current dependence at low magnetic fields indicates the absence of volume pinning centers in the entire volume of the film and reflects a vortex-free state in the superconducting strip. The linear dependence is shown in figure 2(b) by dashed lines. When the applied

magnetic field exceeds a threshold value $B>B_{stop}$, the sample transitions to a mixed superconducting state characterized by vortex penetration. These dependencies is described by solid lines in fig. 2(b).

In figure 2(c) we show dependence of magnetic field B_{stop} on width of strips. Symbols are described experimental values for B_{stop}. Dashed line describes $B_{stop}(w)$ dependence calculated using Ginzburg-Landau model [13]

$$B_{stop}(T) = \Phi_0 / 2\sqrt{3}\pi\xi(T)w,$$

where Φ_0 – magnetic flux quantum, $\xi(E) = 4$ nm is the typical coherence length for NbN [11]. Our experimental B_{stop} values are consistent with the proposed theoretical model. It may indicate the absence of edge defects in the strips. However, we observe a decrease in the critical current value in comparison with the depairing current. This experimental observation suggests the presence of an inhomogeneous energy gap in disordered NbN films. The formation of weak regions (sections of the strip with a locally suppressed superconducting gap) leads to the premature breakdown of superconductivity at current densities below the theoretical depairing current. These defects can be the main limiting factor for the current density [8].

Acknowledgment

The research was supported by the Russian Science Foundation (project No. 24-72-10105).

References

1. *Goltsman G.N. et al*., Applied physics letters **79**(6), 705-707 (2001).
2. *You L*., Nanophotonics **9**(9), 2673-2692 (2020).
3. *Guan Y. et al*., Optics and Lasers in Engineering **156**, 107102 (2022).
4. *Wollman E.E. et al*., Optics Express **32**(27), 48185-48198 (2024).
5. *Vodolazov D.Y. et al*., Physical Review Applied **7**(3), 034014 (2017).
6. *Korneeva Y.P. et al*., Physical Review Applied **9**(6), 064037 (2018).
7. *Clem, J.R*., Phys. Rev. B **84**, 174510 (2011).
8. *Zolotov P.I. et al*., IEEE Transactions on Applied Superconductivity **31**(5), 1-5 (2021).
9. *Zolotov P. et al*., Applied Physics Letters **122**, 15 (2023).
10. *Clem J.R., Kogan V*., Physical Review B–Condensed Matter and Materials Physics **86**(17), 174521 (2012).
11. *Semenov A. et al*., Physical Review B–Condensed Matter and Materials Physics **80**(5), 054510 (2009).
12. *Ilin K. et al.*, Physical Review B **89**(18), 184511 (2014).
13. *Maksimova G.M. et al*., Europhysics Letters **53**(5), 639 (2001).

Control of magnetoresistance of Py/Nb heterostructure using hysteresis properties of magnetic domain structure

L.S. Uspenskaya, S.V. Egorov

ISSP RAS, Chernogolovka, Russia

Magnetoresistance of permalloy-niobium heterostructure is controlled by the type of magnetic domain walls formed in the permalloy layer. Magnetoresistance is negative or positive depending on the type of domain walls, Neel or Bloch one. The effect is greater the more walls are involved in the magnetization reversal process. In this report, we discuss a method for changing the number and direction of walls to provide a wide biased hysteresis loop, thereby expanding the range of fields with increased magnetoresistance and memristor-effect.

Magnetoresistance of permalloy-niobium heterostructure is controlled by the type of magnetic domain walls formed in the permalloy layer [1]. It was stated in [1] that the magnetoresistance is negative or positive depending on the type of domain walls, Neel or Bloch one, Fig. 1. However, it looks like the explanation given in [1] contradicts to the observation of variation of the type of magnetic domain walls in permalloy films fabricated by magnetron evaporation. The change of the type of domain walls from Bloch type in films with thickness of 10 nm by Neel type in films of 30 nm thick, and by cross-tie walls in films of 100 nm were observed by direct imaging in [2], some examples of the structures could be seen in Fig.2 (a-c) (courtesy of Gornakov V.S.). Thus, it have to be the Bloch walls in 20 nm film and Neel walls in 60 nm film.

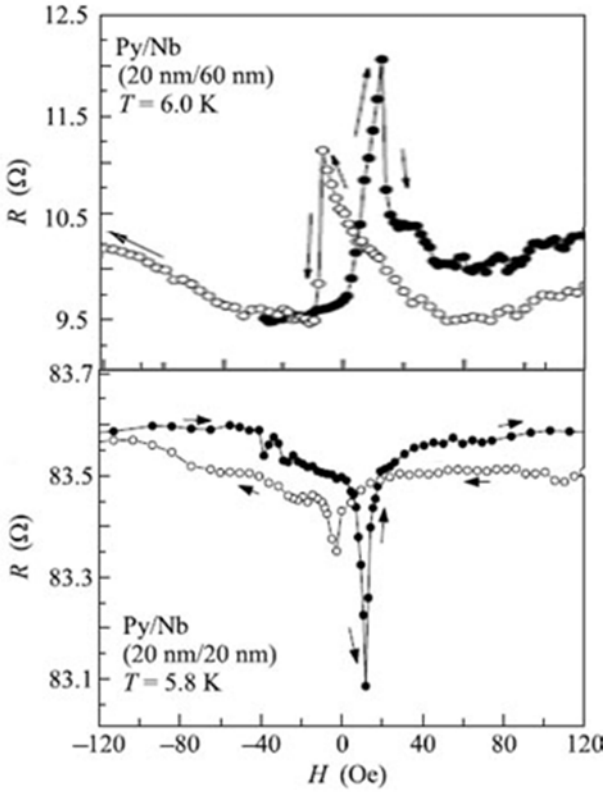

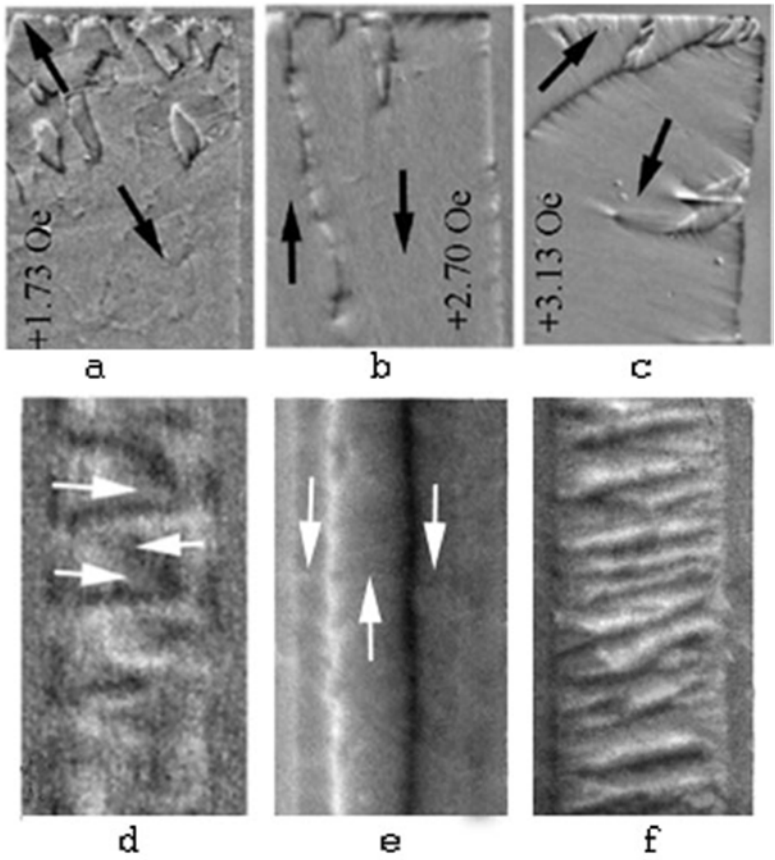

This paper reports on the dependence of the type of magnetic domain wall and the number of the wall in permalloy-niobium heterostructures upon the magnetic prehictory. Fig. 2 (d-f) shows some examples of different type of the walls obtained in the same bilayer stripe at 7 K. Fig. 2d shows the domain structure, obtained following the single-domain state of permalloy, Figs. 2e, 2f correspond to frozen domain structure. The magnitude as well as the sign of the magnetoresistance for these structures is different, since the density of domain walls is different and the direction of the walls is different: dense transverse walls provide large increase in the resistance of the heterostructure, while longitudinal walls reduce to some extent the resistance by creating a "conducting channel" along the structure because of "reentrant" superconductivity [3]. It is important to note also that different types of the formed domain structure correspond to hysteresis loops of different widths and different bias. For example, coercivity for structure like in Fig. 2d equals +7 and -7 Oe, while for structure in Fig. 2e it is +35 and -15 Oe. In conclusion, we discuss the methods for controlling the structure of magnetic domains, which allow changing the number and direction of walls, provided expansion and additional displacement of the hysteresis loop, thereby allowing the widening of the range of fields with increased magnetoresistance and memristor-effect in ferromagnet-superconductor heterostructure.

Usadel theory of dirty altermagnet-superconductor hybrid systems

M.M. Vasiakin, A.S. Mel'nikov

L.D. Landau Institute for Theoretical Physics RAS, 142432 Chernogolovka, Russia, Moscow
Institute of Physics and Technology (National Research University), Dolgoprudnyi, Moscow region, 141701 Russia,
Institute for Physics of Microstructures, Russian Academy of Sciences, 603950 Nizhny Novgorod, GSP-105, Russia

Starting from microscopic Gor'kov theory we derive the Usadel equations describing the superconducting states in dirty superconductor-altermagnet (S/AM) hybrids. We show that the effect of the altermagnetic exchange field can be reduced to effective magnetic impurities in analogy to the Dyakonov-Perel mechanism of spin relaxation. The resulting behaviour of superconducting gap, critical temperature and density of states are studied.

Altermagnetism is a recently discovered type of magnetic ordering. It combines traits of both ferro- and antiferromagnets, such as zero total magnetization and Zeeman-like spin-splitting [1]. Due to strong momentum-dependent exchange field, altermagnetism also bridges the gap between magnetism and spin-orbit coupling. The study of proximity effects in superconducting-magnetic hybrid systems and the influence of spin-orbit coupling (SOC) on superconductivity plays a crucial role in modern solid-state physics, making superconductor-altermagnet (S/AM) hybrids particularly promising as they present an opportunity to study a unique combination of these phenomena. Another important direction in the physics of superconductors is the effects of disorder. In the context of superconducting-antiferromagnet hybrid systems, as demonstrated in Ref. [2], the introduction of non-magnetic impurities may either suppress or restore superconductivity, depending on the chemical potential value.

In our work we focus on the study of possible disorder effects in S/AM structures. As a generic example, we consider a simplified model of S/AM hybrid system: a thin film of dirty superconductor placed on surface of the altermagnetic insulator. The altermagnet is assumed to be planar with the exchange field orthogonal to the interface, meanwhile superconductor in question is assumed to possess a conventional s-wave pairing. We derive the Usadel equation starting from the standard delta-correlated noise to model the disorder. To catch the effect of altermagnetic exchange field we take into account higher momentum harmonics in the expansion of the quasiclassical Green function. After the careful consideration we show that in the leading order the influence of the altermagnetic exchange field can be reduced to the effective magnetic impurities with easy axis and spin-flip time proportional to $[< h_2 >]\tau$, where $[\tau_1]$ is the non-magnetic scattering rate and $[< h_2 >]$ is the average square of the exchange field over the Fermi surface. This result appears to be a direct product of SOC-like nature of altermagnetism. Obtained

scattering rate is in agreement with the estimate based on the consideration of the Dyakonov-Perel mechanism of spin relaxation.

This work has been supported by the Russian Science Foundation (Grant No. 25-12-00042).

References

1. *L. ˇSmejkal, J. Sinova, and T. Jungwirth*, Phys. Rev. X **12**, 040501 (2022).
2. *G.A. Bobkov, I.V. Bobkova, and A.M. Bobkov*, Physical Review B **108**, 10.1103/physrevb.108.054510 (2023).

(A) APPLIED SUPERCONDUCTIVITY

Plenary

Status and trends of large-scale applications of superconductivity in 2025

Vitaly Vysotsky

Russian Scientific R&D Cable Institute

The final result of most old and new discoveries in physics is the development and application of new devices based on them in industry, everyday life, medicine and military equipment. This also applies to the phenomenon of superconductivity, for 114 years now. Considering the large-scale applications of both low and high-temperature superconductivity (LTS and HTS), there are both obvious successes and some failures. Any application of superconductivity can be divided into two types: enabled – that is, allowing you to get a new quality or the only one possible using superconductivity; or replaced – replacing old devices with improved parameters. The division is conditional, but allows us to assess the degree of demand or necessity for a particular application. Taking this division into account, the paper presented provides examples of the most important successes of large-scale applications of superconductivity in recent decades. The successes in obtaining and producing superconducting materials, the main trends and directions of developments in the field of medicine, electrical engineering and power engineering, high-energy physics, controlled thermonuclear fusion, etc. are discussed.

The final result of most old and new discoveries in physics is the development and application of new devices based on them in industry, everyday life, medicine and military equipment. This also applies to the phenomenon of superconductivity, for 114 years now. Considering the large-scale applications of both low and high-temperature superconductivity (LTS and HTS), there are both obvious successes and some failures. Any application of superconductivity can be divided into two types: enabled – that is, allowing you to get a new quality or the only one possible using superconductivity; or replaced – replacing old devices with improved parameters. The division is conditional, but allows us to assess the degree of demand or necessity for a particular application. Taking this division into account, the paper presented provides examples of the most important successes of large-scale applications of superconductivity in recent decades. The successes in obtaining and producing superconducting materials, the main trends and directions of developments in the field of medicine, electrical engineering and power engineering, high-energy physics, controlled thermonuclear fusion, etc. are discussed.

Invited

The development of superconducting materials in Bochvar Institute

Ildar Abdyukhanov

JSC

The results of the development of technical superconducting materials for different applications are presented in this report.

Bochvar Institute (JSC VNIINM) deploies technologies low-temperature superconductors as Nb_3Sn and Nb-Ti and technologies of stating materials for the producing the high temperature superconductors Y(Gd)-Ba-Cu-O.

Presently Bochvar Institute produces new different types of ceramic targets for production of high temperature superconductors Y(Gd)-Ba-Cu-O. These ceramic targets are designed for laser sputtering and contain nanoparticles as doping elements. Developed ceramic targets can be used for producing high temperature superconductors Y(Gd)-Ba-Cu-O with enhanced characteristics.

Also it is shown that the same approaches (using nanoparticles) can be used for improving the properties of Nb_3Sn superconductors.

Design and application of the Muon Source Project at CSNS

Yu Bao, Chen Wu, You Lv, Qiang Li, Yang Li, Cong Chen, Haiyan Du, Meichan Feng, Yan Feng, Xiaoyin Mo, Nikos Vassilopoulos, Lei Liu, Guangyuan Wang, Junsong Zhang, Yongji Yu, Huayan He, Jiaxin Chen, Jiebing Yu, Changdong Deng, Junhao Wei, Yuwen Wu, Wenqin Zhang, Yuntao Liu, Pengcheng Wang, Gang Zhang, Yinglin Ma, Sixuan Zhuang, Huihong Liang, Ning He, Yu Liu, Ao Cao, Congju Yao, Zhiduo Li, Yuanguang Xia, Jun Xu, Yuliang Zhang, Yongcheng He, Xin Qi, Wen Yin, Ziwen Pan, Tianyi Yang, Hao Liang, Bangjiao Ye, Sheng Wang

Institute of High Energy Physics, Chinese Academy of Sciences, Beijing 100049, China,
Spallation Neutron Science Center, Dongguan 523803, China,
State Key Laboratory of Particle Detection and Electronics,
University of Science and Technology of China, Hefei 230026, China,
University of Science and Technology of China, Hefei 230026, China

A Muon station for sciEnce, technoLOgy and inDustrY (MELODY) project has started construction in the beginning of 2024 at China Spallation Neutron Source (CSNS). A stand-alone target station is designed to produce pions and muons.Three muon beamlines are designed for various applications, including a surface muon beam, a dedicated negative muon beam and one decay muon beamline. A muSR spectrometer is designed with 3024 detectors. In this report, we introduce the application of muons in condensed matter and superconducting materials, and describe the design and progress of MELODY.

Muon beams have been used in various applications including particle physics [1] and material research [2]. The muon spin rotation/relaxation/resonance (μSR) techniques use the high sensitivity of polarized muon spins to magnetic fields to study the microscopic magnetic structure and dynamics of condensed matter. In China, we have designed a Muon station for sciEnce, technoLOgy and inDustrY (MELODY) based on China Spallation Neutron Source (CSNS). The project will be constructed during the Phase II upgrade of CSNS. As a start-up project, we will build one surface muon beamline with one μSR spectrometer and leave the decay muon beamline and more terminals for the future. Here we briefly introduce the CSNS facility and report the progress of the design and technique development of MELODY.

References

1. *Kuno Y. and Okada Y.* Rev. Mod. Phys. **73**, 151–202 (2001). (Preprint hep-ph/9909265).
2. *Hillier A.D., Blundell S.J., McKenzie I., Umegaki I., Shu L., Wright J.A., Prokscha T., Bert F., Shimomura K., Berlie A., Alberto H. and Watanabe I.* Nature Reviews Methods Primers **2**, 4 (2022).

Investigation of the vortex structure pinning in irradiated 2G HTS wire

P. Degtyarenko

S-Innovations LLC

In this work the results of investigation irradiated samples of 2G HTS wires is presented. The irradiation is performed by 8 MeV Au, 12 MeV Ni and 15 MeV O ions and Xe, Kr and Bi ions with energies 167, 292 and 670 MeV correspondingly. These results findings demonstrate the potential of ion irradiation as a practical method for enhancing the superconducting properties of 2G-HTS wires, paving the way for their industrial application in high-field environments.

We systematically studied the superconducting properties in magnetic field of 2G HTS wire samples before and after irradiation. The samples were irradiated by different ions (O, Ni, Au, Xe, Bi, Kr) and with different energies. The non-irradiated samples were fabricated by PLD, using commercial production equipment. Superconducting properties of the samples were measured in the field range from 0 to 16 T and various temperatures. The samples were uniformly irradiated at room temperature by scanning the ion beam over their whole surface at different equipment. We performed irradiation experiments using 18 MeV Au, 12 MeV Ni and 15 MeV O ions accelerated by a tandem ion accelerator, targeting 2G-HTS wires composed of YBCO, EuBCO/BHO, GdBCO, or (NdEuGd)BCO and YBCO samples were irradiated on cyclotron U-400 by Xe, Kr and Bi with energies 167, 292 and 670 MeV correspondingly. TRIM simulations suggested that ion penetration and energy loss varied by ion type, affecting defect formation and superconducting performance. The presence of heavy rare-earth elements in the HTS material increased susceptibility to ion irradiation, leading to more pronounced improvements in Ic. The results of microstructural studies by transmission electron microscopy (TEM) and X-ray diffraction methods are given. These results findings demonstrate the potential of ion irradiation as a practical method for enhancing the superconducting properties of 2G-HTS wires, paving the way for their industrial application in high-field environments.

High temperature superconductor: an affordable material for energy, science and transport

M. Moyzykh

SuperOx

High temperature superconductors (HTS) are commercially available since early 2010s. Development of reel-to-reel deposition processes enabled fast scaling of their production volume. Modern producers from Russia, Japan, China, EU and other countries have annual capacities exceeding 1500 km of 4mm HTS wire each. The cost of HTS production per unit length is rather similar between most producers thus the competition occurs in wire current-carrying capacity: each producer aims to provide the best current-to-cost ratio to the customer. Some producers, specifically from Russia and Japan, provide the best current-carrying properties in specific conditions (over 10 T magnetic fields and sub 20 K temperatures), which made these countries dominate at modern HTS market, achieving roughly 90% public market share.

Modern HTS world market is mostly driven by fusion science, followed by energy applications such as HTS fault current limiters and cables, and emerging propulsion applications. HTS utilization in most of these applications provides cost benefit since alternative (non-HTS) options feature significantly higher overall costs. Moreover, HTS cost share for listed applications is in range of 5 – 30% which is marginally less than economic effect, indicating HTS cost does not affect overall economic effect of the project. In other words, for the applications listed, HTS is easily affordable material.

The report supports above-mentioned statements by covering cost structures of modern HTS applications in relation to their economic efficiency as well as discussing determining reasons limiting widespread HTS equipment utilization. It also presents quantitive approaches for cost optimization among potential applications with higher HTS cost sensitivity, motivating targeted project viability determination.

Superconducting magnetic system for small-scale spherical tokamak MEPHIST-1

S. Pokrovskii[1,2], M. Osipov[1,2], I. Martirosian[1,2],
M. Novikov[2], P. Degtyarenko[2], S. Krat[1]

[1] National Research Nuclear University MEPhI, Moscow,
[2] Joint Institute for Nuclear Research, Dubna

The key parameter of any tokamak operation is the magnitude of the magnetic field in the plasma generation region. The report presents the results of conceptual design of superconducting magnetic system for the small spherical tokamak MEPHIST-1 developed in NRNU MEPhI (Russia, Moscow). For design of tokamak magnetic system HTS tapes of SuperOx production as well as modified tapes with artificial pinning centers produced using high energies ion irradiation (more than 100 MeV) were considered. Based on the obtained data, a numerical analysis of the tokamak magnetic system coils (toroidal and poloidal magnets) and operation regimes was performed.

The key parameter of any tokamak is the magnitude of the magnetic field in the plasma generation region. The toroidal (TF) and poloidal (PF) magnetic field coil systems are responsible for generating the primary magnetic field required for plasma formation and stability. Low-temperature superconductors have already been implemented in magnetic systems of nuclear fusion devices. The development of high-temperature superconductivity makes it possible to obtain high magnetic fields at relatively high temperatures, which simplifies the cryogenic system required to cool the magnets. Recently, significant progress has been made in the design and manufacture of superconducting magnetic systems in small-scale tokamaks. An example is the successful generation of plasma in the all-high-temperature superconducting tokamak HH70 in 2024 (the magnetic field was about 0.6 T) [1]. Large-scale low-temperature superconducting (LTS) tokamaks, such as EAST [2] and KSTAR [3], have demonstrated long-pulse and high-performance plasma regime. The development of conceptual compact tokamaks such as SPARC [4] has stimulated interest in high-field designs based on high-temperature superconductors (HTS). In the research by Zhai et al. [5] the superiority of HTS REBCO conductors in high magnetic fields was demonstrated. The transition from LTS to HTS materials, in particular second-generation (2G) REBCO coated conductors, has been recognized as a key step in achieving higher magnetic fields and improving stability.

The report presents the results of conceptual design of superconducting magnetic system for the small spherical tokamak MEPHIST-1 developed in NRNU MEPhI (Russia, Moscow). For the tokamak's magnetic system, HTS tapes produced by SuperOx (4 mm wide, critical current over 160 A at 77 K in self field (SF) with standart lift factor) were considered. Modified tapes with artificial pinning centers created using high energy ion irradiation (over 100 MeV) we're also suggested. In this study, we present the results of magnetic and transport measurements of the pristine and modified

HTS tapes and report an over two-fold increase in the critical current in wide range of temperatures (from 4.2 to 65 K) and magnetic fields (up to 5 T).

Based on the obtained data, a numerical analysis of the coils in the tokamak's magnetic system (toroidal and poloidal magnets) was performed, and the magnetic field distribution in the system was calculated. The target parameter is the value of the working magnetic field at a distance of 25 cm from the tokamak center. The calculation considered the geometric parameters of the vacuum chamber and the required operating modes of the magnetic system for ignition and plasma confinement. Two types of cables for superconducting magnets were analyzed: cables with a conductor on a round core (CORC®), consisting of spirally wound REBCO tapes (the total number of tapes in the cable was 50) and a cable made of HTS tapes tightly stacked on one another. The radial profiles of the magnetic field showed low corrugation and smooth gradients which meets the requirements for effective plasma confinement.

For the proposed configurations, the load curves of superconducting magnets at different temperatures were obtained. The operating points were selected. The mechanical characteristics of the magnetic system were analyzed for the pulsed and steady-state operation regimes of superconducting systems. The distribution of the magnetic field and mechanical stresses in the poloidal and toroidal magnetic field systems of the spherical tokamak was calculated, and the value of the transport current required to achieve the target magnetic field (1 T at 37.1 K) in the steady-state mode was determined. The main parameters such as the maximum toroidal field (more than 1.5 T) and peak current were determined using a standard HTS tape. Using a modified tape, the magnetic field can be increased to 2 T at the same temperature, which corresponds to the latest achievements in magnetic fields in small tokamaks. The results of this study can be used in the development of the Tokamak with Reactor Technologies (TRT), Russia.

Studies of HTS tapes irradiated with high-energy ions was carried out within the project funded by the Ministry of Science and Higher Education of the Russian Federation, Project «Fundamental and applied research at the NICA (JINR) megascience experimental complex» FSWU-2025-0014.

References

1. *Li Z.Y. et al*. Superconductivity **12**, 100137 (2024).
2. *Xiang, G.A.O., et al*. Plasma Science and Technology **23**(9), 092001 (2021).
3. *Kim, Hyun-Seok, et al*. Nuclear Fusion **64**(1), 016033 (2023).
4. *Creely, A.J., et al*. Journal of Plasma Physics **86**(5), 865860502 (2020).
5. *Zhai, Yuhu, et al*. Fusion Engineering and Design **168**, 112611 (2021).

Oral

Development of a superconducting fuse based on second-generation high-temperature superconductors for their use in limiting short-circuit currents in high-voltage networks

N.N. Balashov, A.Yu. Arkhangelsky,
V.V. Zheltov, A.I. Shurkalin, K.L. Kovalev

Joint Institute for High Temperatures of the Russian Academy of Sciences

Examples of major accidents in power systems:

08/14/2003 (USA) power line failure and subsequent rolling blackouts, damage $ 6 billion.

05/23/2005 (Russia) rolling blackouts due to a minor accident at the Chagino substation. Damage in Moscow and the Moscow region is 2.2 billion rubles.

09/28/2003 (Italy) as a result of damage to a power line and subsequent blackouts, 56 million people were left without power for 16 hours.

At the same time, the probability of major accidents (according to the Russian standard, these are accidents with damage from 5 to 500 million rubles) is 10^{-3}–10^{-4}, that is, a major accident is likely on a unit of powerful equipment once every 10 years.

In the event of a short circuit, a tenfold excess of current over the nominal value is considered acceptable. However, in a powerful electrical network, the current can increase 50-100 times already in the first 10-20 ms, while the response time of most used protection relays is 120 ms, and promising (vacuum switches) – about 30-50 ms. Therefore, the problem of creating current-limiting devices has become especially relevant in all developed countries.

1. Relevance

Examples of major accidents in power systems:

08/14/2003 (USA) accident on a power line and subsequent rolling blackouts – damage $ 6 billion.

05/23/2005 (Russia) rolling blackouts due to a minor accident at the Chagino substation. Damage in Moscow and the Moscow region 2.2 billion rubles.

09/28/2003 (Italy) as a result of damage to the power transmission line and subsequent outages, 56 million people were left without power for 16 hours.

At the same time, the probability of major accidents (according to the Russian standard, these are accidents with damage from 5 to 500 million rubles) is 10^{-3}–10^{-4}, that is, a major accident is likely on a unit of powerful equipment once every 10 years.

In the event of a short circuit, a tenfold excess of current over the nominal value is considered acceptable. However, in a powerful electrical network, the current

can increase by 50-100 times already in the first 10-20 ms, while the response time of most used protection relays is 120 ms, and promising (vacuum switches) – about 30-50 ms. Therefore, the problem of creating current-limiting devices has become especially relevant in all developed countries.

2. Novelty

Indeed, by replacing the windings of current-limiting reactors with superconducting ones, it is possible to reduce losses in the operating modes of electrical networks, and the use of superconducting current limiters (SCL), for example, of the resistive type, allows for an additional reduction in the level of shock impact on equipment when a short circuit occurs in the network. However, one cannot count on a reduction in the cost of current limiters. Depending on the power, the estimated cost of one HTSC current limiter, even in serial production, will be from 1 to 10 million $. The question of the service life of this equipment also remains open – in emergency mode, the winding heats up within several ms. With such thermal shocks, it is difficult to avoid degradation of the superconductor. Finally, all versions of HTSC current limiters (possibly with the exception of low-voltage SCL) must be equipped with additional switches with a response time of 30–40 ms. Ensuring such a response time at high currents and voltages is an additional technical problem. The relevance of the task is also confirmed by the intensity of publications devoted to this topic.

There is no information about the SOT variant proposed in this project.

The solution we propose is the use of a superconducting fuse that is devoid of the above-mentioned drawbacks. The working element of the fuse is a fusible link made of HTS tapes, which is completely destroyed when an emergency mode occurs. The current is displaced into the shunt, which limits its value until the network is disconnected by a standard relay protection and automation system (after 120 ms). The design does not require a tracking system – the insert begins to heat up when its critical current is exceeded. No additional switches are required. The destruction time of the insert, due to its special design, should not exceed 5 ms. This is enough to limit the shock current to permissible values in networks of almost any capacity. The length of the insert is about 1 m. Therefore, the power spent on cooling the fuse in the nominal mode will be no more than 10 kW. All other elements of the design are made of ordinary materials and do not require replacement after an accident. As a result, the cost of maintenance is reduced by at least an order of magnitude. The HTSC fuse can also be used in other devices as a high-speed switch.

3. Results

Connection diagram of the HTSC fuse.

The protected section of the network is a generator with the corresponding active resistance and inductance. The current limiter consists of a superconducting fuse and an active non-superconducting shunt. In the nominal mode, the current flows exclusively through the superconducting fuse insert.

The short circuit situation is simulated by closing the related key. During a short circuit, the current through the insert almost instantly exceeds the critical value for its superconducting layer. The insert heats up and completely breaks down, the current is forced into the shunt. The purpose of the shunt is to limit the current until the relay protection is disconnected, that is, within approximately 120 ms.

Experimental studies were carried out at the Scientific and Technical Center of FGC UES. We selected the following operating parameters of the source (generator): U = 1 kV, f = 50 Hz, I = 370 A, Number of phases is one. The surge current value in our experiments was 7-9 standardized values, i.e. 2.6-3.33 kA. Of course, it cannot be chosen arbitrarily, since it depends not only on the insert characteristics, but also on the characteristics of the protected network. The shunt resistance can indeed be chosen arbitrarily. It determines the current in the "current limitation mode", i.e. until the moment the relay protection and automation system is turned on. Our shunt resistance was 1.15 Ohm, and the actual voltage was 1.16 kV. So the effective current value after the insert burnt out was 1 kA. The surge voltage value during insert burnout was from 1.8 to 2.8 kV (depending on the composition of the HTS tape).

4. Application area

In any networks of medium and high voltage (up to 220 kV).

Electric machines with HTS windings

N. Ivanov, V. Kaderov, S. Zanegin, V. Zubko

Moscow Aviation Institute

Development, experimental research and trial operation of systems based on devices with high temperature superconductors (HTS) are the next steps in the field of applied superconductivity. In this case new methods of calculation and design of such systems should be developed. In this paper we provide preliminary scheme of the system which include HTS generator and cable, rectifier, battery and cooling system. Besides main parameters and calculation results of main parameters of the devices are de-scribed in the paper. Considered system will be used for verification of new calculation methods for such systems and for future experimental research of HTS devices behavior

Development, experimental research and trial operation of systems based on devices with high temperature superconductors (HTS) are the next steps in the field of applied superconductivity. In this case new methods of calculation and design of such systems should be developed. In this paper we provide preliminary scheme of the system which include HTS generator and cable, rectifier, battery and cooling system. Besides main parameters and calculation results of main parameters of the devices are de-scribed in the paper. Considered system will be used for verifica-tion of new calculation methods for such systems and for future experimental research of HTS devices behavior.

Superconductive undulators used for synchrothon radiation generation produced by Budker INP

F. Kazantsev, N. Mezentsev, V. Shkaruba

Budker Institute of Nuclear Physics

Modern synchrotron radiation facilities have extremely low electron beam emittance, what allows to generate SR with narrow harmonics using superconductive undulators. Therefore, serious requirements are imposed on the magnetic field structure of the undulators – it's necessary to provide as low as possible phase error value. In this paper recent works and developments in the field of superconductive undulators at Budker INP are descibed.

Nowadays undulators are widely used as synchrotron radiation sources. For example, at the SR facility «SKIF» being built now there would be three stations based on superconductive undulators. This facility belongs to generation 4+ and stands in the same row with such synchrotron radiation facilities as «MAX IV» and «ESRF».

The criterion of a «quality» of the undulator is a phase error. This characterizes uniformness of the magnetic field amplitude from each individual pole – the lower the phase error than the harmonics in the spectra of the output synchrotron radiation become narrower. The influence of the phase error on the synchrotron radiation becomes stronger at the higher harmonics of the undulator spectra.

The main disadvantage of superconducting undulators compared to traditional ones (based on permanent magnets) is the limited adjustment capabilities, in particular, the almost complete impossibility of regulating the magnetic field level of each pole separately. Budker INP is actively working to overcome this drawback. A method for correcting the phase error of the undulator by introducing correcting currents into pole groups, as well as an algorithm for calculating their values, has been developed. Such correction allows one to improve the spectrum of an already manufactured undulator without resorting to, as a rule, extremely labor- and time-consuming operations to fine-tune the magnetic structure.

A full-size prototype of the undulator for SKIF was manufactured with a period of 15.6 mm and a magnetic field of 1.2 T. The initial phase error in it was 8 degrees, but with the help of correction it was possible to reduce it to 2.5-3 degrees.

An attractive way to reduce a phase error is to find out characteristics of each pole of the undulator precisely and then install them in a certain order while assembling the undulator. A device for individual pole magnetic measurements for their further sorting was developed and is being tested and upgrading now. A measurement error of 0.2% was achieved, however long-term repeatability is much worse, about 1.5% – the data floats away monotonously for unknown reasons, likely connected with constructive design features of the system.

Magnetic measurements of a produced undulator should be singled out separately. Currently, a Hall sensor is used for this purpose. This method provides good measurement accuracy, but has limitations – low measurement speed and the need to have a sufficient vertical interpolar gap of the undulator, which tends to decrease constantly. In the foreseeable future, it may be impossible to place a carriage with a Hall sensor. An alternative is methods based on a stretched wire. These methods cannot currently be used as a full replacement for the Hall sensor, due to unresolved difficulties in obtaining high-quality data, but they have two advantages – undemanding to the vertical gap of the undulator and high data acquisition speed. The time of a single measurement with a wire takes about a second, while Hall requires about 1 hour for scanning. Nevertheless, wire measurements are close in accuracy to Hall sensor scans, losing to them by less than one order of magnitude.

Synchronous Electric Machines with Superconducting Stator and Rotor Windings

K.L. Kovalev, D.S. Dezhin, R.I. Ilyasov

Moscow Aviation Institute

This work discusses the current state and prospects of the concept of an aircraft equipped with fully electrified systems, highlighting its advantages and potential impact upon implementation. Currently, airplanes utilize three secondary energy systems: the power supply system, hydraulic system, and pneumatic system. This configuration for onboard power supply systems in future aircraft is not optimal. One of the most promising directions for creating a competitive airplane is transitioning to the concept of an aircraft with fully electrified equipment. A fully electric aircraft (FEA) is defined as one with a centralized power supply system that meets all the aircraft's energy needs.

The FEA concept includes a system that employs superconducting (SC) electric motors to drive the fan thrusters. It is proposed that either an SC generator powered by a gas turbine operating in optimal mode on hydrogen or kerosene-hydrogen fuel be used as the energy source for the motors. This power plant reduces noise, decreases pollutant emissions, and shortens the runway required for takeoff and landing.

The analysis considers the potential use of cryogenic electric machines in aviation. Results of analytical calculations of two-dimensional magnetic field distributions in SC machines, as well as parameters of SC machines in motor and generator regimes are presented. It is shown that the use of modern SC materials enables specific power values exceeding 10-15 kW/kg. This cryoplane integrates several modern trends in aircraft manufacturing:

- The use of liquid hydrogen as a fuel;
- The application of turbojet propulsion that combines high turbine efficiency with a wide range of speed adaptability;
- The incorporation of SC generators and motors, allowing for higher power output than gas turbines;
- The placement of SC generators within the aircraft fuselage, reducing noise and infrared detectability;
- The cryoplane features zero emissions of greenhouse gases and harmful substances.

Alternating Current Oscillation Shaper for Superconductor Research

E.P. Krasnoperov, N.S. Levchenko, A.V. Prutkov

NRC

A power source has been developed that generates various configurations of alternating current oscillations of a given duration. In this way, thermal disturbances are added to the superconductor in small, controlled portions, which allows studying dynamic processes on alternating current with amplitudes I_a exceeding the average critical values I_c.

Measurements allow predicting the appearance of a narrow normal zone and determining the conditions for stable operation of the superconductor at $I_a > I_c$. The process of thermal instability development in liquid nitrogen up to burnout has been studied using electrical and optical methods on 50 μm thick superconducting tapes.

The work was carried out within the state assignment of NRC «Kurchatov Institute».

Combined experimental and numerical study of normal zone propagation in non-insulated HTScoils

I.V. Martirosian, D.A. Aleksandrov, A.Y. Malyavina, S.V. Pokrovskii

National Research Nuclear University MEPhI (Moscow Engineering Physics Institute)

In this work, we present a combined experimental and numerical study of normal zone propagation in pancake coils wound out of REBCO tapes. Longitudinal and transverse NZP have been investigated. To ensure proper thermal contact between the coils and solid nitrogen, a specially modified have been designed. The quench was simulated using resistive heaters embedded between the coil layers. To simulate NZP behavior in HTS coated conductors, a finite element method-based model was developed in COMSOL Multiphysics software.

High-temperature superconductors (HTS), particularly REBCO (rare-earth barium copper oxide) coated conductors, have gained much interest due to their substantial advantages in high-field and high-current applications like superconducting magnetic energy storage (SMES) systems [1], magnetic levitation (maglev) transportation [2], and compact high-field magnets for fusion reactors, nuclear magnetic resonance and magnetic resonance imaging systems [3]. In these applications, thermal stability and effective quench protection are essential for operational reliability. Therefore, one of the key parameters in this context is the normal zone propagation (NZP) velocity. While HTS offer high current densities and better temperature and magnetic field operating intervals, their inherently low NZP velocity–especially compared to low-temperature superconductors–poses a unique challenge. This issue becomes even more pronounced in cryogen-free systems where traditional liquid cryogen immersion is not feasible. Solid nitrogen (SN_2) has emerged as a viable cryogen for HTS applications due to its high volumetric heat capacity, relatively broad operational temperature window (4.2–63.15 K), and mechanical compatibility with compact coil assemblies. However, the phase change peculiarities of SN_2, particularly its sublimation under localized heating under low pressure, introduces new and complex dynamics in NZP behavior that must be studied for future applications.

In this work, we present a combined experimental and numerical study of normal zone propagation in pancake coils wound out of REBCO tapes. Longitudinal and transverse NZP have been investigated. To ensure proper thermal contact between the coils and solid nitrogen, a specially modified have been designed. The quench was simulated using resistive heaters embedded between the coil layers. To simulate NZP behavior in HTS coated conductors, a finite element method-based model was developed in COMSOL Multiphysics software. The model incorporates electromagnetic-thermal coupling, complex temperature and pressure dependencies of nitrogen phases' thermal parameters and phase changes, and temperature dependent current redistribution implementation.

The experimental results reveal that longitudinal NZP velocities were higher than transverse velocities, consistent with expectations for anisotropic thermal conductance in tape geometries. However, under sustained heating a substantial decline in propagation velocity has been observed. This could be explained by the formation of nitrogen vapor pockets due to sublimation and/or rapid melting and evaporation. These vapor pockets effectively decouple the solenoid thermally from the surrounding solid nitrogen, acting as localized thermal insulators. Numerical calculation results are in a good agreement with the experimental data showing similar values for NZP velocities. The model illustrates the normal zone behavior under different applied current and cooling conditions. The model further illustrates how thermal interface degradation due to sublimation and/or rapid melting and evaporation leads to abrupt changes in local heat transfer rates. Notably, in regions where the sublimation occurs, there is a delay in thermal response that may obscure voltage-based quench detection methods.

This study highlights the importance of combined experimental-numerical approaches in understanding quench behavior in SN_2-cooled HTS systems. While solid nitrogen provides favorable bulk thermal stability, its phase-change behavior complicates quench dynamics.

The study was supported by a grant from the Russian Science Foundation No. 24-79-00278, https://rscf.ru/project/24-79-00278/.

References

1. *Gupta R., Anerella M., Joshi P., et al*. IEEE Transactions on Applied Superconductivity **26**(4), 1-8 (2016). DOI: 10.1109/TASC.2016.2517404.
2. *Mun J., Lee C., Lee C., et al*. IEEE Transactions on Applied Superconductivity **31**(5), 1-5 (2021). DOI: 10.1109/TASC.2021.3060692.
3. *Kim W.S., Lee S., Kim Y., et al*. IEEE Transactions on Applied Superconductivity **25**(3), 1-4 (2021). DOI: 10.1109/TASC.2014.2376593.

Calculation and Experimental Measurement of Inductances in Superconducting Structures

F.A. Razorenov[1,2], M.M. Khapaev[3], A.S. Ionin[1,2,4], I.E. Tarasova[1,2], L.N. Karelina[1], N.S. Shuravin[1], V.V. Bol'ginov[1]

[1] Osipyan Institute of Solid State Physics RAS, Chernogolovka, Moscow District, Academician Osipyan str., 142432, Russia,
[2] Moscow Institute of Physics and Technology, 9 Institutskiy per., Dolgoprudny, Moscow Region, 141701, Russia,
[3] Lomonosov Moscow State University, GSP-1, Leninskie Gory, Moscow, 119991, Russia, Joint Venture

Superconducting quantum interferometers (SQUIDs) are key components in digital superconducting electronics, used for information processing and easily tunable by external signals. Their design requires precise inductance calculation, for which wxLL software is applied. Numerical modeling and experiments on two-junction interferometers showed strong agreement, enabling reliable inductance estimation. Additional tests in the 1.2–8 K range confirmed that inductance varies with temperature, offering a way to tune device performance and refine London penetration depth estimates.

For a long time, superconducting quantum interferometers (SQUIDs) are used as a key components of superconducting digital electronics. They are suitable for receiving, transmitting, and converting information, and their properties can be easily tuned by external current signal. Digital superconducting devices are typically designed as multilayer thin-film structures above a superconducting ground plane. While developing their design, one has to shape superconducting lines to achieve optimal inductance values derived from numerical optimization of circuit schematics. To do this, a software is essential capable of calculating inductance for a given sample structure.

We demonstrate that the wxLL software [1], which solves Maxwell's and London equations for a given cross-section, is an effective tool for this task. We numerically modeled two-junction interferometers in four designs, using three superconducting layers separated by insulating layers. The bottom layer serves as a superconducting screen, while the other two form the control line and interferometer loop. The results included per-unit-length values of self- and mutual inductances for stripline structures fabricated in the second and third layers.

To validate these results, we conducted experimental studies of four series of two-junction interferometers with similar cross sections. The interferometers had a U-shape, with Josephson junctions at the ends of the «U», and a variable-length crossbar for different samples of the same design. This configuration enabled determination of per-unit-length and total inductances of the striplines for comparison with the calculated values. The comparison showed agreement within a few percent relative error. The results also allowed us to develop heuristic approaches useful for preliminary estimates.

Experimental studies in the temperature range of 1.2–8 K allowed us to construct the temperature dependencies of self- and mutual inductances. The goal of

these measurements was to evaluate the possibility of ‘tuning’ the transfer function of a superconducting neuron [2] by varying the temperature. The experiment showed a 20–30% increase in inductance within this range and predicted the potential for effective tuning of the transfer function in the 6–8 K range. The good agreement between theory and experiment makes it possible to reconstruct the temperature dependence of the London penetration depth, which is a key parameter in the design of neuromorphic interferometers.

This work was supported by Russian Science Foundation grant No. 23-72-00053. Sample fabrication was performed using the unique scientific facility «Kryointegral» (USF No. 352529), Institute of Radio Engineering and Electronics, RAS.

References

1. *M. Khapaev*, Superconductor Science and Technology **9**(9), 729-733 (1996).
2. *N.S. Shuravin, L.N. Karelina, A.S. Ionin, F.A. Razorenov, M.S. Sidel’nikov, S.V. Egorov, & V.V. Bol’ginov*, JETP Letters **120**(11), 829-836 (2024).
3. *V.V. Shmidt, P. Müller*, The physics of superconductors: Introduction to fundamentals and applications. Springer Science & Business Media, 1997.

The effect of 5 MeV electron irradiation at 165 K on the structure and magnetic properties of YBCO based HTSC tape

Akhmad Shodiev, Malika Mussaeva, Elvira Ibragimova

Institute of Nuclear Physics of the Academy of Sciences of the Republic of Uzbekistan, Tashkent, Uzbekistan

This study investigates the effect of high energy electron irradiation to a fluency of 5×10^{14} cm^{-2} at 165 K just above the superconducting transition onset on the crystal and electronic structure and resistivity/magnetoresistance in applied magnetic field of 0.56 Tesla in the temperature range of 80-300 K. Ten times decrease in magnetoresistance with maximum at 160 K is attributed to paramagnetic charged oxygen vacancy centers acting as effective pinning centers with a separation of ~1 nm. This irradiation method optimizes YBCO tape performance and seems promising for high-field magnet applications.

Metal-coated HTSC-2 tapes are used in high-current cables, energy storage and accelerators [1], although high energy particles (4 MeV electrons, 3×10^{16} e^{-}/cm^{2}) are known to induce defects and deformations that reduce critical current density (J_c) and *E-J* slope [2, 3]. Since this fluency produces defects at a distance <0.1 nm, which is less than the coherence length and therefore destroys Cooper pairs, increases *R* and decreases J_c, the aim of this work was to determine the irradiation conditions when a defect density is much less and possible increases the J_c in multilayer HTSC-YBCO tapes.

Sample details & methods. Material: SuperOx (S-Innovations, Russia-Japan) HTSC-2 tapes (4 mm-wide YBCO layer: 5–8 μm on steel C-276 substrate, coated with Ag/Cu/PbSn microlayers). Irradiation: 5 MeV electrons (fluency 5×10^{14} cm^{-2}, beam current 400 nA) at ~165 K using U-003 accelerator. Measurements: XRD (Empyrean, PANalytical) and Hall effect (HMS-7000 system, Ecopia) of specific resistivity and magnetoresistance [4]. Figure 1 *a,b* shows the temperature dependences for non-irradiated reference (curves 1) and the irradiated sample (curves 2).

Figure1. Resistivity *r* (a), magnetoresistance *R* (b), 1 – before irradiation, 2 – after irradiation at 165 K with the fluency of 5 MeV electron fluency 5×10^{14} cm^{-2}.

The main effects: Irradiation lowered the *r* within 80–300 K and the superconducting transition below 120 K and other transitions at 220 and 300 K. Ten times decrease in the *R* suggests the increased current vortices around strong flux pinning centers at 160 K, which are paramagnetic polarons at *F*-centers in oxygen vacancies generated by the electron beam. The calculated distance between the nearest defects is ~1 nm that is more than the coherence length χ_{ab} in cuprates. The defects act as pinning centers, stabilizing vortices under magnetic field 0.56 Tesla in HMS-7000 system by enhancing the critical current.

Conclusion. Our method of 5 MeV electron irradiation to moderate fluency 5×10^{14} cm^{-2} at 165 K optimized YBCO tape performance and seems promising for applications in high-field magnet coils.

References

1. *Molodyk A. et al*., Sci. Rep. **11**, 2084 (2021).
2. *Fedotov Yu.V. et al*., Low Temp. Phys. **26**, 464 (2000).
3. *Kashurnikov V.A. et al*., Supercond. Sci. Technol. **31**, 115003 (2018).
4. *Shodiev A.A. et al*., Conf.Proc.Nucl. Phys., 76–79 (2023).

Diode effect in bilayer structures based on yttrium iron garnet – superconductor

L.S. Uspenskaya

ISSP RAS, Chernogolovka, Russia

It has been recently shown that in $Y_3Fe_5O_{12}$/Al structures in the region of the superconducting transition temperature it is possible to switch the resistance of the structures both by rotating the magnetic field and by inverting the current. The effect was well described by the influence of the Zeeman field on the superconducting transition of aluminum. In this paper, we propose to use the magnetostriction effect in $Y_3Fe_5O_{12}$ to create structures in which the resistance is switched by inverting the current, and we experimentally demonstrate the possibility of implementing this idea using the example of the $Gd_3Ga_5O_{12}/Y_3Fe_5O_{12}$/Nb structure, where the magnetic domain structure of the garnet film is specifically modified by deformation at a certain choice of the orientation of the niobium strip.

In recent decades, much attention has been paid to the development of cryogenic electronics, including those based on superconducting materials [1, 2]. In particular, spin valves are implemented on the basis of superconductor-magneto-soft and magneto-hard ferromagnets structures [3, 4], magnetoresistive switches are implemented on ferromagnet-superconductor structures [5, 6] that is the superconductor resistance switching by a magnetic field. Currently, the possibilities of field-free switching of hybrid structures are being intensively investigated [7, 8].

Recent results of study of transport properties of aluminium and niobium films and structures fabricated on single-crystal $Y_3Fe_5O_{12}$ films with (111) and (100) orientations in a wide temperature range from 300 K to 4 K are presented by this report.

It is shown in this report that the decrease in the temperature of the superconducting transition and its expanding are more significant at (111) orientation of the films, despite the fact that numerous magnetic domain boundaries localized under the superconductor should enhance the superconductivity.

It is shown that the dependence of the superconductor resistance on the mutual direction of magnetization and current is observed only in narrow and thin stripes of niobium and disappears with their thickening. The rotation of the planar magnetic field makes it possible to effectively switch the resistance of such structures in the region of an expanded superconducting junction only. The effect is as large as 100%.

A scheme for obtaining a diode effect baced on $Y_3Fe_5O_{12}$/Al and $Y_3Fe_5O_{12}$/Nb structures is proposed and implemented. The 25% variation in the resistance is achieved by inverting a relatively low current. The use of the magnetostriction effect in $Y_3Fe_5O_{12}$ is suggested to create structures in which the resistance is switched by inverting the current, and it is experimentally demonstrated the possibility of implementing this idea using the example of the $Gd_3Ga_5O_{12}/Y_3Fe_5O_{12}$/Nb structure,

where the magnetic domain structure of the garnet film is specifically modified by deformation at a certain choice of the orientation of the niobium strip.

The research was carried out at Osipyan Institute of Solid State Physics, Russian Academy of Sciences, within the framework of a state assignment.

References

1. *Sidorenko A.* (Ed.) Functional Nanostructures and Metamaterials for Superconducting Spintronics. NanoScience and Technology, Springer, Cham., 2018.
2. *Mel'nikov A.S., Mironov S.V., Samokhvalov A.V., Buzdin A.I.* Phys. Usp. **65**, 1248–1289 (2022).
3. *Deminov R.G., Tagirov L.R., Gaifullin R.R., et al*. J. Magn. Magn. Mater. **373**, 16-17 (2015).
4. *Stamopoulos D., Manios E., Pissas M.* Supercond. Sci. Technol. **20**, 1205 (2007). DOI: 10.1088/0953-2048/20/12/022.
5. *Karelina, L.N., Bolginov, V.V., Erkenov, S.A. et al*. Jetp Lett. **112**, 705–709 (2020).
6. *Suri D., Kamra A., Meier T.N.G., Kronseder M., Belzig W., Back Ch.H., Strunk Ch*. Appl. Phys. Lett. **121**, 102601 (2022).
7. *Santamaria Ja.* Nature Materials **21**, 993 (2022).
8. *Ustavschikov, S.S., Levichev, M.Y., Pashenkin, I.Y. et al*. J. Exp. Theor. Phys. **135**, 226–230 (2022).

Eigenmodes of the radial current decay in no-insulation HTS coils

D.S. Yashkin, D.N. Diev, A.V. Polyakov, A.V. Naumov

NRC

The problem of non-uniform attenuation of radial current during charging/decharging a NI-HTS coil is considered. An approach is proposed that consists in considering the eigenmodes of the radial current that attenuate with their eigentimes. The approach is substantiated using the equivalent circuit method. The approach is illustrated by a NI-HTS test coil.

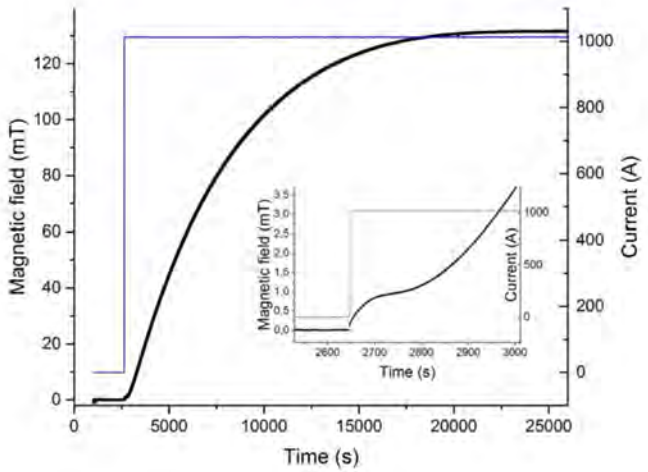

Non-insulated superconducting coils (NI-HTS) [1] differ from isolated ones by the presence of a resistive connection between adjacent turns. This feature leads to fundamental differences in their electromagnetic behavior. Non-insulated coils have a qualitatively specific property: the ability to induce currents in individual turns or groups of turns that close through normal resistance. As a result, dynamic processes in such coils involve redistribution of magnetic flux, current, and energy between turns.

This paper discribes the non-uniform attenuation of radial current during the charging/discharging of an NI-HTS coil. A detailed analysis of the time-dependent magnetic field and voltage graphs reveals that these processes are well described by a superposition of multiple exponential decays (Fig. 1). Notably, the voltages across different coil sections are not always monotonic and may even alternate in polarity (Fig. 2).

This effect occurs because a non-insulated coil comprises multiple inductively coupled circuits through which current can flow. Since each turn contributes differently to the total inductance and has distinct inter-turn resistance, the electromagnetic conditions vary across the coil. Consequently, during dynamic processes, certain sections experience faster current changes, leading to complex current redistribution between turns.

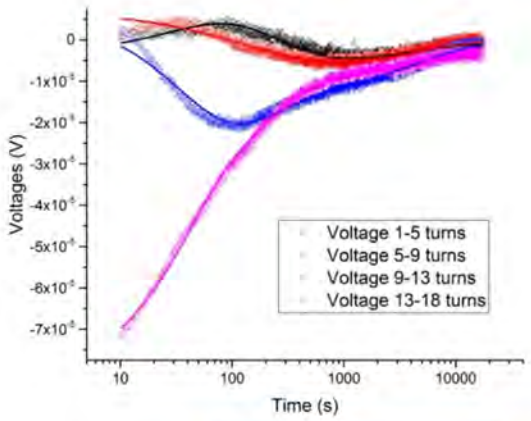

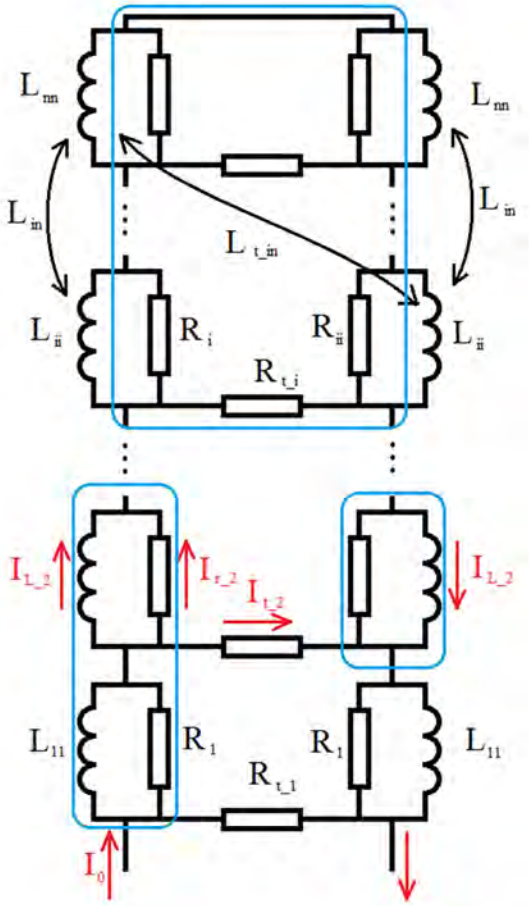

To describe these phenomena, we propose an approach based on the eigenmodes of radial current, each decaying with its characteristic time constant. The approach is substantiated using the equivalent circuit method. A class of equivalent electrical circuits with division into series-connected sections (inductively coupled RL cells) is considered [2]. By the coil current assumed remains below the critical value (dissipative effects in the superconductor are negligible), the system can be described by linear differential equations. The general solution yields a sum of exponential decays, with the decay times and corresponding radial current distributions (eigenmodes) determined by the LDE system's matrix–i.e., the coil geometry and radial resistance profile.

The approach is illustrated by an experiment with a non-insulated HTS test coil. Structurally, the coil is constructed as a double pancake in a monolithic casing, so the equivalent circuit is complicated due to inter-layer currents (Fig. 3). Nevertheless, the system remains linear, preserving the applicability of eigenmode analysis. Fig. 2 shows the voltage dynamics across coil sections during charging process and their joint approximation by the sum of three exponentials. The coefficients of the approximation at the same characteristic times became eigenmodes. In Fig. 4, eigenmodes are shown schematically as relative voltage opposite those sections of the coil where they were measured. The first three eigenmodes obtained from the calculation of the equivalent circuit of Fig. 2 are shown by solid lines. Since it is the voltage that is being measured, it is the eigenmodes by voltage that are compared. The first eigenmode corresponds to the global current injection into the coil, the others reflect internal current redistribution processes. The calculated eigenmodes agree qualitatively with experimental data.

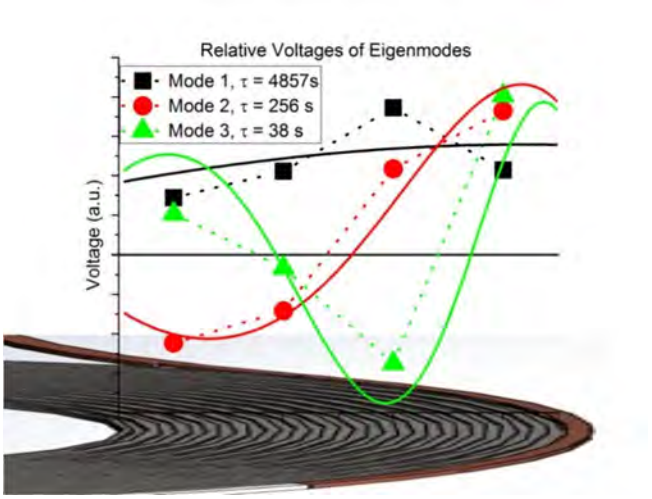

This approach allows one to analyze a current balance in non-insulated coil and provides a predictive tool for their dynamic behavior.

The work was carried out within the state assignment of the NRC «Kurchatov institute».

References

1. *Hahn, S., Park, D.K., Bascunan, J., & Iwasa, Y.* IEEE transactions on applied superconductivity, **21**(3), 1592-1595 (2010).
2. *Yashkin, D.S.* Superconductivity: fundamental and applied research **1**, 41-52 (2024).

Posters

Influence of ion irradiation on superconducting properties of HTSC tapes in a helical cable

D.A. Abin, A.S. Starikovskii, A.Yu. Malyavina,
S.V. Pokrovskii, R.G. Batulin, A.G. Kiiamov,
P.A. Fedin, K.E. Pryanishnikov, T.V. Kulevoy, A.P. Bazakutsa

National Research Nuclear University MEPhI (Moscow Engineering Physics Institute), Moscow, Russia,
Kazan (Volga Region) Federal University, Kazan, Russia,
National Research Center Kurchatov Institute, Moscow, Russia,
Kotelnikov Institute of Radioengineering and Electronics, Russian Academy of Sciences, 125009 Moscow, Russia

The dependence of the critical current of HTS tapes subjected to preliminary ion irradiation on the external magnetic field was studied. Irradiation was carried out with Fe^{2+} ions with an energy of 5.6 MeV and different fluences at room temperature. The samples were 4 mm wide HTS tapes with an open HTS layer wound on a cupronickel tube with a diameter of 5 mm and undeformed tapes. It is shown that with an increase in fluence, a decrease in the critical current occurs in the entire temperature range of 5-100 K for undeformed samples. The appearance of defects associated with compressive deformation during winding has a synergistic effect with defects formed as a result of ion irradiation, which leads to additional degradation of the critical current value.

Currently, there is a tendency in the world to create new generation Megascience installations (tokamaks, synchrotrons, charged particle accelerators) using high-temperature superconducting (HTS) composites. Plasma confinement in such installations is carried out by strong magnetic fields, which can only be created using superconducting magnetic systems (SMS) based on HTS composites. Transport current and magnetic properties of HTS composites included in the SMS windings are highly sensitive to the type and concentration of defects in the superconducting layer. The HTS composite is located in the radiation field of thermonuclear reaction products, including neutrons, which leads to the appearance of additional defects in the superconducting layer of the HTS composite and to the degradation of the current-carrying capacity, which after some time leads to a forced partial or complete replacement of the HTS coils in the tokamak SMS. Thus, a set of experimental data and complex studies that allow answering the question about the terms after which the replacement of the elements of the SMS system will be required is of great interest.

For the most accurate assessment of the service life of the SMS, it is proposed to conduct simulated irradiation of HTS composites with ions under conditions close to operational ones. One of the ways to create superconducting magnets is to form a coil of helical cables (CORC). These cables consist of a cupronickel tube with an

external diameter of 4-8 mm, along which layers of HTS composite are laid with a given rotation angle and tension force. The layers of the HTS composite are constantly under mechanical stress, which is important to consider when conducting research and preparing samples.

In this work, industrial HTS tape of the 2nd generation with a superconducting layer thickness of $YBa_2Cu_3O_{7-x}$ 1-2 μm was considered as samples. Irradiations were carried out on a resonant accelerator TIPr-1 at room temperature. The HTS tape with an open HTS layer 4 mm wide was wound with the HTS layer inside on a cupronickel tube 5 mm in diameter and about 3 cm long with a tension of approximately 0.5 kg. The tape was fixed with clamps at the edges of the tube. The HTS layer was irradiated through a pre-prepared through hole on the tube with a diameter of 3 mm. Thus, during the irradiation, the tape was in a state of mechanical stress similar to tapes wound on a cable in real magnetic systems. Also, for further comparison of the obtained irradiation results and studying the effect of stress created by the tension from winding, an undeformed tape was placed on the holder. The samples were irradiated with Fe^{2+} ions with fluences of 1E12, 5E12, 1E13, 2E13, 5E13 ion/cm^2. The magnetization dependences on the external magnetic field value were measured for the irradiated samples in a wide temperature range of 5-100 K in an external magnetic field of up to 8 T. The measurements were performed on ppms-9 and mpms-5 setups. A set of magnetization loops was obtained for each sample, from which the critical current dependences on the external magnetic field were calculated. It was shown that the deformation from winding the tape on the tube led to an additional decrease in the critical current during irradiation.

Calculation of operating parameters of spherical tokamak's superconducting magnetic system

D. Aleksandrov, I. Martirosian, E. Vinitskiy, M. Osipov

National Research Nuclear University MEPhI (Moscow Engineering Physics Institute)

This work presents a numerical model for calculating the magnetic and mechanical characteristics of the continuous toroidal magnetic field system (CTS) of a superconducting tokamak MEPhIST-1. Three different solenoid configurations were considered. The spherical tokamak's superconducting magnetic system main operating parameters have been calculated. These include: transport current necessary to achieve the required magnetic field of 1 T at 37.1 K, mechanical stress distribution and the peak toroidal magnetic field.

The toroidal field (TF) coil system remains an invaluable part of magnetic confinement fusion devices, responsible for generating the primary magnetic field required for plasma stability and shaping. As efforts to realize practical fusion energy intensify, substantial developments have been undertaken in the design of superconducting TF systems. Recently, large-scale low-temperature superconducting (LTS) tokamaks like EAST [1] and KSTAR [2] have demonstrated long-pulse and high-performance plasma regime. Currently, conceptual compact tokamaks like SPARC are driving interest in high-field designs enabled by high-temperature superconductors (HTS) [3]. The transition from LTS to HTS materials, particularly second-generation (2G) REBCO coated conductors, has been recognized as a transformative step in achieving higher operating fields and improving thermal stability. Studies, such as those by Zhai et al. [4], have emphasized the superiority of REBCO conductors in strong magnetic fields. In high-field compact tokamak designs, high-temperature superconductors have increasingly been used to enable greater flexibility in device geometry and the shaping and stabilization of plasma through magnetic field configuration. Conductor on Round Core (CORC®) cables, consisted of helically wound REBCO tapes, have emerged as a promising candidate for fusion-grade magnets due to their mechanical resilience and ease of winding into complex geometries. Specifically, SuperOx 12 mm REBCO tapes, featuring high critical current performance in excess of 500 A at 20 T and 4.2 K, have been extensively characterized and adopted in experimental and conceptual magnet systems [5].

This work presents a numerical model for calculating the magnetic and mechanical characteristics of the continuous toroidal magnetic field system (CTS) of a superconducting tokamak MEPhIST-1. Three different solenoid configurations were considered. The modelling was performed using the finite element method with the COMSOL Multiphysics software. The mechanical characteristics of the magnetic system were analyzed for pulsed and stationary modes of operation of superconducting solenoids. The calculation of magnetic field and mechanical stress

distributions in the toroidal magnetic field system of a spherical tokamak was carried out for the CTS, and the value of the transport current necessary to achieve the required magnetic field (1 T at 37.1 K) in the steady-state mode of operation was determined. Main parameters such as peak toroidal field (more than 1.5 T) and peak current were determined. Radial magnetic field profiles exhibited low ripple and smooth gradients, consistent with effective plasma confinement requirements. The field symmetry indicated that adequate shielding of the central plasma region was achieved. Current density in the superconducting windings was found to remain below the critical threshold (0.7 Jc) throughout the winding volume, suggesting that thermal and electromagnetic stability could be maintained during stationary operation.

The study was supported by the Russian Science Foundation grant № 24-29-00749, https://rscf.ru/en/project/24-29-00749/.

Magnetorheological polishing of HTSC substrates based on spherical particles obtained by the liquid anode method

Yu.S. Baryshnikov[1], I.A. Rodionov[2], F.A. Orlov[1],
A.D. Trofimuk[1], S.A. Ponyaev[1]

[1] A.F. Ioffe Physical-Technical Institute, Saint Petersburg, Russia,
[2] Peter the Great St. Petersburg Polytechnic University, Russia

The results of polishing stainless steel substrate of HTSC tapes by magnetorheological method using magnetorheological fluid based on spherical particles obtained by liquid anode method are presented. The polishing value achieved was 1.3 nm Sa (1.9 nm RMS), on a scanning section of 10 by 10 μm. Which is an indicator of the possibility of using this method for polishing HTSC substrates in case of scaling the method.

Industrial production of high-temperature superconducting tapes (HTSC tapes) is one of the priorities of technical development in Russia [1], and high-quality polishing with low roughness is one of the important technological stages for their production. To obtain HTSC tapes, it is necessary to achieve a surface roughness after polishing of less than 5 nm RMS [2] or 5 nm Ra [3]. In the cited works, the required roughness value was achieved using electrochemical polishing, and measurement of the surface roughness in a scanning area of 5 by 5 μm showed surface roughness values of 2.3 nm Ra [2] and 3.4 nm Ra [3]. The authors of the work [2] conducted a review of studies of polishing methods and concluded that electrochemical polishing is preferable to ensure a lower surface roughness than when using mechanical and chemical polishing, although the electrochemical polishing method has known disadvantages regarding the disposal of acidic electrolytes and harmful vapors. Also, the researchers in [4] reported the possibility of polishing on an installation for electrochemical polishing of the HTSC tape substrate, which allows obtaining a surface roughness of such tapes of less than 1 nm RMS on a scanning area of 5×5 μm. The magnetorheological polishing method does not have difficulties with acidic electrolytes, as in the case of electrochemical polishing. The method of using magnetorheological fluid for polishing surfaces has been widely studied by researchers from the A.V. Lykov Institute of Heat and Mass Transfer of the National Academy of Sciences of Belarus [5, 6], and the results are known where these researchers achieved a surface roughness of stainless steel of 3.9 Sa on a scanning area of 10×10 μm. It is also known that with magnetorheological polishing of stainless steel, roughness values of 16 nm Ra [7], 23.8 nm Ra [8], 50 nm Ra [9] have been achieved by other researchers. A detailed review of the methods of using magnetorheological polishing in various technical applications is given in [10], without mentioning the possibility of using the method directly for HTSC tapes.

This study presents the results of magnetorheological polishing of stainless substrates of HTSC tapes using a magnetic fluid, which included a diamond

suspension with a diamond fraction of 1 μm and spherical particles obtained by the liquid anode method during plasma spraying of low-carbon steel. The method for obtaining such spherical particles is presented in [11]. In the first case, the preliminary polishing was mechanical polishing with a roughness of 3.4 nm Sa, the roughness was measured on a scanning area of 10 by 10 μm, in the second case, the preliminary polishing was electrolytic-plasma polishing, which gave a roughness of 24.8 nm Sa on a scanning area of 10 by 10 μm. For the first case, after magnetorheological polishing, the obtained roughness value of the HTSC tape substrate was 1.3 nm Sa (1.9 nm RMS), on a scanning section of 10 by 10 μm. For the second case, the best value was 2 nm Ra on a profile length of 8 μm. The surface roughness data were measured using an Ntegra Aura atomic force microscope with an NS15 cantilever in the semi-contact mode. Thus, magnetorheological polishing using spherical particles obtained by the liquid anode method qualitatively reduces the roughness and allows obtaining the required roughness of substrates for HTSC tapes. In the future, it is planned to scale the results of magnetorheological polishing on long sections of HTSC tapes.

References

1. *I. Dorohova*, Atomnyj ekspert. **9**, 21 (2022) [In Russian].
2. *Q. Jia, Y. Wang, H.Suo, P. Wang*, Rare Metals **36**(9), 635 (2017).
3. *S. Hao, Y. Wang, H. Suo, Q. Jia, M. Liu, L. Ma*, Rare Metals, **37**(9), 795 (2018).
4. *S. Lee, V. Petrykin, A. Molodyk, S. Samoilenkov, A. Kaul, A. Vavilov, V. Vysotsky, S. Fetisov*, Supercond. Sci. Technol. **27**(044022), (2014).
5. *A. Hudolej*, Nauka i innovaciya, **11**(189), 30 (2018) [In Russian].
6. *A. Hudolej, G. Gorodkin, L. Gleb, A. Aleksandronec*, Nauka i innovaciya, **6**(148), 20 (2015) [In Russian].
7. *M. Das, V.K. Jain, P. S. Ghoshdastidar*, Machining Science and Technology, **14**(3), 365 (2010).
8. *C. Zheng, X. Gao, F. Zhang, W. Wang, K. Liu, J. Xu*, Precision Engineering, **81**, 104 (2023).
9. *A.W. Hasmi, H.S. Mali, A. Meena, I.A. Khilji, C.R. Chilakamarry, S.N. Saffe*, Materialstoday: Proceedings, **48**(6), 1892 (2022).
10. *F. Zhao, Z. Zhang, J. Yang, J. Yu, J. Feng, H. Zhou, C. Shi, F. Meng*, Chinese Journal of Aeronautics, **37**(4), 54 (2024).
11. *Yu.S. Baryshnikov, R.O. Kurakin, A.V. Chikiryaka, F.A. Orlov, K.V. Tverdokhlebov, S.A. Leukhin, M.I. Yurchenkov, S.A. Ponyaev*, Apllied physics, **3**, 23 (2023).

Structure and electrical conductivity of high-strength Cu-Nb microcomposite depending on deformation

I. L. Deryagina[1], E.N. Popova[1], E.I. Patrakov[1],
M.V. Polikarpova[2], V.I. Pantsyrny[2]

[1] M.N. Miheev Institute of Metal Physics, UB RAS, Ekaterinburg, S. Kovalevskaya, 18, 620108 Russia,
[2] LLC Rosatom Metall Tech, 115230, Moscow, Kashirskoe sh., 3, bld. 2, str. 9

Cu-Nb microcomposites (MCs) with high strength and electrical conductivity are used in various fields, including winding wires for 100 T pulsed magnets, as well as reinforcing elements in Nb_3Sn-based superconducting (SC) strands for SC magnets. The paper studies the Cu-Nb MCs with a reduced Nb content. It is shown that reducing the Nb concentration to 7.7% increases the plasticity of the material, allowing to produce MCs with high true deformation (up to 13.8) and tensile strength of 1200 MPa. The change in MC structure with deformation and its effect on strength and electrical conductivity of the MC wires have been studied by SEM and TEM. The obtained results allow discussing the possibility of using Cu-7.7%Nb composite for reinforcing SC strands.

Cu-Nb microcomposites (MC), possessing high values of both strength and electrical conductivity, are required as contact wires for high-speed railway transport, as microwires for aviation and microelectronics, as winding wires for extremely high-field pulsed magnets (100 T magnet at Los Alamos National Laboratory), as reinforcing components for superconducting (SC) Nb_3Sn-based strands for magnetic coils of Tokamak fusion reactors [1], and 25-30 T laboratory SC magnets [2]. Since requirements for the level of critical current density J_c of SC strands have been increasing throughout the history of the development of the SC industry, it is necessary to improve the strands' resistance to mechanical stresses. High-strength Cu-Nb MCs help to solve this important problem for applied superconductivity. As shown in [2-4], partial replacement of stabilizing copper in the Nb_3Sn-based strands with Cu-Nb inserts results in the enhancement resistance to mechanical stresses during coil winding and operation in SC magnetic systems. Besides, the Cu-Nb MC is promising material for strengthening 2G high-temperature superconducting tapes [5].

The Nb concentration in the Cu-Nb MC traditionally has been 16-20% [6]. In this research we studied Cu-Nb MC with reduced niobium concentration (7.7%Nb). Reducing the niobium concentration allows increasing the ductility of the MC wires, allowing them to be deformed to true strain 13.8 (Fig. 1a) to obtain thin microwires with high tensile strength 1200 MPa [7]. The Cu-7.7Nb MC wires studied in this research were manufactured at LLC Nanoelectro (now Rosatom Metal Tech LLC). We believe these MCs can be used to strengthen the Nb_3Sn-based SCs, which must have high plasticity during drawing and high tensile strength to withstand high stresses during the manufacture and operation of the wires. The Cu-Nb MC structure

at different stages of deformation has been studied using SEM (Fig. 1b) and TEM. The relationship between the strain degree, the structure, strength and conductivity of Cu-7.7Nb MC has been analyzed.

The study was performed using the equipment of the Collaborative Access Center at IMP UB RAS. This work was done within the State Assignment of the Ministry of Science and Higher Education of the Russian Federation for the IMP UB RAS.

Fig. 1. Tensile strength of Cu-7.7Nb MC vs true strain η (a); SEM-image of the composite cross-section, $\eta \approx 7$ (b).

References

1. *V. Pantsyrny, A. Shikov, A. Vorobieva*, Cryogenics **48**, 354-370 (2008).
2. *M. Sugimoto, H. Tsubouchi, H. Li et al*., IEEE Trans. Appl. Supercond. **30**, 6000905 (2020).
3. *N.I. Kozlenkova, V.I. Pantsyrnyi, A.E. Vorobieva et al*., IEEE Trans. Appl. Supercond. **17**, 2599-2602 (2007).
4. *I. Deryagina, E. Popova, E. Patrakov et al*., IEEE Trans. Appl. Supercond. **26**, 600706 (2016).
5. *M.V. Polikarpova, P.A. Lukyanov, I.M. Abdyukhanov et al*., IEEE Trans. Appl. Supercond. **24**, 6644268 (2014).
6. *E.N. Popova, I.L. Deryagina, E.G. Valova-Zaharevskaya et al*., Materials **14**, 7033-7045 (2021).
7. *I.L. Deryagina, E.N. Popova, E.I. Patrakov*, Metals **13**, 1576 (18 pp.) (2023).

Prospects for the Development of Palladium-Based Superconductors: From Theory to Experiment

K.K. Dikhtievskaya, T.Yu. Soboleva,
V.V. Anishchenko, M.V. Maltseva,
Ya.A. Lobkov

NUST MISIS, Laboratory of Functional Quantum Materials, 119049, Moscow

Modern research in the field of high-temperature superconductivity (HTS) has entered a new phase with the emergence of studies predicting the possibility of a superconducting state in palladium-based compounds. Theoretical calculations using quantum chemistry methods and multi-electron models indicate that palladates may possess a unique combination of electronic properties, making them promising candidates for next-generation HTS materials [1, 2].

The key advantage of palladium compared to nickel and copper lies in the peculiarities of its electronic structure. The 4d electrons of palladium demonstrate an optimal balance between localization and delocalization, creating favorable conditions for Cooper pair formation. Of particular interest is the theoretically predicted «Goldilocks effect» – a situation where electronic correlations in palladates are neither too strong (as in nickelates) nor too weak (as in some cuprates). This balance could contribute to an increase in the critical temperature of the superconducting transition [3].

However, the practical realization of superconductivity in palladates faces several significant challenges. The main difficulty lies in the synthesis of stable palladium oxide compounds with the required oxidation state. Unlike nickelates, where the Ni^{1+} electronic configuration can be achieved, palladium requires stabilization of Pd^{2+} or Pd^{3+}, which presents a considerable challenge.

Experimental verification of these theoretical predictions will require the development of new synthesis methods and comprehensive characterization of the obtained samples. At the initial stage, the most promising approach appears to be the fabrication of thin films using molecular beam epitaxy, followed by thorough investigation of their transport and magnetic properties. Particular attention should be paid to searching for signs of superconductivity near the metal-insulator boundary, where the highest T_c (critical temperature) values are theoretically predicted.

Thus, research on superconducting palladates represents a new and promising direction at the intersection of theoretical physics, solid-state chemistry, and materials science. Further development of this field requires close collaboration between theorists working on electronic structure calculations and experimentalists specializing in the synthesis of complex oxide systems.

References

1. *Motoharu Kitatani, Liang Si, Paul Worm, Jan M. Tomczak, Ryotaro Arita, Karsten Held*. Physical Review Letters **130**, 16 (2023). DOI: 1103/PhysRevLett.130.166002.
2. *Yoshiko Nanao, Yoshiharu Krockenberger, Ai Ikeda, Yoshitaka Taniyasu, Michio Naito, and Hideki Yamamoto*. PHYSICAL REVIEW MATERIALS **2**, 085003 (2018).
3. *A.S. Botana and M.R. Norman*. PHYSICAL REVIEW MATERIALS **2**, 104803 (2018).

The essence of the critical current angular dependencies asymmetry observed on coated conductors

V.V. Guryev, S.V. Shavkin, O.A. Kondratiev

NRC Kurchatov institute

The core focus of the present investigation is centered around an analysis of the critical current angular dependencies exhibited by coated conductor samples, which have been sliced in both longitudinal and transverse directions of the tape material. For samples sliced in both directions, a clear dependence of the critical current on the direction of the Lorentz forces is observed. Asymmetry is detected on the longitudinal sample, while this phenomenon is absent for the transverse sample. It is found that such behavior correlates with the predominant tilt of the *ab*-plane around the axis coinciding with the tape direction. An interpretation of this asymmetry is proposed, which naturally follows from the empirically noted dualism of the critical current anisotropy with respect to both directions: magnetic field and the Lorentz force.

The critical current angular dependences observed on coated conductors are of key importance for the efficiency of superconducting devices. However, despite the obvious significance, there is a noticeable gap in our knowledge regarding how the angular dependences relate to the basic microstructural features of the material. In this paper, an experimental study of the angular dependences of the critical current is carried out on samples of REBCO tapes cut in both longitudinal and transverse directions. The obtained angular dependences do not exhibit a strict 180-degree periodicity, and, in addition, the dependence of the critical current on the current polarity is observed. It is shown that both effects are a manifestation of anisotropy with respect to the direction of the Lorentz force, thereby revealing the dual nature of the critical current anisotropy. An asymmetry of the peaks of the angular dependence on the longitudinal sample is noted, in the absence of this phenomenon in the transverse sample.

Using the X-ray rocking curve method, the inclination angle of the crystallographic *ab*-plane with respect to the tape plane was determined: 2.3 degrees around the longitudinal axis and 0.4 degrees around the transverse axis.

A new approach for interpretation the observed phenomena within the framework of the anisotropic pinning model is proposed. By design, this model takes into account the duality of anisotropy [1, 2], and therefore describes well the dependence of the critical current not only with respect to the direction of the magnetic field, but also with respect to the direction of the Lorentz force [3]. However, as it turned out, the same duality is responsible for the asymmetry of the critical current angular dependence and is governed by mismatch of the extreme orientations of the energy and size bodies of the cooperative potential well. A quantitative correlation was established between the fitting parameters of the model and the experimentally measured *ab*-plane tilt. The proposed interpretation gives a plausible explanation for this quantitative agreement.

The work was carried out within the framework of the state assignment of the National Research Center «Kurchatov Institute».

References

1. *E.Yu. Klimenko, S.V. Shavkin*, “Electrodynamics of superconductors with anisotropic pinning” // report at FPS-04.
2. *E.Yu. Klimenko, S.V. Shavkin*, “On the formalism of pinning theory” // report at FPS-06.
3. *V.V. Guryev, I.V. Kulikov, S.V. Shavkin*, “Anisotropy of critical current of technical superconductors: methods of analysis and application examples” **47**, 3 // VANT: thermonuclear fusion (2024).

Fabrication and investigation of superconducting thin Nb-Al films with A15-structure

Selbi Hydyrova[1,2], V. Kulakov[2], S. Romanov[2],
T. Mavliaviev[2], K. Barkov[3], V. Kovalyuk[1,4],
G. Goltsman[5,6], K. Moiseev[2]

[1] University of Science and Technology MISIS,
[2] Bauman Moscow State Technical University,
[3] Voronezh State University,
[4] National Research University Higher School of Economics,
[5] Russian Quantum Center,
[6] Moscow State Pedagogical University

Superconducting properties and structure of Nb-Al thin films fabricated by magnetron co sputtering from two sources on heated substrate were investigated. Fabricated at room temperature Nb-Al films are X-ray amorphous or contain nanocrystalline Nb. In $Nb_{75}Al_{25}$ films deposited at 600°C at Nb magnetron power of 350 W and of 550 W, the $A_{15}Nb_3Al$ phase is obtained; superconducting transition onsets TC0 are ~6,6 K and ~4,1 K correspondingly.

Thin film, Nb_3Al, A_{15} phase, magnetron co-sputtering, superconductivity, critical temperature.

Superconductors with high critical temperature T_C are required for applications such as quantum computing based on trapped ions. One of the most promising materials for superconducting nanowire single-photon detectors is Nb_3Al with A_{15} structure [1], but its ultrathin crystalline films remain unexplored and have not been used in SNSPD, which makes their fabrication and investigation relevant.

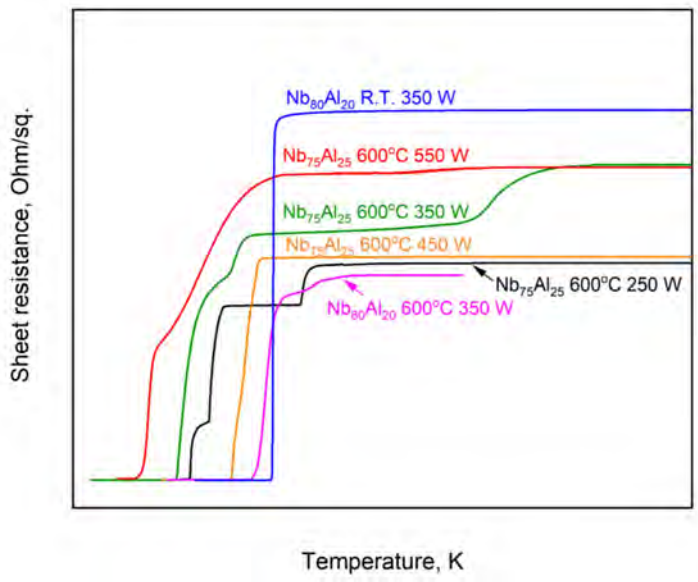

Superconducting Nb-Al thin films can be fabricated by magnetron co-sputtering, and the highest T_C is observed near stoichiometric composition Nb_3Al [2]. There are several phases in Nb-Al system, among them cubic Nb_3Al phase with the A15-structure has the highest $T_C \approx 18.8$ K. It is known that for many compounds with the A15 structure, the critical temperature largely depends on the ordering degree of the compound. Mostly the ordering in films and their degree of crystallinity, and therefore the superconducting properties of Nb_3Al, are influenced by the substrate temperature in film deposition process [3]: one of the most effective methods for T_C enhancement is deposition on a heated substrate at a temperature of 600 °C and above. It has to be mentioned that besides substrate temperature, the film deposition rate, affected by magnetron power, also has a significant influence on film structure and properties.

This work is focused on the effect of the fabrication parameters by magnetron sputtering on the superconducting properties and structure of Nb-Al films.

Nb-Al films are formed by the method of magnetron co-sputtering from two sources on a VUP-11M vacuum setup. The setup is equipped with magnetrons with a target diameter of 2” and a substrate holder with heating up to 600°C. For the magnetron with a Nb target a DC power supply is used, its power is varied from 250 W to 550 W. For the magnetron with an Al target RF power supply is used. Films are deposited with a thickness of 350 nm on R-cut sapphire substrates at the residual pressure less than 5×10^{-3} Pa, the working pressure of 0.2 Pa, the argon flow of 2.6 l/h, the rotation speed of the substrate holder of 15 rpm.

The structure of the films is studied by X-ray diffractometry on a DRON 4-07 diffractometer with a CuKα1 X-ray tube with a wavelength of 1.5406 Å. As a result, it was found that for deposition at room temperature, all the studied Nb-Al films of various compositions, with an Nb fraction from 65 to 85% (at.), are X-ray amorphous or contain nanocrystalline niobium phases.

The superconducting transition temperature, or critical temperature T_C, of the deposited films are studied by measuring the temperature dependence of sheet resistance using a Dewar vessel with liquid helium and a cryogenic insert, in the temperature range from 1.7 to 300 K.

The results of $R_S(T)$ measurements are shown in Fig. 1. It was found that for $Nb_{80}Al_{20}$ film deposited at room temperature with a magnetron power of 350 W for a niobium target, the critical temperature is $T_C = 3.76$ K. Deposition at a temperature of 600°C leads to broadening of the superconducting transition and slightly reduces its temperature to 3.69 K. Moreover, for all samples deposited with heating of the substrate, a stepwise and wider superconducting transition is observed compared to deposition at room temperature, which is presumably due to the non-uniform composition of the film, because the substrate holder in this work could be heated only without rotation.

For $Nb_{75}Al_{25}$ film deposited at 600°C at magnetron power of 350 W, superconducting transition onset T_{C0} is 6,6 K. XRD results indicate that $Nb_{75}Al_{25}$ films deposited at 600°C, at magnetron power of 350 W and of 550 W,

contain only Nb_3Al (A15 phase). Other samples deposited at 600°C contain only Nb phase.

As a result of the experiments, it was found that magnetron sputtering at room temperature ensures the production of superconducting films of $Nb_{80}Al_{20}$ with $T_C = 3.76$ K at a thickness of 350 nm. Deposition of the $Nb_{80}Al_{20}$ film on a heated substrate at 600°C increases the width and decreases the superconducting transition temperature from 3.76 to 3.69 K. For films formed with substrate heating, a stepwise and wider superconducting transition is observed compared to deposition at room temperature, which is presumably due to the non-uniformity of the film composition without rotating the substrate holder. In $Nb_{75}Al_{25}$ films deposited at 600°C at Nb magnetron power of 350 W and of 550 W, the A15 Nb3Al phase is obtained; superconducting transition onsets T_{C0} are ~6,6 K and ~4,1 K correspondingly.

Future plans are to investigate the combined effect of the substrate temperature in the range from room temperature to 600°C, the magnetron power and the film composition on the structure, electrical and superconducting properties of ultrathin Nb-Al films.

The work was supported in fabrication of superconducting films for integrated single-photon detectors by the grant of Ministry of Science and Higher Education of the Russian Federation FSME-2025-0002, in numerical modelling and experimental research – by the Russian Science Foundation grant No. 23-79-00056, in the structure investigation – by the Russian Science Foundation grant No. 23-79-10294.

References

1. *Kovalyuk, V.V., et al*. Radiophysics and Quantum Electronics (2024): 1-54.
2. *Dochev, Dimitar, et al*. Journal of Physics: Conference Series. Vol. 97. No. 1. IOP Publishing, 2008.
3. *Tanabe, K., and O. Michikami*. Journal of applied physics 56.11 (1984): 3261-3270.

Design and analysis of fully superconducting electric machines for transportation systems

N.S. Ivanov, V.V. Zubko, V.A. Kaderov

Moscow Aviation Institute, 125993, Moscow, Russia

A comparative analysis of existing superconducting electric machine projects has been carried out. Based on the findings, new machine configurations were developed using a proposed design methodology that combines analytical and finite element approaches. The calculated machines demonstrate higher specific power compared to reference designs, confirming the effectiveness of the methodology for transport applications.

Design and analysis of fully superconducting electric machines for transportation systems

The electrification of the transportation sector represents a critical direction in the advancement of global transport infrastructure, offering significant benefits in terms of emission reduction, increased energy efficiency, and decreased reliance on hydrocarbon-based fuels. The deployment of electric machines with high efficiency and specific power is essential for the successful implementation of electrified transport solutions. The realization of such machines necessitates the application of advanced materials, engineering approaches, and cutting-edge technologies – among which superconductivity occupies a prominent position.

High-temperature superconducting (HTS) electric machines have the potential to surpass conventional machines by providing superior specific power and efficiency. The present research is primarily focused on the development of methodologies for the design and computational analysis of fully superconducting electric machines intended for transport applications.

To this end, analysis of various transportation systems has been conducted to determine the input parameters required for the development of machines that can be effectively integrated into existing and emerging transport infrastructures. These systems were examined with due consideration of operational and technical constraints specific to each domain. Based on this analysis, several electric machine designs were developed, exhibiting enhanced performance characteristics when compared to existing international benchmark solutions.

Finite element models have been developed, incorporating principal components such as magnetic cores, HTS windings, and selected structural elements. The study investigates machines operating across a range of temperatures (20 K to 77 K) and featuring diverse magnetic core configurations, as illustrated in Figure 1. The finite element analysis provides detailed distributions of magnetic fields within the machine, an example of which is also presented in Figure 1. A key aspect of the modeling process involves the accurate representation of magnetic field behavior

within the HTS winding regions, as these fields directly influence the critical parameters of the superconducting tape.

Table 1 presents a comparative analysis of reference designs and those developed using the proposed methodology. In all examined cases, the newly developed machines demonstrate higher specific power relative to their respective benchmarks. These findings affirm the effectiveness of the proposed methodology in enabling the design of fully HTS-based electric machines with superior performance metrics.

Table 1

Comparative Characteristics of Reference and Calculated Superconducting Electric Machines for Transport Applications

	Machine Type	Rotational Speed, rpm	Power, MW	Operating Temperature, K	Specific Power, kW/kg	Specific Power (Calculated), kW/kg
China [1]	Generator	6000	10	20	13.1	30.4
Korea [2]	Motor	213	5	30	–	2.1
USA [3]	Motor	6800	1.4	60	16	18
Norway [4]	Motor	3500	2.5	45	14.7	17.3

The present work outlines the preliminary design of four HTS electric machines, each characterized by distinct power ratings, rotational speeds, and operational temperatures ranging from 20 K to 77 K, tailored for specific transport applications. The designs are based on a previously established methodology, which integrates analytical methods with finite element modeling, while rigorously accounting for the critical operational parameters of HTS conductors.

References

1. *Zhou X. et al*. Phys. C Supercond. Appl. Elsevier B.V., 2023. Vol. 605, № January. P. 1354207.
2. *Moon H. et al*. IEEE Trans. Supercond. 2016. Vol. 26, № 4. P. 6–10.
3. *Jansen R.H. et al.* AIAA Propuls. Energy Forum Expo, 2019.
4. *Mellerud R., Nøland J., Hartmann C.* Preliminary Design of a 2.5-MW Superconducting Propulsion Motor for Hydrogen-Powered Aviation // 2022 Int. Conf. Electr. Mach. ICEM 2022. 2022. P. 1404–1410.

A Novel Method for Measuring Lower Critical Field of Small-Sized Superconductors

E.M. Ivanova, A.T. Daniyarkhodzhaev,
A.V. Sadakov, A.S. Usoltsev,
A.R. Prishchepa, D.A. Chareev

P.N. Lebedev Physical Institute, Russian Academy of Sciences, 119991, Moscow, Russia,
Institute of Experimental Mineralogy, Russian Academy of Sciences, 142432, Chernogolovka, Moscow District, Russia,
Kazan Federal University, 18 Kremlyovskaya Str., Kazan, 420008, Russia,
Ural Federal University, Yekaterinburg 620002, Russia

Two-coil mutual inductance techniques are widely used to study bulk superconductors by detecting their diamagnetic properties. This approach is a fast and contactless tool for studying magnetic or superconducting materials. Furthermore, it screens the entire volume of the sample, in contrast to resistive measurements.

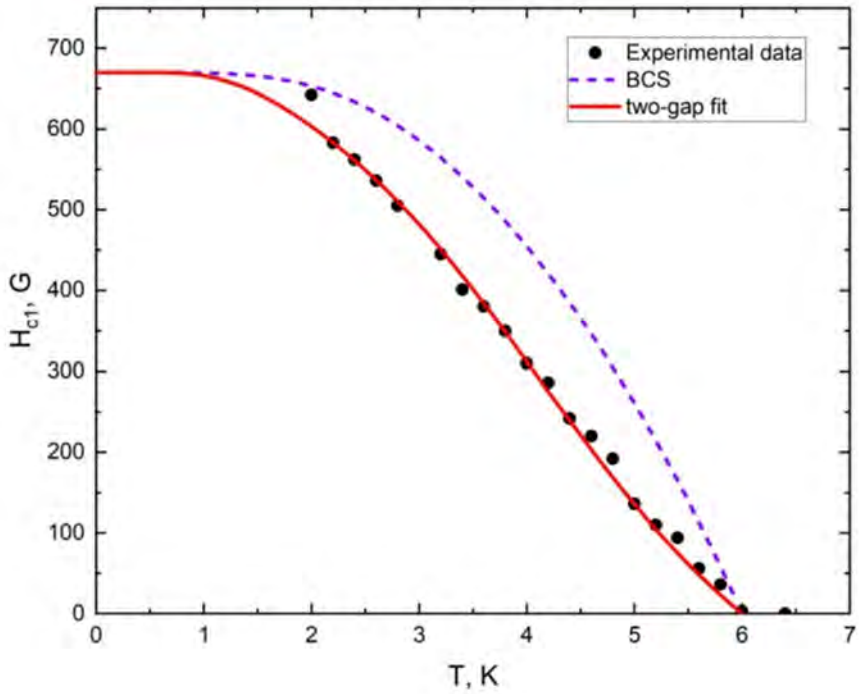

Inductive method can provide such important information about samples as transition temperature and critical fields. The lower critical field, Hc_1, is one of the fundamental parameters of type II superconductors. Hc_1 is related to superfluid density and contains information about penetration depth and Ginsburg-Landau parameter. Additionally, the temperature behavior of Hc_1 can reveal important insights into the nature of the superconducting state and help distinguish various types of paring mechanisms such as conventional s-wave and unconventional d-wave.

The relatively recent interest in two-dimensional superconductors has generated a need to characterize small-sized and thin samples, but traditional techniques might not be completely suitable for that purpose.

A typical scheme of two-coil mutual inductance measurements consists of two coaxial coils, with sample placed inside of them. This setup is placed in an external dc magnetic field, created by superconducting magnet. Applying an alternating current to the outer (drive) coil creates an alternating magnetic field, which in turn generates EFM in the inner (pick-up) coil. In theory, a superconducting sample placed inside pick-up coil will shield the induced magnetic field and decrease the generated voltage. When the external field exceeds Hc1 of the material and enters the sample, EFM increases again. Thus, by tracking this change in generated voltage, one can determine lower critical field of the sample.

The key to accurate measurements in this kind of experiments is high degree of coupling between sample and sensing coil. Also, it is best to place the coil as near to the sample as possible, since the generated signal grows with decreasing distance. Achieving all this is difficult when it comes to the minor samples, and effective volume of the wire coil fitted by the sample stays very small. It results in large signal from background ac field compared to the signal of interest. To solve this issue, we decided to switch from classic wire coils to smaller flat ones.

In this work we present a new technique for lower critical field measurements based on small-sized flat coils. Such approach allows us to increase the sensitivity of the measurements in comparison to the classic setup and to eliminate the influence of the edge effects. To make those coils, we developed microfabrication process that includes optical lithography, thermal evaporation of metals and magnetron sputtering of aluminum oxide. Our goal was to optimize the design and the fabrication process to achieve good sensitivity for accurate determination of Hc1 of small-sized samples.

For testing of our method we used a sample of NbS_2. Measurements were taken in temperature range from 2 to 6,4 K and under DC magnetic fields up to 1200 G. We applied a 1 mA current with frequency of 50 kHz to the excitation coil. Lower critical field as a function of temperature is presented in Fig.1.

To demonstrate the correct work of our set-up, we preformed lower critical field measurements via local magnetization with micro Hall sensor. We found that data collected from two experiments is in good agreement. We conclude that presented method offers a good approach for Hc_1 measurements on small superconducting samples.

Investigation of friction and lifting forces during cryostat movement

D.A. Karpukhin[1], V.V. Koledov[1], A.P. Kamantsev[1], Yu.A. Terentyev[1], M.V. Matyunina[1,2]

[1] Kotelnikov Institute of Radioengineering and Electronics of the Russian Academy of Sciences, Moscow, 125009 Russia,
[2] Chelyabinsk State University, Chelyabinsk, 454001 Russia

Magnetolevitation transport attracts more and more attention due to its inherent high speed and economy. Technical difficulties on the way to its practical implementation gradually recede as technologies develop, new materials and original ideas are developed. The purpose of this work is to study the friction forces during the movement of a cryostat with elements made of high-temperature superconductor ceramics. One of the principles of operation of magnetic-levitation transport systems is based on the use of the phenomenon of magnetic levitation of HTSC of the second kind.

A cryostat with a high-temperature superconductor (HTSC) of the Y-Ba-Cu-O composition is cooled above a track assembled from permanent magnets. The temperature of the HTSC transition to the superconducting state is approximately 93 K, which allows cooling the cryostat with liquid nitrogen, the boiling point of which is 77 K. During the experiment, the cryostat is first installed at room temperature at a certain height (the cool-down height) on a non-magnetic support above the track. Then it is filled with liquid nitrogen. The HTSC goes into the superconducting state upon reaching the critical temperature. Magnetic lines of force emerging from the linear magnets of the track are “frozen” into the HTSC elements. This also provides a counter-gravitational force, providing levitation and a lateral stabilizing force [1].

In our previous experiments, cryostats with bulk HTSC materials made of $YBa_2Cu_3O_7$ levitate over linear tracks of permanent magnets (PM) NdFeB, laid out in a special way. To estimate the levitation force between HTSC and PM, original installations were created.

References

1. *Karpukhin D.A., Petrov A.O., Koledov V.V. et al*. Journal of Radio Electronics. – 2022. – No. 11. – P. 8.

Modifying thermal coupling in superconducting nanowire single-photon detector by tuning amorphous sub-layer

K.I. Khilay, M.D. Soldatenkova, E.M. Baeva,
S.S. Svyatodukh, N.A. Titova, A.I. Kolbatova, G.N. Goltsman

MPSU, Malaya Pirogovskaya st. 1/1, Moscow 119435, Russia,
HSE MIEM, Tallinskaya st. 34, Moscow 123592, Russia

In recent decades, methods for controlling heat transfer between thin-film structures and substrates have been actively studied to improve the efficiency of superconducting nanowire single-photon detectors (SNSPDs) [1]. One of the enigmatic factors affecting SNSPD performance is the thermal contact between the superconducting film and the substrate, the influence of which remains poorly understood. In this work, we propose modifying the thermal link between the SNSPD and the thermal bath by varying the thickness of an amorphous dielectric interlayer between the superconducting film and the crystalline substrate.

In recent decades, methods for controlling heat transfer between thin-film structures and substrates have been actively studied to improve the efficiency of superconducting nanowire single-photon detectors (SNSPDs) [1]. One of the enigmatic factors affecting SNSPD performance is the thermal contact between the superconducting film and the substrate, the influence of which remains poorly understood. Recently, it was demonstrated that weakening the thermal link between the film and the substrate by using suspended membranes for SNSPDs allows achieving nearly 100% internal detection efficiency [4]. Various technological approaches are used to control the thermal coupling between the superconducting film and the thermal bath: reducing thermal contact by substrate etching [3], creating suspended structures [3], or changing the substrate material [5].

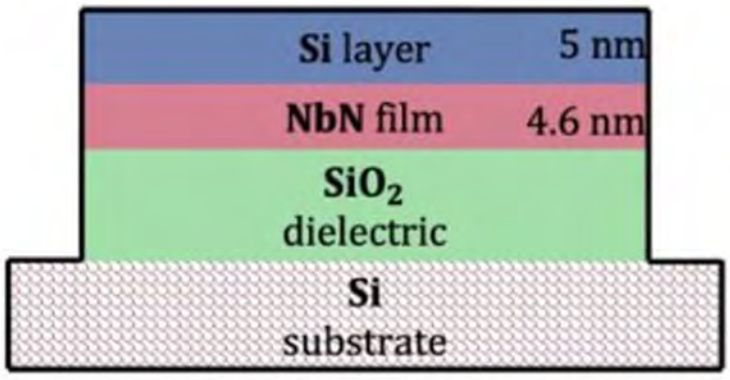

In this work, we propose modifying the thermal link between the SNSPD and the thermal bath by varying the thickness of an amorphous dielectric interlayer between the superconducting film and the crystalline substrate. Increasing the thickness of the amorphous dielectric layer introduces additional thermal resistance

due to the short phonon mean free path [3]. In this study, we fabricated meander-shaped structures from a 4.6 nm niobium nitride (NbN) film on dielectric layers (SiO_2 in our case) of varying thickness (from 10 nm to 1 μm) and investigated their current-voltage characteristics. Figure 1 shows a schematic of the deposited layers on the sample, while Figure 2 presents the obtained current-voltage characteristics of the samples with different thicknesses.

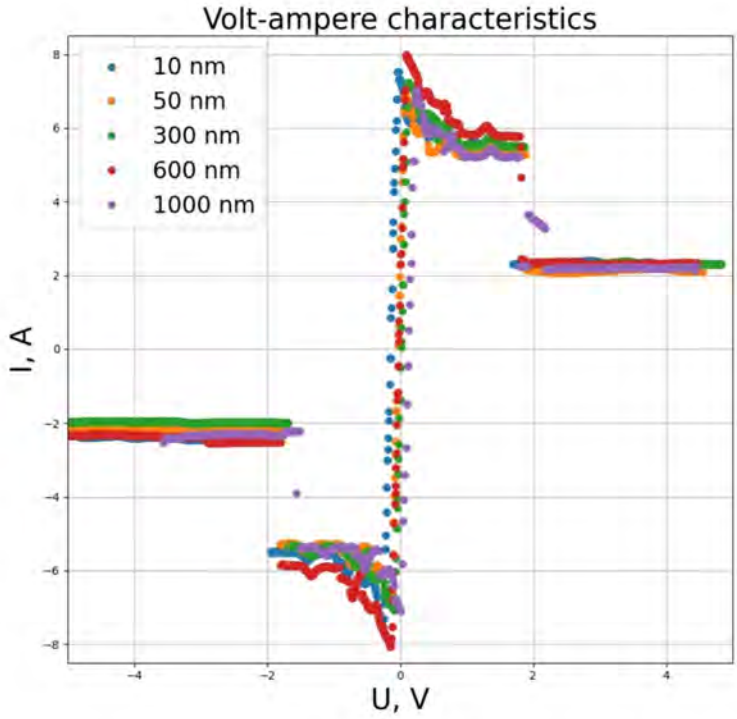

This work was supported by the Russian Science Foundation (RSF grant no. [24-72-10105]).

References

1. *Dane A. et al*., Nature Communications **13**(1), 5429 (2022).
2. *Stockhausen A. et al*., Superconductor Science and Technology **25**(3), 035012 (2012).
3. *Baeva E.M. et al*., Physical Review Applied **15**(5), 054014 (2021).
4. *Chang J. et al*., APL Photonics **6**, 3 (2021).
5. *Zhang L. et al*., Scientific reports **8**(1), 1486 (2018).

Helium-free magnetic system MRI 1.5T

O. Kovalchuk, A. Glushaev, N. Shatil,
V. Tanchuk, A. Labusov, E. Startsev

JSC NIIEFA (The D.V. Efremov Institute)

In modern magnetic resonance imaging (MRI) systems, a vital task is to abandon liquid helium in favor of helium-free cooling, which allows to significantly reduce operating costs owing to the absence of liquid helium in a cooling system, as well as to simplify the cryostat design due to no need in helium utilities (helium bath, discharge pipes, etc.). It, in turn, lowers the building infrastructure requirements and simplifies maintenance. In addition, the MRI systems with helium-free cooling are high-demand in remote regions with a limited access to liquid helium. However, the transition to helium-free cooling requires a revision of the key technical and design solutions which provide stable cryostatting of superconducting windings. The paper considers the features of cryostats and helium management systems operating on cryocoolers, as well as the specific requirements to ensure magnetic field stability in such operating conditions by the example of the first Russian helium-free 1.5 T MRI system to be developed and manufactured in the JSC «NIIEFA» (Rosatom State Corporation). When developed, particular attention has been paid to the design of superconducting switches which shall maintain «frozen current» conditions with low heat inputs in a magnetic field shimming/removal mode, as well as to the analysis of engineering solutions and compromises with respect to thermal and electrical insulation, stability and uniformity of the magnetic field, cooling efficiency and operational reliability.

R&D of TRT central solenoid model coil

O. Kovalchuk, E. Zapretilina, E. Bondarchuk, A. Volkov,
T. Marchenko, S. Shliykov, D. Glushaev, A. Bursikov

JSC NIIEFA (The D.V. Efremov Institute)

The article will present the intermediate results of the development, manufacture and testing of the model central solenoid coil of the HTSC tokamak TRT (tokamak with reactor technologies).

Model coils are necessary to confirm the adequacy of solutions to specific problems arising in the process of developing a superconducting EMS. The design of model coils is developed in such a way as to meet the conditions of the tasks set. As a rule, modeling during the development of large-scale EMS is carried out in stages – a short sample of conductor (1-10 m); a long sample of conductor manufactured close to the industrial technics (up to 100 m); a large-scale model coil – the closest in design and operating conditions of the conductor to the real EMS winding.

At the previous stages of the work, samples of HTSC conductors up to 3 meters long and joints corresponding to the operating conditions of the TRT and the central solenoid coil in particular were manufactured and tested. Successful test results allowed to move on to the next stage of work – development of «industrial length of conductor and model coil».

The TRT tokamak, currently being designed in the Russian Federation, is unique in a number of its characteristics. The electromagnetic system of the tokamak consists entirely of HTSC coils. Main parameters of the TRT:

Major radius (R0) m 2.15
Minor radius (a) m 0.57
Aspect ratio (R/f) – 3.77
Magnetic field on the spine (Bt0) T 8
Plasma current (Ip) MA 5
Elongation – 1.8
Triangularity – 0.3
Discharge duration s 100
Average density 102 m-3 ≤2
Additional heating power (Paux) MW ≤40
Plasma composition H, He, D
Thermonuclear power (Pfus) D MW ~0.5
Average thermal load on material surfaces facing the plasma not less than MW/m2 0.2

The central solenoid must be a self-supporting structure that includes four sections (colenoids), a power structure, a pre-compression mechanism, a centering mechanism, supports, terminals and brackets for holding the current-supplying busbar, and collectors. Central solenoid must provide a change in magnetic flux to ensure breakdown, lift, and maintenance of plasma current Ipl = 5 MA for more than 100 s. The TRT central solenoid is designed to operate in the temperature range of 4-20 K, in fields up to 20 T with a change rate of up to 12 T/s, and currents of 63 kA.

Internal Josephson effect in laboratory and space conditions

Yu.A. Kovalev

P.N. Lebedev Physical Institute of the Russian Academy of Sciences

The internal Josephson effect observed in laboratory layered superconductors with many hundreds of internal Josephson junctions can be considered as a radiating model of Josephson microstructures in a proton type-II superconductor – in the shells of Abrikosov quantum vortex filaments inside neutron stars. Coherent radio emission from a multitude of Josephson micro-junctions in these shells exits from the subcortical layer of the superconducting core into the star's magnetosphere along a strong magnetic field through cracks in the crust after "starquakes". The rotation of magnetized neutron stars explains the main properties of the observed pulsed radiation of pulsars, fast radio bursts and magnetars. Partial absorption of radiation at the core-crust boundary can lead to acceleration of protons by the Faraday mechanism and to the production of high-energy neutrinos.

The internal Josephson effect observed in laboratory layered superconductors with many hundreds of internal Josephson junctions [1] can be considered as a radiating model of Josephson microstructures [2] in a proton type-II superconductor – in the shells of Abrikosov quantum vortex filaments inside neutron stars [3]. Coherent radio emission from a multitude of Josephson micro-junctions in these shells exits from the subcortical layer of the superconducting core into the star's magnetosphere along a strong magnetic field through cracks in the crust after "starquakes" [4]. The rotation of magnetized neutron stars explains the main properties of the observed pulsed radiation of pulsars [3-5], fast radio bursts and magnetars [2]. Partial absorption of radiation at the core-crust boundary can lead to acceleration of protons by the Faraday mechanism and to the production of high-energy neutrinos [5,2]. The basic assumption: a mixture of non-superconducting electrons and neutrons with proton pairs forms an interacting mixture in the star – a "spongy" microstructure of weakly coupled Josephson micro-junctions [4-5] with electrodynamics [6] in the shells of vortex filaments, similar to junctions in laboratory conditions [7-8]. The wave function of bosons can be distorted near fermions because of the proximity effect, forming weak couplings (when the coherence length is greater or of the order of the distance between fermions in the mixture, or/and near the normal filament cores). The examples of such types of coupling see in the paragraphs 15, 20 of the book [7]; see also [8]. The role of the external current through the junctions is played by eddy currents associated with the magnetic field of the filament. The theory gives a criterion for weak coupling. Estimates for the star satisfy it with a large margin. Thus, the Josephson effect can exist inside the neutron stars – with the emission and without it, and with the coherence length in the superconductor eight orders of magnitude smaller than in laboratory conditions.

References

1. *Charikova T.B. et al*. Usp. Fiz. Nauk **194**, 377 (2024); *Kleiner R. et al*. Appl. Phys. **126**, 171101 (2019).
2. *Kovalev Yu.A*. HEA-2024 Conference, collection of abstracts, pp. 56-57, IKI RAS, Moscow (2024).
3. *Ginzburg V.L*. UFN **97**, 601 (1969) and **104**, 393 (1971); *Potekhin A.Yu*. UFN **180**, 1279 (2010).
4. *Kovalev Yu.A*. Astrophys.Space Sci. **63**, 19 (1979); **67**, 397 (1980); Pis'ma AZH **5**, 390 (1979); *Kovalev Yu.A*., in Proc.IAU 128 (ed. Hankins T.H. et al.), (Zielona Gora: Poland, 1992), p. 130.
5. *Kovalev Yu.A*. Conference VAK-2024, collection of abstracts, pp. 34-35, SAO RAS, M. (2024).
6. *Aslamazov L.G., Larkin A.I.* – Letters to JETP **9**, 150 (1969).
7. *Schmidt V.V*. Introduction to the Physics of Superconductors (M.: MCNMO, 2000).
8. *Fominov Ya.V., Shchelkachev N.M*. Josephson Effect (M.: MIPT, 2010).

Study of the dependence of electron-phonon scattering time on disorder in thin NbN films

A.I. Lomakin, E.M. Baeva, N.A. Titova,
A.V. Semenov, A.I. Kolbatova, G.N. Goltsman

National Research University Higher School of Economics, 20 Myasnitskaya St, Moscow 101000, Russia,
Moscow Pedagogical State University, 29 Malaya Pirogovskaya St, Moscow 119435, Russia,
LLC Superconducting Nanotechnology (SCONTEL), 11A Derbenevskaya Naberezhnaya, Moscow 115114, Russia

The dependence of the inelastic relaxation of nonequilibrium electrons in ultrathin NbN films on the degree of their disorder is experimentally studied by the magnetoresistance method in the temperature range from T_c to $\approx 3T_c$. It is observed that the inelastic relaxation, which is determined by electron-phonon scattering, is insensitive to changes in the disorder in the films.

Introduction

The study of the influence of disorder on electron transport in superconducting films is important for understanding the physical mechanisms that determine the superconducting and electronic properties of ultrathin films. Despite the fundamental importance, these studies also have practical applications in many modern microelectronic devices. For example, it is known that increasing disorder has a positive effect on the quantum efficiency of SSPD [1]. But the degree of disorder affects the electron transport parameters, which also matter for SSPD. For example, the scattering rate contributes to the detector dead time, thus largely determining the SSPD performance.

Thin films of niobium nitride (NbN) has been extensively used for production of modern electronic devices such as SNSPDs [2], HEB (hot electron bolometer) mixers [3], microwave nanoinductors [4], etc. It is a typical material, in which disorder can be tuned from moderate to strong limit [5].

Measurement setup

To study transport properties of NbN, we patterned films into 500-μm-wide and 1000-μm-long Hall bars. The level of disorder was varied by different heating of the film substrate during its deposition or by changing the partial pressure of nitrogen. The thickness of all films was 2.5 nm. The film square resistance R_S in the normal state was measured in a four-probe configuration. The measurements were carried out in a homemade cryogenic insert immersed in a Dewar with liquid helium ^{4}He and performed in a wide temperature range (from 300 K to 1.7 K). At low temperatures, we measured the magnetoresistance $R_S(B)$, the temperature dependences of the second critical magnetic field $B_{c2}(T)$ (to determine the diffusion coefficient), and the Hall constant (to determine the concentration of charge carriers) by applying a perpendicular magnetic field B up to 4 T. Here the critical temperature T_c is determined by us as the temperature at $R_S = R_{max}/2$ (Table 1).

Table 1

Parameters of NbN films

	s1	s2	s3	s4	s5	s6
R_S^{300}, Ohm/sq	437	509	815	912	1025	1574
$k_F l$	6.3	5.5	3.5	3.2	2.8	2.1
T_c, K	11.54	10.76	8.43	7.02	6.03	3.40
D, cm^2/s	0.59	0.57	0.36	0.35	0.34	0.27
n, $x10^{29}$ m^{-3}	1.9	1.8	1.7	1.6	1.6	1
τ_{e-ph}	8.3	7.0	20.5	21.0	20.0	30.0

Results and discussion

The dimensionless change in magnetoconductance at the fixed T was determined from the measured $R_S(B,T)$ using the following expression:

$$\delta G(B,T) = \frac{2\pi^2\hbar}{e^2}\left[R_S(B,T)^{-1} - R_S(0,T)^{-1}\right]. \quad (1)$$

Figure 1 shows typical experimental dependences $\delta G(B,T)$ for NbN samples obtained in the experiment. The change in resistance occurs due to the influence of the magnetic field on superconducting fluctuations [6] and weak localization.

The data in Figure 1 was compared with

$$\delta G(B,T) = G^{SC}(B,T) - G^{SC}(0,T). \quad (2)$$

where $G^{SC}(B,T)$ and $G^{SC}(0,T)$ are a sum of four terms of quantum corrections to conductivity at finite and zero magnetic fields: the weak localization, the Aslamazov-Larkin term, the density of states contribution term, and Maki-Thomson term[7]. The final expression for $\delta G(B,T)$ contains only one unknown parameter – the phase breaking time of the electron wave function τ_ϕ – present in the Maki-Thompson correction and weak localization. We obtain this parameter as a result of data processing.

Figure 1. Experimental dependencies of the normalized magnetoconductance $\delta G(B,T)$ for a representative sample (s5). Different colors of the curves correspond to different operating temperatures marked on the $R_S(T)$ curve in the inset. The dashed black curves represent fits by Eq. 2.

The dependence $\tau\phi(T)$ extracted from the magnetoresistance measurements is displayed in fig. 2 (a).

The exact expression for $\tau\phi^{-1}$ is represented by sum of scattering mechanisms due to superconducting fluctuations τ_{SC}^{-1}, the electron-electron (e-e) scattering rate τ_{e-e}^{-1}, the spin-flip scattering rate τ_s^{-1}, and the electron-phonon (e-ph) scattering rate τ_{e-ph}^{-1} as follows [8]:

$$\tau\phi^{-1} = \tau_{SC} i^{-1} + \tau_{e-e}^{-1} + 2\tau_s^{-1} + \tau_{e-ph}^{-1}. \quad (3)$$

It was found that a passivating Si layer over NbN films prevents the appearance of magnetic moments on the surface of the film. Calculating $\tau_{SC}i^{-1}$ and τ_{e-e}^{-1} and using the experimental values of $\tau\phi(T)$, we obtained the dependence of *e-ph* scattering time on temperature (Fig. 2(b)).

We find that the inelastic scattering rates of electrons and their temperature dependencies are close for NbN films of different microscopic quality and with different levels of disorder. The observed results are not described by existing models of e-ph scattering in disordered metals. The values of τ_{e-ph}^{-1} obtained above 10 K are proportional to T^3 expected for electron scattering by three-dimensional acoustic phonons in the pure case. At lower temperatures, changes to T^2 (not shown here), which is probably due to a decrease in the dimensionality of the phonons involved in e-ph scattering. Our results call for further theoretical andexperimental studies of the e-ph scattering in thin disordered films. The study is described in more detail in [9].

Figure 2. Temperature dependencies of (a) the electron dephasing rate $\tau\phi^{-1}$ extracted from magnetoconductance measurements and (b) the *e-ph* scattering time τ_{e-ph} extracted from $\tau\phi^{-1}$. The data are plotted in symbols on a log-log scale. In (a) the solid curves show the best fits of $\tau\phi^{-1}$ by Eq. (3).

Acknowledgments

Authors wishing to acknowledge the RSF project 23-72-00014 for the transport measurements.

References

1. *P.I. Zolotov, G.N.Goltsman, T.M. Klapwijk et al*. IEEE Trans. Appl. Supercond. **31**, 1 (2021).
2. *G.N. Gol'tsman, O. Okunev, G. Chulkova et al*. Applied Physics Letters **79**, 705 (2001).
3. *I. Tretyakov, S. Ryabchun, M. Finkel et al*. Applied Physics Letters **98**, 033507 (2011).
4. *A.J. Annunziata, D.F. Santavicca, L. Frunzio et al*. Nanotechnology **21**, 445202 (2010).
5. *S.P. Chockalingam, M. Chand, J. Jesudasan et al*. Phys. Rev. B **77**, 214503 (2008).
6. *D. Destraz, K. Ilin, M. Siegel, A. Schilling, and J. Chang*. Phys. Rev. B **95**, 224501 (2017).
7. *J.M. B. Lopes dos Santos and E. Abrahams*. Phys. Rev. B **31**, 172 (1985).
8. *A.A. Varlamov, A. Galda, and A. Glatz*. Rev. Mod. Phys. **90**, 015009 (2018).
9. *A.I. Lomakin, E.I. Baeva, A.I. Kolbatova et al*. Phys. Rev. B **107**, 054205 (2023).

Effect of vortex pinning configuration on transient processes during a microsecond current pulse

A. Maksimova, A. Moroz,
S. Pokrovskii, V. Kashurnikov

National Research Nuclear University MEPhI

The form of the response of a vortex system in a high-temperature superconductor to a current pulse of microsecond duration has been numerically calculated. The presence of a voltage peak on the superconductor at the moment of switching on the pulse in a sample with strong pinning is shown. The amplitude of the peak is several tens of times higher than the steady-state value of the voltage. The expression of the peak decreases with decreasing defect efficiency. In the case when a current pulse is applied to a specimen initially loaded with a current less than critical, the peak amplitude decreases. Calculations were performed at different values of current amplitude in the pulse and temperature.

The effect of transport current pulse on a high-temperature superconductor is of considerable practical importance. In [1-3], the pulse method was used to measure the critical current of a superconductor. The necessity of the pulse method appears, for example, in high magnetic fields, when heating of the sample during current flow makes it impossible to obtain the volt-ampere characteristic. The study of the pulse effect on the superconductor is also important in the design of current limiters [4,5]. The pulsed current effect on the superconductor was also studied in [6-9]. In [6], the current amplitude in the pulse was 10-30 times higher than the typical value (normal operating current) of the sample, at temperatures of 60 and 80 K. The current value used resulted in degradation of the sample, however, it was shown that the degradation depends on the peak temperature of the sample rather than on the initial current value at a pulse duration of 1 s. The maximum peak temperature at which degradation is not yet observed was shown to be 400-600 K.

Transport characteristics of a superconductor, such as the magnitude of the critical current and the shape of the current-voltage characteristic, depend on the interaction of the vortex system in the sample with pinning centres. In the experiment, burnout of the sample often occurs when the supercritical current flows. Therefore, the application of numerical modelling preceding the experiment is preferred. The aim of our work is to model the response of a vortex system to a current pulse, revealing the features of the response under varying defect efficiencies and at different temperatures. We also analyze the influence of the current flowing through the sample before the pulse is applied.

The calculations were performed by the Monte Carlo method in the framework of the two-dimensional model of a layered high-temperature superconductor (see [10,11]). Yttrium-based cuprates, the most used in practice, are layered anisotropic substances; the vortex filament in such a superconductor can be represented as a stack of two-dimensional

planar vortices – pancakes. Pancakes in planes are connected by inter-plane coupling, and in general case the vortex is a three-dimensional system. However, at low anisotropy $(\gamma \sim 10)$, the average deviations of the pancakes from the filament axis are small and a two-dimensional model of the vortex system can be used in calculations. The total energy of the vortices is composed of the intrinsic energy per unit length, pairwise interaction energy, interaction with Meissner and transport currents, reflection from the boundary and pinning centres. The rectangular shape of the current pulse is assumed in the calculation, with a leading edge duration of 2 μs and a pulse duration of 100 μs. A Monte Carlo step equivalent of $\sim 10^{-8}$ s, estimated by us from comparison with experimental current-voltage characteristics, was used.

The response to the current pulse is calculated as a time dependence (in Monte Carlo steps) of the electric field strength in the sample. Under the action of the overcritical transport current, vortices are depinned and move under the Lorentz force to the centre of the sample, where annihilation of vortices of opposite sign takes place. The electric field strength is calculated as $E=vB/c$, where v is the velocity of the viscous flow of vortices and B is the magnetic field in the superconductor. At typical current densities of $3 \cdot 10^6$ A/cm^2 the vortex velocities are a few tens of cm/s. A sample containing 1600 pinning centres (the size of the simulated region is $6 \cdot 6 \mu$m) was considered. The defect is characterized by its effective depth of the potential well α.

In the Monte Carlo calculation, it is more convenient to use not the current density, but the value of the magnetic field HI generated by the current at the sample boundaries. The value H_I=1200 Gs adopted in the calculation corresponds to a current slightly exceeding the critical current at α=1 eV. The response of the vortex system to a rectangular pulse of supercritical current (at α=0.5 eV and α=0) is also rectangular, but has a longer leading edge. The calculated response shapes are shown in the figure. The response of the sample at α=1 eV has a pronounced peak at the moment when the pulse is switched on, later the intensity decreases to the threshold value of 1 μV/cm. The origin of this peak is related to the motion of vortices: at the moment of current switching on, the vortices enter the sample and move freely to the centre of the sample. At subsequent moments of time, the vortices are gradually fixed on the defects and prevent further free flow of the vortex lattice.

More realistic is the case when the current less than critical I_0 is already flowing in the sample before the pulse action. In our calculation we assume $I_0 = 0.42 I_c$. The presence of current before the action of the pulse at strong pinning reduces the magnitude of the pinch and does not affect the shape of the pulse at weaker pinning.

The calculation results will be useful in the design of superconducting keys, where it is necessary to estimate the configuration of pinning centres required to achieve the given properties.

This work was supported by the Ministry of Science and Higher Education of the Russian Federation within the State Assignment (project FSWU-2025-0008).

Joint influence of different types of artificial defects on the critical current of HTS tape

A. Maksimova, A. Moroz,
S. Pokrovskii, V. Kashurnikov

National Research Nuclear University MEPhI, 115409 Kashirskoe shosse, 31, Moscow, Russia

The dependences of the critical current of the sample on the magnetic field have been calculated by the Monte Carlo method in the framework of a two-dimensional model of a layered high-temperature superconductor (HTS). Two types of defects of different concentration were taken into account in the calculation. It is shown that the contribution to the critical current from two types of pinning centres is not additive. This property is fulfilled at all considered temperature values. In the presence of a regular (rectangular) lattice of pinning centres, the additivity of the critical current is also not fulfilled.

At magnetic fields and currents used in practice, the superconductor passes into a mixed state, and its magnetic and transport properties are determined by the motion of Abrikosov vortices and their interaction with pinning centres. The task of optimization of pinning centres is still topical; many works are devoted to this question. In [1], the influence of the electron free path length in $YBa_2Cu_3O_{6+x}$ on the critical current was investigated. In [2], the enhancement of the critical current of $YBa_2Cu_3O_{6+x}$ by the addition of nanoscale Dy_2O_3 particles was investigated. The pinning efficiency depends not only on the efficiency of vortex pinning, but also on the mutual arrangement of defects.

In [3], the possibility of pinning enhancement at the same defect concentration is shown for conformal mapping applied to a square lattice. The study was carried out by the molecular dynamics method. When a superconductor is irradiated with high energy ions, columnar defects appear [4, 5]. The radius of such defect is usually a few nanometres, which is close to the coherence length of the superconductor, and this accounts for the pinning efficiency. In [4], the optimal fluence of irradiation of $YBa_2Cu_3O_{6+x}$ with Bi ions was determined. In [5], the angular dependences of the critical current on the magnetic field during the irradiation of ReBCO with Ag ions were investigated. However, new defects often appear in the superconductor during the operation of the HTS tape; this is relevant, for example, for magnets at accelerators. Therefore, it is necessary to investigate the question of the ratio of the critical current before and after a new irradiation pulse. The aim of our work is to obtain the dependences of the critical current on the magnetic field in the presence of two types of defects, to check the additivity of the critical current due to each group of defects.

The calculations were performed by the Monte Carlo method in the framework of a two-dimensional model of a layered high-temperature superconductor. For a detailed description of the model see [6-8]. The energy of interaction of a vortex with a defect is chosen as follows

$$U_{\pm} = -\alpha \frac{1}{1 + r_{ij}/\xi} e^{r_{ij}/2\xi},$$

where α – effective depth of defect potential well, ξ – coherence length of superconductor and r_{ij} – distance between i-th defect and j-th vortex. Two types of defects were introduced into the model: first with effective radius x_i and depth $\alpha = 1$ eV (strong pinning), second with radius $3x_i$ and depth $\alpha = 0.4$ eV (weak pinning). Concentration of defects was chosen $\sim 10^9$ cm^{-2}.

The figure shows the calculated dependences of the critical current on the magnetic field at T=4.2 K. The calculations were performed at magnetic field values up to 2000 Gs. The obtained dependences are decreasing, one can only note a small peak near zero field for weak pinning. The figure shows the curves corresponding to each defect type separately and the dependence in the presence of two defect types at once. It can be seen that the type 1 and 2 curve does not correspond to the sum of the type 1 and type 2 curves. However, we can expect that additivity will be fulfilled if we subtract from the critical current of the defective sample the critical current of the sample without defects (near the zero magnetic field, the critical current is not equal to 0, since there is a field of superheating of the Meissner state, and vortices enter the sample only when the current reaches a certain value). The dependences of jc(type 1 and 2) and jc(type 1)+jc(type 2) do not coincide, as the calculation shows. This result is also obtained for other defect concentrations as well as for their regular distribution (rectangular lattice). Thus, the additivity of the critical current, at least for the investigated configurations, is not fulfilled.

In the future, it is planned to extend the range of magnetic fields taken into account in the calculation to 2 Tesla. These calculations will be useful in assessing the influence of radiation defects on the critical current in superconducting magnets used in accelerators.

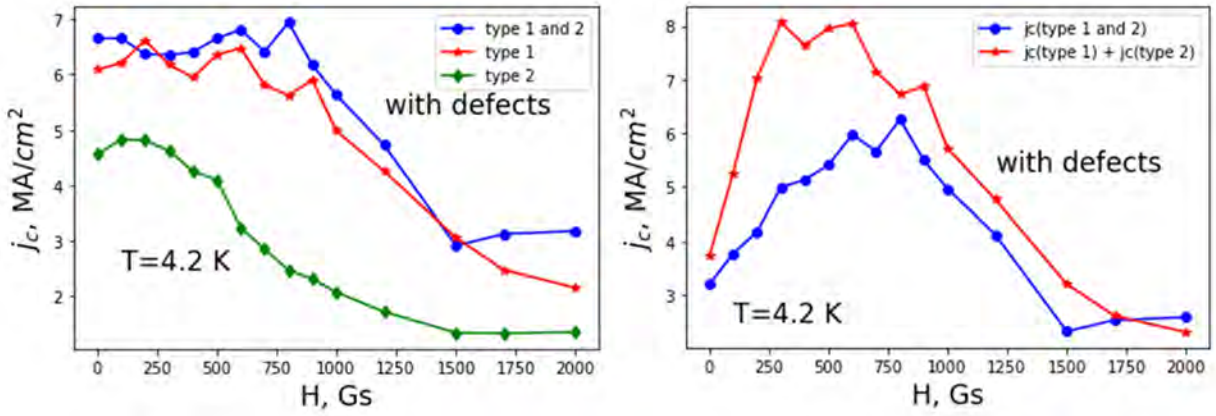

Fig. 1. *Jc*(*H*) curves at *T*=4.2 K. Defects are randomly distributed.

The work was funded by the Ministry of Science and Higher Education of the Russian Federation, Project “Fundamental and applied research at the NICA (JINR) megascience experimental complex”” FSWU-2025-0014.

References

1. *Paturi P., Huhtinen H.* Supercond. Sci. Technol. **35**(065007), 10.1088 (2022).
2. *Algarni R. et al*. Journal of Alloys and Compounds **852**, 157019 (2021).
3. *Zoveydavi S. et al*. Physica C: Superconductivity and its Applications **620**, 1354498 (2024).
4. *Liu L. et al.* Physica C: Superconductivity and its Applications **592**, 1354000 (2022).
5. *Strickland N.M. et al.* Superconductor Science and Technology **36**(5), 055001 (2023).
6. *Maksimova A.N. et al*. Chinese Journal of Physics, 2025.
7. *Moroz A.N. et al*. Journal of Physics: Condensed Matter. **33**(14), 145902 (2021).
8. *Moroz A.N. et al*. Journal of Physics: Condensed Matter. **33**(35), 355901 (2021).

Comprehensive analysis of normal zone propagation in multi-tape superconducting cables for magnetic energy storage

I.V. Martirosian, D.A. Alexandrov, A.Y. Malyavina,
D.A. Abin, S.V. Pokrovskii

National Research Nuclear University MEPhI (Moscow Engineering Physics Institute)

This study aims to characterize NZP behavior in multi-tape superconducting cables, focusing on the influence of geometrical configuration, thermal coupling, and current-sharing mechanisms. This study presents the results of the analysis of the NZP processes in multilayer HTS cables for several geometric configurations: CORC cable, twisted stack of tapes, Rebel cable. The study of electrodynamic and thermal processes in cables was performed in a wide range of operating temperatures. The investigation seeks to provide a detailed analysis of how different design parameters affect the propagation of normal zones and the overall stability of the cable.

The performance and reliability of superconducting cables are critical for their application in high-field magnets, fusion energy devices and magnetic energy storage [1]. These cables serve as the backbone of technologies that require extreme operational conditions, such as magnetic confinement fusion reactors, particle accelerators, and high-capacity electrical grids. The practical implementation of these systems is contingent upon the robustness of superconducting cables under varying operating conditions. Even minor deviations in cable performance can lead to catastrophic failures, making it imperative to address the underlying mechanisms that govern their behavior.

A key challenge in these systems is understanding and controlling normal zone propagation (NZP) [2]. NZP refers to the transition of a superconducting material from its zero-resistance state to a resistive state due to localized heating or external disturbances. This phenomenon poses significant risks to the stability and safety of superconducting systems, as it can trigger a cascade of thermal and electrical instabilities known as a “quench.” A quench occurs when the heat generated in the resistive zone spreads uncontrollably, potentially damaging the entire system. Therefore, gaining a comprehensive understanding of NZP dynamics is crucial for ensuring the reliable operation of superconducting cables in demanding applications.

This study aims to characterize NZP behavior in multi-tape superconducting cables, focusing on the influence of geometrical configuration, thermal coupling, and current-sharing mechanisms. This study presents the results of the analysis of the NZP processes in multilayer HTS cables for several geometric configurations: CORC cable, twisted stack of tapes, Rebel cable. The study of electrodynamic and thermal processes in cables was performed in a wide range of operating temperatures. The investigation seeks to provide a detailed analysis of how different design parameters affect the propagation of normal zones and the overall stability of the cable. Multi-tape configurations are of particular interest because they offer higher current-

carrying capacities compared to single-tape systems, but they also introduce additional complexities in terms of thermal and electrical interactions. By systematically examining the interplay between tape arrangement, thermal properties, and current distribution, this research aims to identify strategies for enhancing the resilience of superconducting cables against quenches. The results indicate that enhanced transverse heat transfer reduces the risk of quenching. By improving the lateral conduction of heat between tapes and their surroundings, the system can more effectively dissipate localized hotspots before they escalate into full-blown quenches. When multiple tapes share the transport current, the load can be redistributed in response to localized heating, reducing the likelihood of a runaway quench. However, this redistribution can also create uneven heat dissipation profiles, which may necessitate careful design considerations to ensure uniform thermal management. In summary, this research provides a comprehensive analysis of NZP behavior in multi-tape superconducting cables, highlighting the critical role of geometrical configuration, thermal coupling, and current-sharing mechanisms. The findings demonstrate that the arrangement of tapes, material properties, and cooling conditions significantly influence NZP dynamics and quench resilience.

The work was carried out under the State Assignment (project FSWU-2025-0008) with the support of the Ministry of Science and Higher Education of the Russian Federation.

References

1. *H. Maeda, Y. Yanagisawa*, IEEE Trans. Appl. Supercond. **24**(3), 1 (2014).
2. *M. Marchevsky*, Instruments **5**(3), 27 (2021).

A trapped field in a rings stack of high temperature superconducting tape

A. Mashirov, K. Kolesov, A. Petrov,
D. Suslov, A. Orlov, A. Kamantsev, V. Koledov

Kotelnikov Institute of Radioengineering and Electronics of Russian Academy of Sciences, Laboratory of magnetic phenomena, Moscow, Russian Federation

This work presents the results of a study of the process of capturing and holding magnetic fields in a super permanent magnets based on high-temperature superconducting tapes.

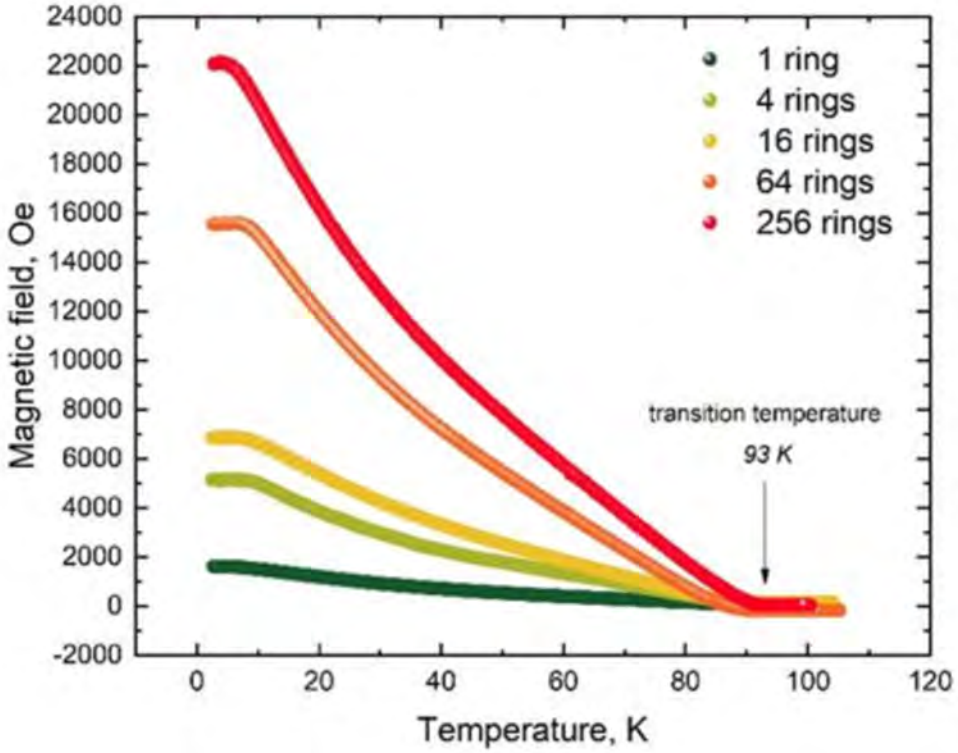

High-temperature superconductors the Y-Ba-Cu-O families in the form of bulk ceramics and tapes of film composites have the necessary properties to create super permanent magnets that capture and maintain a constant magnetic field for a long time at temperatures of 90 K and below [1]. This paper presents the results of a comparative study of the process of capturing and retaining magnetic fields in the super permanent magnets of high-temperature superconductors tape elements of two configurations: in the gap between two stacks of tape segments and in a cylindrical hole in a stack of tape segments. The experiments were carried out at temperatures from 3 to 90 K, in a magnetic field up to 10 T. We experimental consider trapped field stacks of rings of high-temperature superconductors tapes. The results of the study of the process of capture and retention of magnetic fields in a ring stacks are presented, including the dependence of the magnetic field in the center of the trapped field stacks on the temperature after cooling of the trapped field stacks in an external

magnetic field, followed by switching off the external field source. The stability of the magnetic field in the trapped field stacks at a constant temperature is also considered. The experiments were carried out at temperatures from 3 to 100 K, in a magnetic field of up to 6.4 T. The maximum trapped magnetic field of a 256 rings stack is 2.2 T at temperature 10 K and 0.22 T at 77 K (figure). The possibility of using super permanent magnets in promising solid-state cooling systems based on the magnetocaloric effect is discussed.

The study was supported by the Russian Science Foundation grant No. 25-19-00942, https://rscf.ru/project/ 25-19-00942/.

References

1. *Wang, Qi, et al*. Superconductor Science and Technology **37**(12), 123005 (2024).

Study of critical current of industrial 2G HTS-wire with different stoichiometry of Gd-based composition in strong magnetic fields

B.I. Massalimov, A.R. Prishchepa, A.V. Sadakov, P.N. Degtyarenko

Ginzburg Center for High-Temperature Superconductivity and Quantum Materials,
P.N. Lebedev Physical Institute of the Russian Academy of Sciences (LPI RAS), LLC S-Innovations

This work is devoted to a systematic study of 2nd generation GdBCO-based HTS wires with different yttrium stoichiometry. All wires were grown by pulsed laser deposition (PLD) and characterized by transport measurements over a wide range of temperatures and magnetic fields.

This work is devoted to a systematic study of 2nd generation GdBCO-based HTS wires with different yttrium stoichiometry. All wires were grown by pulsed laser deposition (PLD) and characterized by transport measurements over a wide range of temperatures and magnetic fields. The samples were fabricated on commercial production equipment of S-Innovations LLC and contained different concentrations of yttrium +0%Gd, +15%Gd, +30%Gd. The investigated 12 mm wide tape sample was modified using laser cutting and focused ion beam (FIB) to form a microbridge with dimensions on the order of 3 μm by 100 μm. The critical current densities were measured by volt-ampere characteristics using the four-pin method in fields from 0 to 16 T at temperatures of 65 K and 77 K. The obtained research results will be used in the design of various kinds of superconducting research and industrial equipment in different fields of power engineering, medicine and science.

Microscopic Parameters of Superconducting MoRe Ultra-Thin Films for Single-Photon Detection

I.N. Pavlov, S.S. Svyatodukh, A.I. Lomakin, N.A. Titova,
K.I. Khilay, E.M. Baeva, M.D. Soldatenkova, S.A. Evlashin,
A.I. Kolbatova, G.N. Goltsman

MPSU, Malaya Pirogovskaya st. 1/1, Moscow 119435, Russia,
HSE MIEM, Tallinskaya st. 34, Moscow 123592, Russia,
SCONTEL, Derbenevskaya nab. 11 bld.A, Moscow 115114, Russia,
Skoltech, Bolshoy Blvd. 30 bld.1, Skolkovo 143026, Russia

Here, we report on the fabrication and characterizaton of ultrathin MoRe films for superconducting nanowire single-photon detectors (SNSPDs). MoRe films were deposited onto sapphire substrate at room temperature using DC magnetron sputtering. We studied 1.8 nm and 4.3 nm thick films with sheet resistances of 350 and 660 $\Omega/\square$ and critical temperatures of 5.9 K and 4.6 K, respectively. The inelastic scattering rate was investigated using magnetoconductance, showing a temperature dependence of $\tau_{e-ph}^{-1} \propto T^3$ with values from 40 to 10 ps at 8-15 K. These findings suggest ultrathin MoRe films could be a viable alternative to NbN in low-temperature applications.

In recent years, superconducting nanowire single-photon detectors (SNSPDs) have been successfully applied in a variety of fields, including quantum information technology and space-to-ground communication systems [1]. The growing demand for these devices with enhanced performance has stimulated research activity in material science [2, 3]. One area of this research focuses on improving the properties of superconducting materials used in the fabrication of SNSPDs, while another area seeks to find alternative materials that could enhance the performance of existing devices. When exploring new materials for use in SNSPDs, several important factors need to be considered. These include the inelastic electron-phonon scattering rate, phonon escape rate, ratio between electron and phonon heat capacities, density of electronic states, and diffusivity, all of which affect the transfer of energy from electromagnetic radiation to electrons and subsequently to the surrounding environment [4]. The growing interest in thin molybdenum rhenium (MoRe) films has emerged among researchers working on sensitive single-photon detectors [5, 6]. These materials exhibit excellent superconducting properties and stable chemical, electrical and mechanical characteristics [5]. In this study, we focus on the fabrication and investigation of few-nanometers-thick superconducting MoRe films on sapphire substrates.

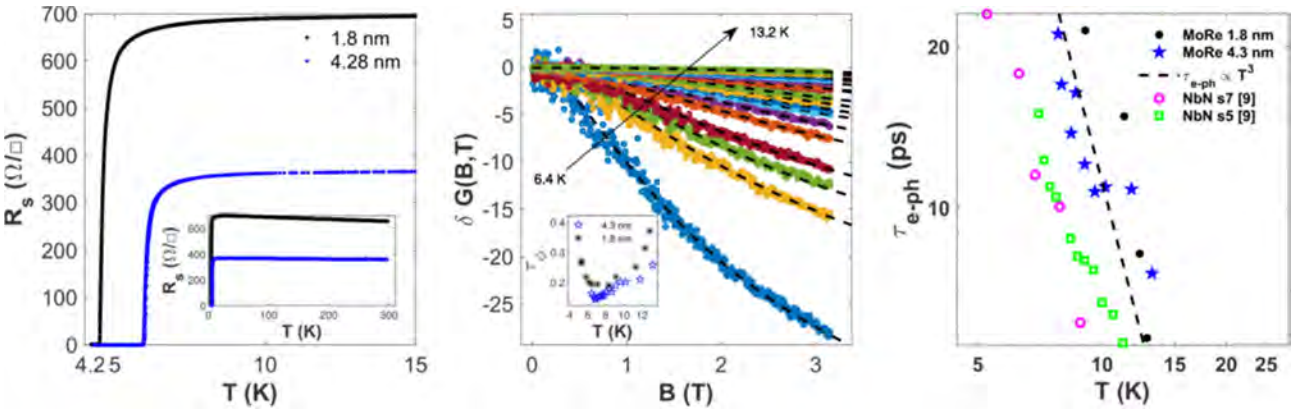

Figure 1. (a) Temperature dependence of resistance for the investigated samples; (b) Magnetic field dependence of conductivity for the 4.3 nm MoRe film on an Al_2O_3 substrate, with τ_ϕ as a fitting parameter (the inset shows the dependence of the electron wave function phase coherence time on temperature); (c) Temperature dependence of electron-phonon relaxation time for MoRe films on an Al_2O_3 substrate, compared with that of NbN [9].

These films were grown by DC magnetron sputtering at room temperature from a composite target containing 40% Mo and 60% Re. We studied two film thicknesses, 1.8 nm and 4.3 nm. For these films, the sheet resistance at room temperature was 350 and 660 $\Omega/\square$, and the critical temperature values were 5.9 and 4.6 K, as shown in Figure 1 – in the temperature dependencies of resistance for these films. Using standard transport measurements at low temperatures, we determined electron coherence length, the carrier density and diffusion coefficient in the normal state, corresponding to the following values: 4.5 and 4.4 nm, $3*10^{23}$ and $2.8*10^{23}$ cm^{-3}, 0.4 and 0.3 cm^2/s, respectively. The level of disorder in the films is characterized by the Ioffe-Regel parameter, which is 3.8 and 5.0, respectively.

We also investigate the inelastic scattering rate in MoRe films using the magnetoconductance method. This method allows to determine the phase-breaking rate of the electron wave function, which is usually the sum of inelastic scattering rates in thin metal films. These rates include the electron-phonon, electron-electron, and electron-fluctuation scattering rates [7]. Figure 1b shows the experimental magnetoconductance data for a 4.2-nm-thick MoRe sample at different bath temperatures. By analyzing the data with quantum corrections to conductivity, we extract the phase-breaking rates (inset in Figure 2a) and estimate the electron-phonon scattering time (Figure 1c) for the studied MoRe films. The rates for both samples show a temperature dependence that is close to a power law $\tau_{e-ph}^{-1} \propto T^3$ and with values in the range 40 to 10 ps in the temperature range of 8 to 13 K, correspondingly. These results are consistent with previous measurements of τ_{e-ph} in thin NbN films, which were 20 to 5 ps in a similar temperature range [8, 9]. This work demonstrates some of the unique properties of ultra-thin MoRe that may make it a viable alternative to more commonly used materials such as NbN for low-temperature applications.

The work was supported by the Russian Science Foundation grant No. 24-72-10105.

References

1. *You L.* Nanophotonics **9**, 2673–92.2 (2020).
2. *Esmaeil Zadeh I., Chang J., Los J.W.N., Gyger S., Elshaari A.W., Steinhauer S., Dorenbos S.N. and Zwiller V*. Appl. Phys. Lett. **118**, 190502 (2021).
3. *Shibata H.* IEICE Trans. Electron. E **104-C**, 429–34 (2021).
4. *Vodolazov D.Y.* Phys. Rev. Applied **7**, 034014 (2017).
5. *Zhukova E. et al*. Mesoscience & Nanotechnology **1**, 01002 (2023).
6. *Seleznev V.A., Tarkhov M.A., Voronov B.M., Milostnaya I.I., Lyakhno V.Y., Garbuz A.S., Mikhailov M.Y., Zhigalina O.M., Gol'tsman G.N*. Supercond. Sci. Technol. **21**, 115006 (2008).
7. *Lin J.J., Bird J.P.* J. Phys.: Condens. Matter **14**, R501–R596 (2002).
8. *Sidorova M., Semenov A., H¨ubers H.-W., Ilin K., Siegel M., Charaev I., Moshkova M., Kaurova N., Goltsman G.N., Zhang X., Schilling A*. Phys. Rev. B **102**, 054501 (2020).
9. *Lomakin A.I. et al*. Phys. Rev. B **107**, 054205 (2023).

Influence of cooling conditions and the field cooling gap on bearings functional characteristics based on the HTS tapes

S. Pokrovskii, I. Martirosian, M. Osipov,
A. Starikovskii, D. Aleksandrov, P. Erykov

National Research Nuclear University

In this work we present a combined experimental and numerical study of high-temperature superconducting bearing as the support element for a wide range devices consisting of HTS and permanent magnet parts. As the results of this study, dependencies of vertical and lateral levitation forces on the magnitude of levitation gap at different initial field cooling heights of the HTS block were obtained (for 77.4 K in the experimental part and in a wide temperature interval in the numerical part).It was found the existence of the optimal field cooling conditions (temperature and the gap) to obtain high characteristics. The initial levitation height (maximum levitation gap magnitude) spans from 5 mm to 100 mm in both numerical and experimental part of this study.

Contactless magnetic suspensions or bearings can be divided into two major groups: systems based on permanent magnets and conventional materials and systems based on superconductors [1]. The main difference between traditional contactless magnetic systems is, first of all, that in such systems it is necessary to organize feedback loop to maintain the levitation gap within specified boundaries, which in turn entails the necessity to organize somewhat complicated active control of the magnetic system. Unlike traditional magnetic suspensions and bearings, superconducting systems are stable because of the unique properties of superconducting material to capture the external magnetic flux and «memorize» its configuration [2]. Thus, a superconducting levitation system does not require stability maintenance feedback loop. It is possible to organize a superconductor-based levitation suspension or bearing using high-temperature superconductors (HTS) based on REBCO (where RE is a rare-earth element). Tape superconductors can be effectively used as an alternative to bulk materials in levitation applications, with composite tapes leading to improved device (particularly bearing) efficiency, simplified manufacturing processes, enabling more complex and optimized geometries of system components, showing higher mechanical strength, improved thermal performance, higher availability and therefore potential monetary cost reductions [3].

In this work we present a combined experimental and numerical study of support high-temperature superconducting bearing. The bearing consists of two main parts: HTS block and permanent magnet (PM) block. For the HTS part we used the «S-Innovations» 12 mm REBCO tape assemblies. NdFeB permanent magnets were used for the PM block. The numerical model is based on finite elements method. To calculate magnetic and force characteristics of HTS bearing we employed the H-

formulation of Maxwell's equations. The calculations were performed for several PM configurations in a wide temperature interval. The numerical model was verified by the experimental data. The field cooling initial levitation height (maximum levitation gap magnitude) spans from 5 mm to 100 mm in both numerical and experimental part of this study. In the experimental part, measurements of levitation forces were carried out at the boiling temperature of liquid nitrogen (77.4 K).

As the results of this study, dependencies of vertical and lateral levitation forces on the magnitude of levitation gap at different initial field cooling heights of the HTS block were obtained. Additionally, analogous results were obtained for zero-field cooling mode. At the boiling point of liquid nitrogen, numerical and experimental data are in good agreement with each other for both vertical and lateral levitation forces. Moreover, the effect of temperature on the levitation force dependencies was numerically investigated.

The study was funded by the Russian Science Foundation grant No. 23-19-00394, https://rscf.ru/project/23-19-00394/.

References

1. *Arani, A.K., Karami, H., Gharehpetian, G.B., & Hejazi, M.S.A*. Renewable and Sustainable Energy Reviews, **69**, 9-18 (2017).
2. *Supreeth, D.K., Bekinal, S.I., Chandranna, S.R., & Doddamani, M.* IEEE Transactions on Applied Superconductivity, **32**(3), 1-15 (2022).
3. *Osipov, M., Abin, D., Pokrovskii, S., & Rudnev, I.* IEEE Transactions on Applied Superconductivity, **26**(4), 1-1 (2016).

Strain Assessment in YBCO Layer of Industrial 2G HTS Wires

M.O. Rikel[1], V.A. Amelichev[1], A.V. Markelov[1], P.N. Degtyarenko[1], A.A. Kamenev[1], A.L. Vasiliev[1,2]

[1] S-Innovations LLC, Moscow, Russia,
[2] Shubnikov Institute of Crystallography, Russian Academy of Sciences, Moscow, Russia

We report on the progress in quantifying the strain state in YBCO layer of 2G HTS wires produced at S-Innovations for low-temperature magnet applications. The focus is on developing the methodology of XRD measurements for determination of out-of-plane and in-plane lattice parameters of Y123 phase and distinguishing the contributions from strain and oxygen nonstoichiometry. The limitations in accuracy due to uncertainties in accounting for noticeable bulk compressive strain and strain gradients are analyzed. Correlations between the strain state and nanostructure morphology revealed by TEM and mechanisms by which the strain state of Y123 affects wire performance are discussed.

Controlling the strain state is important for performance optimization in industrial 2G HTS wires. The strain in YBCO layer depends on wire architecture (difference in thermal expansion coefficients of constituent layers) and nanostructure (lattice mismatch between Y123 matrix and nanoparticles) and may affect the fundamental properties of Y123 (Tc, Bc2, …) and, thus, the pinning energy, as well as the nanostructure (twinning in Y123 matrix due to Tetra => Ortho transformation during oxidation is very sensitive to the strain state).

In this contribution, we report on the progress in quantifying the strain state in YBCO layer of 2G HTS wires produced at S-Innovations for low-temperature magnet applications. The focus is on developing the methodology of XRD measurements for determination of out-of-plane (c) and in-plane (a, b) lattice parameters of Y123 phase and distinguishing the contributions from strain and oxygen nonstoichiometry. The accuracy of the developed method is currently limited by the uncertainties in accounting for (1) a noticeable bulk compressive strain that likely originates from the presence of small Y2O3 nanoparticles fully coherent to the Y123 matrix and (2) strain gradients in the Y123 matrix that may cause a difference in orthorhombicity, $2(b–a)/(b + a)$, values assessed from different (HKL, KHL) doublets.

We also analyze correlations between the changes in the strain state and nanostructure morphology revealed by TEM. Mechanisms by which the strain fields in Y123 matrix may affect wire performance are discussed.

550 GHz mixer prototype

K. Rudakov[1,2], G. Nazarov[1,2], Ya. Vodzyanovsky[1],
A. Khudchenko[1], I. Tretyakov[2], L. Filippenko[1],
A. Chekushkin[2], V. Koshelets[2]

[1] ASC LPI,
[2] IRE RAS

Receivers based on the superconductor-insulator-superconductor (SIS) tunnel junction are one of the most sensitive heterodyne systems for detecting submm and mm-band waves. In this work, we present numerical simulation results and preliminary SIS mixers design at 550 GHz. The mixer includes RF probe, filters, tuning structure, contact pads on a single quartz substrate. The developed designs sensitivity to major technological deviations in dimensions and parameters is evaluated. The prototype receiving element under development has the potential to be used in future on the astronomy observatory.

The study of water transport origin in the universe is an important goal for astronomy [1]. The frequency band 500-600 GHz includes the information about water vapor's spectral lines in the Universe and considered for astronomy observations [e.g. 2-4]. We are working on the DSB (double side band) receiver based on the SIS (superconductor isolater superconductor) junction. We have evaluated the DSB mixer designs for the 505-600 GHz frequency range. The mixer microstructure is incorporated into an RF waveguide block connected to the input feed horn and to magnet field support systems.

These microstructure designs were developed using numerical calculations provided by a 3d modeler program with including the superconducting material properties. We used a waveguide probe placed orthogonally to the waveguide. We have found an optimal waveguide and fused quartz substrate dimensions: 60 μm thick, 210×420 μm cross-section respectively. The designed mixers include the SIS junctions with approximately 0.5 μm^2 area and normal resistance of Rn ~ 20 Ohm. The SIS (Nb/AlOx/NbN) junctions is embedded into 200 nm Nb wiring and separated by a 250 nm SiO_2 layer. The current density of the SIS bath thrilayer is about 21 kA/cm^2 and the estimated quality factor R_j/R_n should be about 18, where R_j is a sub-gap resistance, R_n is a normal state resistance.

Optimal coupling between the waveguide and the SIS junction is achieved by using a probe with the impedance close to 4 – 18i Oms, a microstrip line transformers and tuners. These SIS junctions are small and very thin structures that leds to significant junction's capacitance which should be untuned. These lines between the probe and the SIS junction act as a microstrip line impedance transformers and tuners for the SIS junction. Using 0.5 μm^2 area SIS junctions allows to achieve a good matching between the waveguide input and the junctions using only microstrip structures. In addition, the small SIS junction can leds for sower IF band degradation. Now we are working on fabrication the designs and the assembly.

References

1. *V. Tretyakov et al*., IEEE TST, **15**(2), march 2025.
2. *S. Kardashev et al*., Physics Uspekhi **57**(12), 1199-1228 (2014).
3. *D. Novikov et al*., Physics Uspekhi **64**(4), 386–419 (2021).
4. *F. Likhahev and T.I. Larchenkova*, Physics Uspekhi, accepted for publication. DOI: 10.3367/UFNe.2024.03.039662.

Superconducting magnets for synchrotron radiation source, developed at the BINP

A. Sedov

BINP

Review of superconducting magnets produced at ISF SB RAS. This paper presents superconducting wigglers, shifters, and quadrupole lenses developed for new SR sources such as SKIF, KCSRN 2, and SCFT.

Superconductivity has become one of the most influential accelerator technologies in the last 30 years, and superconducting magnets have become the indispensable choice for large colliders, as well as cyclotrons and synchrotrons. Accelerator magnets vary depending on the type of accelerator and the required tasks for which they are intended.

The Budker Institute of Nuclear Physics is one of the leaders in the production of superconducting insertion devices for SR generation, such as wigglers and undulators [1]. Insertion devices developed at the INP have been installed in many storage rings around the world. Currently, the INP is developing insertion devices for the new synchrotron center Siberian Ring Photon Source (SKIF) and for the Kurchatov Synchrotron Radiation Source (KISI).

It is planned that SKIF will operate at an energy of 3 GeV and with a horizontal natural emittance of 75 pm · rad, generating synchrotron radiation with a maximum brightness in the range from 100 eV to 100 keV for 30 different experimental stations [2]. Of the 30 planned stations, 6 stations will be put into operation first, including station 1-3 “Fast processes” and station 1-5 “Diagnostics in the high-energy X-ray range”, which will use superconducting wigglers as a radiation source.

As a result of the work done, a 144-pole superconducting wiggler with a period of 27 mm and a magnetic field level of 2.7 T and a 36-pole superconducting wiggler with a period of 48 mm and a magnetic field level of 4.5 T were assembled and tested.

Also, work has begun at INP on creating insertion devices for the upgraded KCSRN 2 source. As a result of the KCSRN upgrade, a third-generation synchrotron with a power of 2.5 GeV will be created, capable of operating in the “infinite” beam lifetime mode. In addition to the existing insertion devices, it is planned to install a 5-pole shifter, an undulator with a period of 18 mm and a field of 1.4 T, and a spiral undulator [3].

The development of final focus magnets for the Super Charm-Tau Factory (SCTF) accelerator complex is also underway. To test the crab-waist technology, it is planned to create an experimental setup for the beam collision point at VEPP-4M with a FF system similar to the system planned for SCTF. The beams are supposed to

be focused at the collision point using superconducting quadrupole lenses, which will be placed inside the detector solenoid [4].

References

1. *V.A. Shkaruba, A.V. Bragin, A.A. Volkov, A.I. Erokhin, A.V. Zorin, V.Kh. Lev, N.A. Mezentsev, A.N. Safronov, V.M. Syrovatin, O.A. Tarasenko, S.V. Khrushchev, V.M. Tsukanov*, Physics of Particles and Nuclei Letters, **17**(4), 542–547 (2020).
2. *E.B. Levichev, A.N. Zhuravlev, K.V. Zolotarev, Ya.V. Zubavichus, K.I. Shefer*, Project for the creation of a 4+ generation synchrotron source at the SKIF Center for Collective Use in Koltsovo, Novosibirsk Region: general information and implementation status: Electronic collection of articles. Novosibirsk. – 2022. – Volume 1. – P. 5–12.
3. *N. Barbashina, I. Astapov, M. Delov, D. Moshkova, A. Vasiliev*, New challenges and approaches in training personnel for research projects of the “MegaScience” class. Journal of Physics: Conference Series, pp. 3-5.
4. *A. Bogomyagkov, E. Levichev and S. Sinyatkin*, J. Instrum. **19**, P02017 (2024).

High-Q superconducting terahertz Fabry-Pérot resonator

A.V. Terentiev

Moscow Institute of Physics and Technology, Dolgoprudny, Russia

We fabricate high-Q monolithic THz Fabry-Pérot resonators by depositing SC $Mo_{0.6}Re_{0.4}$ films (T_c=7−8 K) on plane-parallel slabs of high-resistivity silicon. Transmission coefficient of the resonators is measured at frequencies ν=3–50 cm−1 and at temperatures T=2.5–300 K. In the SC state, the interferometric peaks exhibit a dramatic increase in quality factor Q and a reduction in FWHM Δν. Record values are obtained at T = 2.5 K: Q=830 (peak at ≈6 cm−1), Δν=0.005 cm−1 (peak at ≈3 cm−1). The resonator is compact, portable, and mechanically robust which makes it promising for applications with stringent weight and size constraints, such as astronomy and atmospheric science.

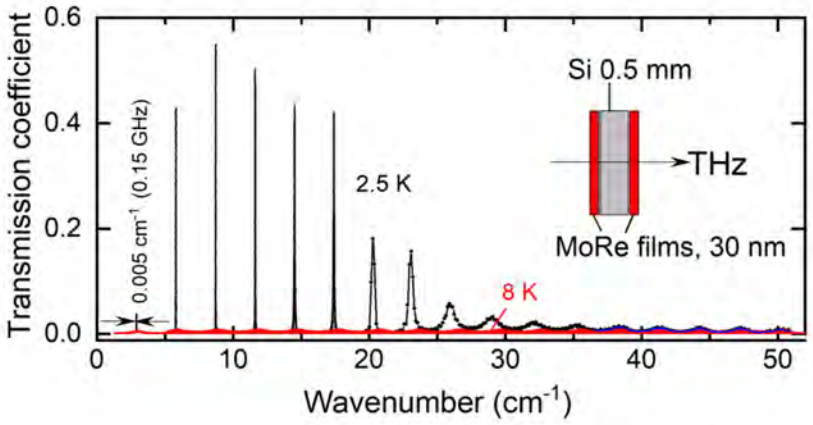

Fig. 1. THz transmission coefficient of a Fabry-Pérot resonator with SC $Mo_{0.6}Re_{0.4}$ films as reflectors measured above (8 K) and below (2.5 K) T_c≈8 K.

High-Q Fabry-Pérot resonators are made by depositing SC $Mo_{0.6}Re_{0.4}$ films (10, 20, 30 nm thick, T_c=7-8 K) on both sides of plane-parallel slabs of highly resistive silicon. Performance of resonators, as well as films parameters (SC energy gap, London penetration depth, SC condensate plasma frequency) are characterized by measuring transmissivity of resonators at frequencies 3–50 cm^{-1} and at temperatures 2.5–300 K. Dramatic increase in reflectivity of the films and drop in losses in SC state lead to record values of quality factor Q and finesse F of interferometric peaks at T=2.5 K: Q=830 (peak at ≈6 cm^{-1}), F=580 (peak at ≈3 cm^{-1}; FWHM=150 MHz, Fig.1). Despite the need for deep cooling, due to extreme compactness (8*8 mm^2, 0.5 mm thick) and simple design, the resonator is promising for applications in THz technology, especially in situations with stringent weight and size constraints.

The work was supported by the Ministry of Science and Higher Education of the Russian Federation: projects FSMG-2025-0005 (THz experiments), 075-15-2025-010 (sample preparation and characterization).

Influence of Filamentation on Magnetization Losses in Laser-Processed 2G HTS Tapes

S.V. Veselova, M.A. Osipov, D.A. Abin, S.V. Pokrovskii

This study investigates filamentation of 2G HTS tapes to mitigate energy dissipation caused by Abrikosov vortex motion in alternating magnetic fields. Laser segmentation into parallel conductors reduces hysteresis losses by restricting vortex mobility, while copper-coated filaments enhance thermal stability during quenches. Optimal laser ablation parameters (19±1 μm depth, 10 passes) were determined via profilometry (Ra/Rz analysis). Magneto-optical imaging confirmed isolated filament formation. MPMS-5 measurements (4.2–77.4 K, ±5 T) revealed filamentation-dependent magnetization losses: significant reduction at 4.2 K, weakening at 40 K, and minimal effect at 77.4 K.

During operation in alternating magnetic fields, non-filamented high-temperature superconducting (HTS) tapes experience movement of Abrikosov vortices, leading to energy dissipation. Laser or mechanical segmentation into parallel insulated conductors reduces hysteresis losses during magnetization reversal by restricting lateral vortex motion through the creation of physical barriers [1, 2]. Additionally, filamentation localizes heat generation during quench events. Each filament is surrounded by a copper coating that enhances heat dissipation and prevents overheating of the entire tape.

This work focused on optimizing laser cutting parameters for second-generation (2G) HTS tapes to establish conditions for forming filamentary structures. Samples with varying numbers of filaments were produced. Surface morphology was analyzed using a profilometer via longitudinal scanning, enabling quantitative evaluation of average roughness (Ra) and mean depth (Rz). Samples with optimal laser ablation depth (19±1 μm), achieved through 10 laser passes, were selected for reproducible filamentation.

Magneto-optical imaging confirmed spatial separation of the superconducting layer into isolated filaments. Quantitative analysis of magnetic properties was performed using an MPMS-5 system in the temperature range of 4.2-77.4 K under cyclic magnetic fields of ±5 T. The obtained magnetization hysteresis curves demonstrate the dependence of magnetization losses on the degree of filamentation. At 4.2 K, a significant reduction in hysteresis losses was observed. This effect diminished at 40 K and further degraded at 77.4 K.

The study was supported by the Russian Science Foundation grant No. 23-19-00394, https://rscf.ru/project/23-19-00394/.

References

1. *Lan, Tian, et al*., IEEE, **33**(6), 1-12 (2023).
2. *Skov-Hansen, P., Z. Han, and Jakob Ilsted Bech*. IEEE, **9**(2), 2617-2620 (1999).

Application of the 3D-MLSI program for designing superconducting interferometers

E.N. Zhardetsky, A.S. Ionin, F.A. Razorenov, V.V. Bolginov, I.E. Tarasova, L.N. Karelina, N.S. Shuravin, M.M. Khapaev

Institute of Solid State Physics, Russian Academy of Sciences, Chernogolovka 142432, Moscow oblast, Russia, HSE University, Moscow 101000, Russia, Moscow Institute of Physics and Technology, Dolgoprudnyi 141700, Moscow oblast, Russia,
OOO "SP "Quant", Moscow 121205, Russia, Moscow State University, Moscow 119991, Russia

The increasing data processing demands in neuromorphic computing raises the issue of using superconducting electronics, which offer advantages in speed and energy efficiency. Josephson interferometers have previously been proposed (for example, [1]) which have the necessary type of transfer function (TF) for the implementation of a superconducting perceptron or radial basis function networks. However, the necessary type of TF depends on specific, optimal ratios between the inductors of the neuron elements. Therefore, when designing experimental samples, numerical modeling of the proposed interferometer design, taking into account the shape of the superconducting connecting lines, becomes particularly important.

In this paper, we want to demonstrate the capabilities of the 3D-MLSI program [2], developed by researchers at Moscow State University and which is the most accessible for Russian users. The program solves Maxwell's and London's equations for a given configuration and geometry of inductive superconducting lines. The capabilities of the program are illustrated by comparing simulated results with those of an experimental study of two-junction superconducting interferometers of four different designs. All designs involved the use of three superconducting layers separated by layers of Insulation. The bottom layer performed the functions of a superconducting screen, while the other two were intended to create a control line and an interferometer loop. The interferometers were U-shaped, with the Josephson junctions located at the base of the "U", and the "crossbar" had a variable length for different samples of the same design. Experimental and numerical studies of interferometers of a more complex shape, representing partial circuits of a sigma neuron, were also conducted. A good agreement between the calculated and experimental results (at the level of several percent) was obtained, which confirms the high potential of the 3DMLSI program for designing elements of digital superconducting electronics.

This work was supported by the Russian Science Foundation grant No. 23-72-00053. Samples were fabricated using the «Cryointegral» unique scientific facility (USF No. 352529) of the V.A. Kotelnikov Institute of Radio Engineering and Electronics of the Russian Academy of Sciences.

References

1. *E. Schegolev, N.V. Klenov, I.I. Soloviev, M.V. Tereshonok*, Beilstein journal of nanotechnology **7**(1), 1397-1403 (2016).
2. *M. Khapaev*, System **3**(D2D), 6 (2004).

SPONSOR PRESENTATIONS

CRYOTRADE engineering
...WE MAKE IDEAS WORK

Cryotrade Engineering Ltd.
125367, Moscow, st. Gabrichevsky, 5к1, p. 1/2
Tel./fax: +7 (495) 374-69-52
Web: www.cryotrade.ru E-mail: sales@cryotrade.ru

Cryotrade Engineering is engaged in the production of cryostats, as well as the supply of various equipment for scientific laboratories. For 15 years of work in the Russian market we have completed more than 1000 contracts for the various equipment supply. Main areas of activity: vacuum, cryogenic, magnetic, sputtering equipment, consumables; turnkey laboratory equipment.

Our company manufactures the following equipment:

- LN-120 and LN-121-SPECTR are standard compact nitrogen variable temperature dewars, which have proven themselves in the market;
- Nitrogen and helium flow and closed-loop cryostats – standard or customized, including helium closed-loop cryostats with ultra low vibration for optics and microscopy;
- closed-type cryostats with a third cooling stage, allowing operation at temperatures up to 0.3 / 0.9K;
- superconducting magnets with room temperature bore (RTB) or variable temperature insert (VTI), filled and closed-loop type, optical and non-optical;
- transfer lines for LN_2 and LHe with vacuum insulation and LN_2 dispensing systems;
- liquid nitrogen generators with capacity from 10 to 360 liters/day (more productive systems - on order)

Supplied equipment:

- Cryorefrigerators cooled to 4K and below, on the Gifford-McMahon or Pulse tube cycle;
- helium liquefiers and re-liquefiers with capacity from 20 to 200 l/day;
- cooled and heating stages with temperature range from -190 to + 1200 ºC;
- accessories and consumables – cryogenic wires, temperature sensors, temperature monitors and controllers, current sources, Dewar vessels;

- vacuum turbo pumping stations, gauges, fittings and all related products;
- equipment for vacuum systems - ultra-high vacuum portable chambers, linear motion systems (from 1 to 5 axes), high-temperature and ion-beam evaporators, gates, etc.;
- Electromagnets, Helmholtz coils and installations based on them (VSM, MOKE, Hall effect measurement systems, demagnetizing installations and many others);

- optical and laser equipment and vibration isolation tables;
- lock-in amplifiers with frequency range from 100 kHz to 300 MHz;
- electrical measuring equipment (multimeters, current sources, LCR meters, etc.);
- all type of CVD systems, and also lithography, furnaces, etc.,
- piezo motion stages and scanners, including cryogenic systems;
- HF components and lines: detectors, circulators, insulators, coaxial wires, etc.;
- Chillers and thermal stabilizers - from compact table-top units for lasers to industrial systems (from room to full building);
- optical components, semiconductor substrates and wafers, scintillators, crystals for lasers, transparency windows, SOI, heterostructures, etc.

Microtechpro

«Microtechpro» LLC - Equipment, Service, Parts and Consumables for FIB SEM TEM

We provide support for your high-performance SEM, FIB, and TEM systems with consumables, parts, and service maintenance.

Company "**Microtechpro**" is a group of enthusiasts engineers, focused on the production and restoration of FIB, SEM, TEM consumables. Our company offers a full range of service and technical and engineering services, as well as conducts scientific research and produces experimental design work.

Our engineers have official certificates from well-known world manufacturers (FEI, Physical Electronics (PHI), EDAX Inc., Fisçhione, Kleindiek, etc.).

Equipment for electron microscopy

New & refurbished. We offer new, refurbished and upgraded systems and equipment for electron microscopy from the largest original equipment manufacturers

FIB, SEM, TEM Direct replacement consumables and parts

Sources, extractors, suppressors, aperture strips, detectors, gas chemistries. Every item is a direct replacement for original components, delivering the same or better performance with substantial cost savings

Refurbished electronic components:

Scintillators, ion pumps, controllers, power supply and other items. We have extensive stock of new and used electronic components for electron microscopes

R&D

We conduct scientific research and produce experimental design work. Quantifoil modification, development of new compositions

Service & Support

We provide comprehensive support for all aspects ranging from installation to maintenance services, diagnosis of the installation environment, and training on the use of equipment in order to ensure stable equipment operation and maximum utilization of the equipment by the customer

+7 (495) 363-52-38 sales@microtechpro.ru

microtechpro.ru vk.com/schottky t.me/microtechpro

Advatex

advatex.ru

Вакуумные системы для анализа поверхности

XPS, ARPES, NAP-XPS, SPM, PEEM/LEEM, HAXPES, AES, MBE, UPS, SIMS и другие

Насосы, компоненты и комплектующие вакуумных систем

Системы позиционирования, манипуляторы и трансляторы

Рентгеновские дифрактометры

Настольные порошковые дифрактометры

Дифрактометры с точечным и линейным детектором

Дифрактометры с высоким разрешением для анализа тонких пленок

Монокристальные дифрактометры

Источники излучения, испарители и детекторы

Рентгеновские, УФ, ионные и плазменные источники

Электронные источники и электронно-лучевые испарители

Рентгеновские детекторы и детекторы электронов

ООО «Адватекс»
Тел.: +7 (499) 964-47-00
e-mail: sales@advatex.ru

providing advanced technologies

Advatex

advatex.ru

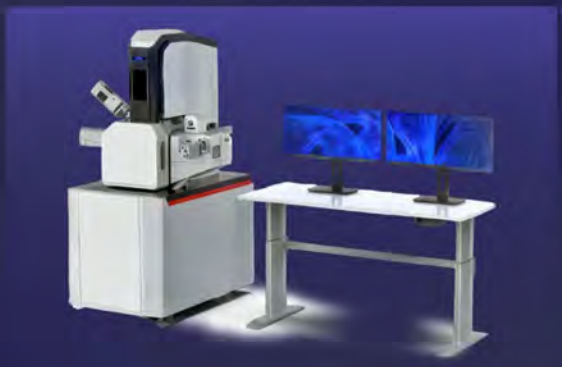

Сканирующие электронные микроскопы

«Рабочие лошадки» с вольфрамовым катодом

Высокоразрешающие СЭМ с катодом Шоттки

Множество опций и приставок: EDS, EBSD, CL, WDS, литография, STM, AFM, столики нагрева/ охлаждения, микро- наноманипулятор

Пробоподготовка

Металлографические шлифовочные/ полировочные машины

Металлографические отрезные станки

Металлографические запрессовщики

Установки нанесения проводящих покрытий

Системы ионного утонения образцов

Термообработка и термоанализ

Системы Вакуумной Термообработки:

Искровое плазменное спекание

Горячее изостатическое прессование

Дуговая плавка

Закалка, пайка, сварка

Спиннингование

Рост кристаллов

Газофазное осаждение и др.

Системы Термоанализа (TDA, DSC, STA, TMA и др.)

ООО «Адватекс»
Тел.: +7 (499) 964-47-00
e-mail: sales@advatex.ru

providing advanced technologies

ЭМТИОН | INNOVATIONS FOR SCIENCE AND TECHNOLOGY

STC MTEON - Innovations for Science and Technology

+ **20 years** of successful projects in science and education market
+ **Life time support** service with engineers and service centres in Russia
+ **DEMO lab** to explore equipment features in Moscow
+ **Self-made innovative equipment** and investigations
+ **Customized solutions** and full support during the project implementation

X-RAY PHOTOELECTRON SPECTROSCOPY

Flexible configuration system for user tasks:

+ X-ray source
+ Monochromator 500mm
+ 150mm Analyzer
+ Ion source
+ UV source
+ Electronic source
+ Charge neutralization
+ Sample Preparation Chamber
+ Five-axis manipulator
+ E-beam heating and LN2 cooling
+ Loading Camera
+ Film thickness control

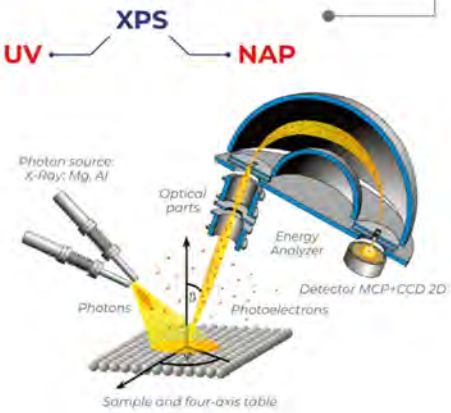

XAFS X-RAY ABSORPTION SPECTROMETER

XAFS spectroscopy is based on measuring the absorption coefficient of an atom of matter near the absorption edge (XANES) and in the region beyond the absorption edge (EXAFS).

+ the electronic structure of the atoms of matter
+ the number of nearby atoms and their positions
+ link lengths
+ Valence angles and more

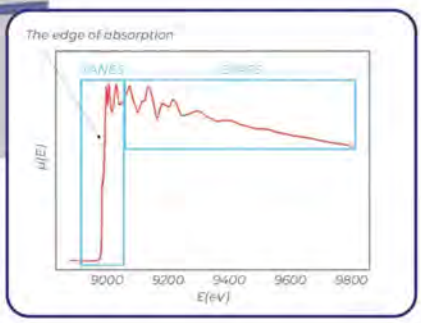

The XANES spectrum provides information about the valence state and geometry of the atoms' surroundings, while the EXAFS spectrum provides information about bond lengths, coordination numbers, types of neighbouring atoms, etc.

ЭМТИОН

STC MTEON / ITN 7735195944 / Tel. +7-499-390-90-81
Address: 4 Savelkinsky proezd, Zelenograd, Moscow, Russian Federation
www.mteon.ru
info@mteon.ru

X-RAY DIFFRACTOMETRY

DIFFRACTOMETERS
POWDER — SINGLE-CRYSTAL

- **High speed and precision**
  Matrix 1D, SDD, SC detectors and scanning in 0.0001° increments
- **Automation without compromise**
  Auto-changer for 12 samples + 360° rotation
- **Extreme conditions — stable results**
  Operate in the range from -196°C to 1600°C
- **Smart analysis**
  Built-in spectrum database and processing software - turn data into discoveries in minutes

ELECTRON MICROSCOPY

Choose options for your tasks and get maximum opportunities with an optimal budget.

- SE (SE LV) surface topography
- BSE (BASE LV) composition analysis
- EDS elementary microanalysis.
- EBSD crystallographic studies WDS elemental analysis
- CL optical properties
- STEM translucent mode
- Electronic lithography

SEM
TEM
FIB SEM

Gold spheres, spatial resolution is 1.5nm

PPMS / VSM / MO KERR

Measurement of a wide range of physical properties of materials under controlled conditions (temperature, magnetic field, pressure):

- Electrical properties (resistance, conductivity, Hall effect)
- Magnetic properties (magnetization, magnetic susceptibility)
- Thermal properties (heat capacity, thermal conductivity)
- Mechanical properties (e.g. magnetostriction)

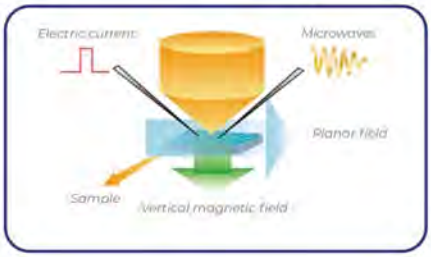

ЭМТИОН
STC MTEON / ITN 7735195944 / Tel. +7-499-390-90-81
Address: 4 Savelkinsky proezd, Zelenograd, Moscow, Russian Federation
www.mteon.ru
info@mteon.ru

ООО «ЛАНХИТ» производит высокочистые неорганические материалы для:

❖**Электроники**
❖**Фотоники**
❖**Фармацевтики**
❖**Ядерной медицины**
❖**Научных исследований**

Используя собственные научные исследования и разработки ООО «ЛАНХИТ» производит:

- ультрасухие галогениды металлов: хлориды, бромиды, иодиды. Эти соединения чувствительны к кислороду и влаге, все ультрасухие материалы (примеси кислорода и влаги в диапазоне 50–100 ppm) ампулируются в атмосфере аргона. Продукция соответствует международным стандартам качества, степень чистоты материалов составляет от 99,9% до 99,999%, что обуславливает возможность применения галогенидов в различных областях науки и техники. Большинство ультрасухих материалов производится в виде гранул сферической формы (менее 2 мм), а также в виде кристаллов и порошков. Соединения доступны в количествах от граммов до сотни килограммов;
- соли редкоземельных металлов (гидраты нитратов, галогенидов, сульфатов, ацетатов, карбонатов, оксалатов, нанодисперсные оксиды);
- оксиды редких металлов;
- высокочистые металлы (мышьяк, молибден, стронций, Рений и др.);
- щелочные металлы (натрий, калий, рубидий, цезий).

Синтезируем материалы по индивидуальному запросу заказчика.

Выбирайте надежность и высокое качество – выбирайте продукцию ООО «ЛАНХИТ»!

ООО «ЛАНХИТ»
105118, г. Москва, ш. Энтузиастов, 34
Телефон: +7 (499) 948-23-44
E-mail: info@lanhit.ru
Сайт: www.lanhit.ru

LLC «LANHIT» produces high-purity inorganic materials for the following industries:

❖**Electronics**
❖**Photonics**
❖**Pharmaceutical**
❖**Nuclear medicine**
❖**Scientific research**

Based on its own scientific research and in-house developments, LLC «LANHIT» manufactures:

- Ultra dry metal halides: chlorides, bromides, and iodides. These compounds are highly sensitive to oxygen and moisture. All ultra dry materials (with oxygen and moisture impurities in the range of 50–100 ppm) are sealed in ampoules under an argon atmosphere. The products meet international quality standards, with material purity levels ranging from 99.9% to 99.999%, which allows their use in a wide range of scientific and technological applications. Most ultra dry halides are produced as spherical granules (less than 2 mm), as well as in crystalline and powder forms. Quantities are available from grams to hundreds of kilograms;
- Rare-earth metal salts (hydrates of nitrates, halides, sulfates, acetates, carbonates, oxalates, and nanodispersed oxides);
- Rare metal oxides;
- High-purity metals (arsenic, molybdenum, strontium, rhenium, etc.);
- Alkali metals (sodium, potassium, rubidium, cesium).

We also offer custom synthesis of materials based on individual customer requests.

Choose reliability and exceptional quality – choose LANHIT products!

LLC «LANHIT»
105118, Moscow, Shosse Entuziastov, 34
Phone: +7 (499) 948-23-44
E-mail: info@lanhit.ru
Website: www.lanhit.ru

Группа Компаний «Криосистемы»
111250, г. Москва, проезд Завода Серп и Молот, д. 10, БЦ «Интеграл», офис 404,
Телефон: +7 (495) 215-55-65,
info@cryosystems.ru, www.cryosystems.ru

Группа компаний «Криосистемы» была создана в 2002 году высокопрофессиональной командой российских инженеров, конструкторов и технических специалистов.

Решение о создании ГК «Криосистемы» было вызвано необходимостью сохранения знаний и опыта, а также в целях получения возможности для развития научно-технического потенциала в области криогенных и вакуумных технологий.

Нашими постоянными заказчиками являются ведущие государственные предприятия, корпорации и технические объединения, составляющие научный, космический, атомный, военный и оборонно-промышленный комплексы Российской Федерации. Более двадцати лет ГК «Криосистемы» тесно сотрудничает с акционерным обществом «Корпорация космических систем специального назначения «Комета», акционерным обществом «Научно-производственное предприятие «Исток» имени А. И. Шокина», акционерным обществом «Научно-производственная корпорация «Системы прецизионного приборостроения», федеральным государственным унитарным предприятием «Российский федеральный ядерный центр – Всероссийский научно-исследовательский институт экспериментальной физики», публичным акционерным обществом «Ракетно-космическая корпорация «Энергия» имени С.П. Королёва», акционерным обществом «Научно-производственное объединение им. С.А. Лавочкина», и многими другими государственными предприятиями, корпорациями и техническими объединениями.

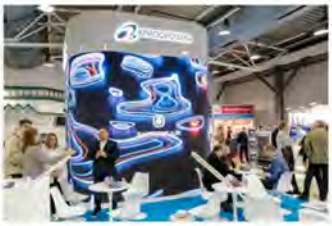

Основные направления деятельности:

♦ **Проектный инжиниринг и разработка под задачу заказчика.**
Индивидуальные инженерные решения с учётом специфики отрасли, условий эксплуатации и технологических требований.

♦ **Производство вакуумного и криогенного оборудования.**
Сборка сложных систем: от криостатов и имитаторов до стендов и камер. Работаем с нестандартными задачами, обеспечивая точность и надёжность.

♦ **Поставка, сервис и ремонт оборудования.**
Обслуживаем вакуумное, криогенное, испытательное и лабораторное оборудование. Выполняем ремонт любой сложности, проводим модернизацию и дооснащение систем.

♦ **Высокоточная металлообработка.**
Собственный парк станков с ЧПУ позволяет изготавливать узлы и детали с высокой точностью. Обрабатываем сложные материалы и отвечаем требованиям оборонной, аэрокосмической и научной отрасли.

Наши компетенции:

- **Сверхвысоковакуумные установки** для осаждения материалов, создания микроконтактов, меток, электродов и туннельных переходов.
- **Криостаты оптические и растворения** для исследований квантовой логики, нанофотоники, наномеханики и метрологии при сверхнизких температурах.
- **Криогенные и исследовательские установки** для лабораторных и прикладных задач.
- **Имитаторы космического пространства** с контролем температурных и вакуумных параметров.
- **Автоматизированные стенды контроля герметичности** для серийных и опытных производств.